Title
Interactions of Water and Energy Mediate Responses of High-Latitude Terrestrial Ecosystems to Climate Change

Author
Subin, Zachary Marc

Publication Date
2012

Peer reviewed|Thesis/dissertation

Interactions of Water and Energy Mediate Responses of High-Latitude Terrestrial Ecosystems to Climate Change

By

Zachary Marc Subin

A dissertation submitted in partial satisfaction of the

requirements for the degree of

Doctor of Philosophy

in

Energy and Resources

in the

Graduate Division

of the

University of California, Berkeley

Committee in charge:

Adjunct Associate Professor Margaret S. Torn, Chair
Professor William D. Collins
Dr. William J. Riley

Spring, 2012

Abstract

Interactions of Water and Energy Mediate Responses of High-Latitude Terrestrial Ecosystems to Climate Change

By

Zachary Marc Subin

Doctor of Philosophy in Energy and Resources

University of California, Berkeley

Adjunct Associate Professor Margaret Torn, Chair

Both biogeophysical and biogeochemical feedbacks to climate change from high-latitude terrestrial ecosystems may be mediated by permafrost thaw. For instance, lakes may expand as relatively intact permafrost begins to thaw but experience drainage with continued permafrost degradation; thawing permafrost also increases the vulnerability of soil carbon to decomposition. In order to quantify these feedbacks, Earth System Models (ESMs) need to adequately represent a number of sub-surface processes.

I improved the lake model in the land-surface component (CLM4) of an ESM by including the physics of snow, ice, and underlying sediment, allowing shallow high-latitude lakes to be adequately simulated. After evaluating the model, I investigated the sensitivity of regional surface fluxes to included lake model processes. The inclusion of snow insulation and lake water phase change each cause 15-30 W m^{-2} changes in seasonal surface fluxes, altering the forcing of lakes on the atmosphere. With realistic inclusion of these processes, I predict that the presence of high-latitude lakes causes little net change in mean annual air temperature. However, due to increased sub-surface thermal inertia, lakes moderate the seasonal and diurnal cycle in regions of large lake area like the Canadian Shield. Consequently, the loss of lake area in areas of disappearing permafrost could exacerbate increases in summer daily maximum temperatures due to climate warming by up to 1°C.

Snow insulation has long been recognized as a key control on permafrost soil thermal regime. I show that the snow thermal rectifier can interact with hydrology to cause significant changes in soil temperature associated with non-thermal anthropogenic forcings. Elevated CO_2 or increased summer rainfall could increase soil water-filled pore space by 0.1-0.2 in some permafrost areas, associated with 1-2°C increases in mean soil temperature. This warming results from both the increased thermal conductivity of the soil and the increased latent heat of fusion. Because these mechanisms saturate once soils are relatively saturated, the initial soil moisture state is crucial in determining susceptibility to these warming mechanisms. In this model, these warming mechanisms were not effective in substantially increasing permafrost vulnerability to thaw in a severe 21st century transient warming scenario.

In summary, I have shown that explicit representation of snow insulation and of freezing and thawing in lakes and soils can alter the predicted responses of soil and air temperatures to changes in climate.

Table of Contents

Acknowledgements

I would like to recognize all the people who helped make this dissertation possible. Most importantly, my committee members Margaret Torn, Bill Riley, and Bill Collins have provided consistently excellent academic guidance while remaining personally approachable and supportive throughout my studies. Secondly, I would like to thank additional members of my Qualifying Exam committee, John Harte and Rob Rhew. Finally, the Lawrence Berkeley Lab and Energy and Resources Group staff, and all the Berkeley professors and teaching fellows who instructed me in coursework, played a crucial role in the academic process.

In addition, the following colleagues contributed intellectually to this research: Charlie Koven, Lisa Murphy, Fuyu Li, Céline Bonfils, Dmitrii Mironov, David Lawrence, and Sean Swenson. Andy Jones, Sebastien Biraud, and Jinyun Tang consistently helped bounce off ideas and provided helpful computational scripts. Additional insight and assistance was provided by Andrey Martynov, Victor Stepanenko, Annika Nordbo, Marjorie Perroud, Michael Wehner, John Chiang, Sarah Kang, and Ben Santer. Feedback on this research was provided by colleagues at presentations and conferences, particularly members of the Climate Sciences Department at the Lawrence Berkeley Lab and the Earth, members of the CESM Land Model Working Group, and attendees at the 2nd Workshop on Parameterization of Lakes in Numerical Weather Prediction and Climate Modeling. Anonymous reviewers improved the writing of Chapters 2 and 3 and caught several errors.

My parents, friends, and roommates provided entertaining diversions and emotional support: especially Craig Hetherington, David Hembry, Rita Hamad, Elliot Reed, Kris Hartley, Jordan Chan, Nir Krakauer, Scott Zimmerman, Elissa Sato, Ari Turner, Toyotaka Ishibashi, Alexei Painter, Kristen Durham, and Casey Mullin.

Finally, this work was made possible by a research grant from the Department of Energy to the Lawrence Berkeley National Lab, paid for by the U.S. taxpayers.

Chapter 1: Introduction

Chapter 1 Table of Contents

1. Introduction

High-latitude terrestrial ecosystems are expected to experience greater than global-mean warming under 21st century climate change (Solomon et al. 2007). "High-latitude" as used here roughly encompasses the Northern Hemisphere Boreal and Arctic zones, where mean-annual air temperatures are near or below 0°C. This warming has the potential to provide multiple feedbacks to global climate change, many of them positive (Schuur et al. 2008; Tarnocai et al. 2009; Walter et al. 2007a; Zimov et al. 2006a; Zimov et al. 2006b). In this Chapter, unless otherwise stated, I use "feedback" to denote one-half of a feedback loop, i.e., a response of terrestrial ecosystems to climate change that will likely have a follow-on effect on large-scale climate. Positive biogeophysical feedbacks that may increase surface energy fluxes to the atmosphere include: retreating ice and snow or expanding dark vegetation cover (Chapin et al. 2005; Eugster et al. 2000), which may decrease albedo; changes in lake area, discussed below; and reduced permafrost area, discussed below. Positive biogeochemical feedbacks include increased greenhouse gas emissions from expanding and deepening thermokarst lakes, thawing permafrost, fire, and wetlands experiencing hydrological disruptions (Grosse et al. 2011; Schuur et al. 2011). Increased anaerobic decomposition in warming and/or wetting thermokarst lakes, peatlands, and wet tundra is of particular concern because methane fluxes respond highly nonlinearly to environmental conditions (Smith et al. 2003), and methane has 26 times the effective molar instantaneous radiative forcing as CO_2 (Forster et al. 2007). Negative biogeophysical and biogeochemical feedbacks are also possible from changes in lake area, disturbance of wetland hydrological regimes, and increased ecosystem carbon uptake from increased vegetation productivity.

To better understand how these forcings and feedbacks interact with climate change, General Circulation Models (GCMs) and Earth System Models (ESMs) need to accurately simulate a variety of processes. However, current formulations and evaluation of these processes in ESMs are limited. Many GCMs lack even a 1-dimensional (1D) mechanistic treatment of lake thermodynamics, which is a pre-requisite to understanding physical and biogeochemical changes in thermokarst lakes (defined below). Only recently have GCM soil physics schemes begun to include features such as deep soil and organic matter content that could be important for determining permafrost thaw rates (Lawrence et al. 2008a). GCMs included in the Climate Model Intercomparison Project 5 (CMIP5) have widely divergent predictions of permafrost thaw resulting from variations in soil physics (Koven et al., in preparation); some models even lack phase change (Romanovsky and Osterkamp 2000) and snow insulation (Zhang 2005) mechanisms that may be critical to simulating active layer thickness (ALT) and soil temperatures. Wetland treatments in GCMs (Ringeval et al. 2010), if included at all, are very limited in mechanistic fidelity compared to treatments in stand-alone dynamic vegetation models (Wania et al. 2009a, 2009b) and relative to the processes expected to be important for understanding changes in northern peatland dynamics (Frolking et al. 2009).

In the following sections, I expand on some of the most important dynamics for understanding climate feedbacks and the current state of modeling capabilities, before outlining the new research undertaken in this dissertation.

1.1 Permafrost Thaw

Recent modeling work in the Community Land Model (CLM) [the land component of the Community Earth System Model (CESM)] suggests that much of the near-surface permafrost currently found at high latitudes is vulnerable to thaw within the next century (Lawrence et al. 2011; Lawrence et al. 2008a; Lawrence et al. 2008b), although alternative models do show greater persistence of permafrost during this period (Delisle 2007). Other modeling work (Camill 2005; Sazonova et al. 2004; Zhang et al. 2008a, 2008b), combined with observations of current thawing and warming rates (Akerman and Johansson 2008; Camill 2005; Osterkamp and Romanovsky 1999; Osterkamp and Jorgenson 2006; Romanovsky et al. 2007; Smith et al. 2005b) suggests ample reason for concern, although some studies show that certain areas are experiencing cooling or are protected by ice-rich organic soil layers with low effective thermal diffusivity (Serreze et al. 2000; Tarnocai et al. 2004). Permafrost thaw can accelerate summertime warming by reducing the seasonal thermal inertia of the soil (Lawrence et al. 2011). Increases in thawed soil volume can allow soil decomposition to occur during a greater part of the year, and even make available previously frozen stocks of soil carbon for decay. The large size of potential permafrost-zone soil carbon stocks relative to the size of the atmospheric carbon stock (Tarnocai et al. 2009) means that this positive feedback could be severe and is deserving of extensive scientific attention.

Many subsurface models driven by prescribed atmospheric temperatures, from local to pan-Arctic spatial scale, have been developed to predict permafrost thaw (Couture and Pollard 2007; Delisle 2007; Hinzman et al. 1998; Khvorostyanov et al. 2008; Riseborough 2007; Saito 2008; Salzmann et al. 2007; Sazonova and Romanovsky 2003; Zhang et al. 2008b). These often include processes that GCMs currently do not, like excess ice and thaw subsidence, 2-dimensional (2D) or 3-dimensional (3D) heat transport and hydrology (particularly for modeling mountainous areas), and heat generated by organic matter decomposition. A recent review summarizes permafrost models (Riseborough et al. 2008). Several modeling groups have incorporated permafrost into coupled regional climate models (Stendel et al. 2007; Sushama et al. 2007). The extent of permafrost thaw predicted during the 21st century in all of these models varies considerably, but most find substantial increases in active layer thickness (ALT), increased area of soil with taliks (zones of annually unfrozen soil beneath the active layer), and some reduction in permafrost extent in the areas studied, though reductions in permafrost areas are often modest (e.g. 16-20% reductions in Canada predicted by Zhang et al. (2008a)). However, some of the apparent discrepancies between model predictions [i.e., global losses of 80% in Lawrence et al. (2011; 2008a) as compared with Zhang et al. (2008a)] merely result from differing scope: Lawrence et al. (2011; 2008a), partially limited by model capabilities, only predicted losses of near-surface (top 4 m) permafrost. Even substantial losses of near-surface permafrost, though, could make large amounts of previously frozen soil carbon accessible to soil decomposers (Tarnocai et al. 2009).

While process comprehensiveness may not be expected to be as complete in ESMs as stand-alone permafrost models, ESMs should still include a minimum of processes in order to properly model permafrost thaw and potential carbon mineralization. Realistically, the next generation of ESM soil models should include: (1) vertically resolved soil columns; (2) snow insulation; (3) heat of fusion for phase change; (4) soil organic matter content (which is needed for soil thermal properties as well as biogeochemical modeling); (5) dynamic thermal and hydraulic properties; and (6) a deep enough column to encompass at least the depth of permafrost thaw during the time frame of interest. Moreover, while near-surface permafrost thaw has been modeled

primarily as a result of increased air temperatures (Schaefer et al. 2011), other factors can be at least as important in determining soil temperature and active layer depth: the seasonally asymmetric presence of snow insulation (i.e., the "snow thermal rectifier") is a major control on soil temperature (Goodrich 1982; Zhang 2005). Changes in snowfall, snow properties, and snow season length could alter soil temperatures (Iijima et al. 2010; Lawrence and Slater 2010; Pavlov and Moskalenko 2002; Stieglitz et al. 2003; Westermann et al. 2011; Zhang et al. 2005). In addition, increased soil moisture could interact with the snow thermal rectifier (Goodrich 1982; Zhang and Stamnes 1998). I explore the implications of these processes in Chapter 4. Other biogeophysical forcings such as shrub expansion could contribute to soil temperature changes, addressed in some recent studies [e.g., Bonfils et al. (2012) and Lawrence and Swenson (2011)].

1.2 Thermokarst Lakes

Thermokarst lakes are a dynamic feature of high-latitude landscapes containing permafrost. Formed primarily by thaw subsidence (in soils containing ice in excess of the structural porosity, referred to here as "excess ice") and secondarily by wind, wave, and gravity-induced bank erosion, lakes and drained-lake basins are present in permafrost-affected landscapes throughout the West Canadian Arctic, Siberia, Arctic Coastal Plain, & Bering Strait (West and Plug 2008). Active (i.e., expanding and non-drained) lakes cover as much as 20-40% of the surface area of affected landscapes (Frohn et al. 2005; Hinkel et al. 2005; Hinkel et al. 2003; Jorgenson et al. 2006; Jorgenson et al. 2001; Osterkamp et al. 2000; Plug et al. 2008). Existing lakes span a large range of sizes and ages, with new thermokarst pits several meters in diameter barely detectable from satellite, and others, which formed in the early Holocene, covering tens of square kilometers. Lakes deeper than the maximal thickness of winter ice generally have an unfrozen volume of soil, or talik, below them and to their sides.

Thermokarst lake dynamics can interact with climate change in several ways. Atmospheric warming can dramatically increase the rate of lake formation and expansion (Jorgenson et al. 2006; Jorgenson et al. 2001; Kaab and Haeberli 2001; Plug and West 2009), but it can also induce abrupt drainage (Smith et al. 2005a; Smith et al. 2007) as cracks develop in underlying permafrost to permeable rock beneath or lateral lake walls are breached towards a downhill grade. Meanwhile, the effect of lakes on their surroundings is large enough that simulating lakes appropriately has been shown to improve simulation of regional climate (Bates et al. 1993; Goyette et al. 2000). Thaw lakes increase the absorption of solar radiation at the surface and so warm their surroundings and increase thaw rates (Jeffries et al. 1999). Thaw subsidence reduces the soil thickness separating the permafrost from the atmosphere and interacts with snow in ways that further increase the rate of permafrost thaw (Buteau et al. 2004; Osterkamp et al. 2009) (although this would also temporarily remove more heat from the atmosphere). In the winter, freezing lake surfaces are a large source of latent heat flux that can be comparable in size to the energy flux supplied by the Arctic Ocean to some terrestrial regions (Frohn et al. 2005). Expanding taliks beneath lakes can moderate summer temperatures (Kaab and Haeberli 2001), but they can undergo extensive organic decomposition, releasing carbon dioxide and methane to the atmosphere in a positive feedback to climate change (Schuur et al. 2008).

Because of the anaerobic environment in the bottoms of, and beneath, lakes, methane emissions can be especially pronounced; while large-scale estimates are highly uncertain, these emissions could represent ~3% of the global methane budget at present, with larger emissions

potentially occurring during the Last Glacial Termination and under climate change (Walter et al. 2007a; Walter et al. 2007b). Unlike the active layer in nearby permafrost, taliks can produce as much methane during the winter as during the summer, and can release much of this methane quickly during the spring thaw (Phelps et al. 1998); because the decomposition is isolated from the atmosphere during the winter and the release is abrupt upon thaw, little of the methane is oxidized before reaching the surface. Since the methane release is highly concentrated in space as well as time, much of it has been missed by previous observations (Walter et al. 2007a; Walter et al. 2006). The per-area methane emissions from thermokarst lakes, particularly around the expanding edges of lakes in the Siberian Yedoma region [where organic matter is present in up to 60 m of loess (Zimov et al. 2006b)], can be much larger than that found in undisturbed high-latitude wetlands: isotopic analysis suggests that more concentrated sources of emissions tend to result from the decomposition of older carbon (Walter et al. 2008). Indeed, it seems reasonable to assume that, once thawed, organic material that has persisted in permafrost may be substantially more labile than organic matter that has accumulated in peatlands primarily because of biogeochemical rather than thermal constraints on decomposition. The mechanical erosion and slumping present at thermokarst edges also allows material from a range of depths to slide into the lake and undergo anaerobic decomposition. All of these thermokarst-specific factors are poorly treated in current ESMs that do not capture thermokarst processes in detail.

Thermokarst has generally been modeled only at a local or landscape scale. Thaw subsidence is included in several permafrost models (Buteau et al. 2004; Couture and Pollard 2007). Thermokarst lakes have been modeled thermally before and after drainage (Ling 2003; Ling and Zhang 2004), and their formation has been modeled in order to better understand their non-random orientation with respect to the prevailing wind (Pelletier 2005). The most detailed thermokarst lake models include a 2D lake and soil thermal model with thaw subsidence (West and Plug 2008) and a 3D finite-element model with thermal diffusion and mass transport at lake edges, allowing the lake to expand horizontally via gravity- and wind-induced erosion (Plug and West 2009). Recent work also includes an extension of the Plug and West (2009) model to larger scales and the inclusion of biogeochemistry (Kessler et al. 2012). One pan-Arctic scale study with dynamic thermokarst lake area has been conducted (van Huissteden et al. 2011), finding that lake drainage may limit the potential for methane emissions; however, this study used a relatively simple empirical parameterization of thermokarst lake area dynamics and focused on lateral drainage without inclusion of sub-surface drainage.

In any case, a prerequisite to including mechanistic thermokarst lake dynamics in ESMs is a faithful representation of lake thermodynamics, particularly for the regime of small, high-latitude, shallow lakes. Only recently have 1-dimensional (1D) lake models been commonly included in GCMs, and careful evaluation of these models is still underway, with no individual model formulation yet proving superior in both small and large lakes (Martynov et al. 2010; Perroud et al. 2009; Stepanenko et al. 2010). Many lake models currently integrated into climate models (Bonan 1995; Samuelsson et al. 2010) lack processes likely to be critical for high-latitude lake thermodynamics, such as snow insulation and phase change (Brown and Duguay 2010; Dutra et al. 2010). I explore the sensitivity of lake thermodynamics to these processes in Chapter 2.

While much of the current interest in thermokarst lakes focuses on biogeochemical impacts, current GCMs may be better suited to investigate whether expanding or contracting lake area

could have significant effects on surface energy fluxes and regional air temperatures. A number of studies have investigated the seasonal effects of lakes (Bonan 1995; Dutra et al. 2010; Krinner 2003; Lofgren 1997; Long et al. 2007; Rouse et al. 2005; Samuelsson et al. 2010). While studies tend to agree that temperate lakes increase surface fluxes and air temperatures in the fall and decrease them in the spring as compared with nearby land, there is some disagreement as to the net effects in the summer and winter, especially at high latitudes. Only one of these studies has examined effects on diurnal temperature range (DTR) of surface air temperature (Samuelsson et al. 2010) but empirical studies suggest they could be important (Geerts 2003). As most of the world's lake area is at high latitudes (Lehner and Doll 2004), there is high potential for change in lake area with changing climate. Krinner and Boike (2010) found that loss of high-latitude lakes and wetlands in areas of disappearing permafrost could slightly exacerbate summer warming under climate change (with only small effects of increasing lake area in remaining permafrost), but they did not investigate DTR or perform experiments long enough to investigate the possibility that lake area changes could have more than local effects. I explore these issues in Chapter 3.

1.3 Wetlands

High-latitude wetlands are an important component of the global carbon cycle, comprising the largest wetland complex in the world (MacDonald et al. 2006) and contributing from 10-30% of global methane emissions from natural wetlands (Bergamaschi et al. 2009; Christensen et al. 1996; Wania et al. 2009b; Zhuang et al. 2004). Most high-latitude wetlands are peatlands, with more than ~0.5 m accumulation of organic soil (Frolking et al. 2011), representing a large carbon stock. These peatlands could interact with climate change in several ways: melting permafrost could release currently dormant stores of soil carbon for degradation (Anisimov 2007; Schuur et al. 2009); temperature increases may alter the kinetics of soil biochemistry (Segers 1998); changes in the balance between precipitation and evapotranspiration could alter water table depth and soil moisture, which are strong controls on methane emissions (Smith et al. 2003) and on peatland carbon accumulation (Frolking et al. 2011); changes in both temperature and precipitation could change the net primary productivity (NPP) of existing plants or cause plant types to change (Christensen et al. 2004); and changes in soil hydrology or fire disturbance regimes could destabilize peatlands (Grosse et al. 2011). Fine-scale thermokarst activity can even convert forests into wetlands, changing the dominant vegetation from trees to aquatic herbaceous plants (Jorgenson et al. 2001).

Many Arctic permafrost peatlands developed in the early Holocene, spurred by high summer insolation, and have since frozen due to Arctic cooling in the late Holocene (MacDonald et al. 2006): moreover, in some aggrading permafrost peatlands, each year some fraction of litter and soil organic material freezes, thereby raising the soil surface and effectively moving the active layer upward (Kuhry et al. 2010). This carbon-rich material is vulnerable to decomposition if it thaws (Kuhry et al. 2010). Within the active layer, increasing temperatures may increase the rates of decomposition relative to primary production. If they have ample substrate, methanogens seem to have a higher sensitivity to temperature than typical aerobic soil decomposers (Lloyd and Taylor 1994; Segers 1998; Walter and Heimann 2000; Zhuang et al. 2004), so increased soil temperatures could increase the ratio of methane to carbon dioxide production associated with soil carbon mineralization. Moreover, because methanogens seem to also have higher temperature sensitivity than methanotrophs (Segers 1998; Walter and Heimann

2000; Whalen 2005; Zhuang et al. 2004), increased temperatures may increase the proportions of methane that escape to the atmosphere rather than being oxidized in the soil. However, it is uncertain whether either of these factors will dominate in the field as opposed to the laboratory. If methanogens are primarily limited by the availability of fermented substrate (e.g., acetate and hydrogen), and the production of that substrate does not have the same high temperature sensitivity of the methanogens, then the ratio of methane to CO_2 production may not increase; some studies (Basiliko et al. 2007; Bergman et al. 1998) and one review (Whalen 2005) suggest that high-latitude methanogens are primarily substrate-limited. Likewise, if methanotrophs are primarily limited by methane and oxygen diffusion rates rather than internal kinetics, as is frequently the case (Smith et al. 2003), then increasing temperatures (with constant methane production) may have little effect on the proportion of methane escaping oxidation, as diffusion rates vary relatively slowly with temperature. However, in areas where the primary mode of methane emission is ebullition rather than diffusion through the soil or through aerenchyma, then increased temperature will likely increase methane emissions by lowering the solubilities of both methane and oxygen, reducing the activity of methanotrophs and thus the proportion of methane oxidized before escaping. Also, as soil decomposition tends to have a much stronger temperature sensitivity (Lloyd and Taylor 1994) than diffusion, so as long as the ratio of methane to CO_2 production did not *decrease* with increasing temperature, then the proportion of methane escaping oxidation would increase, as the oxidative capacity would be increasingly overwhelmed by the faster production. An effective methane emissions model should represent each of these processes and factors explicitly.

Although some high-latitude terrestrial ecosystems may get wetter under climate change due to enhanced high-latitude atmospheric moisture convergence, some may experience drying because increases in evapotranspiration outpace increases in precipitation. Moreover, permafrost areas whose current wetness is due to a perched water table may experience drainage as permafrost thaws. This process could be accelerated as the surface peat layer that insulates the permafrost begins to degrade due to the initial drainage or warming. The timing of precipitation is critical: increased winter snow may merely run off during the snowmelt (and potentially help to keep the winter season long) without helping to keep soils moist during the growing season.

Peatlands have been a consistent source of methane and sink of CO_2 throughout the Holocene (Frolking and Roulet 2007), and either wetting or drying would influence the net fluxes of methane and CO_2. Wetting may tend to suppress decomposition and increase the net uptake of carbon by the soils over the long term (reducing atmospheric CO_2), but the concomitant increase in methane emissions may increase the net contribution to global warming potential in the short term; drying would have the opposite effect. The fine-scale spatial heterogeneity of both the terrestrial systems and likely changes in atmospheric forcing, and the complex dependence on seasonal hydrological dynamics, argues for modeling within a GCM to predict the relative areas experiencing wetting vs. drying.

As temperature increases and soil moisture changes, the productivity and composition of plant species will shift. These plant species shifts will affect the wetland carbon cycle, and accurately modeling these effects requires distinguishing between several classes of plant types that have different effects on methane emissions. In particular, the model should at least be able to distinguish between graminoids like Carex, whose high productivity, root exudation, and extensive aerenchyma can enhance methane emissions, and mosses like Sphagnum, which lack

aerenchyma and have acidic, recalcitrant litter that tends to suppress soil decomposition (MacDonald et al. 2006).

A few terrestrial methane models have been developed to understand the controls on methane biogeochemistry and how these might interact with climate change. These models are challenging to develop because net methane fluxes are often the small residual of larger gross production and oxidation fluxes, and production is itself highly sensitive to aqueous chemical controls that are poorly understood at large scales. Some models have been designed to be run at a local scale and include more extensive mechanistic detail (Grant and Roulet 2002; Segers and Leffelaar 2001; Segers et al. 2001) than could easily be incorporated into an ESM. Grant and Roulet (2002) include explicit representation of several different soil organic substrates, with microbial populations broken down into aerobic decomposers, anaerobic fermenters, methanotrophs, and both acetotrophic and hydrogenotrophic methanogens. They also model convective fluid transport within the soil and roots in addition to diffusion. Segers and Leffelaar (2001) have an explicit characterization of the geometry of the rhizosphere, with oxygen diffusing outwards and methane diffusing into cylindrical roots within the soil. The model detailed in Grant and Roulet (2002) was used to predict how methane and CO_2 fluxes in an Alaskan coastal Arctic tundra would change during 100 years of warming and increased nitrogen deposition (Grant et al. 2003). They found that methane fluxes would roughly double from 20 gC m^{-2} yr^{-1} to 40 gC m^{-2} yr^{-1}, due primarily to increased heterotrophic respiration rates (partially compensated by increased NPP in its effect on soil carbon balance), which increased both the rate of methane production and the anoxia of the soil, allowing more methane to escape without being oxidized. This analysis provides some support for the possibility that high-latitude methane emissions could provide a substantial positive feedback even without assuming a high temperature sensitivity of methanogens.

A series of models of increasing complexity have been used to predict high-latitude or global methane emissions and their sensitivity to climate change when driven by atmospheric forcing (Cao et al. 1996; Cao et al. 1998; Gedney et al. 2004; Riley et al. 2011; Ringeval et al. 2011; Ringeval et al. 2010; Walter et al. 2001a, 2001b; Wania et al. 2009a, 2009b; Zhuang et al. 2004; Zhuang et al. 2006). They generally have found the potential for a wetland methane emission feedback that is substantial compared to anthropogenic methane emissions but small compared to total anthropogenic greenhouse gas emissions: for instance, Gedney et al. (2004) find a doubling of wetland methane emissions by 2100, which would represent only a fraction of the radiative forcing of 21st century anthropogenic CO_2 at that time. However, these models have several limitations (Riley et al. 2011): they typically use many fixed parameters that have been tuned to limited site data, such as the Q_{10} of methane production or the ratio of methane escape to methane oxidation in aerenchyma, without characterizing the effects of uncertainty in these parameters on predictions of global emissions or how emissions might change with climate. In particular, several models use values for the Q_{10} of methanogenesis much larger than would typically be used to model aerobic soil decomposition: Walter et al. (2001b) use 6, and Zhuang et al. (2006) use ecosystem-specific values for Q_{10}, based on site tuning, ranging from 3.5-7.5. These high values could over-estimate prediction of the methane feedback if the methanogens tend to be more substrate-limited than rate-limited, and if the production of substrate has a smaller temperature dependence. Only a few models (Riley et al. 2011; Ringeval et al. 2010) have included the ability for wetland area to change seasonally or under climate change, and only one other (Volodin 2008) simulated the effect of increased methane emissions on atmospheric

chemistry and radiation. Zhuang et al. (2004; 2006) have included the effects of pH and redox potential on methanogenesis, but without considering the differences between pH in wetlands and the soils used to generate the pH distribution data, the time variation of redox potential in response to environmental conditions, or the potential for anti-correlation of the two factors across wetland types. Finally, in general, these models have poorly characterized model uncertainty both due to the large potential for parametric uncertainty of microbial biochemistry and the large structural uncertainty of missing processes in these models, including characteristics of peatland ecosystems (Frolking et al. 2009; Frolking et al. 2011), thermokarst lake dynamics, and the potential availability of thawing permafrost carbon (Koven et al. 2011) for anaerobic decomposition. I participated in a recent study (Riley et al. 2011) that attempted to quantify the importance of some of these limitations in previous studies and of the parametric and structural uncertainty inherent in these models; some implications of this study in the context of the research presented in Chapters 2-4 will be discussed in Chapter 5.

1.4 Earth System Modeling

Climate models of different levels of complexity complement each other, as each represents a different compromise between mechanistic detail, overall realism, faithful representation of dominant dynamic drivers, clarity of interpretation, ability to adequately represent feedbacks, and ability to represent spatial heterogeneity at different scales:

> An important concept in climate system modelling [sic.] is that of a spectrum of models of differing levels of complexity, each being optimum for answering specific questions. It is not meaningful to judge one level as being better or worse than another independently of the context of analysis. What is important is that each model be asked questions appropriate for its level of complexity and quality of its simulation. (Randall et al. 2007)

GCMs and ESMs may be so complicated that they can suffer from hidden and compensating errors and make simple interpretation difficult. They may model processes at such a coarse spatial scale that it is difficult to adequately represent the processes responsible for fine-scale spatial heterogeneity in dynamics. Attempts to maintain mechanistic clarity can conflict with large-scale realism when processes do not scale linearly. However, they are the only models capable of bringing together all of the feedback processes with atmospheric and oceanic dynamics while being faithful to processes finely resolved in time (like methane production, oxidation, and transport) and with large-scale 2D spatial heterogeneity. They are capable of fully closing feedback loops, integrating not only first-order effects of climate on feedback variables, but the follow-on effect of changes in climate and atmospheric chemistry on the feedback variables. They are also capable of being run in "offline" or in partially coupled mode in which first-order effects can be isolated from each other; e.g., they can calculate each of the separate components of the feedback *g* factor (Friedlingstein et al. 2006; Torn and Harte 2006). Furthermore, there are specific details of the processes discussed here that make them particularly suitable for analysis within ESMs, especially their dependence on regionally varying below-ground properties and the balance between precipitation and evaporation. Although ESMs (and certainly not a single ESM) cannot give a conclusive answer to the questions of how much area of permafrost will undergo thaw, what will be the balance between expanding and draining thermokarst lakes, and what will be the balance between expanding and drying wetlands, it is difficult to fully address these questions without reference to an ESM, as

atmospheric forcing (and subsequent responses of forcing to feedbacks via changes in large-scale circulation of the atmosphere and ocean) will vary between high-latitude gridcells.

In any case, ESMs as currently run typically include these feedback loops crudely or implicitly, or they require their effects to be prescribed based on offline simulations with simpler models that may make assumptions or have responses that are inconsistent with the ESMs using their results. For instance, ESMs have typically used prescribed atmospheric methane concentrations calculated offline. ESMs also require surface fluxes to be calculated in a land model that includes some treatment of albedo and surface resistance to evaporation, but these treatments may poorly represent biogeophysical features of high-latitude ecosystems highlighted here. Friedlingstein et al. (2006) argued for inclusion of a prognostic CO_2 cycle to avoid inconsistencies between offline carbon models and GCM predictions using their results. GCMs have long included prognostic calculation of the effect of anthropogenic greenhouse gas forcing on atmospheric concentrations of water, the most important greenhouse gas (with follow-on calculations of hydrologic feedbacks). Over the last several years, GCMs have increasingly incorporated fully prognostic CO_2 cycles that include online calculation of the effects of increased CO_2 and higher temperatures on ocean physical uptake and on terrestrial net ecosystem exchange (i.e., becoming ESMs). Incorporating a fully prognostic methane cycle, for instance, would be a logical next step, as methane has the third largest radiative forcing among greenhouse gases (and the second largest that is subject to direct anthropogenic alteration).

Nevertheless, as suggested by Held (2005), GCMs and ESMs must not be developed and run mechanically without insightful analysis. A hierarchy of models is crucial for understanding emergent behavior in coupled dynamical systems. I attempt to adhere to this principle in this dissertation. Before applying a new lake model to predict effects on regional climate in Chapter 3, I evaluated the model offline with prescribed atmospheric conditions compared to observations at thirteen lakes in Chapter 2. To complement the surprising prediction of effects on the Southern Hemisphere from changes in Boreal lakes in Chapter 3, I analyze idealized "aqua-planet" simulations to investigate potential mechanisms. Finally, in Chapter 4 I complement new results from a GCM land-surface model (CLM4) with a simplified analysis that allows us to understand the mechanisms in back-of-the-envelope, or a "Spherical Cow" (Harte 1988), style.

1.5 Hydrology as a Unifying Control on Permafrost-Zone Ecosystem Dynamics

Hydrology is a unifying thread for all the terrestrial ecosystem climate responses discussed above, and in particular on the future state of permafrost. The spatial and temporal distribution of water in terrestrial ecosystems governs the nature of ecosystem responses to warming (Jorgenson et al. 2010; Schuur et al. 2008), and future changes in hydrology will interact with ecosystem responses to changes in temperature (Grosse et al. 2011). Ice and snow properties further influence the effects of warming on ecosystems (Brown and Duguay 2010; Shur and Jorgenson 2007; Zhang 2005). These influences can be divided into biogeophysical and biogeochemical effects.

Hydrological regimes interact with biogeophysics to control the timing and form of surface energy fluxes, affecting both equilibrium soil thermal regimes and the sensitivity of soil temperatures to future climate change. The presence of surface water (e.g., lakes) can increase seasonal thermal inertia and cause shifts from sensible to latent heat fluxes. Under unfrozen

conditions, lakes can increase shortwave absorption and increase ground heat flux to soils. Increased soil moisture can cause shifts from sensible to latent heat fluxes but also increase the thermal inertia and conductivity of the soil. Snow increases albedo but also insulates soils and lakes from the atmosphere during the cold season. Excess ground ice can cause increases in thermokarst activity that increases surface water storage and mechanically mixes the soil, but it can also transiently retard permafrost thaw by serving as a latent heat sink.

Hydrological regimes also modify biogeochemistry: changes in soil moisture and surface water cause shifts in vegetation community composition and shift soil decomposition between predominately aerobic and predominately anaerobic processes. While anaerobic decomposition can release methane in addition to CO_2, with larger global warming potential per carbon atom, reductions in overall rates of carbon mineralization could compensate for increased methane fluxes.

Some biogeochemical effects of hydrology feed back to biogeophysics. Anaerobic conditions favor non-vascular vegetation and accumulation of soil organic matter that can decrease summer sub-surface thermal conductivity, cooling soils. The effectiveness of this cooling mechanism could be reduced if climate change causes drying or causes reduced stocks of near-surface organic matter and moss.

1.6 Outline of Research Included in This Dissertation

Because of the high degree of complexity of biogeochemical responses to climate change and their relatively poor treatment in existing ESMs, and because a number of tractable outstanding questions remain about biogeophysical effects of changes in hydrology on atmospheric and soil warming, I focused on biogeophysical interactions of climate and hydrology in this dissertation. I performed model development, evaluation, and experimental analyses in CLM4 and CESM1 to understand the effects of changes in lake area and soil moisture on surface energy fluxes, regional air temperatures, and soil temperatures.

In Chapter 2, I identify deficiencies in the current CLM4 lake thermodynamics sub-model, particularly for simulating high-latitude lakes like thermokarst lakes. I develop improvements in model structure and parameterization to address these deficiencies, and evaluate the model at 13 lakes of varying depth and horizontal extent, optical properties, and climate. In sensitivity experiments, I quantify the importance of ice and snow properties to regional high-latitude surface energy fluxes.

In Chapter 3, I apply the lake model developed in Chapter 2 to investigate atmospheric responses to changes in lake area. I first examine the role of current lake distributions in regulating high-latitude climate before investigating how future changes in lake distribution in permafrost regions could perturb responses to climate change. Because the potential for terrestrial surface properties to have large-scale and remote effects on atmospheric conditions has been little investigated, I investigate the surface forcing of small Boreal lakes in idealized aquaplanet simulations. Experiments in this reduced-complexity system may yield insights relevant for understanding effects of other extra-tropical terrestrial surface forcings that could be associated with climate change, such as changes in vegetation distribution, increased deposition of absorbing aerosols on ice and snow, and seasonal or regional loss of ice and snow cover.

In Chapter 4, I investigate whether future hydrological forcings, such as increased summer rainfall or reduced transpiration due to elevated CO_2, could warm permafrost soils by increasing soil moisture independently of increases in air temperatures. Responses are analyzed using perturbed physics experiments that isolate the mechanisms linking soil moisture and soil temperature. After understanding how soils may respond to forcing that increases moisture under equilibrium conditions, I investigate whether these mechanisms could be important during transient 21st century climate change.

Finally, in Chapter 5, I include summary conclusions, synthetic discussion, and address implications for opportunities for future research.

1.7 References

Akerman, H. J., and M. Johansson, 2008: Thawing permafrost and thicker active layers in sub-arctic Sweden. *Permafrost and Periglacial Processes*, **19,** 279-292.

Anisimov, O. A., 2007: Potential feedback of thawing permafrost to the global climate system through methane emission. *Environ. Res. Lett.*, **2,** 7.

Basiliko, N., C. Blodau, C. Roehm, P. Bengtson, and T. R. Moore, 2007: Regulation of decomposition and methane dynamics across natural, commercially mined, and restored northern peatlands. *Ecosystems*, **10,** 1148-1165.

Bates, G. T., F. Giorgi, and S. W. Hostetler, 1993: Towards the Simulation of the Effects of the Great-Lakes on Regional Climate. *Mon. Weather Rev.*, **121,** 1373-1387.

Bergamaschi, P., and Coauthors, 2009: Inverse modeling of global and regional CH4 emissions using SCIAMACHY satellite retrievals. *Journal of Geophysical Research-Atmospheres*, **114,** 28.

Bergman, I., B. H. Svensson, and M. Nilsson, 1998: Regulation of methane production in a Swedish acid mire by pH, temperature and substrate. *Soil Biology & Biochemistry*, **30,** 729-741.

Bonan, G. B., 1995: Sensitivity of a GCM Simulation to Inclusion of Inland Water Surfaces. *J. Clim.*, **8,** 2691-2704.

Bonfils, C. J. W., T. J. Phillips, D. M. Lawrence, P. Cameron-Smith, W. J. Riley, and Z. M. Subin, 2012: On the influence of shrub height and expansion on northern high latitude climate. *Environ. Res. Lett.*, **7**.

Brown, L. C., and C. R. Duguay, 2010: The response and role of ice cover in lake-climate interactions. *Progress in Physical Geography*, **34,** 671-704.

Buteau, S., R. Fortier, G. Delisle, and M. Allard, 2004: Numerical simulation of the impacts of climate warming on a permafrost mound. *Permafrost and Periglacial Processes*, **15,** 41-57.

Camill, P., 2005: Permafrost thaw accelerates in boreal peatlands during late-20th century climate warming. *Clim. Change*, **68,** 135-152.

Cao, M. K., S. Marshall, and K. Gregson, 1996: Global carbon exchange and methane emissions from natural wetlands: Application of a process-based model. *Journal of Geophysical Research-Atmospheres*, **101,** 14399-14414.

Cao, M. K., K. Gregson, and S. Marshall, 1998: Global methane emission from wetlands and its sensitivity to climate change. *Atmospheric Environment*, **32,** 3293-3299.

Chapin, F. S., and Coauthors, 2005: Role of land-surface changes in Arctic summer warming. *Science*, **310,** 657-660.

Christensen, T. R., I. C. Prentice, J. Kaplan, A. Haxeltine, and S. Sitch, 1996: Methane flux from northern wetlands and tundra - An ecosystem source modelling approach. *Tellus Series B-Chemical and Physical Meteorology*, **48,** 652-661.

Christensen, T. R., and Coauthors, 2004: Thawing sub-arctic permafrost: Effects on vegetation and methane emissions. *Geophysical Research Letters*, **31,** 4.

Couture, N. J., and W. H. Pollard, 2007: Modelling geomorphic response to climatic change. *Clim. Change*, **85,** 407-431.

Delisle, G., 2007: Near-surface permafrost degradation: How severe during the 21st century? *Geophysical Research Letters*, **34**.

Dutra, E., V. M. Stepanenko, G. Balsamo, P. Viterbo, P. M. A. Miranda, D. Mironov, and C. Schar, 2010: An offline study of the impact of lakes on the performance of the ECMWF surface scheme. *Boreal Environment Research*, **15,** 100-112.

Eugster, W., and Coauthors, 2000: Land-atmosphere energy exchange in Arctic tundra and boreal forest: available data and feedbacks to climate. *Glob. Change Biol.*, **6,** 84-115.

Forster, P., and Coauthors, 2007: Changes in Atmospheric Constituents and in Radiative Forcing. *Climate Change 2007: The Physical Science Basis. Contribution of Working Group I to the Fourth Assessment Report of the Intergovernmental Panel on Climate Change*, S. Solomon, and Coauthors, Eds.

Friedlingstein, P., and Coauthors, 2006: Climate-carbon cycle feedback analysis: Results from the (CMIP)-M-4 model intercomparison. *J. Clim.*, **19,** 3337-3353.

Frohn, R. C., K. M. Hinkel, and W. R. Eisner, 2005: Satellite remote sensing classification of thaw lakes and drained thaw lake basins on the North Slope of Alaska. *Remote Sens. Environ.*, **97,** 116-126.

Frolking, S., and N. T. Roulet, 2007: Holocene radiative forcing impact of northern peatland carbon accumulation and methane emissions. *Glob. Change Biol.*, **13,** 1079-1088.

Frolking, S., N. Roulet, and D. Lawrence, 2009: Issues Related to Incorporating Northern Peatlands Into Global Climate Models. *Carbon Cycling in Northern Peatlands*, A. J. Baird, L. R. Belyea, X. Comas, A. S. Reeve, and L. D. Slater, Eds., American Geophysical Union, 19-35.

Frolking, S., J. Talbot, M. C. Jones, C. C. Treat, J. B. Kauffman, E. S. Tuittila, and N. Roulet, 2011: Peatlands in the Earth's 21st century climate system. *Environmental Reviews*, **19,** 371-396.

Gedney, N., P. M. Cox, and C. Huntingford, 2004: Climate feedback from wetland methane emissions. *Geophysical Research Letters*, **31,** 4.

Geerts, B., 2003: Empirical estimation of the monthly-mean daily temperature range. *Theoretical and Applied Climatology*, **74,** 145-165.

Goodrich, L. E., 1982: The Influence of Snow Cover on the Ground Thermal Regime. *Canadian Geotechnical Journal*, **19,** 421-432.

Goyette, S., N. McFarlane, and G. Flato, 2000: Application of the Canadian Regional Climate Model to the Laurentian Great Lakes region: Implementation of a lake model. *Atmosphere-Ocean*, **38,** 481-503.

Grant, R. F., and N. T. Roulet, 2002: Methane efflux from boreal wetlands: Theory and testing of the ecosystem model Ecosys with chamber and tower flux measurements. *Global Biogeochemical Cycles*, **16**.

Grant, R. F., W. C. Oechel, and C. L. Ping, 2003: Modelling carbon balances of coastal arctic tundra under changing climate. *Glob. Change Biol.*, **9,** 16-36.

Grosse, G., and Coauthors, 2011: Vulnerability of high-latitude soil organic carbon in North America to disturbance. *Journal of Geophysical Research-Biogeosciences*, **116**.

Harte, J., 1988: *Consider a Spherical Cow: A Course in Environmental Problem Solving.* University Science Books.

Held, I. M., 2005: The gap between simulation and understanding in climate modeling. *Bulletin of the American Meteorological Society*, **86,** 1609-+.

Hinkel, K. M., R. C. Frohn, F. E. Nelson, W. R. Eisner, and R. A. Beck, 2005: Morphometric and spatial analysis of thaw lakes and drained thaw lake basins in the western Arctic Coastal Plain, Alaska. *Permafrost and Periglacial Processes*, **16,** 327-341.

Hinkel, K. M., W. R. Eisner, J. G. Bockheim, F. E. Nelson, K. M. Peterson, and X. Y. Dai, 2003: Spatial extent, age, and carbon stocks in drained thaw lake basins on the Barrow Peninsula, Alaska. *Arctic Antarctic and Alpine Research*, **35,** 291-300.

Hinzman, L. D., D. J. Goering, and D. L. Kane, 1998: A distributed thermal model for calculating soil temperature profiles and depth of thaw in permafrost regions. *Journal of Geophysical Research-Atmospheres*, **103,** 28975-28991.

Iijima, Y., A. N. Fedorov, H. Park, K. Suzuki, H. Yabuki, T. C. Maximov, and T. Ohata, 2010: Abrupt Increases in Soil Temperatures following Increased Precipitation in a Permafrost Region, Central Lena River Basin, Russia. *Permafrost and Periglacial Processes*, **21,** 30-41.

Jeffries, M., T. Zhang, K. Frey, and N. Kozlenko, 1999: Estimating late-winter heat flow to the atmosphere from the lake-dominated Alaskan North Slope. *J. Glaciol.*, **45,** 315-324.

Jorgenson, M. T., Y. L. Shur, and E. R. Pullman, 2006: Abrupt increase in permafrost degradation in Arctic Alaska. *Geophysical Research Letters*, **33**.

Jorgenson, M. T., C. H. Racine, J. C. Walters, and T. E. Osterkamp, 2001: Permafrost degradation and ecological changes associated with a warming climate in central Alaska. *Climatic Change*, **48,** 551-579.

Jorgenson, M. T., and Coauthors, 2010: Resilience and vulnerability of permafrost to climate change. *Canadian Journal of Forest Research-Revue Canadienne De Recherche Forestiere*, **40,** 1219-1236.

Kaab, A., and W. Haeberli, 2001: Evolution of a high-mountain thermokarst lake in the Swiss Alps. *Arctic Antarctic and Alpine Research*, **33,** 385-390.

Kessler, M. A., L. J. Plug, and K. M. Walter Anthony, 2012: Simulating the decadal- to millennial-scale dynamics of morphology and sequestered carbon mobilization of two thermokarst lakes in NW Alaska. *J. Geophys. Res.*, **117,** G00M06.

Khvorostyanov, D. V., G. Krinner, P. Ciais, M. Heimann, and S. A. Zimov, 2008: Vulnerability of permafrost carbon to global warming. Part I: model description and role of heat generated by organic matter decomposition. *Tellus Series B-Chemical and Physical Meteorology*, **60,** 250-264.

Koven, C. D., and Coauthors, 2011: Permafrost carbon-climate feedbacks accelerate global warming. *Proc. Natl. Acad. Sci. U. S. A.*, **108,** 14769-14774.

Krinner, G., 2003: Impact of lakes and wetlands on boreal climate. *Journal of Geophysical Research-Atmospheres*, **108,** 18.

Krinner, G., and J. Boike, 2010: A study of the large-scale climatic effects of a possible disappearance of high-latitude inland water surfaces during the 21st century. *Boreal Environment Research*, **15,** 203-217.

Kuhry, P., E. Dorrepaal, G. Hugelius, E. A. G. Schuur, and C. Tarnocai, 2010: Potential Remobilization of Belowground Permafrost Carbon under Future Global Warming. *Permafrost and Periglacial Processes*, **21,** 208-214.

Lawrence, D. M., and A. G. Slater, 2010: The contribution of snow condition trends to future ground climate. *Climate Dynamics*, **34,** 969-981.

Lawrence, D. M., and S. C. Swenson, 2011: Permafrost response to increasing Arctic shrub abundance depends on the relative influence of shrubs on local soil cooling versus large-scale climate warming. *Environ. Res. Lett.*, **6,** 045504.

Lawrence, D. M., A. G. Slater, and S. C. Swenson, 2011: Simulation of Present-Day and Future Permafrost and Seasonally Frozen Ground Conditions in CCSM4. *J. Clim.*, **25,** 2207-2225.

Lawrence, D. M., A. G. Slater, V. E. Romanovsky, and D. J. Nicolsky, 2008a: Sensitivity of a model projection of near-surface permafrost degradation to soil column depth and representation of soil organic matter. *Journal of Geophysical Research-Earth Surface*, **113,** 14.

Lawrence, D. M., A. G. Slater, R. A. Tomas, M. M. Holland, and C. Deser, 2008b: Accelerated Arctic land warming and permafrost degradation during rapid sea ice loss. *Geophysical Research Letters*, **35**.

Lehner, B., and P. Doll, 2004: Development and validation of a global database of lakes, reservoirs and wetlands. *Journal of Hydrology*, **296,** 1-22.

Ling, F., 2003: Numerical simulation of permafrost thermal regime and talik development under shallow thaw lakes on the Alaskan Arctic Coastal Plain. *Journal of Geophysical Research-Atmospheres*, **108**.

Ling, F., and T. J. Zhang, 2004: Modeling study of talik freeze-up and permafrost response under drained thaw lakes on the Alaskan Arctic Coastal Plain. *Journal of Geophysical Research-Atmospheres*, **109**.

Lloyd, J., and J. A. Taylor, 1994: On the Temperature-Dependence of Soil Respiration. *Functional Ecology*, **8,** 315-323.

Lofgren, B. M., 1997: Simulated effects of idealized Laurentian Great Lakes on regional and large-scale climate. *J. Clim.*, **10,** 2847-2858.

Long, Z., W. Perrie, J. Gyakum, D. Caya, and R. Laprise, 2007: Northern lake impacts on local seasonal climate. *J. Hydrometeorol.*, **8,** 881-896.

MacDonald, G. M., D. W. Beilman, K. V. Kremenetski, Y. W. Sheng, L. C. Smith, and A. A. Velichko, 2006: Rapid early development of circumarctic peatlands and atmospheric CH4 and CO2 variations. *Science*, **314,** 285-288.

Martynov, A., L. Sushama, and R. Laprise, 2010: Simulation of temperate freezing lakes by one-dimensional lake models: performance assessment for interactive coupling with regional climate models. *Boreal Environment Research*, **15,** 143-164.

Osterkamp, T. E., and V. E. Romanovsky, 1999: Evidence for warming and thawing of discontinuous permafrost in Alaska. *Permafrost and Periglacial Processes*, **10,** 17-37.

Osterkamp, T. E., and J. C. Jorgenson, 2006: Warming of permafrost in the Arctic National Wildlife Refuge, Alaska. *Permafrost and Periglacial Processes*, **17,** 65-69.

Osterkamp, T. E., L. Viereck, Y. Shur, M. T. Jorgenson, C. Racine, A. Doyle, and R. D. Boone, 2000: Observations of thermokarst and its impact on boreal forests in Alaska, USA. *Arctic Antarctic and Alpine Research*, **32,** 303-315.

Osterkamp, T. E., M. T. Jorgenson, E. A. G. Schuur, Y. L. Shur, M. Z. Kanevskiy, J. G. Vogel, and V. E. Tumskoy, 2009: Physical and Ecological Changes Associated with Warming Permafrost and Thermokarst in Interior Alaska. *Permafrost and Periglacial Processes*, **20,** 235-256.

Pavlov, A. V., and N. G. Moskalenko, 2002: The thermal regime of soils in the north of Western Siberia. *Permafrost and Periglacial Processes*, **13,** 43-51.

Pelletier, J. D., 2005: Formation of oriented thaw lakes by thaw slumping. *Journal of Geophysical Research-Earth Surface*, **110**.

Perroud, M., S. Goyette, A. Martynov, M. Beniston, and O. Anneville, 2009: Simulation of multiannual thermal profiles in deep Lake Geneva: A comparison of one-dimensional lake models. *Limnology and Oceanography*, **54,** 1574-1594.

Phelps, A., K. Peterson, and M. Jeffries, 1998: Methane efflux from high-latitude lakes during spring ice melt. *Journal of Geophysical Research-Atmospheres*, **103,** 29029-29036.

Plug, L., and J. West, 2009: Thaw lake expansion in a two-dimensional coupled model of heat transfer, thaw subsidence, and mass movement. *Journal of Geophysical Research-Earth Surface*, **114,** -.

Plug, L. J., C. Walls, and B. M. Scott, 2008: Tundra lake changes from 1978 to 2001 on the Tuktoyaktuk Peninsula, western Canadian Arctic. *Geophysical Research Letters*, **35,** 5.

Randall, D. A., and Coauthors, 2007: Climate Models and Their Evaluation. *Climate Change 2007: The Physical Science Basis. Contribution of Working Group I to the Fourth Assessment*

Report of the Intergovernmental Panel on Climate Change, S. Solomon, D. Qin, M. Manning, Z. Chen, M. Marquis, K.B. Averyt, M.Tignor and H.L. Miller, Ed., Cambridge University Press.

Riley, W. J., and Coauthors, 2011: Barriers to predicting changes in global terrestrial methane fluxes: analyses using CLM4Me, a methane biogeochemistry model integrated in CESM. *Biogeosciences*, **8,** 1925-1953.

Ringeval, B., P. Friedlingstein, C. Koven, P. Ciais, N. de Noblet-Ducoudre, B. Decharme, and P. Cadule, 2011: Climate-CH(4) feedback from wetlands and its interaction with the climate-CO(2) feedback. *Biogeosciences*, **8,** 2137-2157.

Ringeval, B., and Coauthors, 2010: An attempt to quantify the impact of changes in wetland extent on methane emissions on the seasonal and interannual time scales. *Global Biogeochemical Cycles*, **24,** GB2003.

Riseborough, D., 2007: The effect of transient conditions on an equilibrium permafrost-climate model. *Permafrost and Periglacial Processes*, **18,** 21-32.

Riseborough, D., N. Shiklomanov, B. Etzelmuller, S. Gruber, and S. Marchenko, 2008: Recent advances in permafrost modelling. *Permafrost and Periglacial Processes*, **19,** 137-156.

Romanovsky, V. E., and T. E. Osterkamp, 2000: Effects of unfrozen water on heat and mass transport processes in the active layer and permafrost. *Permafrost and Periglacial Processes*, **11,** 219-239.

Romanovsky, V. E., T. S. Sazonova, V. T. Balobaev, N. I. Shender, and D. O. Sergueev, 2007: Past and recent changes in air and permafrost temperatures in eastern Siberia. *Proceedings of the Ninth International Conference on Permafrost*, 399-413.

Rouse, W. R., and Coauthors, 2005: The role of northern lakes in a regional energy balance. *J. Hydrometeorol.*, **6,** 291-305.

Saito, K., 2008: Arctic land hydrothermal sensitivity under warming: Idealized off-line evaluation of a physical terrestrial scheme in a global climate model. *Journal of Geophysical Research-Atmospheres*, **113**.

Salzmann, N., J. Notzli, C. Hauck, S. Gruber, M. Hoelzle, and W. Haeberli, 2007: Ground surface temperature scenarios in complex high-mountain topography based on regional climate model results. *Journal of Geophysical Research-Earth Surface*, **112,** 10.

Samuelsson, P., E. Kourzeneva, and D. Mironov, 2010: The impact of lakes on the European climate as simulated by a regional climate model. *Boreal Environment Research*, **15,** 113-129.

Sazonova, T. S., and V. E. Romanovsky, 2003: A model for regional-scale estimation of temporal and spatial variability of active layer thickness and mean annual ground temperatures. *Permafrost Periglacial Process*, **14,** 125-139.

Sazonova, T. S., V. E. Romanovsky, J. E. Walsh, and D. O. Sergueev, 2004: Permafrost dynamics in the 20th and 21st centuries along the East Siberian transect. *Journal of Geophysical Research-Atmospheres*, **109,** 25.

Schaefer, K., T. J. Zhang, L. Bruhwiler, and A. P. Barrett, 2011: Amount and timing of permafrost carbon release in response to climate warming. *Tellus Series B-Chemical and Physical Meteorology*, **63,** 165-180.

Schuur, E., and Coauthors, 2008: Vulnerability of permafrost carbon to climate change: Implications for the global carbon cycle. *Bioscience*, **58,** 701-714.

Schuur, E. A. G., B. Abbott, and N. Permafrost Carbon, 2011: High risk of permafrost thaw. *Nature*, **480,** 32-33.

Schuur, E. A. G., J. G. Vogel, K. G. Crummer, H. Lee, J. O. Sickman, and T. E. Osterkamp, 2009: The effect of permafrost thaw on old carbon release and net carbon exchange from tundra. *Nature*, **459,** 556-559.

Segers, R., 1998: Methane production and methane consumption: a review of processes underlying wetland methane fluxes. *Biogeochemistry*, **41,** 23-51.

Segers, R., and P. A. Leffelaar, 2001: Modeling methane fluxes in wetlands with gas-transporting plants 3. Plot scale. *Journal of Geophysical Research-Atmospheres*, **106,** 3541-3558.

Segers, R., C. Rappoldt, and P. A. Leffelaar, 2001: Modeling methane fluxes in wetlands with gas-transporting plants 2. Soil layer scale. *Journal of Geophysical Research-Atmospheres*, **106,** 3529-3540.

Serreze, M. C., and Coauthors, 2000: Observational evidence of recent change in the northern high-latitude environment. *Clim. Change*, **46,** 159-207.

Shur, Y. L., and M. T. Jorgenson, 2007: Patterns of permafrost formation and degradation in relation to climate and ecosystems. *Permafrost and Periglacial Processes*, **18,** 7-19.

Smith, K. A., T. Ball, F. Conen, K. E. Dobbie, J. Massheder, and A. Rey, 2003: Exchange of greenhouse gases between soil and atmosphere: interactions of soil physical factors and biological processes. *European Journal of Soil Science*, **54,** 779-791.

Smith, L., Y. Sheng, G. MacDonald, and L. Hinzman, 2005a: Disappearing Arctic lakes. *Science*, **308,** 1429-1429.

Smith, L. C., Y. W. Sheng, and G. M. MacDonald, 2007: A first pan-Arctic assessment of the influence of glaciation, permafrost, topography and peatlands on northern hemisphere lake distribution. *Permafrost and Periglacial Processes*, **18,** 201-208.

Smith, S. L., M. M. Burgess, D. Riseborough, and F. M. Nixon, 2005b: Recent trends from Canadian Permafrost Thermal Monitoring Network Sites. *Permafrost and Periglacial Processes*, **16,** 19-30.

Solomon, S., and Coauthors, Eds., 2007: *Contribution of Working Group I to the Fourth Assessment Report of the Intergovernmental Panel on Climate Change, 2007*. Cambridge University Press.

Stendel, M., V. E. Romanovsky, J. H. Christensen, and T. Sazonova, 2007: Using dynamical downscaling to close the gap between global change scenarios and local permafrost dynamics. *Global and Planetary Change*, **56,** 203-214.

Stepanenko, V. M., S. Goyette, A. Martynov, M. Perroud, X. Fang, and D. Mironov, 2010: First steps of a Lake Model Intercomparison Project: LakeMIP. *Boreal Environment Research*, **15,** 191-202.

Stieglitz, M., S. J. Dery, V. E. Romanovsky, and T. E. Osterkamp, 2003: The role of snow cover in the warming of arctic permafrost. *Geophysical Research Letters*, **30,** 4.

Sushama, L., R. Laprise, D. Caya, D. Verseghy, and M. Allard, 2007: An RCM projection of soil thermal and moisture regimes for North American permafrost zones. *Geophysical Research Letters*, **34,** 6.

Tarnocai, C., F. M. Nixon, and L. Kutny, 2004: Circumpolar-active-layer-monitoring (CALM) sites in the Mackenzie Valley, northwestern Canada. *Permafrost and Periglacial Processes*, **15,** 141-153.

Tarnocai, C., J. G. Canadell, E. A. G. Schuur, P. Kuhry, G. Mazhitova, and S. Zimov, 2009: Soil organic carbon pools in the northern circumpolar permafrost region. *Global Biogeochemical Cycles*, **23**.

Torn, M., and J. Harte, 2006: Missing feedbacks, asymmetric uncertainties, and the underestimation of future warming. *Geophysical Research Letters*, **33,** -.

van Huissteden, J., C. Berrittella, F. J. W. Parmentier, Y. Mi, T. C. Maximov, and A. J. Dolman, 2011: Methane emissions from permafrost thaw lakes limited by lake drainage. *Nature Climate Change*, **1,** 119-123.

Volodin, E. M., 2008: Methane cycle in the INM RAS climate model. *Izv. Atmos. Ocean. Phys.*, **44,** 153-159.

Walter, B. P., and M. Heimann, 2000: A process-based, climate-sensitive model to derive methane emissions from natural wetlands: Application to five wetland sites, sensitivity to model parameters, and climate. *Global Biogeochemical Cycles*, **14,** 745-765.

Walter, B. P., M. Heimann, and E. Matthews, 2001a: Modeling modern methane emissions from natural wetlands 2. Interannual variations 1982-1993. *Journal of Geophysical Research-Atmospheres*, **106,** 34207-34219.

——, 2001b: Modeling modern methane emissions from natural wetlands 1. Model description and results. *Journal of Geophysical Research-Atmospheres*, **106,** 34189-34206.

Walter, K. M., L. C. Smith, and F. S. Chapin, 2007a: Methane bubbling from northern lakes: present and future contributions to the global methane budget. *Philosophical Transactions of the Royal Society a-Mathematical Physical and Engineering Sciences*, **365,** 1657-1676.

Walter, K. M., S. A. Zimov, J. P. Chanton, D. Verbyla, and F. S. Chapin, 2006: Methane bubbling from Siberian thaw lakes as a positive feedback to climate warming. *Nature*, **443,** 71-75.

Walter, K. M., M. E. Edwards, G. Grosse, S. A. Zimov, and F. S. Chapin, 2007b: Thermokarst lakes as a source of atmospheric CH4 during the last deglaciation. *Science*, **318,** 633-636.

Walter, K. M., J. P. Chanton, F. S. Chapin, E. A. G. Schuur, and S. A. Zimov, 2008: Methane production and bubble emissions from arctic lakes: Isotopic implications for source pathways and ages. *Journal of Geophysical Research-Biogeosciences*, **113,** 16.

Wania, R., I. Ross, and I. C. Prentice, 2009a: Integrating peatlands and permafrost into a dynamic global vegetation model: 1. Evaluation and sensitivity of physical land surface processes. *Global Biogeochemical Cycles*, **23,** 19.

——, 2009b: Integrating peatlands and permafrost into a dynamic global vegetation model: 2. Evaluation and sensitivity of vegetation and carbon cycle processes. *Global Biogeochemical Cycles*, **23**.

West, J. J., and L. J. Plug, 2008: Time-dependent morphology of thaw lakes and taliks in deep and shallow ground ice. *Journal of Geophysical Research-Earth Surface*, **113**.

Westermann, S., J. Boike, M. Langer, T. V. Schuler, and B. Etzelmuller, 2011: Modeling the impact of wintertime rain events on the thermal regime of permafrost. *Cryosphere*, **5,** 945-959.

Whalen, S. C., 2005: Biogeochemistry of methane exchange between natural wetlands and the atmosphere. *Environ. Eng. Sci.*, **22,** 73-94.

Zhang, T., and K. Stamnes, 1998: Impact of climatic factors on the active layer and permafrost at Barrow, Alaska. *Permafrost and Periglacial Processes*, **9,** 229-246.

Zhang, T. J., 2005: Influence of the seasonal snow cover on the ground thermal regime: An overview. *Rev. Geophys.*, **43,** 26.

Zhang, Y., W. J. Chen, and D. W. Riseborough, 2008a: Disequilibrium response of permafrost thaw to climate warming in Canada over 1850-2100. *Geophysical Research Letters*, **35**.

——, 2008b: Transient projections of permafrost distribution in Canada during the 21st century under scenarios of climate change. *Global and Planetary Change*, **60,** 443-456.

Zhang, Y., W. J. Chen, S. L. Smith, D. W. Riseborough, and J. Cihlar, 2005: Soil temperature in Canada during the twentieth century: Complex responses to atmospheric climate change. *Journal of Geophysical Research-Atmospheres*, **110,** 15.

Zhuang, Q., and Coauthors, 2004: Methane fluxes between terrestrial ecosystems and the atmosphere at northern high latitudes during the past century: A retrospective analysis with a process-based biogeochemistry model. *Global Biogeochemical Cycles*, **18**.

Zhuang, Q. L., and Coauthors, 2006: CO2 and CH4 exchanges between land ecosystems and the atmosphere in northern high latitudes over the 21st century. *Geophysical Research Letters*, **33**.

Zimov, S., E. Schuur, and F. Chapin, 2006a: Permafrost and the global carbon budget. *Science*, **312,** 1612-1613.

Zimov, S., S. Davydov, G. Zimova, A. Davydova, E. Schuur, K. Dutta, and F. Chapin, 2006b: Permafrost carbon: Stock and decomposability of a globally significant carbon pool. *Geophysical Research Letters*, **33,** -.

Chapter 2: An Improved Lake Model for Climate Simulations: Model Structure, Evaluation, and Sensitivity Analyses in CESM1

Chapter 2 Table of Contents

2. An Improved Lake Model for Climate Simulations: Model Structure, Evaluation, and Sensitivity Analyses in CESM1

This chapter is based on the article published in 2012 in the Journal of Advances in Modeling Earth Systems, with co-authors William J. Riley (Lawrence Berkeley National Lab) and Dmitrii Mironov (German Weather Service). The article was published open-access by the American Geophysical Union.

Citation:

Subin, Z. M., W. J. Riley, and D. Mironov (2012), An improved lake model for climate simulations: Model structure, evaluation, and sensitivity analyses in CESM1, *J. Adv. Model. Earth Syst.*, 4, M02001, doi:10.1029/2011MS000072.

http://www.agu.org/pubs/crossref/2012/2011MS000072.shtml

2.1 Summary

Lakes can influence regional climate, yet most general circulation models have, at best, simple and largely untested representations of lakes.

We developed the Lake, Ice, Snow, and Sediment Simulator (LISSS) for inclusion in the land-surface component (CLM4) of an earth system model (CESM1). The existing CLM4 lake model performed poorly at all sites tested; for temperate lakes, summer surface water temperature predictions were 10-25°C lower than observations. CLM4-LISSS modifies the existing model by including (1) a treatment of snow; (2) freezing, melting, and ice physics; (3) a sediment thermal submodel; (4) spatially variable prescribed lake depth; (5) improved parameterizations of lake surface properties; (6) increased mixing under ice and in deep lakes; and (7) correction of previous errors. We evaluated the lake model predictions of water temperature and surface fluxes at three small temperate and boreal lakes where extensive observational data was available. We also evaluated the predicted water temperature and/or ice and snow thicknesses for ten other lakes where less comprehensive forcing observations were available. CLM4-LISSS performed very well compared to observations for shallow to medium-depth small lakes. For large, deep lakes, the under-prediction of mixing was improved by increasing the lake eddy diffusivity by a factor of 10, consistent with previous published analyses. Surface temperature and surface flux predictions were improved when the aerodynamic roughness lengths were calculated as a function of friction velocity, rather than using a constant value of 1 mm or greater.

We evaluated the sensitivity of surface energy fluxes to modeled lake processes and parameters. Large changes in monthly-averaged surface fluxes (up to 30 W m^{-2}) were found when excluding snow insulation or phase change physics and when varying the opacity, depth, albedo of melting lake ice, and mixing strength across ranges commonly found in real lakes. Typical variation among model parameterization choices can therefore cause persistent local surface flux changes much larger than expected changes in greenhouse forcing.

We conclude that CLM4-LISSS adequately simulates lake water temperature and surface energy fluxes, with errors comparable in magnitude to those resulting from uncertainty in global lake properties, and is suitablefor inclusion in global and regional climate studies.

2.2 Introduction

Lakes typically have different albedo, greater subsurface heat conductance and effective heat capacity, and much lower surface roughness than surrounding land area. These properties are important for accurate prediction of climate at the regional scale in regions with large lake area (Dutra et al. 2010; Krinner 2003; Lofgren 1997; Long et al. 2007; Rouse et al. 2005; Samuelsson et al. 2010), and are important in regional energy budgets (Jeffries et al. 1999). Several modeling studies (Bonan 1995; Dutra et al. 2010; Krinner 2003; Samuelsson et al. 2010) have found significant changes in regional temperature with prognostic 1-dimensional (1D) lake models integrated in climate models.

The impacts of lakes on regional climate vary with location and season. In general, unfrozen lakes tend to suppress diurnal temperature variation as compared to surrounding land (Samuelsson et al. 2010). Some temperate and high-latitude lakes tend to be cooler than surrounding land in the early summer, which, combined with their smaller surface roughness, tends to reduce heat fluxes to the atmosphere during this season (Dutra et al. 2010; Krinner 2003; Lofgren 1997; Rouse et al. 2008), though in some locations decreases in albedo and cloudiness compensate for this reduction (Samuelsson et al. 2010). At sufficiently high surface temperatures typical of low latitudes, lakes can increase latent heat fluxes relative to surrounding land in all seasons (Dutra et al. 2010). Temperate and high-latitude lakes tend to be warmer than surrounding land in autumn, resulting in increased surface heat fluxes (Dutra et al. 2010; Lofgren 1997; Long et al. 2007; Rouse et al. 2008; Samuelsson et al. 2010). Autumn and early winter overturning and freezing lakes warm and moisten the boundary layer (Jeffries et al. 1999) until substantial snow insulation is present (Dutra et al. 2010), and can cause lake-effect precipitation downwind (Bates et al. 1993; Goyette et al. 2000; Kristovich and Braham 1998; Laird et al. 2009; Lofgren 2004; Samuelsson and Tjernstrom 2001). In contrast, melting lakes cool the boundary layer (Samuelsson et al. 2010) as compared to adjacent land.

Lake area, lake physical properties, and lake biogeochemistry may interact with climate change and other anthropogenic forcings. Climate warming can alter lake mixing regimes (Fang and Stefan 2009; King et al. 1997; Kirillin 2010; MacKay et al. 2009; McCormick and Fahnenstiel 1999; Perroud and Goyette 2010; Verburg and Hecky 2009) and ice cover duration (Blenckner et al. 2002; Brown and Duguay 2010; Fang and Stefan 2009; Mueller et al. 2009; Saloranta et al. 2009; Vavrus et al. 1996; Vincent et al. 2008; Zhang and Jeffries 2000), which can cause feedbacks to regional climate change. Changes in temperature, mixing regimes (Peeters et al. 2007; Verburg and Hecky 2009), watershed hydrology (Kosten et al. 2009), and anthropogenic nutrient deposition in the watershed may alter lake biology (MacKay et al. 2009), which is a primary determinant of lake optical properties (Cristofor et al. 1994), itself a strong control over lake mixing regime (Cristofor et al. 1994; Hocking and Straskraba 1999; Houser 2006; Mazumder and Taylor 1994; Mazumder et al. 1990; Persson and Jones 2008). Changes in the balance of precipitation and evaporation in lake watersheds (Schindler 2009; Small et al. 2001) and anthropogenic diversion of source rivers (Small et al. 2001) may change lake depth or area. Climate warming may interact with thermokarst lake dynamics at high latitudes (Smith et

al. 2005). Lakes may be significant components of the global carbon cycle (Duarte et al. 2008; Tranvik et al. 2009; Walter et al. 2007), so alterations in their biochemistry under climate change could be important (Cardille et al. 2009; Walter et al. 2006).

Current numerical weather prediction (NWP) models, regional climate models (RCMs), and global climate models (GCMs) typically have a highly simplified, and often untested, treatment of lakes. The Weather Research and Forecasting Model 3 (WRF3) (Skamarock et al. 2008) and versions of the HTESSEL land-surface scheme prior to recent model development (Dutra et al. 2010) prescribe temperatures of large lakes using sea surface temperature interpolation and ignore subgrid-scale lakes. Simple fixed mixed-layer or heat penetration models have been used in previous studies with the Canadian Regional Climate Model (Goyette et al. 2000; Plummer et al. 2006), Geophysical Fluid Dynamics Laboratory GCM (Lofgren 1997), RAMS (Lofgren 2004), and ECHAM (Hagemann et al. 2006). Some models with more sophisticated treatment of lakes ignore lake water freezing [e.g., Bonan (1995)] or snow insulation [e.g., Samuelsson et al. (2010)]. Most coupled land-surface/atmosphere models use datasets that under-estimate global lake area (Downing et al. 2006) and treat lakes as having constant depth and optical properties. However, lake depth (Rouse et al. 2005), optical properties (Hocking and Straskraba 1999), sediment (Fang and Stefan 1998; Golosov and Kirillin 2010), freezing (Brown and Duguay 2010), and snow insulation (Brown and Duguay 2010; Dutra et al. 2010) are important for accurately modeling lakes and their interactions with the atmosphere.

Efforts are underway to develop, refine, and integrate lake models into NWP models, RCMs, and GCMs (MacKay et al. 2009; Mironov et al. 2010a); to develop global datasets required to run these models (Kourzeneva 2010); and to compare the performance of these models across lakes of different geometries, optical properties, and climates (Martynov et al. 2010; Perroud et al. 2009; Stepanenko et al. 2010). Several different types of one-dimensional (1D) lake models have been developed [reviewed in Martynov et al. (2010), Perroud et al. (2009), and Stepanenko et al. (2010)]: (1) relatively simple 2-layer models based on similarity theory [e.g., FLake (Mironov et al. 2010b)]; (2) thermal diffusion models with parameterized eddy diffusivity [e.g., the Hostetler Model (Hostetler and Bartlein 1990) and Minlake (Fang and Stefan 1996)]; (3) and more complex turbulence models [e.g., the Lagrangian model DYRESM (Yeates and Imberger 2003) and the k-ε turbulence closure models SIMSTRAT (Goudsmit et al. 2002) and LAKE (Stepanenko and Lykossov 2005; Stepanenko et al. 2011)].

Each of these 1D lake model types has advantages and disadvantages (Martynov et al. 2010; Perroud et al. 2009; Stepanenko et al. 2010). FLake is computationally efficient and performs reasonably across lake categories in predicting surface temperatures and ice characteristics. However, seasonal stratification is not always predicted well, and the model's two-layer structure causes difficulties simulating the water temperature near the bottom of deep lakes. The Hostetler Model predicts Sparkling Lake water temperatures well (Martynov et al. 2010; Stepanenko et al. 2010) but under-predicts mixing for several deep lakes (Martynov et al. 2010; Perroud et al. 2009; Stepanenko et al. 2010). Turbulence models improve characterization of Lake Geneva and Lake Michigan (Perroud et al. 2009; Stepanenko et al. 2010) by including additional sources of turbulence such as seiches (lake-scale wave motions), but over-predict mixing in Sparkling Lake (Stepanenko et al. 2010). Turbulence models can be computationally expensive, may require extensive lake-specific data or calibration, and have not yet been integrated into climate models.

In this study, we focused on the treatment of lakes in CLM4 (Community Land Model 4) (Lawrence et al. 2011; Oleson et al. 2010), the land component of the Community Earth System Model 1 (CESM1, http://www.cesm.ucar.edu/models/cesm1.0/) (Gent et al. 2011). The existing CLM4 lake model is identical to the version in CLM2 (Bonan et al. 2002b; Zeng et al. 2002), is based on Hostetler and Bartlein (1990), and incorporates code from LSM (Bonan 1995) and CoLM (Dai et al. 2003), but it has not been compared to observations in its current form. We created CLM4-LISSS (Lake, Ice, Snow, and Sediment Simulator) by (1) including a comprehensive treatment of snow; (2) including freezing and melting (hereafter referred to as "phase change") and ice physics; (3) including a sediment thermal submodel; (4) allowing for variable prescribed lake depth; (5) improving the parameterization of lake surface properties such as roughness lengths; (6) increasing mixing under ice and in deep lakes, and (7) correcting several errors in the calculation of surface fluxes and lake temperature. We evaluated CLM4-LISSS at thirteen lakes and performed sensitivity experiments in order to characterize the effect of dominant processes and poorly constrained parameters on lake water temperature and surface energy flux predictions.

2.3 Methods

2.3.1 Model Description

2.3.1.1 Overview

CLM4-LISSS solves the 1D thermal diffusion equation by dividing the lake vertical profile into several discrete layers corresponding to: snow (when snow is present and greater than a minimum thickness); lake liquid water and ice (referred to collectively as the "lake body"); and underlying substrates (sediment, soil, and bedrock; hereafter referred to collectively as "sediment" except where otherwise noted). Sensible heat, latent heat, momentum, and radiation fluxes are calculated between the surface and the lower atmosphere (i.e., an observation height or atmospheric model bottom level, ~2 – 60 m). The residual energy flux at the surface is then used as a top boundary condition for thermal diffusion in the snow, lake body, and sediment. Constant lake body water content and saturated sediments are assumed, although the snow depth and properties are prognosed (Section 2.3.1.3). CLM4 uses a subgrid "tile" approach in which several landunit types are modeled separately (without explicit subgrid location or distribution) and the surface fluxes are averaged to the gridcell weighted by landunit area (Bonan et al. 2002a; Oleson et al. 2010), so lakes need not be resolved at the grid scale in order to be included. (The CLM software includes a four-level hierarchy containing gridcells, landunits, columns, and plant functional types. There are five distinct 1D landunits which do not exchange horizontal fluxes: soil, urban, lake, wetland, and glacier.) Currently, only one lake is modeled in each gridcell, but the CLM4 software allows the flexibility for multiple lakes (e.g., of different depth or optical categories) to be modeled in each gridcell (as multiple columns in the lake landunit).

In the lake body, mixing is caused by wind-driven eddies (Hostetler and Bartlein 1990), convection (Hostetler and Bartlein 1990), molecular diffusion, and unresolved 3D mixing processes (Fang and Stefan 1996). Shortwave [i.e., solar visible and near-infrared (NIR)] radiation is distributed among the snow and lake body according to their diagnosed optical properties. The submodels for friction velocity, aerodynamic resistances, snow, and sediment are

similar to those in CLM4 (Oleson et al. 2010). The lake model is summarized in Fig. 2.1 and described in the following subsections; more details are included in the technical note available at http://www.agu.org/pubs/crossref/2012/2011MS000072.shtml. The CLM4-LISSS model also includes a correction of several structural deficiencies and errors in formulation in the existing CLM4 lake model (Appendix, Section 2.8.1).

2.3.1.2 Phase Change and Ice in the Lake Body

The lake body consists of a number of combined liquid water and ice layers; 25 layers are currently used for site evaluations, while 10 layers are currently used for global simulations in order to reduce computational expense. Each of these layers has a fixed water mass and fixed nominal thickness Δz (m), while the ice fraction (f_i) may vary from 0 to 1. The ice thermal conductivity is decreased by the ratio of ice density to water density, and the diffusivities are calculated using the layer-mean specific heat, to account for the increased physical thickness of the ice relative to the same mass of water. The heat capacity of each layer is the sum of the heat capacity of the ice mass and liquid water mass. The net thermal conductance κ (m s^{-1}) of layers containing both liquid water and ice is calculated by adding the respective resistances r (s m^{-1}) in series, assuming that the ice is stacked vertically on the liquid water:

$$\kappa = \left(r_w + r_i\right)^{-1} = \frac{1}{\Delta z}\left(\frac{1-f_i}{d_w} + \frac{f_i}{d_i}\right)^{-1}, \qquad \textbf{Eq. 2.1}$$

where d_w (m^2 s^{-1}) is the liquid water diffusivity and d_i (m^2 s^{-1}) is the ice diffusivity reduced by the ratio of ice density to water density. Liquid water diffusivity includes wind-driven eddy diffusivity (when there is no ice above the liquid), molecular diffusivity, and enhanced diffusivity (Section 2.3.1.6); ice diffusivity contains only molecular diffusivity.

At each time step, diffusion is first calculated ignoring phase change, and then phase change is calculated as a correction. This procedure is similar to the phase change solution for soil water and ice in CLM4. After the diffusion equation is solved (Section 2.3.1.9), any layer containing nonzero ice fraction at a temperature above freezing (or nonzero liquid fraction at a temperature below freezing) undergoes freezing (melting) until either the energy excess (deficit) is consumed, or all the ice (liquid) is melted (frozen). Heat capacities are adjusted to precisely conserve energy as the ice fraction changes. After this process is complete, every layer containing both liquid water and ice must have a temperature at the freezing point. [Except for sensitivity experiments, ice is immediately aggregated at the top of the lake (Section 2.3.1.6).] This approach is a flexible solution to the Stefan problem (diffusion in the presence of a phase boundary) that (1) allows for an arbitrary temperature profile to occur in the ice (within the precision of the resolved layer thicknesses); (2) allows complex layering of water and ice (e.g., slush); (3) precisely conserves energy; and (4) is computationally simple.

2.3.1.3 Snow

The lake snow model used here is nearly identical to the snow model used over non-lake landunits in CLM4 (Lawrence et al. 2011). Once the snow thickness exceeds a small threshold, one or more snow layers are explicitly resolved with state variables including temperature, water content, ice content, density, snow grain radius, and accumulated deposited aerosols of several

species. The shortwave radiation absorption, reflection, and transmission of each snow layer are calculated as a function of the snow grain radius and aerosol content (Flanner and Zender 2006; Flanner et al. 2007). Top snow layers can undergo evaporation, sublimation, and deposition of dew and frost. All snow layers can partially melt, refreeze, and allow infiltration of water into snow layers below. Currently, the model has up to 5 resolved snow layers, with explicit rules for subdividing thick snow layers and combining thin snow layers. Because a temperature gradient may occur between the top snow layer and the top lake layer, and the snow conductivity [based on the 1991 version of SNTHERM (Jin et al. 1999; Oleson et al. 2010)] considers air, water, and ice content, snow insulation is modeled explicitly in the diffusion solution.

There are several differences between the snow model used here over lakes and the model used for non-lake landunits in CLM4. The phase change solution is analogous to the solution used for lake layers (Section 2.3.1.2), except that layer ice and liquid water masses are the state variables rather than lake layer ice mass fraction. Snow falling on unfrozen lakes will thermally mix with the top lake body layer and cannot accumulate until the top lake body layer is brought to freezing (see below). Rarely, if the top of the lake body is warmed sufficiently from below while resolved snow layers persist above, they may be eliminated (with details in the technical note). Note that lake snow and ice mechanical dynamics, such as snow causing disintegration of ice or falling into lake water, are not considered.

When the snow is less than 40 mm thick, it does not form a resolved layer, and the only state variables are the ice mass and snow thickness. When the top lake layer is above freezing after the thermal transport solution with less than 40 mm of snow, the excess heat content (above freezing) is used to melt the snow. In effect, this requires melting of the snow before melting of lake body ice can be completed. For non-lake landunits in CLM4, the minimum resolved snow layer thickness is 10 mm. However, during testing, we found occasional numerical instability when the Courant-Friedrich-Lewy condition (Hazewinkel 1995) was violated in the top snow layer. The semi-implicit Crank-Nicholson method (Section 2.3.1.9) should be stable even when this condition is violated, but the surface flux solution method (Section 2.3.1.8) acts as a fully explicit time-stepping component in the integration method and may compromise stability. We addressed this problem by requiring resolved snow layers to be at least 40 mm thick over lakes for the default 30 min model timestep, with appropriate adjustment to the rules for subdividing and combining snow layers. This type of instability has not been observed in non-lake landunits in CLM4, where the surface flux solution method differs somewhat (Section 2.3.1.8).

2.3.1.4 Sediment, Soil, and Bedrock

The new lake sediment model is similar to the soil and bedrock model for the CLM4 soil landunit. Soil physical properties, including the pore volume, heat capacity, and thermal conductivity, are set as in CLM4 (Farouki 1981; Lawrence et al. 2008; Oleson et al. 2010), based on the prescribed soil texture and organic matter content in addition to the time-varying water and ice contents. The treatment of organic matter interpolates between pure mineral soil and pure peat properties as the organic matter fraction increases (Lawrence and Slater 2008). Dry, hydrologically inactive bedrock layers are found beneath the soil layers, with thermal conductivity [Clauser and Huenges in Ahrens (1995)] and heat capacity (Farouki 1981) set as in CLM4.

The primary difference between the treatment of soil in the CLM4 soil landunit and in CLM4-LISSS is that the sediment layers beneath the lake are maintained at hydraulic saturation. In addition, the thermal conductivity is adjusted during freezing to account for frost heave (e.g., a slight physical expansion in the layer due to the freezing of the saturated pore space, which for computational simplicity is treated by altering the thermal conductivity rather than the layer thickness), allowing excess ground ice in permafrost regions to be readily modeled in future experiments. We note that frost heave is ignored in the CLM4 soil landunit. Finally, freezing point depression (the persistence of some liquid water at temperatures less than the freezing temperature of fresh water) is not allowed under lakes, as the freezing point depression in the CLM4 soil landunit is intended primarily to smoothly modulate the hydraulic conductivity and microbial activity just below freezing (Lawrence et al. 2011). The phase change solution for lake sediment is conceptually identical to the solution for phase change in lake water (Section 2.3.1.2) and snow (Section 2.3.1.3).

Currently, 3.8 m of sediment layers under lakes are included and initialized using the same global geographic soil texture and organic content data as for the soil landunit in CLM4 (Lawrence et al. 2008), with 38 m of bedrock below. This approximation may be reasonable for thermokarst and other transient or shallow lakes, but it is likely to be less accurate for deep lakes. However, deep lakes will be relatively insensitive to the thermal properties of the sediment, so this approximation should suffice until geographic data on sediment properties are available.

2.3.1.5 Radiation Transfer in Lake Body

For unfrozen lakes, radiation transfer is calculated similarly to Bonan (1995), with a fraction of the non-reflecting shortwave radiation absorbed near the lake surface (top 0.6 m), and the remainder absorbed in the lake according to the Beer-Lambert Law with a constant extinction coefficient. However, the fraction of non-reflected shortwave radiation absorbed at the surface, β, is set equal to the NIR fraction (> 700 nm) predicted by the atmospheric model or forcing data, which is typically ~0.5. When only the total shortwave radiation is provided as forcing data, CESM1 calculates a diagnostic NIR fraction. Any shortwave radiation penetrating the bottom layer of the lake body is assumed to be absorbed in the top layer of sediment, which is a good approximation except for an especially shallow and clear lake, where some radiation might be reflected by the lake bottom and either absorbed in the layers above or released to the atmosphere, increasing the lake albedo.

The extinction coefficient, η (m^{-1}), is allowed to vary between gridcells. If not provided to the model as external data, η is calculated as a simple empirical function of lake depth, based on data from 88 Swedish lakes (Hakanson 1995) [using the Poole-Atkins expression (Idso and Gilbert 1974) to substitute η for the regressed Secchi Depth]:

$$\eta = 1.1925 d^{-0.424}, \qquad \textbf{Eq. 2.2}$$

where d is the lake depth (m). For the lakes simulated in this study, the observed η varied between 0.05 and 7.1 m^{-1}. This parameter cannot be consistently calculated from physical properties of the lake or its climate, as it depends on lake biology that itself depends on nutrient runoff from the watershed (Cristofor et al. 1994). However, we hypothesize that shallow lakes may tend to have higher concentrations of suspended sediment and nutrients. Even though the

regression to lake depth only explains 46% of the variance in Secchi Depth [Hakanson (1995), Table 4D], and the sample used in this regression may not be representative of lake optical variation globally, we contend that it is better to capture some of this variation than use a single global constant value, as lake optics are a strong control on lake mixing regime (Cristofor et al. 1994; Hocking and Straskraba 1999; Houser 2006; Mazumder and Taylor 1994; Mazumder et al. 1990; Persson and Jones 2008). Eq. 2.2 will introduce error for deep, turbid lakes, and we analyze the model sensitivity to opacity in Section 2.4.2.4.

For frozen lakes with snow less than 40 mm deep, CLM4-LISSS assumes that the surface absorption (β) equals the NIR fraction of incident shortwave, and the remainder of non-reflected shortwave radiation is absorbed in the top lake body layer. For lakes with resolved snow layers (i.e., deeper than 40 mm), CLM4 contains a snow-optics and radiation transfer submodel that predicts snow layer optical characteristics, including transmissivity, based on predicted snow-grain radius and deposited aerosol species (Flanner and Zender 2006; Flanner et al. 2007). In this case, the CLM4 snow-optics submodel predictions are used in assigning absorbed shortwave radiation to snow layers. Because CLM4-LISSS, unlike non-lake CLM4 landunits, includes an infinitesimal surface interface used for calculating surface fluxes, we set β to be the fraction of shortwave radiation predicted to be absorbed by the top layer in the CLM4 snow-optics submodel. For this model version, we assumed that any shortwave radiation penetrating the snow is absorbed in the top layer of lake ice, although some studies have suggested that radiation penetrating ice in the spring might induce convection (Mironov et al. 2002); future model versions should investigate this mechanism.

2.3.1.6 Mixing in the Lake Body

There are four types of mixing among layers of the lake water and ice: wind-driven eddy diffusion, buoyant convection, molecular diffusion, and additional background mixing due to unresolved processes (referred to as "enhanced diffusion"). In lake liquid water, CLM4-LISSS assumes the wind-driven eddy diffusivity, molecular diffusivity, and enhanced diffusivity are added independently; this approach differs little in practice from using the maximum over these different diffusivities, as they tend to vary by at least an order of magnitude (when present). For lake ice, only the molecular diffusivity is used. For model layers containing both water and ice, the ice is assumed to be stacked vertically on top of the water, so that the respective thermal resistances add in series to yield the total resistance of the layer (Eq. 2.1).

Wind-driven eddy diffusivity for unfrozen lakes is evaluated at each depth as a function of the 2 m windspeed, the Brunt-Väisälä frequency implied by the lake density gradient, and the latitudinally-dependent Ekman decay (Hostetler and Bartlein 1990). Although the friction velocity might be a better predictor than the 2 m windspeed, we chose to keep this portion of the Hostetler Model formulation unchanged. Wind-driven mixing tends to be stronger at higher wind speeds and for weakly stable stratification of the lake water, and it tends to penetrate deeper into lakes at low latitude.

Enhanced diffusion in lake water is intended to partially account for sources of turbulence other than wind-driven eddies that lead to mixing in frozen lakes and below the depth where wind-driven mixing can penetrate, including lake-scale wave motions like seiches and advection due to horizontal temperature gradients in large lakes. The Hostetler lake model, mixed primarily

by wind-driven eddies, tends to under-predict mixing for frozen and deep lakes (Martynov et al. 2010; Perroud et al. 2009; Stepanenko et al. 2010), leading to insufficient heat loss for deep lakes in the winter, excessively fast warm-up in the spring (Martynov et al. 2010), and insufficient seasonal variation in lake bottom temperature (Perroud et al. 2009). Fang and Stefan (1996) reasoned that in real lakes there will generally be some source of turbulence in addition to eddies created by wind at the surface, even below ice or at large depth. Turbulent kinetic energy tends to be reduced as a function of the Brunt-Väisälä frequency: under stably stratified conditions, the greater the density gradient, the faster turbulent kinetic energy will be dissipated, leading to a smaller effective diffusivity. Fang and Stefan (1996) suggest using the following expression for thermal diffusivity, D_{ed} (m^2 s^{-1}), derived from measurements under an ice-covered lake (Ellis et al. 1991):

$$D_{ed} = 1.04 \times 10^{-8} \left(N^2\right)^{-0.43}, \qquad \textbf{Eq. 2.3}$$

where N (s^{-1}) is the Brunt-Väisälä frequency. N^2 is limited to a minimum value of 7.5×10^{-5} s^{-2} (Fang and Stefan 1996; Hondzo and Stefan 1993), which leads to a maximum D_{ed} of about 6 times larger than the molecular thermal diffusivity of water. For comparison, wind-driven eddy diffusivities calculated according to Hostetler and Bartlein (1990) are typically 2 to 3 orders of magnitude larger than the molecular diffusivity. Consequently, enhanced diffusion tends to only be important for frozen or deep lakes. We incorporated enhanced diffusion while noting that this is a somewhat ad hoc formulation and is not intended to fully compensate for missing 3D mixing processes: much stronger mixing (equivalent to a factor of ~10^3 increase in eddy diffusivity) may sometimes be required to provide satisfactory simulations of deep lakes like Lake Michigan (Martynov et al. 2010). Therefore, given the information available for a GCM, unrealistically large eddy diffusivity values may be sometimes be predicted and can degrade the simulation quality for shallow lakes; we avoid increasing eddy diffusivities beyond the Hostetler and Bartlein (1990) or Fang and Stefan (1996) values in the baseline model configuration. We do, however, perform sensitivity experiments when evaluating model performance at deep lakes by increasing enhanced and wind-driven eddy diffusivities by factors of 10 – 100.

The lake density is recalculated after surface fluxes, radiation, diffusion, and phase change are calculated. If there is an unstable density profile between any two model layers j and $j + 1$, fast convection is assumed to occur that leaves the lake completely well-mixed (i.e., constant temperature, except in the presence of ice, as described below) from the top down through layer $j + 1$ (Hostetler and Bartlein 1990). This convective adjustment procedure is repeated iteratively, starting with the top two layers and proceeding downwards towards the bottom of the lake, so that the density profile becomes stable or neutral. For the simulation of Lake Michigan and for the archived model version, we modified the adjustment procedure when an unstable density profile occurs between the bottom two layers, in order to avoid thermal instability originating in the lake sediments from causing a complete mixing to the surface of the lake (Section 2.4.1.3); instead, we mix iteratively from the bottom layer upwards only so far as is needed to eliminate any unstable density profiles.

Except for sensitivity studies, the model assumes that all ice is at the top of the lake. Consequently, convection is triggered any time ice occurs below water after phase change has been calculated. The model conserves total heat content and ice mass during this convection. If

the total prior heat content of the layers undergoing convection is greater than that required to bring them to freezing, then the excess heat is assigned uniformly to the layers that are fully unfrozen after convection; otherwise, the heat deficit is assigned uniformly to the layers that are completely frozen after convection.

2.3.1.7 Surface Properties and Parameters

The albedo, *a,* for direct shortwave radiation striking unfrozen lakes is based on the form in Pivovarov (1972), with coefficients incorporated into CLM from BATS (Zeng et al. 2002) (Yongjiu Dai, personal communication, 2010):

$$a = \frac{0.05}{\cos z + 0.15}, \qquad \textbf{Eq. 2.4}$$

where z is the zenith angle. As the diffuse radiation calculated by the atmosphere or diagnosed from the atmospheric forcing is integrated over all angles, the albedo for diffuse radiation is the integral of Eq. 2.4 over the full sky, or 0.10. For cold, frozen lakes with snow depth < 40 mm, the albedo is set to 0.60 for visible radiation (< 700 nm) and 0.40 for NIR (> 700 nm), as in LSM (Bonan 1998; Bonan 1995). When snow is present, the albedo of the snow is calculated as in CLM4 for non-lake landunits (Flanner and Zender 2006; Flanner et al. 2007), and the overall albedo is the average of the snow albedo and ice albedo, weighted by the snow fraction (Lawrence et al. 2011). As real melting lakes can form puddles of liquid water above the ice or undergo disintegration of the ice surface, lowering the albedo and increasing the melt rate, we reduce the albedo for frozen lakes with snow depth < 40 mm whose top layer is close to freezing, following Mironov et al. (2010a):

$$a = a_0(1-x) + a_1 x, x = \exp\left(-95\frac{T_f - T_s}{T_f}\right), \qquad \textbf{Eq. 2.5}$$

where a_0 is the albedo for cold, frozen lakes with snow depth < 40 mm, T_f is the freezing temperature, $a_1 = 0.10$, and T_s is the surface ice temperature. We restrict a to be no smaller than that defined by Eq. 2.4.

The model assumes that lakes have a fixed emissivity of 0.97 (Oleson et al. 2010). The fraction of radiation absorbed near the surface of the lake (β) is described in Section 2.3.1.5.

The momentum roughness length (z_{0m}) for lakes with resolved snow layers is 2.4 mm as in CLM4 , with the scalar roughness lengths calculated as a function of the momentum roughness length and the friction velocity in the atmospheric surface layer (u_*), as in CLM4 over non-vegetated soil and snow (Zilitinkevich 1972):

$$R_0 = \frac{z_{0m} u_*}{\nu}, \qquad \textbf{Eq. 2.6}$$
$$z_{0h} = z_{0q} = z_{0m} \exp\left\{-0.13 R_0^{0.45}\right\}$$

where R_0 is the near-surface atmospheric roughness Reynolds number, z_{0h} is the roughness length for sensible heat, z_{0q} is the roughness length for latent heat, and v is the kinematic viscosity of air.

In the absence of significant snow accumulation, z_{0m} is a crucial parameter for determining the friction velocity and thus the strength of the coupling between the lake and the atmosphere. We detail the treatment of unfrozen lakes below; for frozen lakes with snow depth < 40 mm, we apply z_{0m} = 1 mm, which is roughly consistent with literature values (Andreas 1987; Morris 1989; Vavrus et al. 1996). Scalar roughness lengths for frozen lakes with snow depth < 40 mm are calculated according to Eq. 2.6.

The roughness elements of unfrozen lakes are moving surface waves, whose development depends on the forcing wind, friction velocity, and fetch. The momentum transfer from the atmosphere to the lake depends on the size of the waves and the relative motion of the waves and the wind. Consequently, the effective z_{0m} is larger for lakes with small fetch, where the waves have not had a chance to equilibrate with the mean forcing wind (Donelan et al. 1993; Geernaert et al. 1987; Smith et al. 1992).

For the deep, open-water limit, z_{0m} is well-established (Atakturk and Katsaros 1999). In the limit of aerodynamically smooth flow and an established viscous sub-layer just above the lake surface (Fairall et al. 1996):

$$z_{0m} = \frac{\gamma \nu}{u_*}, \qquad \textbf{Eq. 2.7}$$

where $\gamma = 0.1$ is a dimensionless empirical constant. In the limit of highly turbulent flow just above the surface:

$$z_{0m} = \frac{\alpha u_*^{\,2}}{g}, \qquad \textbf{Eq. 2.8}$$

where g is the acceleration of gravity and α is the dimensionless Charnock coefficient (Charnock 1955), equal to about 0.01 (Smith 1988). In CLM4-LISSS, we choose the appropriate limit by using the maximum of Eq. 2.7 and Eq. 2.8, which is equivalent to keeping R_0 no less than 0.1.

Under fetch-limited conditions, such as small lakes or lakes or oceans near the shoreline, the phase speed of the dominant wave mode is less than the forcing wind, and α is larger than the open water value (Donelan et al. 1993; Maat et al. 1991; Smith et al. 1992; Vickers and Mahrt 1997), though the precise value is not as well-characterized as the open water value. Moreover, small depth also limits the dominant phase speed (equal to $\sqrt{dg}$, where d is the depth, when the wavelength is much larger than the depth). Shoaling waves are steeper (Freilich and Guza 1984; Freilich et al. 1990) and so yield a larger α (Anctil and Donelan 1996; Vickers and Mahrt 1997), and it is typically asserted that small depth will increase the roughness length (Atakturk and Katsaros 1999; Smith et al. 1992). Panin et al. (2006) showed that without correcting for small depth, sensible and latent heat fluxes may be underestimated. However, we could not find systematic empirical relationships between α and d in the literature, and waves may be smaller for constant-depth shallow lakes than shoaling waves at the same depth near the shoreline of deep lakes. In addition, Gao et al. (2009) seemed to find smaller roughness lengths in a coastal zone as compared to open water, although they still observed larger roughness lengths for immature waves. Nevertheless, we tentatively included an increase in α for shallow lakes.

We based our formulation for α loosely on Vickers and Mahrt (1997), who found a mean value of α of 0.073 for offshore flow. The drag coefficient or roughness length is often expressed as a function of the dimensionless wave age, which is captured by the ratio u_*/c or u/c between the friction velocity or forcing wind and the dominant wave phase speed (Gao et al. 2009; Maat et al. 1991; Smith et al. 1992). In the absence of detailed wave information, this can be related to a power-law function f of the dimensionless fetch (Mahrt 1999):

$$f = \left(Fg/u_*^{\,2}\right)^{1/3}, \qquad \textbf{Eq. 2.9}$$

where F is the fetch (m), and u is sometimes used instead of u_*. Vickers and Mahrt (1997) developed an expression for the drag coefficient that tends from the maximum fetch-limited value to the open-water value with $\exp\left\{-\frac{f}{f_c}\right\}$, where $f_c = 100$. We adjusted f_c to correspond to using u instead of u_* in Eq. 2.9, assuming a drag coefficient of 0.1, yielding $f_c = 22$. (As the drag coefficient varies over a large range, future model versions should eliminate this assumption by setting $f_c = 100$ and directly applying Eq. 2.9.) We used this relationship to calculate the fetch-limited α, and we also assumed that the depth limitation on c acts similarly to the fetch limitation in its effect on α:

$$\alpha = \alpha_{\min} + (\alpha_{\max} - \alpha_{\min})\exp\{-\min(A, B)\}$$
$$A = \left(\frac{Fg}{u^2}\right)^{1/3} \Big/ f_c \qquad , \qquad \textbf{Eq. 2.10}$$
$$B = \varepsilon \frac{\sqrt{dg}}{u}$$

where A and B define the fetch- and depth-limitation, respectively. We assumed $\alpha_{\min} = 0.01$ (the open-water limit) and $\alpha_{\max} = 0.11$, extrapolating roughly to the upper limit of the data in Vickers and Mahrt (1997). We tentatively set $\varepsilon = 1$, to be adjusted as data becomes available. For global simulations when the approximate fetch is unavailable, we may assume the fetch is 25 times the depth, a crude relationship characterizing typical lakes (Hutchinson 1957; Wetzel and Likens 1991). In this case, the depth limitation rarely takes precedence over the fetch limitation. This relationship will underestimate the fetch of broad, shallow lakes, but we reason that it is better to under-estimate the fetch than over-estimate it, as non-stationary wind will tend to keep the wave development farther from equilibrium. Alternatively, to reduce the number of unconstrained parameters causing differences between gridcells in global simulations, we can assume a fetch large enough that only the depth limitation on wave development applies. Either choice is crude and should be replaced by global gridded data when available; we analyze the model sensitivity to fetch below.

For unfrozen lakes, the modeled scalar roughness lengths are separate functions of R_0 and z_{0m} (Zilitinkevich et al. 2001):

$$z_{0h} = z_{0m} \exp\left\{-\frac{\kappa}{P_r}\left(4\sqrt{R_0} - 3.2\right)\right\},$$
$$z_{0q} = z_{0m} \exp\left\{-\frac{\kappa}{S_c}\left(4\sqrt{R_0} - 4.2\right)\right\}, \quad \textbf{Eq. 2.11}$$

where κ is the von Karman constant, $P_r = 0.71$ is the molecular Prandt number for air, and $S_c = 0.66$ is the molecular Schmidt number for water in air. We arbitrarily imposed a lower limit of 0.01 mm on predicted scalar roughness lengths (coming into effect for $u_* > \sim 0.2$ m s^{-1}), as the Zilitinkevich et al. (2001) expressions have not been validated for very large u_*; we checked that the model predictions were not overly sensitive to this assumption, and relaxing this limit should be considered for future model versions.

2.3.1.8 Surface Fluxes Solution

Surface fluxes are solved using the conditions at the atmospheric reference height as a top boundary condition and the top lake model layer temperature (in the lake body for snow depth < 40 mm and in the snow otherwise) as a bottom boundary condition, both evaluated at the end of the previous timestep. The surface temperature T_g is solved simultaneously with the friction velocity, surface roughnesses, and aerodynamic resistances in order to balance the surface energy budget. Note that T_g is associated with an infinitesimal interface between the top lake model layer and the atmosphere and thus can vary freely during the surface flux solution. This approach is in contrast with the surface flux solution over bare ground for non-lake landunits in CLM4, where the surface temperature is restricted to equal the top soil or snow layer temperature from the previous timestep (although the effective thickness is tuned to achieve appropriate diurnal temperature range), and the thermal diffusion solution includes the first-order dependence of the surface temperature on the surface fluxes, which are then corrected after the diffusion solution.

Conservation of energy at the lake surface requires:

$$S + L = H + \lambda E + G, \quad \textbf{Eq. 2.12}$$

where S is the absorbed shortwave radiation flux at the surface, L is the net longwave (thermal infrared) radiation flux at the surface, H is the upward sensible heat flux, λE is the upward latent heat flux, and G is the downward heat flux into the lake. These terms are calculated as:

$$S = \beta S_a,$$
$$L = -\varepsilon(\sigma T_g{}^4 - L_{atm}),$$
$$H = \rho_{atm} c_p \frac{T_g - \theta_{atm}}{r_{ah}}, \quad \textbf{Eq. 2.13}$$
$$\lambda E = \lambda \rho_{atm} \frac{q_g - q_{atm}}{r_{aw}},$$
$$G = k \frac{T_g - T_T}{\Delta z_T / 2},$$

where β is the fraction of the total surface absorbed shortwave radiation S_a (see Section 2.3.1.5), ε is the lake emissivity, σ is the Stefan-Boltzman constant, L_{atm} is the downward longwave radiation flux, ρ_{atm} is the moist atmospheric density, c_p is the specific heat of air at constant pressure, θ_{atm} is the potential temperature at the atmospheric reference height with respect to the surface (i.e., normalized to the reference height with an assumed lapse rate, not 1000 hPa), r_{ah} is the aerodynamic resistance with respect to sensible heat, λ is the latent heat of vaporization or sublimation (depending on the surface temperature), q_g is the saturated specific humidity at the surface temperature, q_{atm} is the specific humidity at the reference height, r_{aw} is the aerodynamic resistance with respect to latent heat, k is the thermal conductivity of the top lake model layer, T_T is the temperature of the top lake model layer, and Δz_T is the top lake model layer thickness. For unfrozen lakes, k includes eddy and enhanced diffusivities (Section 2.3.1.6) in addition to molecular diffusivity, as calculated at the previous timestep.

The energy fluxes, aerodynamic resistances, and friction velocity all depend on the surface temperature. The friction velocity depends on the surface roughnesses, which in turn are functions of the friction velocity (Section 2.3.1.7). The system of equations is iterated four times to find the unique surface temperature T_g that balances the surface energy budget. During each iteration, the friction velocity and aerodynamic resistances are calculated according to the method for lakes or bare ground in CLM4, with the surface roughnesses calculated as in Section 2.3.1.7, using the values from the previous timestep for the first iteration. The updated aerodynamic resistances are used to re-evaluate the surface fluxes, which are used to update the solution for surface temperature following the Newton-Raphson Method applied to Eq. 2.12.

After the surface temperature iteration yields a tentative solution T_g' for Eq. 2.12, several restrictions are imposed on T_g before the diffusion solution (Section 2.3.1.9) to maintain consistency with the top lake model layer temperature T_T:

$$\begin{aligned} &1)\ T_T \le T_f < T_g' \Rightarrow T_g = T_f, \\ &2)\ T_T > T_g' > T_m \Rightarrow T_g = T_T, \\ &3)\ T_m > T_g' > T_T > T_f \Rightarrow T_g = T_T. \end{aligned} \qquad \textbf{Eq. 2.14}$$

The first condition requires that, if there is any ice or snow present (except for newly incident snow of less than 40 mm), the surface temperature is restricted to be less than or equal to freezing. The second and third conditions maintain convective stability in the top lake layer. For instance, if the surface temperature is less than the top lake layer temperature but greater than the maximum density temperature [T_m = 3.85°C as in Hostetler and Bartlein (1990), though we recommend 3.98°C for future model versions (Gebhart and Mollendorf 1977)], the water at the surface will be heavier than in the middle of the top layer, and mixing will immediately occur to homogenize the temperature in the top layer, so we reset the surface temperature to equal that of the top layer. This condition, which effectively extends the explicit convection to the top half of the top lake layer, is important for preventing unrealistic declines in lake surface temperature during night or during the autumn.

After T_g is potentially reset (Eq. 2.14), the longwave radiation and heat fluxes L, H, and λE are re-evaluated. Finally, G is set as the residual energy flux in Eq. 2.12, in order to precisely conserve energy: this may differ from the expression for G in Eq. 2.13 because of the restrictions

imposed in Eq. 2.14 and the numerical precision of the iterative surface temperature solution. However, during model testing, the difference between the residual energy flux and the Eq. 2.13 expression for G in the absence of application of Eq. 2.14 was small (i.e., discrepancies at each timestep were generally less than 0.01 W m^{-2}, were always less than 2 W m^{-2}, and averaged to zero). Separate testing confirmed that the diagnostic calculation of surface roughness as a function of friction velocity, itself depending on surface roughness, did not adversely affect convergence of the T_g solution.

2.3.1.9 Diffusion Solution

After the surface fluxes, radiation transfer, and thermal conductivities are calculated, and before phase change, convection, and snow dynamics are evaluated (in that order), the 1D thermal diffusion equation is solved for the full lake column, including snow, ice, water, sediment, and bedrock:

$$c_w \frac{\partial T}{\partial t} = \frac{\partial}{\partial z}\left(k \frac{\partial T}{\partial z} \right) - \frac{d\phi}{dz}, \qquad \textbf{Eq. 2.15}$$

where c_w is the specific heat (per unit volume) at depth z (the sum of the respective heat capacities of the water, ice, and mineral constituents), T is the temperature, t is time, k is the thermal conductivity, and ϕ is the radiation flux reaching depth z. The top boundary condition prescribes the residual heat flux G calculated during the surface flux solution (Section 2.3.1.8) to flow into the top layer, and the bottom boundary condition beneath the sediment prescribes zero heat flux to flow out of the bottom layer. Eq. 2.15 is discretized and solved using the semi-implicit Crank-Nicholson method; details are found in the technical note.

After diffusion, phase change, and convection are evaluated, an energy balance check is evaluated to make sure that the total change in lake enthalpy over the course of the timestep (including the latent heat associated with phase change and correcting for the discontinuity in specific heat at the freezing point) is equal to the shortwave radiation flux penetrating the lake surface $(1-\beta)S_a$ plus the heat flux transmitted from the lake surface G, to a precision of 10^{-7} W m^{-2}.

2.3.1.10 Hydrology

In CLM4-LISSS, the water content of melting snow is immediately added to runoff, as is done currently for glacier and wetland landunits in CLM4. Since the water level of the lake is fixed and watershed runoff into the lakes is not tracked, the water is balanced for global simulations by removing lake evaporation and sublimation from the runoff to the ocean, and adding dew, frost, and precipitation reaching the lake surface. Snow is accumulated for frozen lakes, and dew, frost, and precipitation are added to the top snow layer if present. Evaporation or sublimation may be removed directly from the top snow layer.

2.3.2 Model Evaluation

We evaluated CLM4-LISSS at two small temperate lakes (Sparkling Lake and Kossenblatter Lake) and one small boreal lake (Lake Valkea-Kotinen) where extensive observations were

available, including lake water temperature, surface fluxes, optical extinction coefficient, and 2 m meteorological forcing observations above the lake including air temperature, humidity, pressure, and wind speed, with incoming longwave and shortwave radiation observations from nearby weather stations (Table 2.1). (We use "small lakes" to mean lakes smaller than ~2 km^2 in area, and "shallow lakes" to mean lakes with less than 20 m depth. "Large" and "deep" lakes mean the opposite.) We followed a similar evaluation procedure to that used in the Lake Model Intercomparison Project (LakeMIP) (Stepanenko et al. 2010) for Sparkling Lake, and CLM-LISSS is participating in the LakeMIP for Kossenblatter Lake and Lake Valkea-Kotinen.

We also tested CLM4-LISSS at ten other lakes where complete meteorological forcing observations were unavailable and lake observation data were less comprehensive, including lakes spanning a large range of geometry, climate, and opacity (Table 2.1). Since most lake observations are limited to water temperature or water surface temperature and because snow and ice are key components of this lake model, we emphasized lakes where observations of snow and ice thickness were simultaneously made. Because we lacked meteorological forcing observations for any of these lakes, we sought several lakes in each category and for each observed variable of interest to compensate for the unpredictable discrepancies between coarse-scale meteorology and local conditions. Unfortunately, insufficient data were available to effectively evaluate the lake sediment temperature predictions. Finally, we evaluated the existing CLM4 lake model at four lakes for comparison: Sparkling Lake, Lake Michigan, Great Slave Lake, and Lake McIlwaine.

Each evaluation simulation was performed in single-point mode with a single lake column, using soil properties and aerosol deposition based on the nearest gridcell in the CLM4 1.9° x 2.5° dataset. For the large and deep lakes, we repeated the simulations with non-molecular thermal diffusivities multiplied by 10 in case the model (even with enhanced diffusion as in Section 2.3.1.6) insufficiently accounted for unresolved 3D processes; for Great Slave Lake we also performed a simulation with 100 times increased diffusivities.

In Section 2.4.1.1, we first analyze results from the three small temperate lakes where forcing observations were available, including testing the effects of the roughness length formulation. In Section 2.4.1.2, we examine ice and snow observations from Ryan Lake, Thrush Lake, Lake Gogebic, Big Island Lake, and Karujärv, with additional water temperature comparisons for boreal lakes Raksjo, Karujärv, and Thrush. We continue in Section 2.4.1.3 by considering Lake Michigan, a large, deep, temperate lake that undergoes mixing in excess of wind-driven eddies (Martynov et al. 2010), to characterize how the model fares under these conditions and to test the effects of enhanced diffusion and 10 times increased eddy diffusivity. Great Slave Lake provides a similar test where some surface flux observations were also available. Finally, we briefly examine one very deep caldera lake (Crater Lake) and one mid-size tropical lake (McIlwaine).

2.3.3 Modeled Sensitivity of Surface Fluxes and Water Temperature to Processes and Parameters

Many lake models integrated in climate models lack some of the processes included in CLM4-LISSS, such as phase change and the insulation of frozen lakes by snow. There are also many lake characteristics and model parameters which are poorly constrained in global simulations and are sometimes characterized crudely in existing lake models, such as depth,

surface roughness, and optical extinction coefficient. We performed sensitivity experiments to isolate the effects of each excluded process or typical range of parameter uncertainty on lake model predictions. We were primarily interested in the effects of these processes and parameters on global climate model predictions, so we examined the sensitivity of surface fluxes averaged over all the lake area in several regions, and examined changes in lake water temperatures for several representative gridcells to better understand the causes of flux changes. To understand the changes in surface fluxes, we also examined the rate of change of lake enthalpy, which we calculated as the sum of the rate of shortwave radiation absorption beneath the surface and the rate of heat diffusion into the lake at the surface (i.e., $(1-\beta)S_a + G$). For brevity, we analyzed averages for North Eurasian lakes only (e.g. 60 – 90°N, 0 – 175°E) in Section 2.4.2, using the simulated lake co-located with Finnish Lake Inari ("*Inarijärvi*", 69.05°N, 27.81° E; simulated depth = 11 m) as a test case; figures for two warmer regions are available in the Supplemental (Supp.) Figures. In order to isolate the primary effects of processes and parameters without atmospheric feedback, we used offline experiments forced by bias-corrected NCEP atmospheric reanalysis data (Qian et al. 2006).

We performed 14 total experiments, all independently varied from the reference case, detailed below. The reference case was a global 1.9° x 2.5° CLM4 simulation (with CLM4-LISSS) using year 2000 conditions for aerosol deposition and repeated 25-year periods of atmospheric forcing from 1980-2004 (Qian et al. 2006), with 110 years for spinup and 15 years (1990-2004) for analysis. In order to make the reference simulation more realistic, we used lake depth and lake area data not available in the standard CLM4 surface datasets. The global lake area in the standard CLM4 dataset is about 0.7 million km^2, far less than the 2.7 million km^2 from the Global Lake and Wetland Database (GLWD) (Lehner and Doll 2004), which itself is probably an underestimate of the true lake area; Downing et al. (2006) estimated a total lake area of 4.6 million km^2. We used the GLWD lake area interpolated to 1.9° x 2.5° resolution and excluding the Caspian Sea (which is treated as ocean in CESM1), yielding 2.3 million km^2, shown in Supp. Fig. 2.1a.

To our knowledge, the first extensive global gridded lake depth dataset has been recently developed at 30 arcsec. resolution (Kourzeneva 2010) (http://www.flake.igb-berlin.de/ep-data.shtml). This dataset includes real data from a variety of sources for over 13,000 lakes and uses default depths of 10 m when a lake is present but the depth is not known, which is likely to be more realistic for the small lakes for which data are likely to be unavailable than the 50 m default lake depth in the existing CLM4. (Rivers are included in this dataset and assigned a depth of 3 m; even though the lake model may not be appropriate for rivers, we could not easily remove the rivers from the depth dataset, though these are not included in the GLWD that we used to determine the lake area simulated in each gridcell.) We interpolated this data to 1.9° x 2.5° resolution by using the mean depth from each 1 km gridcell in the lake-depth dataset where a lake was present, whether or not the real depth was available for that 1 km gridcell. Because the mean depth was used, each represented lake does not correspond to the depth of any particular real lake unless that lake dominates the 1.9° x 2.5° gridcell. This approximation is a crude first step intended to be more realistic than a constant global lake depth: future work should use multiple lake depth categories in each gridcell. Other interpolation approaches could have been used, such as using the mode rather than the mean lake depth when interpolating to the coarse gridcell, or ignoring 30 arcsec. gridcells assigned to the default 10 m in the lake depth

dataset if at least one lake with known depth is available in the CLM4 gridcell; these alternative approaches are compared in Supp. Fig. 2.1b-d.

Each 25-year experiment started with the initial conditions after 100 years of spinup for the reference case and allowed 10 additional years for spinup (1980-1989 atmosphere) unless otherwise specified, using the final 15 years (1990-2004) for analysis, retaining year 2000 aerosol deposition. For simplicity, we assumed no small-fetch limitation on wave development (Section 2.3.1.7) in the reference case. The fourteen sensitivity experiments are described below. In addition to these fourteen experiments, we also investigated the effects of vertical discretization by comparing the model predictions when using 10 lake body layers for these global simulations as opposed to 25, which we used for the site evaluations.

1. *No heat of fusion for phase change*. We set the heat of fusion for water equal to 1 J kg^{-1}. All other effects of phase change (e.g., changes in albedo and thermal properties, suppression of wind-driven eddies) remained unchanged.
2. *No snow insulation*. We multiplied the thermal conductivity of snow by 10^6. All other snow properties remained unchanged.
3. *No enhanced diffusion.* The "enhanced diffusion" defined in Section 2.3.1.6 was turned off, leaving only the wind-driven eddy and molecular diffusion.
4. *Lake puddling*. We suppressed convection (which is normally responsible for aggregating ice at the surface) when more than 0.3 m of ice was present, allowing some liquid water to remain above ice and for arbitrary mixtures of ice and water to be present below. Wind-driven eddy diffusivity was added to liquid water present above ice. This case was compared to Case 11, as this mechanism independently allows a decrease in albedo when water is present over melting ice.
5. *Lake depth = 50 m*. All lakes had constant 50 m depth. Twenty years of additional spinup were used. This case was compared to a perturbed reference case with η = 0.22 m^{-1}, the default 50 m lake value (Section 2.3.1.5), so that the lake depth was the only change.
6. *Lake depth = 5 m*. All lakes had constant 5 m depth. This case was compared to a perturbed reference case with η = 0.60 m^{-1}, the default 5 m lake value (Section 2.3.1.5), so that the lake depth was the only change.
7. *η = 1.0 m^{-1}*. All lakes had constant extinction coefficient of 1.0 m^{-1}, instead of being a function of depth as in the reference case (Section 2.3.1.5). This represented an increase in extinction coefficient for most gridcells.
8. *z_{0m} = 1 mm.* All unfrozen lakes had constant roughness lengths (both momentum and scalar roughness lengths) equal to 1 mm, instead of the diagnostic values (Section 2.3.1.7).
9. *z_{0m} = 10 mm.* All unfrozen lakes had constant roughness lengths (both momentum and scalar roughness lengths) equal to 10 mm (the value used in the existing CLM4 lake model), instead of the diagnostic values (Section 2.3.1.7).

10. *Unfrozen albedo = 0.07*. All lakes had constant unfrozen albedo for both direct and diffuse shortwave radiation, instead of the relationships in Section 2.3.1.7.
11. *No albedo correction for melting lakes*. All frozen lakes had constant albedo (0.60 for visible and 0.40 for NIR), without reduction as the ice surface temperature approaches freezing (Section 2.3.1.7).
12. *Mixing times 2.* Wind-driven eddy and enhanced diffusion (Section 2.3.1.6) were multiplied by 2.
13. *Mixing times 10.* Wind-driven eddy and enhanced diffusion (Section 2.3.1.6) were multiplied by 10.
14. *100 m fetch.* The fetch was set to 100 m for all lakes, as opposed to the unlimited value in the reference case.

2.4 Results

2.4.1 Model Evaluation

2.4.1.1 Shallow Lakes with Forcing; Roughness Length Sensitivity

The existing CLM4 lake model performed poorly for Sparkling Lake (Fig. 2.2). During the summer, the lake was barely stratified and remained cold, with predicted surface water temperature averaging 15°C too low. In the winter, the surface temperature sometimes rose well above freezing during warm spells, because of the model's lack of thermal inertia from the presence of ice. Latent heat fluxes were consistently high during the early summer and peaked too early in the season. Sensible heat fluxes were negative throughout the year. The model simulated an unrealistically high average diurnal surface temperature range exceeding 13°C during the summer, comparable to the average diurnal range in observed 2 m air temperature but not the average diurnal range in observed near-surface water temperature (0.5°C). Because the unphysical behavior of the existing CLM4 lake model at Sparkling Lake was evident at all other lakes tested, it served as a poor point of comparison for CLM4-LISSS, and we present further evaluation results only in the Appendix (Section 2.8.2).

CLM4-LISSS simulated medium-depth Sparkling Lake surface and 10 m water temperatures and sensible and latent heat fluxes well (Fig. 2.2). The latent heat flux predictions were higher than observations for 2002-2003 but accurate for 2004-2005, and the seasonal timing of the peak in latent heat flux was well reproduced. Sensible heat flux predictions were largely consistent with observations, though they peaked later in the season than observations. Predictions of summer diurnal temperature range were 0.8°C for the surface and 0.5°C for the water at 0.05 m, the latter being consistent with observations (not shown).

Degrading the roughness lengths from the diagnostic values (which ranged between 0.01 and 1 mm but were generally between 0.1 and 0.5 mm) to a constant 1 or 10 mm caused excessive outgoing latent heat flux and cold surface temperatures (Fig. 2.3). For 10 mm roughness lengths, summer latent heat flux was 46 W m^{-2} higher than when using the diagnostic roughness lengths, and near-surface summer water temperatures were 4.2°C too low compared to observations. This cold bias persisted into the winter, causing early freeze-up and late thaw dates.

The model evaluations at the two relatively shallow, turbid lakes (Kossenblatter and Valkea-Kotinen) showed similar results (Fig. 2.4 and Fig. 2.5). CLM4-LISSS simulated the Kossenblatter surface and 1 m temperatures relatively accurately, while using fixed 10 mm roughness lengths caused a cold bias. CLM4-LISSS mildly over-predicted Kossenblatter heat fluxes while reproducing the temporal patterns of variability; with fixed 10 mm roughness lengths latent heat fluxes were excessively high and sensible heat fluxes were excessively low. CLM4-LISSS reproduced the observed vertical and seasonal patterns for water temperature and the seasonal patterns for afternoon heat fluxes for Lake Valkea-Kotinen [although these eddy covariance data are limited to conditions when the fetch is along the lake (Nordbo et al. 2011)].

2.4.1.2 Small Temperate and Boreal Lakes: Ice, Snow, and Sediment

We evaluated simulated ice and snow thicknesses for Big Island Lake, Lake Gogebic, Ryan Lake, Thrush Lake, and Karujärv (Fig. 2.6 and Supp. Fig. 2.2). The model performed acceptably by correctly predicting the range of thickness magnitudes and the range of inter-annual variability among modeled years and between lakes. Freeze and thaw dates were approximately correct, given the sporadic available observations. As in the observations, the model showed a strong anti-correlation between snow and ice thicknesses, demonstrating that it correctly represented the inhibition of ice formation from snow insulation (Brown and Duguay 2010). However, predictions of snow thickness for a given year or lake were not consistently accurate. These differences were possibly influenced by inconsistencies between actual local snowfall and the snowfall predicted by the 2° reanalysis dataset.

We also evaluated water temperature predictions for temperate Thrush Lake (Supp. Fig. 2.3) and boreal lakes Raksjo (Supp. Fig. 2.4) and Karujärv (Supp. Fig. 2.2). The model predicted temperatures accurately for Thrush and Karujärv. The seasonal variation was mildly delayed and the heat penetration mildly under-predicted for Raksjo compared with observations, though the surface temperature variation was accurate.

2.4.1.3 Deep Lakes; Mixing Sensitivity

The parameterization of wind-driven eddy mixing (Hostetler and Bartlein 1990) apparently led to under-predicted mixing in all four simulated deep lakes, as slight improvement was obtained for some lakes with enhanced diffusion and substantial improvement was usually obtained for all four lakes when increasing eddy diffusivity by factors of 10 – 100. Even without these improvements, performance of CLM4-LISSS was adequate in the context of uncertain lake properties at the global scale (Section 2.4.2).

We evaluated Lake Michigan with CLM4-LISSS, CLM4-LISSS without enhanced diffusion, and CLM4-LISSS with 10 times increased eddy diffusivity, compared to vertical water temperature observations (Fig. 2.7) and surface temperature observations (Fig. 2.8) for 1990. CLM4-LISSS accurately predicted the observed seasonal and vertical patterns of variation in water temperature including summer stratification, although the predicted summer thermocline was too shallow and the surface temperature too low both with the baseline CLM4-LISSS and with 10 times increased eddy diffusivity (Fig. 2.7).

Typical of the difficulties of evaluating 1D models for large lakes, surface temperature observations differed between the two mid-lake buoys closest to the simulated location by up to

5°C (Fig. 2.8). The warmer buoy had surface temperature observations colder than those of the nearby vertical water temperature observations (Fig. 2.7) during the same time period. CLM4-LISSS predicted an earlier spring warm-up and fall cool-down than the observations (Fig. 2.8). Including enhanced diffusion had little effect on this timing. When 10 times increased eddy diffusivity was used, the spring warm-up and fall cool-down were delayed, bringing the model closer to observations, though a 5°C warm bias remained in the spring and early summer. During the late summer, all model versions corresponded well to the warmer buoy observations, which were bracketed by the surface temperatures indicated by the cooler buoy and those from the contemporaneous vertical water temperature observations (Fig. 2.7).

In our original simulations of Lake Michigan (not shown), several unobserved abrupt and complete overturning events occurred in the summer season. We determined that these events were caused by an unrealistic interaction of the sediments with the original convective adjustment algorithm (Hostetler and Bartlein 1990): slight diffusion of heat from the sediments during atmospheric cooling was causing the bottom layer to become slightly warmer than the layer above, triggering a complete mixing to the lake top, with the time of this occurrence highly sensitive to the model state. We modified the convective algorithm (Section 2.3.1.6) to prevent the unrealistic behavior. This correction only caused insignificant changes in other lakes, where sediment-initiated overturning events were rare and small in magnitude.

We evaluated Great Slave Lake with CLM4-LISSS, CLM4-LISSS without enhanced diffusion, and CLM4-LISSS with 100 times increased eddy diffusivity, compared to vertical water temperature observations and surface flux observations for 1997-2002 (Fig. 2.9). Compared to observations, CLM4-LISSS tended to under-predict mixing, as evidenced by over-predicted surface temperatures, under-predicted autumn 40 m water temperatures, an early peak in surface heat fluxes, and an early freeze-up date. These errors were most pronounced when enhanced diffusion was turned off, while substantial improvements were obtained with 100 times increased eddy diffusivity. A comparison of each year's freeze-up and thaw dates between CLM4-LISSS simulations and observations (not shown), though complicated by the lack of fractional ice cover predictions, also suggested that the simulated seasonal dynamics were several weeks too early in the default version and about one week early with 100 times increased eddy diffusivity. We note that errors in all simulations may have been exacerbated by the use of coarse resolution (~2°) reanalysis-derived meteorological forcing rather than local forcing, as air temperatures over Great Slave Lake tend to have a substantial seasonal lag compared to air temperatures over nearby land (Rouse et al. 2008).

We also evaluated model predictions for the very deep (594 m) Crater Lake with mild Pacific Northwest climate and for tropical Lake McIlwaine. CLM4-LISSS reproduced the vertical and seasonal patterns of temperature variation in Crater Lake, which is well-mixed in the winter and mildly stratified in the summer, although it under-predicted seasonal temperature variability and summer stratification (Supp. Fig. 2.5 and 2.6). Predictions are closer to observations with 10 times increased eddy diffusivity and farther from observations with no enhanced diffusion. CLM4-LISSS performed similarly for Lake McIlwaine, capturing the increased stratification and surface warming in the summer (Supp. Fig. 2.7). It over-predicted stratification in this case, but predictions were closer to observations with 10 times increased eddy diffusivity and farther from observations with no enhanced diffusion.

2.4.2 Model Sensitivity

We evaluated the sensitivities to modeled processes and parameters for the average monthly surface energy fluxes for North Eurasian lakes and the water temperatures of the 11 m deep lake approximating Finnish Lake Inari. Summarizing the results detailed in the following subsections (2.4.2.1-2.4.2.7), we found very high sensitivity to the inclusion of snow insulation and high sensitivity to the inclusion of the heat of fusion for phase change, lake depth, extinction coefficient, and the albedo of melting lakes. Sensitivities to roughness lengths and mixing strength depended on the perturbation magnitudes. We found low sensitivities to enhanced diffusion (Case 3), the inclusion of puddling on thick melting ice (Case 4), the unfrozen albedo (Case 10), and the fetch (Case 14), so we do not discuss these cases below. Surface flux sensitivity and water temperature figures for all cases are available in the Supplemental Information (Supp. Figs. 2.10 – 2.18). Compared to the results detailed below, results from warmer regions (i.e., U.S. lakes and Eastern Hemisphere tropical lakes) showed reduced sensitivity to snow insulation and phase change and increased sensitivity to the roughness lengths, enhanced diffusion, and mixing strengths.

2.4.2.1 Snow Insulation

In Case 2, we eliminated snow insulation by multiplying the thermal conductivity of snow by 10^6, keeping all other snow properties constant. North Eurasian lakes were predicted to lose ~20 W m^{-2} more to the atmosphere during the winter (Fig. 2.10a). Compared with the baseline simulation (Fig. 2.11a), Inari ice increased in thickness (~ 1 m) and duration (1 week) and cooled (~8°C) at the surface (Fig. 2.11b). North Eurasian lakes remained cooler in the summer, leading to an extra 30 W m^{-2} energy absorption in July, manifesting as large declines in summer longwave, latent, and sensible energy fluxes.

2.4.2.2 Heat of Fusion for Phase Change

In Case 1, we eliminated the heat of fusion of water. This modification dramatically increased the thickness of Inari winter lake "ice" and cooled its top layer by up to 4°C (Supp. Fig. 2.14b). The decline in North Eurasian lake surface temperatures caused less heat to be lost to the atmosphere during the winter, while faster spring melt decreased the lake energy uptake by 14 W m^{-2} in June, causing 2 – 3 W m^{-2} increases in longwave, latent, and sensible energy fluxes (Fig. 2.10b). It is noteworthy that both eliminating the heat of fusion and eliminating snow insulation caused declines in ice surface temperatures but with opposite effects on atmospheric fluxes and lake summer temperatures.

2.4.2.3 Lake Depth

In Case 5, we increased the depth of modeled North Eurasian lakes from an average of 14 m (with a median of 10 m) to a constant 50 m, while in Case 6, we decreased the depth to a constant 5 m. Decreasing the depth led to the expected summer warming and autumn cooling of the Inari surface due to decreased thermal inertia (Supp. Fig. 2.15d), associated with a decrease in energy uptake of North Eurasian lakes by 5 W m^{-2} in the summer and an increase in lake energy loss of 12 W m^{-2} in October (Fig. 2.10c). During the summer, sensible and latent fluxes

increased while net longwave fluxes remained nearly unchanged, indicating that the warming occurred primarily during the day.

The seasonal pattern of surface flux change was more complicated when the depth was increased. In June, North Eurasian lakes lost an extra 10 W m^{-2} to the atmosphere, primarily via longwave radiation (Fig. 2.10d). This loss is consistent with the predicted greater winter and spring temperature stratification under the ice and consequent delay in overturning as compared to the baseline simulation with identical constant η (not shown). This change may have been unrealistic if winter below-ice mixing was too weak (Martynov et al. 2010). In contrast, energy uptake by the lakes increased by 14 W m^{-2} in September when the depth was increased to 50 m, primarily via decreases in latent heat fluxes. The lakes then returned an extra 8 W m^{-2} to the atmosphere in November.

2.4.2.4 Extinction Coefficient

Increasing the optical extinction coefficient of North Eurasian lakes from an average of 0.46 m^{-1} to a constant 1.0 m^{-1} (Case 7) acted analogously (though more strongly, in this case) to a decrease in lake depth, increasing thermal stratification and decreasing the effective mixing depth of Lake Inari during the summer (Fig. 2.11c). North Eurasian lake energy uptake in July decreased by 17 W m^{-2}, primarily via increased latent heat flux associated with a daytime surface warming; lake energy loss in October decreased by 16 W m^{-2}, about equally via sensible, latent, and longwave fluxes (Fig. 2.12a).

2.4.2.5 Melting Lake Albedo

In Case 11, we maintained the albedo of melting ice at the winter value rather than allowing it to decline to 0.10 as the exposed ice surface reached the melting temperature. This change caused a median of 8 days delay in melt for North Eurasian lakes, though much larger delays were observed in some gridcells. Energy uptake by lakes decreased by 15 W m^{-2} and energy fluxes to the atmosphere decreased by 16 W m^{-2} in June (Fig. 2.12b), associated with a loss of 31 W m^{-2} in absorbed shortwave radiation (not shown). Lakes remained colder in July, taking up an extra 15 W m^{-2}.

2.4.2.6 Roughness Lengths

In Case 8, we fixed roughness lengths for unfrozen lakes to a constant value of 1 mm [instead of the diagnostic values (Section 2.3.1.6), which varied but were generally less than 0.5 mm], while in Case 9, we increased roughness lengths to 10 mm, which is unrealistically high but equal to the value used in the existing CLM4 lake model. Fixing the roughness lengths at 1 mm caused about a 15 W m^{-2} increase in the sum of summer sensible and latent heat fluxes for North Eurasian lakes, at the expense of lake energy uptake and longwave fluxes (Fig. 2.12c). The Lake Inari peak summer surface temperature declined by 2°C (Supp. Fig. 2.16c). Lakes remained colder in the autumn, with lake energy loss decreasing by 9 W m^{-2}, primarily via decreased longwave fluxes. These effects were magnified when roughness lengths were fixed at 10 mm, with about a 20 W m^{-2} summer increase in the sum of latent and sensible heat fluxes for North Eurasian lakes, a 19 W m^{-2} decline in October lake energy loss (Supp. Fig. 2.12a), and a 4°C decline in peak Inari summer surface temperature (Supp. Fig. 2.16d). In both cases, decreased

summer energy uptake by Lake Inari led to an annually colder lake, with ~ 1 week earlier freeze-up and later thaw (Supp. Fig. 2.16c-d).

2.4.2.7 Mixing Strength

In Case 12, we multiplied eddy diffusivities by 2, and in Case 13 we multiplied by 10. Results were modest for the factor of 2 increase in eddy diffusivity, increasing the July energy uptake and October energy loss for North Eurasian lakes by about 4 W m^{-2} (Supp. Fig. 2.12d). For the factor of 10 increase, the increase in seasonal energy exchange was about 20 W m^{-2} (Fig. 2.12d); Lake Inari summer thermal stratification also decreased (Fig. 2.11d). Normally, a low sensitivity to a 100% parameter change would be considered as evidence of low uncertainty, but the results in Section 2.4.1.3 suggested that the uncertainty in mixing strength for large, deep lakes is very large, and a factor of 10 increase usually improved the realism of simulated water temperatures. Consequently, the 20 W m^{-2} increase in seasonal energy exchange associated with Case 13 may be realistic.

2.4.2.8 Discretization

We also compared the model predictions when using 10 lake body layers for these global simulations as opposed to 25, which we used for the site evaluations. We found that errors in surface energy flux predictions may result from using 10 layers instead of 25 layers, with annual-mean errors of a few W m^{-2}. Much larger errors may occur for short time periods when energy exchange between the lake body and atmosphere are large. We therefore recommend increasing the number of layers for global simulations when sufficient computational resources are available.

2.5 Discussion

2.5.1 Performance of CESM/CLM4 Lake Models

Due to the lack of phase change physics and snow insulation, unrealistically large roughness lengths, and errors in the calculation of surface fluxes, surface temperature, and eddy diffusivity, predictions of the existing CLM4 lake model poorly matched observations at all lakes tested (Sections 2.4.1.1 and 2.8.2). For the three small, shallow temperate and boreal lakes with available meteorological forcing observations, CLM4-LISSS predictions for water temperature were excellent, and predictions for surface fluxes were good. We note that there are important uncertainties associated with eddy-covariance observations, particularly in the presence of land-surface heterogeneity (Foken 2008), which certainly applies to these small lakes. For other small shallow temperate and boreal lakes without forcing observations, water temperature predictions were good, with no systematic biases. CLM4-LISSS performance was adequate for large and deep lakes (Section 2.5.3), although we note that there are substantial horizontal variations in temperature which CLM4-LISSS cannot resolve. Insufficient data were available to conclusively test the performance of the ice, snow, and sediment schemes in CLM4-LISSS, although there appear to be no systematic biases in the ice and snow thickness predictions, and the model showed the right seasonal behavior and a realistic anti-correlation between snow depth and ice thickness (Brown and Duguay 2010). The new roughness length formulations for momentum, heat, and moisture fluxes were clearly superior to fixed values of 1 mm or greater, although

insufficient data were available to test the relatively uncertain enhancement of surface exchange due to depth and fetch limitation on wave development. However, sensitivity to fetch limitation appeared to be very small compared to the other parametric uncertainties, with a maximum of 2 W m^{-2} effects on monthly surface fluxes for North Eurasian lakes when changing from an unlimited to a 100 m fetch. Evaluation of model predictions of snow, ice, and sediment would benefit from the greater availability of measurements of snow thickness, ice thickness, and sediment temperatures at the same location as above-lake meteorological observations, including incident snowfall.

2.5.2 Ice and Snow

The largest model sensitivity we found for North Eurasian lakes was the presence or absence of snow insulation, which caused greater than 30 W m^{-2} monthly average changes in lake energy exchanges in the winter and summer. Indeed, while the historical development of climate models has generally emphasized snow over land surfaces rather than over lake and sea ice, snow there may have relatively larger importance (per unit area) because of the relatively larger sub-surface heat capacity and conductivity for water and ice in the absence of snow insulation. The inclusion of snow insulation may affect predictions of lake-climate interactions (Section 2.5.5).

We successfully introduced a new method for modeling ice in lakes, allowing each layer to have an independently variable ice fraction rather than separately modeling ice above water layers. This framework may allow for more realistic prediction of temperature gradients in ice and more flexible treatment of surface ice fractionation or slushy mixtures of ice and water. Using this framework, we tested the impact of suppressing convection and allowing mixtures of ice and water to occur when ice is greater than 0.3 m thick, and found relatively low impacts on regional surface energy exchanges.

Future work could improve the treatment of lake ice during periods of marginal ice cover. It may be possible to parameterize surface ice fractional cover, which can be important for large lakes (Goyette et al. 2000). Such an approach may be more robust than simply decreasing the albedo over melting ice to account for puddling and disintegration, by being able to predict the large observed albedo variability during melt. Our current implementation caused large changes in surface fluxes (16 W m^{-2}) compared to assuming a constant winter-time ice albedo, and may be an over-estimate of the albedo decrease, as it allows melting lakes to have an albedo as low as unfrozen lakes under some combinations of zenith angle and ice surface temperature. For small high-latitude lakes, recent work suggests that puddling over melting ice may be more typical for lakes that freeze to the bottom each winter (Arp et al. 2011); this information could be used in predicting albedo declines and suppression of convection in melting lakes.

2.5.3 Mixing in Small and Large Lakes

Previous studies have shown that lake models parameterizing total thermal diffusivity based on wind-driven eddies (Hostetler and Bartlein 1990) and molecular diffusivity alone under-predict mixing for large, deep lakes (Martynov et al. 2010; Perroud et al. 2009; Stepanenko et al. 2010). That behavior was confirmed for all four simulated deep lakes, except perhaps at one of three observation sites for Lake Michigan. In some cases, we found slight improvement when adding enhanced diffusivity under conditions of neutral stability to represent unresolved 3D

mixing processes (Fang and Stefan 1996), but this change was insufficient to bring thermal diffusivity to realistic levels. For deep lakes, we nearly always obtained substantial improvements in lake water temperature and surface flux predictions when we increased eddy diffusivity by 10, and in one case predictions were further improved when increasing by 100. This sensitivity is consistent with the large thermal diffusivities found by Martynov et al. (2010) to be required to substantially improve the simulation of Lake Michigan compared to surface temperature observations.

Some 1D lake models tend to assume greater mixing, including both simpler models like FLake and more sophisticated k-ε models like SIMSTRAT that predict the production, dissipation, and diffusion of turbulent kinetic energy. Consequently, these models can sometimes more accurately predict temperatures in large, deep lakes like Lake Michigan and Lake Geneva than does the Hostetler Model (Martynov et al. 2010; Perroud et al. 2009; Stepanenko et al. 2010). However, when these turbulence models are applied to small, shallow lakes (e.g., Sparkling Lake), they can sometimes over-predict mixing, causing temperature predictions to not match observations as well as simpler models (Stepanenko et al. 2010). This discrepancy may be because the additional sources of turbulent kinetic energy parameterized in these models may be serving as a proxy for advection induced in large lakes by horizontal temperature gradients not able to be represented in 1D models, or that these models parameterize insufficient dissipation of turbulent kinetic energy for small lakes.

Further research is needed to bridge the gap between large and small lakes in GCM-scale lake models. For global simulations with CLM4-LISSS described here, it may be advisable to increase eddy diffusivity by a factor that depends on lake shape, and future research should systematically investigate the relationship between mixing strength and lake geometry. For now, we recommend increasing the eddy diffusivity by 10 for lakes larger and deeper than some threshold (e.g., 5 km^2 and 30 m). Additional research should also be undertaken to couple k-ε models into climate models. Another approach would be to couple 3D models into climate models for large lakes where detailed bathymetry is available (Leon et al. 2007; Song et al. 2004).

In any case, surface flux changes resulting from 10 times increased eddy diffusivity in our model were comparable in magnitude to those changes resulting from changes in modeled lake depth. Given the challenges in interpolating from fine-scale variation in lake depth to a single or small number of lake depths at the GCM scale, under-prediction of mixing for large lakes may be relatively unimportant for global simulations except in the vicinity of very large lakes like the Great Lakes. Indeed, the majority of global lake area is occupied by much smaller lakes (Kourzeneva 2010; Lehner and Doll 2004) for which CLM4-LISSS performance is very good.

2.5.4 Uncertain Parameters for Global Simulations

We found moderate changes in surface fluxes when the modeled lake depths of North Eurasian lakes were varied across a typical range. Until recently, most global simulations assumed constant lake depth. Fine resolution global data on lake depth are becoming available (Kourzeneva 2010), although spatial coverage is far from complete. It may also be possible to invert for lake depth by comparing modeled surface temperature to remotely sensed surface temperature (Balsamo et al. 2010; Dutra et al. 2010). However, in our current implementation, as

in many other GCMs, only one lake is modeled in each gridcell, so even allowing the lake depth to vary between gridcells is a crude representation of real lake depths since most lakes are much smaller than the grid scale. Different interpolation approaches could be used to aggregate observed lake depths at finer scales to calculate the single representative gridcell lake depth, but it is not clear what the optimum gridcell depth would be. The optimum lake depth may depend on the model structure and intended application. A more sophisticated approach would be that used in Samuelsson et al. (2010), where several lakes of different depth categories are explicitly modeled in each RCM gridcell. Further research is needed to identify how best to aggregate lakes into depth categories.

Increasing the extinction coefficient from an average of 0.46 m^{-1} to a constant 1.0 m^{-1} for North Eurasian lakes caused large changes in surface fluxes and differences between summer surface and lake bottom temperatures, despite being a relatively small change compared to the large variability of observed values (0.05 to 7.1 m^{-1} just for the lakes simulated in this study). Such increases in thermal stratification with increased opacity have been observed elsewhere and could affect lake-climate interactions (Section 2.5.5). The surface flux changes were similar in seasonal pattern but larger in magnitude than those resulting when decreasing the depth from a median of 10 m to a constant 5 m. Consequently, global data on lake opacity may be as important as, or more important than, global data on lake depth. It may be possible to retrieve lake opacity from satellite observations (Gomez et al. 2009; Koponen et al. 2002; Zhang et al. 2003). However, without explicitly modeling several lakes of different optical categories in each gridcell, it is unclear what the optimum extinction coefficient should be for the single modeled lake in each gridcell, or whether such an optimum value would be model-dependent. Moreover, we assumed that the extinction coefficient is not related to albedo, but further work is needed to understand the relationship, if any, between lake opacity and albedo.

In contrast, global data on lake fetch may be less important. While using excessively large values of roughness lengths may degrade simulations, and lake geometry may influence lake temperature in other ways, model predictions were relatively insensitive even to extreme changes in the fetch from unlimited to 100 m. This low sensitivity may be because, using the Zilitinkevich et al. (2001) relationships, predicted scalar roughness lengths were relatively insensitive to changes in the momentum roughness length with fetch. However, we did not analyze changes in momentum flux, and it is unclear if these changes could be important in coupled simulations. In any case, retrieval of approximate lake horizontal dimensions from remote sensing should be relatively straightforward, so we still recommend the creation of a global dataset to eliminate this small source of uncertainty in global simulations.

2.5.5 Lake-Climate Interactions

Reducing surface roughness lengths and correcting errors in surface flux calculation reduced latent heat fluxes and delayed their seasonal peak in CLM4-LISSS compared to the existing CLM4 lake model, consistent with observations. While Bonan (1995) found large summer increases in latent heat fluxes at all latitudes when adding lakes to a GCM, the decreased roughness length and increased thermal inertia of lakes could tend to decrease latent heat fluxes compared to surrounding land area in the early summer, particularly at high latitudes, where there is large seasonal temperature variation and soil evaporation tends not to be moisture-limited. Samuelsson et al. (2010) found net regional summer warming resulting from lakes in

Northern Europe. Dutra et al. (2010) found regional cooling at all latitudes, but increases in latent heat fluxes only occurred at low latitudes, while decreases occurred at high latitudes, consistent with the findings of Lofgren (1997) for the Great Lakes and Krinner (2003) and Krinner and Boike (2010) for high latitudes. These results suggest that energy uptake by lakes may be more important than increasing latent heat fluxes as a summer cooling mechanism at temperate and high latitudes.

Studies tend to agree that lakes increase autumn heat fluxes and surface temperatures (Bonan 1995; Dutra et al. 2010; Lofgren 1997; Rouse et al. 2008; Samuelsson et al. 2010). In the winter, however, ice and snow model details are important. For example, studies tend to find that lakes cause warming when snow insulation is not modeled (Bonan 1995; Lofgren 1997; Samuelsson et al. 2010), while Dutra et al. (2010) found slight, if any, warming when snow insulation was present. (We note that the winter warming reported in Lofgren (1997) may be realistic, as the Great Lakes often do not completely freeze.) Krinner and Boike (2010), using a model with snow insulation, found that a fraction of the predicted autumn warming caused by lakes extended into the winter under present climate, while most of the autumn warming persisted into the winter under future climate; this discrepancy may be due to decreased snow thickness, but these results were not reported. The dependency on snow insulation of the winter atmospheric response to lakes is consistent with the large increases we found in winter energy fluxes from lakes to the atmosphere when eliminating snow insulation. We note that ignoring the heat of fusion caused half as large changes in flux but of the opposite sign, even though both changes tended to make lake ice surfaces colder in the winter: snow insulation keeps the lake ice from being exposed to cold atmospheric temperatures, while heat of fusion increases the thermal inertia of the lake itself.

Due to the potential for climate change to interact with thermokarst lake area (Smith et al. 2005), future studies should investigate the effects of these changes on regional climate (Krinner and Boike 2010). Other land cover change experiments have shown changes in atmospheric circulation or remote atmospheric conditions (Bala et al. 2007; Feddema et al. 2005a; Feddema et al. 2005b), but it is not clear if this could result from changing lake area. For studies showing increasing summer latent heat fluxes and surface cooling for regions with large lake area, it is unclear how this additional water vapor affected atmospheric conditions elsewhere. We address some of these questions in Chapter 3.

Lake opacity may also interact with climate change, as both increasing opacity and increasing air temperatures can enhance summer stratification. Changes in climate and watershed properties can affect lake biology by changing temperature and the concentrations of dissolved nutrients and oxygen (Kosten et al. 2009; MacKay et al. 2009; Peeters et al. 2007; Verburg and Hecky 2009), and lake biology is a primary determinant of opacity (Cristofor et al. 1994). Like previous observational and modeling studies (Cristofor et al. 1994; Hocking and Straskraba 1999; Houser 2006; Mazumder and Taylor 1994; Mazumder et al. 1990; Persson and Jones 2008), we found that increased opacity increases summer stratification, and we also found large effects on surface energy fluxes. Although the extinction coefficient may be estimated using remote sensing or model inversions, these approaches will not be able to predict future changes in opacity under climate change or anthropogenic manipulation of watersheds. To do so would require explicitly modeling lake hydrology and biogeochemistry, including water and nutrient

inputs, so that the lake water content, dissolved nutrient and oxygen concentrations, and biological activity can be predicted.

2.6 Conclusions

The existing CLM4 lake model performance was poor, with unrealistic predictions of water temperatures and surface fluxes for all four lakes simulated, likely attributable both to deficiencies in model structure and to errors in surface flux and lake temperature calculations (Section 2.8). The new CLM4 lake model (CLM4-LISSS) matched observations of water temperatures and surface fluxes very well for three small temperate and boreal lakes where local meteorological forcing observations were available. Biases in larger lakes were modest and comparable to those associated with uncertainty in lake characterizations (e.g., depth, opacity). Based on our analyses, we conclude that CLM4-LISSS is suitable for inclusion in global climate studies.

Neglecting the fact that lakes have much smaller effective aerodynamic roughness lengths than other land types represented in land surface models will lead to large biases in predicted surface fluxes and surface temperature. These resulting biases will be large compared to the effects of fetch and depth limitations on wave development.

Other missing processes in lake models or unavailable parameter data for global simulations can cause very large seasonal biases in local surface flux predictions of up to 30 W m^{-2}, highlighting needs for future research. Either neglecting snow insulation or the energy exchanges associated with phase change will lead to large declines in predicted winter lake ice temperatures, but with opposite effects on predicted surface fluxes and summer lake water temperatures. Observed lake opacity varies over more than two orders of magnitude, but even moderate variation in opacity caused larger changes in predicted surface fluxes than typical lake depth variation in our simulations. Consequently, global datasets of lake opacity should be developed based on remote sensing, and research should be undertaken to predict how lake optics might change under anthropogenic climate change and watershed manipulation. Decreases in frozen lake albedo during spring thaw can accelerate melt by a week or more at high latitudes, but current 1D model parameterizations are relatively crude.

Wind-driven eddy mixing predicted by the Hostetler Model was insufficient for simulating large lake surface fluxes and water temperatures; predictions were nearly always improved by increasing eddy diffusivity by a large factor to account for unresolved 3D processes. Errors in surface fluxes that might result from insufficient mixing in large lakes were comparable to errors resulting from missing information on lake depth or opacity. Further research is needed to bridge the gap in model performance between small and large lakes for lake models coupled into climate models.

2.7 Acknowledgements

Andrey Martynov (Université du Québec à Montréal) provided processed data for Sparkling Lake (collected by the University of Wisconsin Center for Limnology) and important insight during model development. Victor Stepanenko (Moscow State University) provided processed data for Kossenblatter Lake (collected by the Lindenberg Meteorological Observatory and Richard Aßmann Observatory), helpful feedback during discussion of model results, and detailed

comments on a draft manuscript. Marjorie Perroud (Switzerland Federal Office for the Environment) provided detailed comments on a draft manuscript. Annika Nordbo (University of Helsinki) provided processed data for Lake Valkea-Kotinen. Margaret Torn (Lawrence Berkeley National Laboratory) provided high-level guidance and advice. David Lawrence (National Center for Atmospheric Research) provided support in using and modifying the CLM code and getting feedback from the CLM community. Two anonymous reviewers also provided very helpful suggestions for revising the manuscript. This work was supported by the Director, Office of Science, Office of Biological and Environmental Research, Climate and Environmental Science Division, of the U.S. Department of Energy under Contract No. DE-AC02-05CH11231 to Berkeley Lab.

2.8 Appendix: Deficiencies in the Existing CLM4 Lake Model

2.8.1 Comments on Model Formulation

In addition to the structural simplifications of the existing CLM4 lake model (e.g., lack of phase change and snow insulation), there are a number of unrealistic assumptions and errors in model formulation that contribute to the unphysical behavior of the model: an error in the eddy diffusivity calculation; the assumption that convection does not occur when the top of the lake is colder than freezing; excessively large surface roughness lengths; an error in the calculation of surface fluxes and surface temperature; and an unrealistic decoupling of the surface and the top water layer.

Two issues contribute to predictions in the existing CLM4 lake model of excessively mixed lakes in the summer and insufficiently mixed lakes in the winter. In the calculation of the wind-driven eddy diffusivity (Oleson et al. (2010), p. 184, Eq. 9-45), the equation is not corrected for the fact that the CLM4 code defines the z-coordinate as positive downwards while Hostetler and Bartlein (1990) define it as positive upwards. Thus, the square of the Brunt-Väisälä frequency is always calculated as negative and reset to zero by a flag in the code restricting it to be non-negative before a square root is taken. Consequently, the eddy diffusivity is always calculated as if the lake were perfectly neutrally stable, making the eddy diffusivity much larger than it should be when stratification occurs. In addition, the model does not allow convection to occur in the liquid portion of the lake when the top of the lake is colder than freezing, but this constraint is unphysical.

In the existing CLM4 lake model, the surface roughness lengths are set to constant values of 10 mm for unfrozen lakes and 40 mm for frozen lakes, which are much larger than values found in the literature for lakes, ocean, and sea ice. In Section 2.4.1.1, we showed that such large roughness lengths (in an otherwise unchanged CLM4-LISSS) yielded low surface temperatures, high latent heat fluxes, and low sensible heat fluxes during the summer over two lakes, as compared with observations.

An error and an unrealistic assumption in the calculation of surface fluxes tend to decrease water temperatures, increase latent heat fluxes, and increase diurnal surface temperature variation. In both the existing CLM4 lake model and CLM4-LISSS, Eq. 2.13 is solved using the Newton-Raphson method:

2.33

$$\Delta T_g = \frac{S + L - H - \lambda E - G}{-\frac{\partial L}{\partial T_g} + \frac{\partial H}{\partial T_g} + \lambda \frac{\partial E}{\partial T_g} + \frac{\partial G}{\partial T_g}}, \quad \textbf{Eq. 2.16}$$

where ΔT_g is the change in predicted surface temperature between iterations. However, in the existing CLM4 lake model [Eq. 9.10 on p. 176 in Oleson et al. (2010)], the term *S* corresponds to the *total* absorbed shortwave radiation for the lake, *not* the fraction absorbed at the surface (as is used in Eq. 2.14 here). Energy is still conserved, as the correct expression is used when calculating *G*, which is then used as the top boundary condition for the temperature solution of the lake body. However, this tends to increase the surface temperature and heat fluxes during the daytime at the expense of energy entering the lake. In addition, the thermal diffusivity between the surface and the top model layer only includes molecular diffusivity, which will be several orders of magnitude smaller than the eddy diffusivity for unfrozen lakes. Moreover, the surface temperature T_g is not corrected for convection within the top lake layer when the calculated T_g implies an unstable density profile in the top lake layer. These two assumptions create an unrealistic decoupling between the surface and the top lake layer, hiding the effect of the error in *S* during the daytime but also allowing for unrealistically low night-time and autumn surface temperatures and large daily temperature variability.

2.8.2 Unphysical Behavior of the Existing CLM4 Lake Model Compared to Observations

The issues described above have a synergistic effect in producing excessively cold, well-mixed lakes with excessive latent heat flux, insufficient or negative sensible heat flux, low night-time and autumn surface temperatures, and excessive surface temperature variability. These effects were evident in Sparkling Lake (Section 2.4.1.1) and all three other lakes where the existing CLM4 lake model was evaluated. The simulated Lake Michigan remained well-mixed (not shown) at a constant temperature during the entire unfrozen season (Supp. Fig. 2.8). Summer near-surface water temperatures were too cold, and the lack of phase change and the suppression of convection for lakes with surface temperature below freezing contributed to unrealistic autumn temperature variability and a sometimes unstable vertical temperature profile. The surface and 0.05 m water temperatures are shown separately to illustrate their unrealistic decoupling; the simulated surface temperature had unrealistically large daily variability and tended to closely follow the air temperature (not shown), seasonally leading both the observed and simulated lake near-surface temperatures. The simulation of Great Slave Lake yielded an early summer peak in both latent and sensible heat fluxes, insufficient summer stratification, a very early initial autumn surface freeze-up, and unrealistic autumn near-surface water temperature variability with a sometimes unstable vertical temperature profile (Supp. Fig. 2.9). The surface temperature showed the same unphysical behavior as for Lake Michigan. Lake McIlwaine was predicted to be well-mixed throughout the year with little seasonal temperature variation, inconsistent with observations (Supp. Fig. 2.7c-d).

2.9 Figures

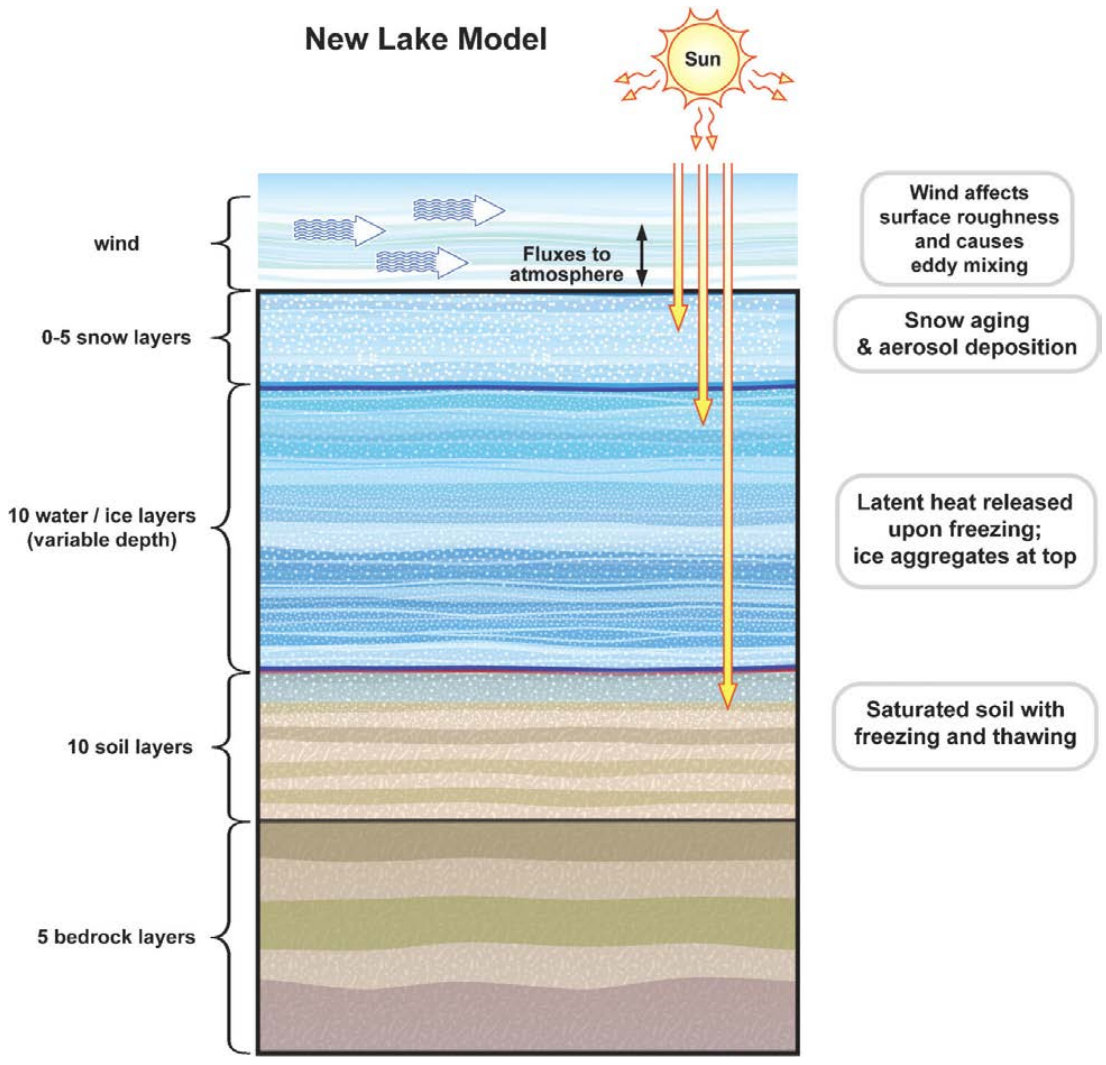

Fig. 2.1: Lake model schematic.

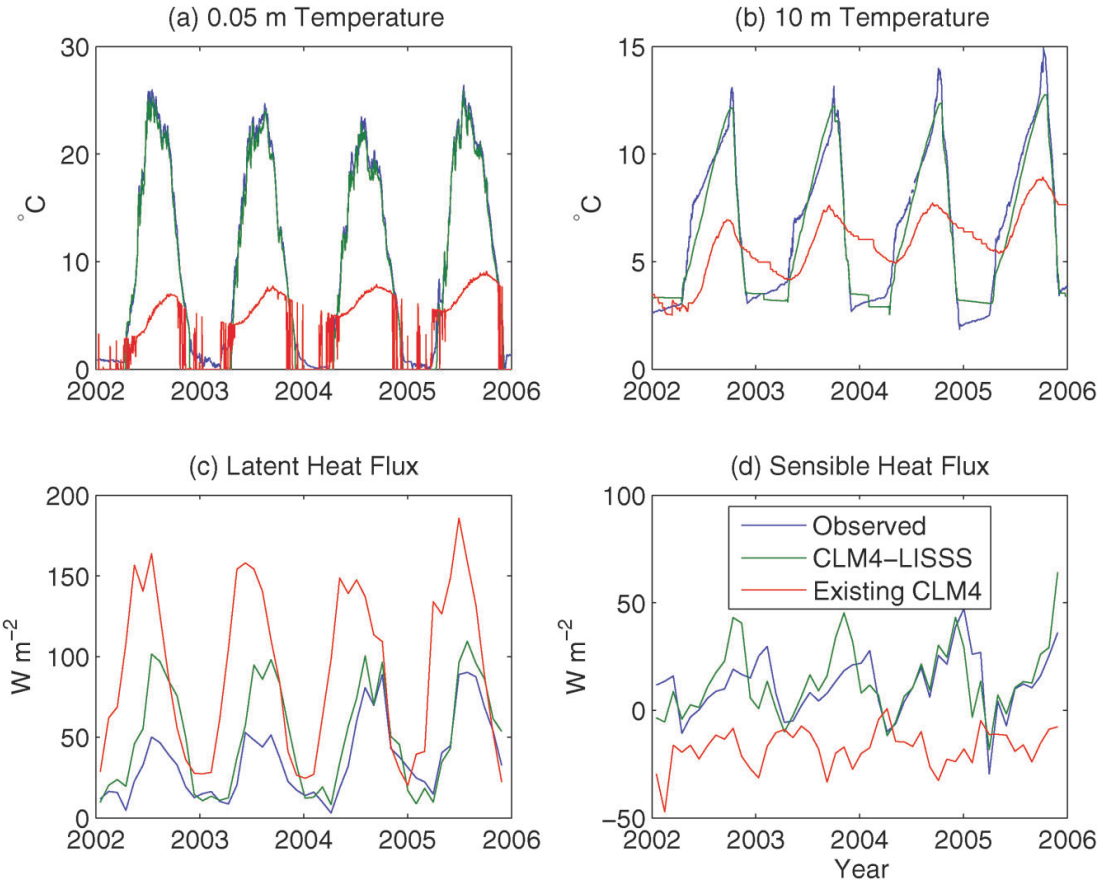

Fig. 2.2: Daily mean Sparkling Lake water temperatures and 30-day mean surface energy fluxes, 2002-2005, observed, simulated by CLM4-LISSS, and simulated by the existing CLM4 lake model: (a) 0.05 m water temperature (below-freezing temperatures are not shown, as surface observations are typically flawed during these periods); (b) water temperature at 10 m depth; (c) latent heat flux; and (d) sensible heat flux.

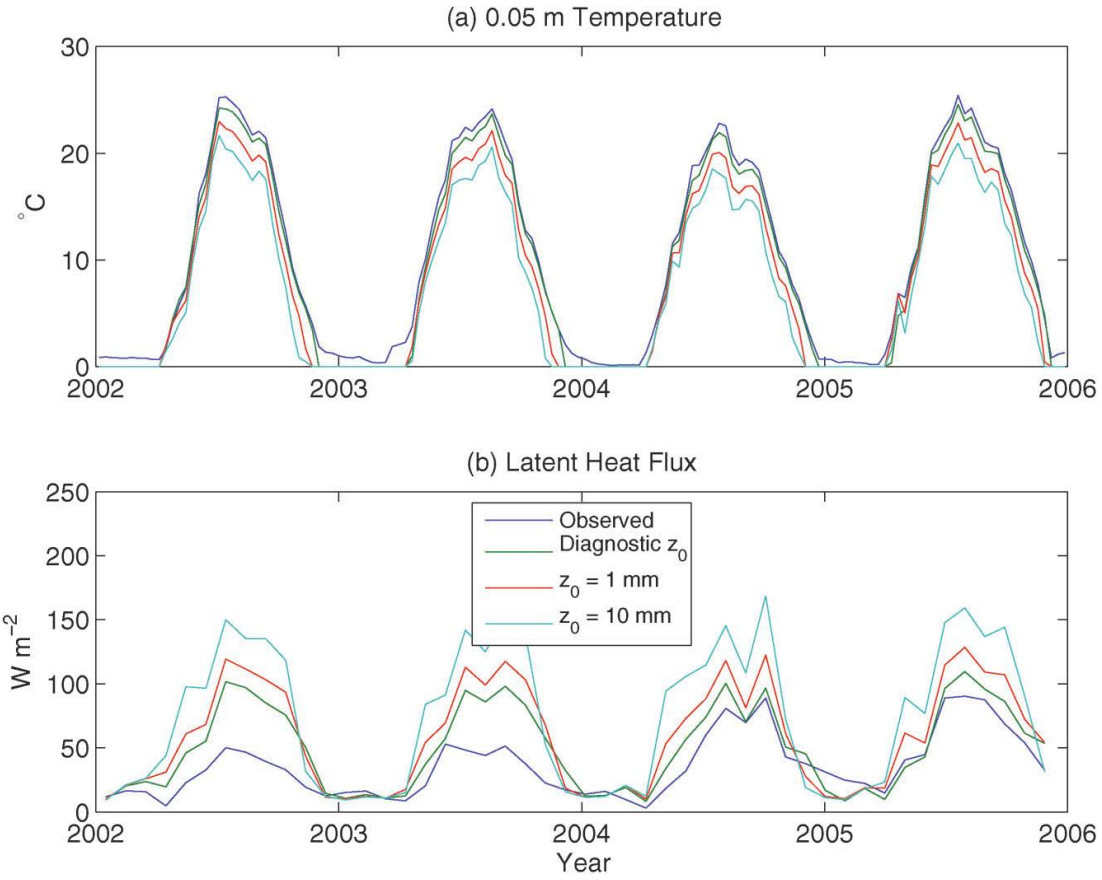

Fig. 2.3: Ten-day mean Sparkling Lake (a) 0.05 m temperature and (b) latent heat flux, 2002-2005, observed and simulated by CLM4-LISSS with diagnostic roughness lengths, fixed 1 mm roughness lengths, and fixed 10 mm roughness lengths. Near-surface below-freezing temperatures are not shown, as surface observations are typically flawed during these periods.

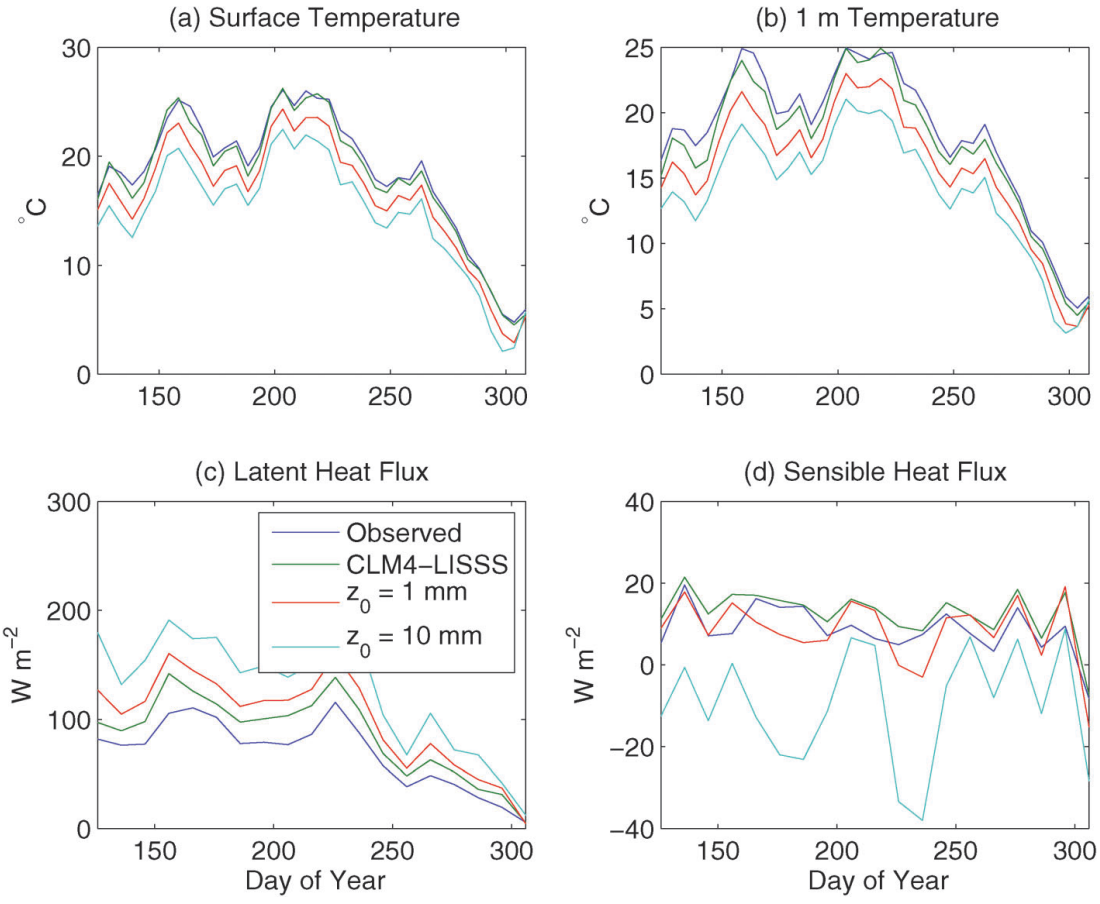

Fig. 2.4: Five-day mean Kossenblatter water temperatures and surface energy fluxes, May – November, 2003, observed and simulated by CLM4-LISSS with diagnostic roughness lengths, fixed 1 mm roughness lengths, and fixed 10 mm roughness lengths: (a) surface temperature; (b) temperature at 1 m depth; (c) latent heat flux; and (d) sensible heat flux.

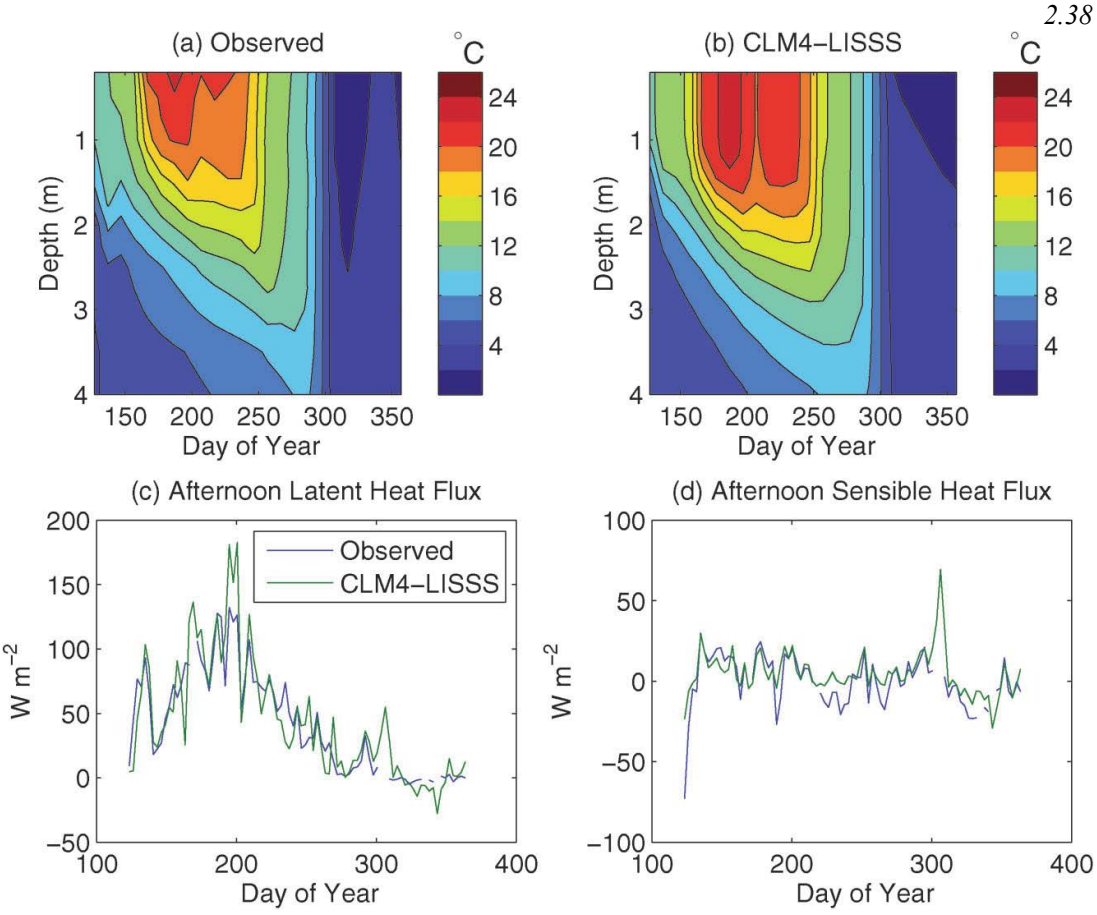

Fig. 2.5: Lake Valkea-Kotinen, May – December, 2006. Ten-day mean water temperatures: (a) observed (Nordbo et al. 2011); and (b) simulated by CLM4-LISSS. Three-day mean (over available data for the sporadic observations) 12-6 PM surface energy fluxes, observed and simulated: (c) latent heat flux; and (d) sensible heat flux.

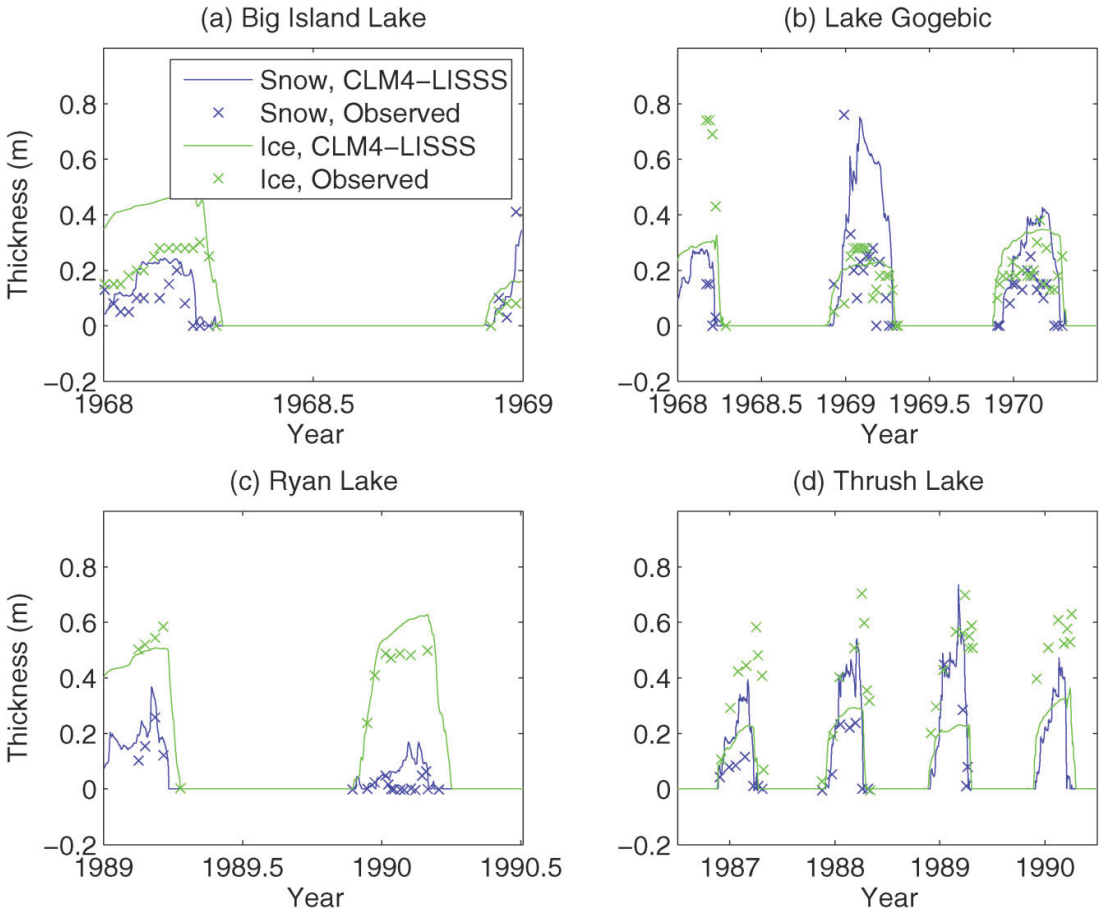

Fig. 2.6: Snow thickness and ice thickness, simulated by CLM4-LISSS and observed, for (a) Big Island Lake; (b) Lake Gogebic; (c) Ryan Lake (Gu and Stefan 1993); and (d) Thrush Lake (Fang and Stefan 1996).

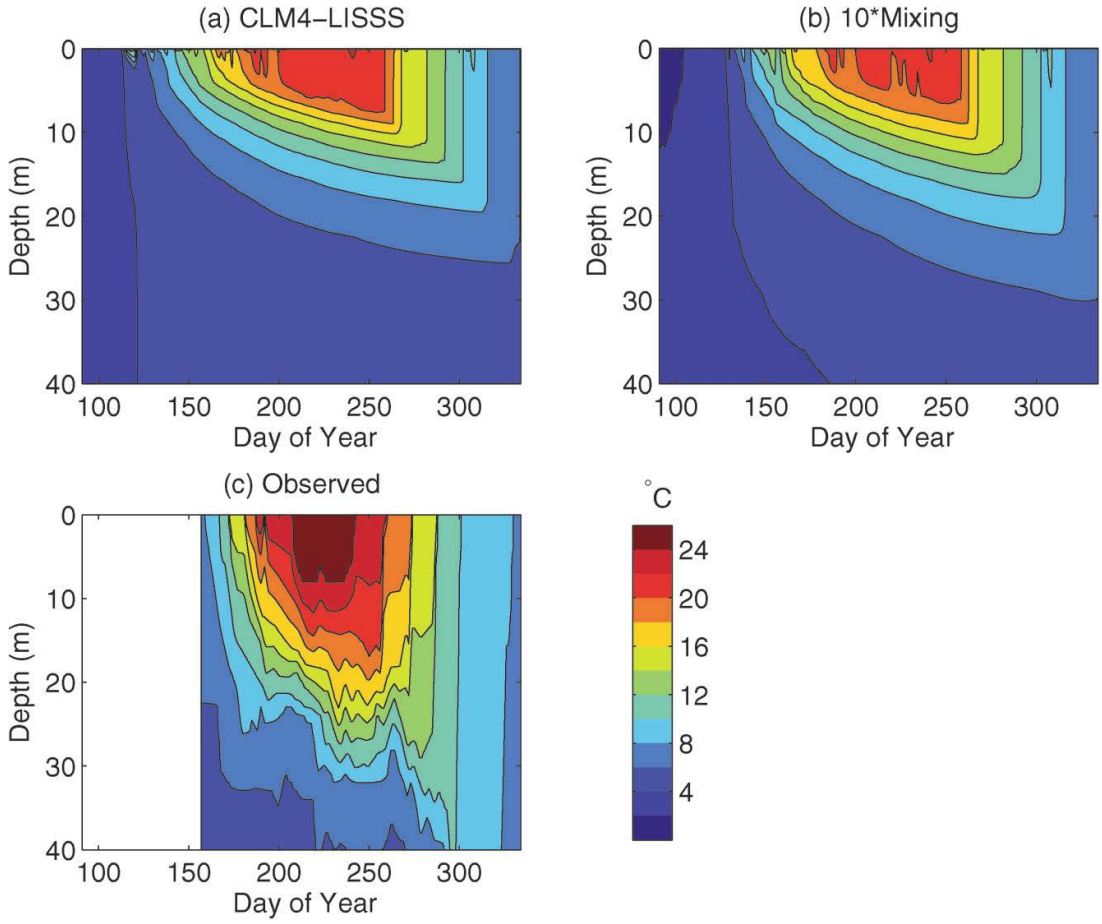

Fig. 2.7: Daily mean Lake Michigan water temperatures for 1990: (a) CLM4-LISSS; (b) CLM4-LISSS with eddy diffusivity increased by 10; and (c) observed (McCormick and Pazdalski 1993).

2.41

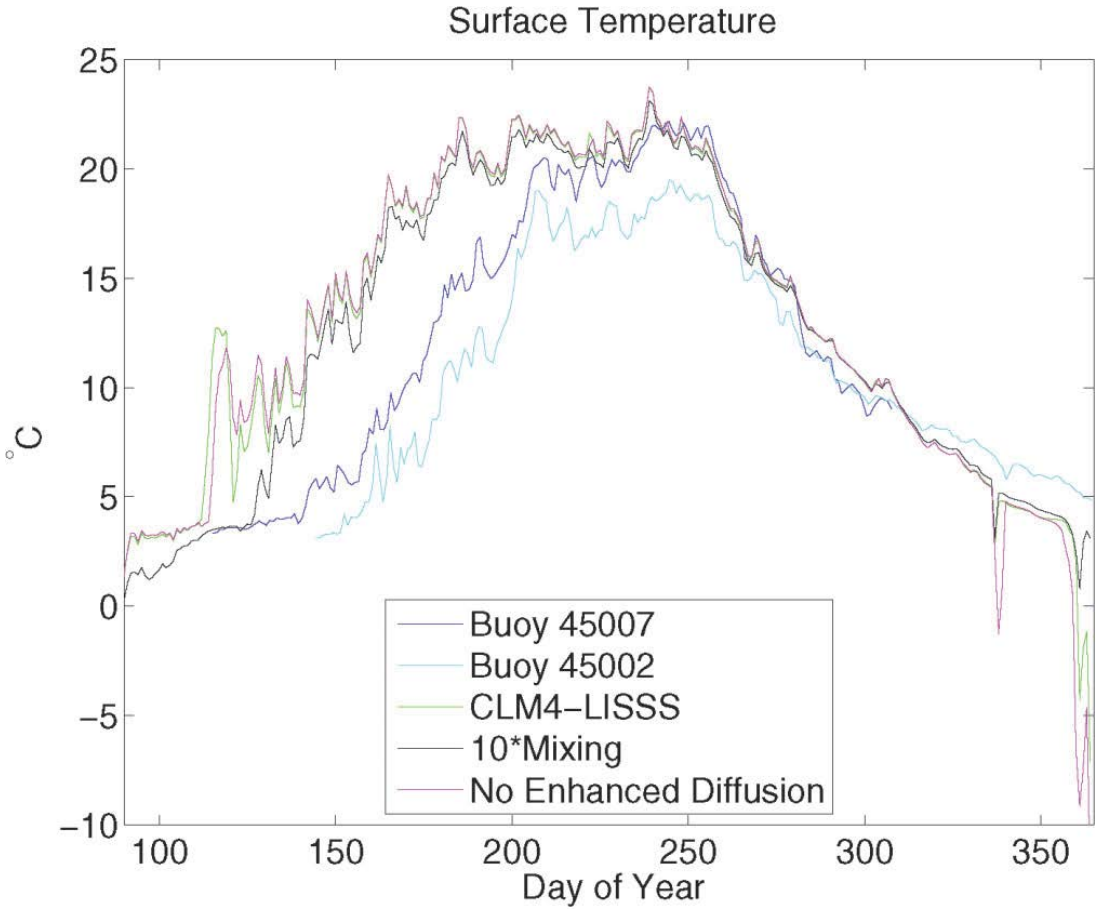

Fig. 2.8: Daily mean Lake Michigan surface temperatures for 1990: National Data Buoy Center Station 45007 observations, National Data Buoy Center Station 45002 observations, and simulated by CLM4-LISSS, CLM4-LISSS with eddy diffusivity increased by 10, and CLM4-LISSS with no enhanced diffusion.

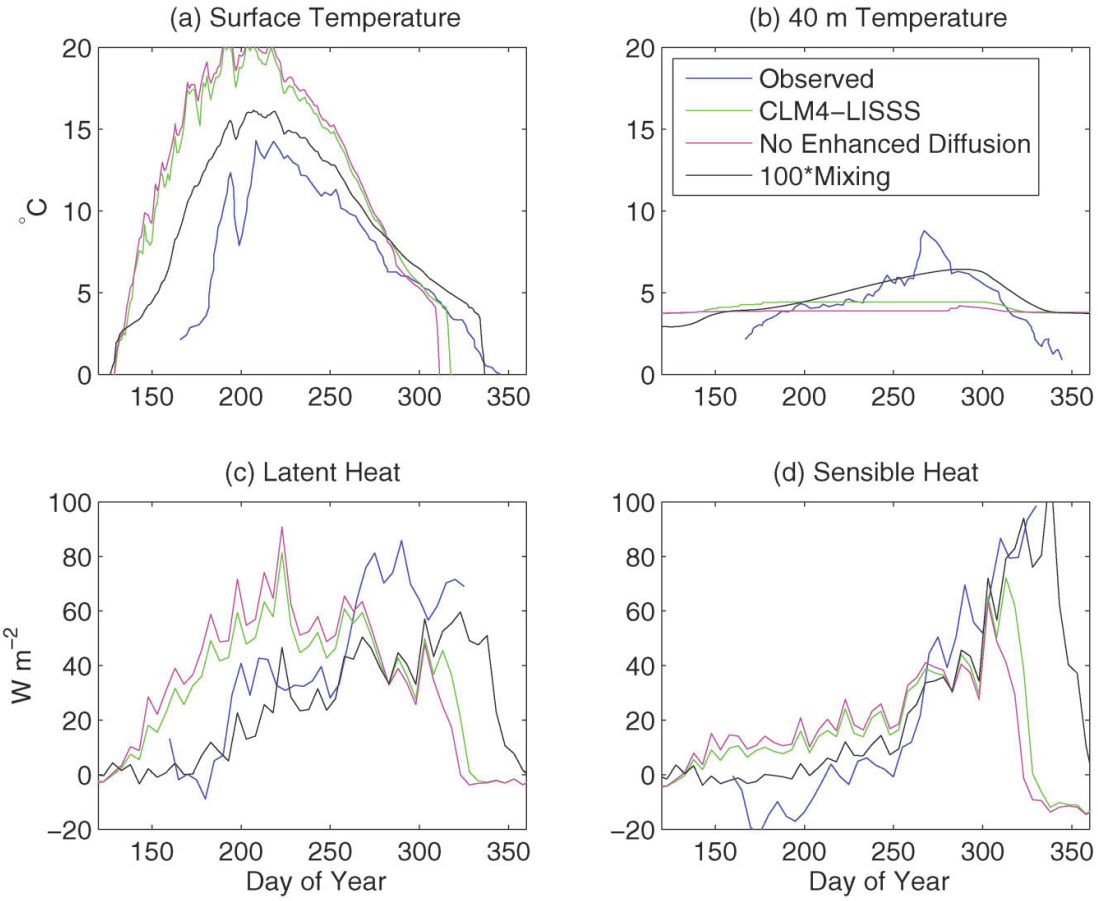

Fig. 2.9: Daily-averaged Great Slave Lake water temperatures and surface fluxes from 1997-2003 excluding 2001, observed (Rouse et al. 2008) and simulated by CLM4-LISSS, CLM4-LISSS with no enhanced diffusion, and CLM4-LISSS with eddy diffusivity increased by 100: (a) surface temperature; (b) temperature at 40 m depth; (c) latent heat; and (d) sensible heat.

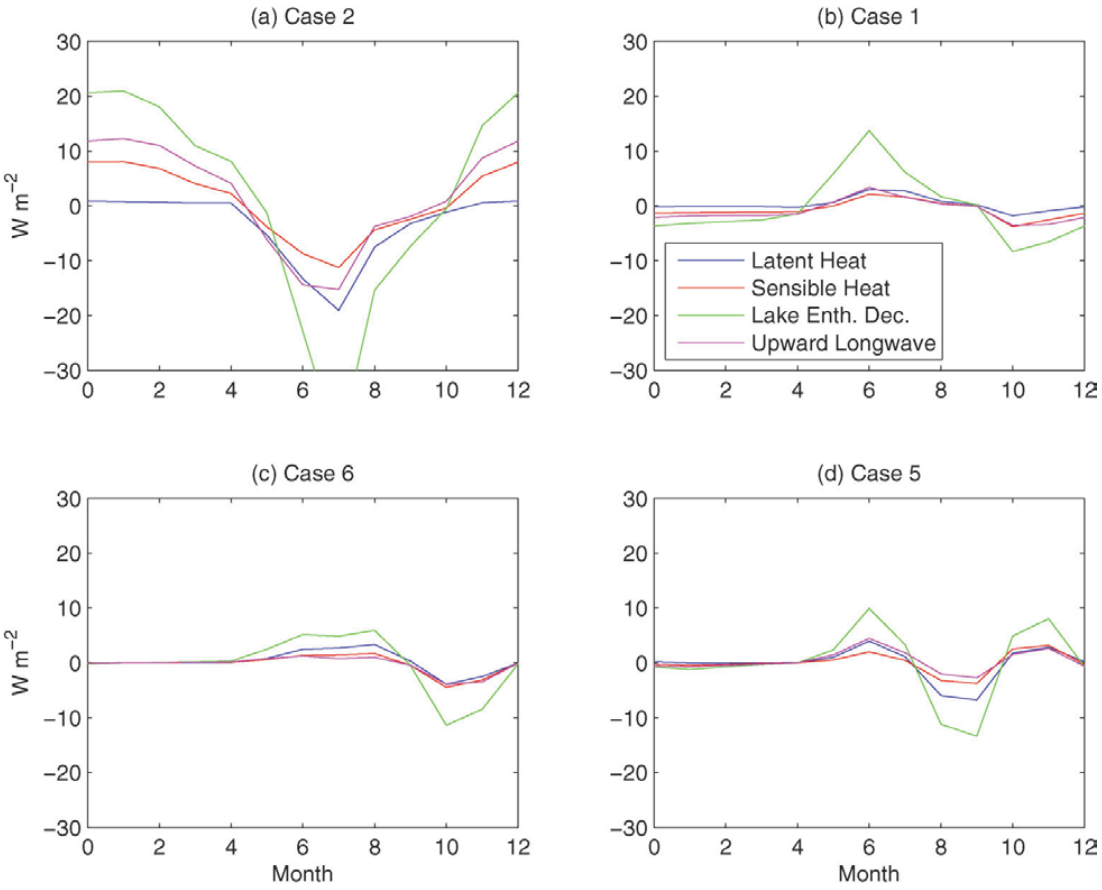

Fig. 2.10: Monthly average surface flux anomalies for North Eurasian (60 – 90°N, 0 – 175°E) lakes, latent heat, sensible heat, rate of lake enthalpy decrease, and upward longwave: (a) Case 2, no snow insulation; (b) Case 1, no heat of fusion for phase change; (c) Case 6, lake depth = 5 m; and (d) Case 5, lake depth = 50 m.

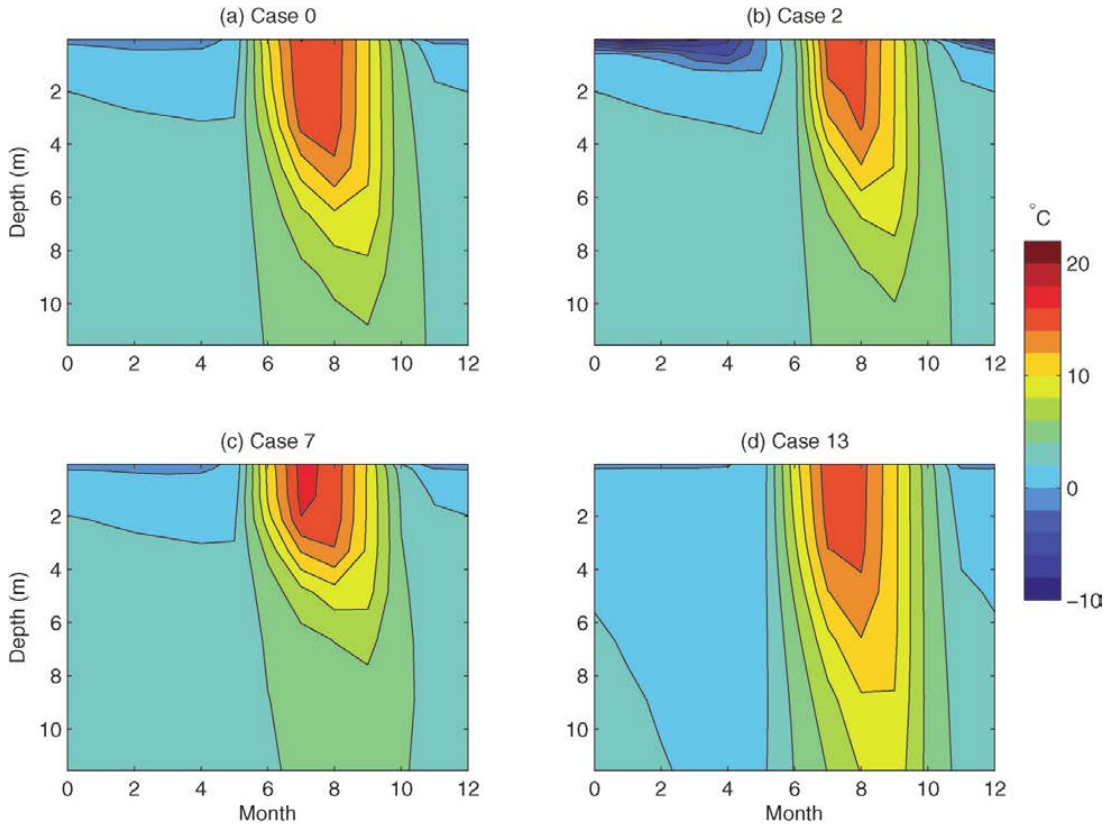

Fig. 2.11: Monthly average water temperatures for the gridcell co-located with Finnish Lake Inari: (a) Case 0, baseline; (b) Case 2, no snow insulation; (c) Case 7, extinction coefficient = 1.0 m^{-1}; and (d) Case 13, eddy diffusivities increased by 10.

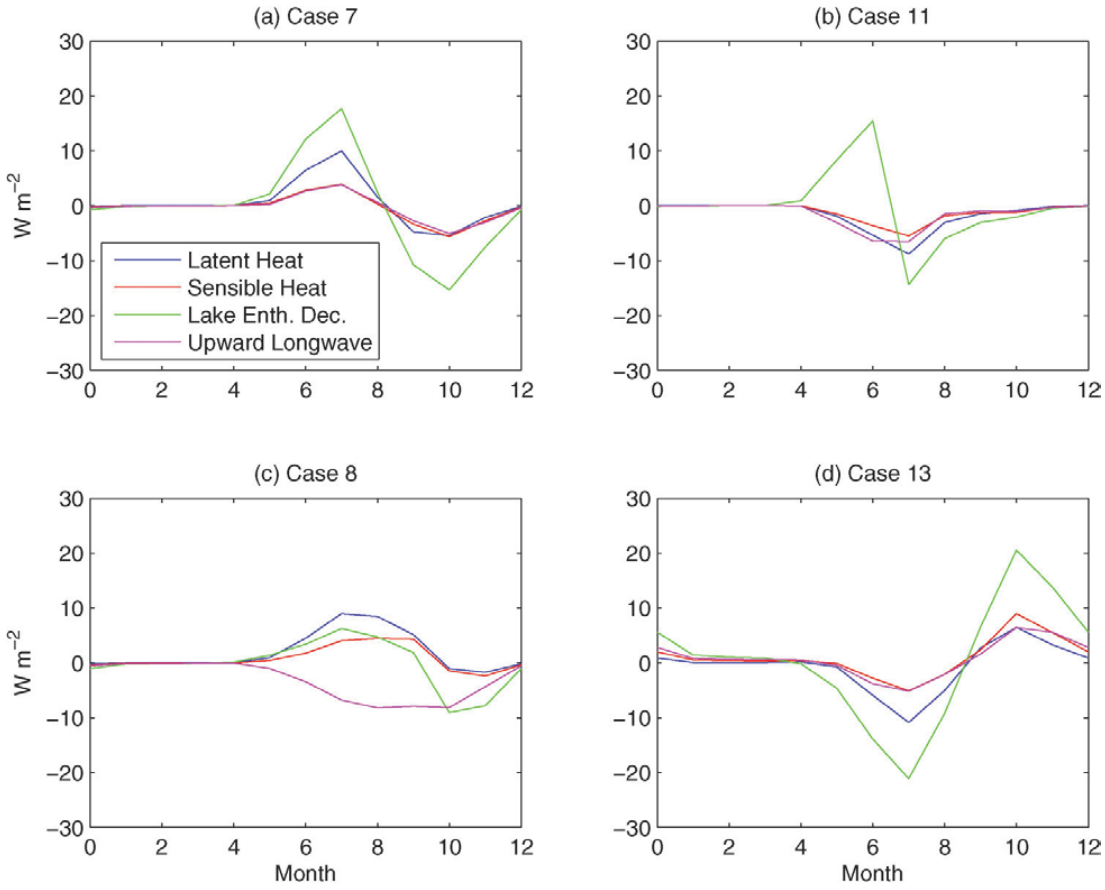

Fig. 2.12: Monthly average surface flux anomalies for North Eurasian (60 – 90°N, 0 – 175°E) lakes, latent heat, sensible heat, rate of lake enthalpy decrease, and upward longwave: (a) Case 7, extinction coefficient = 1.0 m^{-1}; (b) Case 11, no albedo correction for melting lakes; (c) Case 8, roughness lengths = 1 mm; and (d) Case 13, eddy diffusivities increased by 10.

2.10 Tables

Table 2.1: Simulated Lakes

Name	*Location (°N, °E)*	*Depth (m)*	*η (m^{-1})*	*Fetch (km)*	*Forcing*	*Spinup (yr)*	*Evaluation Period*	*Variables Evaluated*	*References*
Sparkling	46.01, -89.70	18	0.27	0.5	Obs.	5	2002-2005	WT, SF	(Martynov et al. 2010); lter.limnology.wisc.edu
Kossenblatter	52.13, 14.1	2	7.08	1.0	Obs.	5	05/2003-11/2003	WT, SF, ST	(Beyrich et al. 2006); Lindenberg Meteorological Observatory, Richard Aßmann Observatory, DWD, Germany
Valkea-Kotinen	61.24, 25.06	6	3.1	0.3	Obs.	2	05/2006-12/2006	WT, SF	(Nordbo et al. 2011; Vesala et al. 2006); www.atm.helsinki.fi
Michigan	44, -87	160	N/A	60	NCEP	40	04/1990-12/1990	WT, ST	(McCormick and Pazdalski 1993); www.ndbc.noaa.gov (Stat. 45002, 45007)‡
Great Slave	61.6, -114.0	90	N/A	65	NCEP	40	1997-2003	WT, SF	(Rouse et al. 2008)
Ryan	45.04, -93.32	11	0.5	0.2	NCEP	9	1989-1990	IsT	(Gu and Stefan 1993)
Thrush	47.90, -90.50	14	0.45	0.2	NCEP	10	1986-1991	WT, IsT	(Fang and Stefan 1996)
Big Island	46.18, -86.50	11	N/A	0.2	NCEP	8	1968	IsT	(Sleator 1995); nsidc.org/data/g00803.html (Stat. 210)
Gogebic	46.60, -89.58	5	N/A	3.0	NCEP	7	1968-1970	IsT	(Sleator 1995); nsidc.org/data/g00803.html (Stat. 128)
Karujärv	58.38, 22.22	2	2.0	0.15	NCEP	3	1979-1987	WT, IsT	(Vassiljev et al. 1994)
Raksjo	60.03, 17.08	10	0.54	0.6	NCEP	4	05/1995-09/1995	WT, ST	(Elo 2007)
Crater	42.93, -122.10	500	0.05	4.0	NCEP†	64**	1988-2000	WT	(Larson et al. 2007)
McIlwaine*	-17.90, 30.80	25	N/A	2.0	NCEP	45	08/1975-02/1976	WT	(Robarts and Ward 1978)

Notes. **McIlwaine*: Now appears to be part of Zimbabwe and renamed Lake Chivero. *Depth*: The depth used for simulation, which is the mean depth, the maximum depth, or the depth at the measurement site. η: The extinction coefficient used for simulation; N/A

means the default depth-based expression based on Hakanson (1995) was used. *Forcing*: NCEP = 2° global reanalysis data processed for CESM (1948-2004) (Qian et al. 2006). †Because Crater Lake is about 900 m above the forcing gridcell average altitude, we subtracted 6°C from the forcing temperature and 7500 Pa from the forcing pressure. ***Spinup*: Crater Lake was spun up for 25 years (1948-1972) with 10,000 times increased eddy diffusivity before 39 years of conventional spinup. *Variables evaluated*: WT = water temperature; SF = surface fluxes; ST = surface temperature; IsT = ice & snow thickness. We note that a short period of data on sediment temperatures was available in Gu and Stefan (1993), but this data were insufficient to effectively evaluate CLM4-LISSS in the absence of more detailed data (e.g., sediment characteristics, near-lake meteorological conditions). ‡*References*: for Lake Michigan, these 2 buoys were selected because they were located mid-lake and relatively close to the simulated point corresponding to the McCormick and Pazdalski (1993) observations; several other buoys were located on the shoreline.

References

Ahrens, T. J., 1995: *Rock physics & phase relations : a handbook of physical constants.* American Geophysical Union.

Anctil, F., and M. A. Donelan, 1996: Air-water momentum flux observations over shoaling waves. *J. Phys. Oceanogr.*, 26, 1344-1353.

Andreas, E. L., 1987: A Theory For The Scalar Roughness and the Scalar Transfer-Coefficients over Snow and Sea Ice. *Boundary-Layer Meteorology*, 38, 159-184.

Arp, C. D., B. M. Jones, F. E. Urban, and G. Grosse, 2011: Hydrogeomorphic processes of thermokarst lakes with grounded-ice and floating-ice regimes on the Arctic coastal plain, Alaska. *Hydrological Processes*, 25, 2422-2438.

Atakturk, S. S., and K. B. Katsaros, 1999: Wind stress and surface waves observed on Lake Washington. *J. Phys. Oceanogr.*, 29, 633-650.

Bala, G., K. Caldeira, M. Wickett, T. J. Phillips, D. B. Lobell, C. Delire, and A. Mirin, 2007: Combined climate and carbon-cycle effects of large-scale deforestation. *Proceedings of the National Academy of Sciences of the United States of America*, 104, 6550-6555.

Balsamo, G., E. Dutra, V. M. Stepanenko, P. Viterbo, P. M. A. Miranda, and D. Mironov, 2010: Deriving an effective lake depth from satellite lake surface temperature data: a feasibility study with MODIS data. *Boreal Environment Research*, 15, 178-190.

Bates, G. T., F. Giorgi, and S. W. Hostetler, 1993: Towards the Simulation of the Effects of the Great-Lakes on Regional Climate. *Mon. Weather Rev.*, 121, 1373-1387.

Beyrich, F., and Coauthors, 2006: Area-averaged surface fluxes over the litfass region based on eddy-covariance measurements. *Boundary-Layer Meteorology*, 121, 33-65.

Blenckner, T., A. Omstedt, and M. Rummukainen, 2002: A Swedish case study of contemporary and possible future consequences of climate change on lake function. *Aquat. Sci.*, 64, 171-184.

Bonan, G., 1998: The land surface climatology of the NCAR Land Surface Model coupled to the NCAR Community Climate Model. *J. Clim.*, 11, 1307-1326.

Bonan, G., S. Levis, L. Kergoat, and K. Oleson, 2002a: Landscapes as patches of plant functional types: An integrating concept for climate and ecosystem models. *Global Biogeochemical Cycles*, 16, -.

Bonan, G. B., 1995: Sensitivity of a GCM Simulation to Inclusion of Inland Water Surfaces. *J. Clim.*, 8, 2691-2704.

Bonan, G. B., and Coauthors, 2002b: The land surface climatology of the community land model coupled to the NCAR community climate model. *Journal of Climate*, 15, 3123-3149.

Brown, L. C., and C. R. Duguay, 2010: The response and role of ice cover in lake-climate interactions. *Prog. Phys. Geogr.*, 34, 671-704.

Cardille, J., S. Carpenter, J. Foley, P. Hanson, M. Turner, and J. Vano, 2009: Climate change and lakes: Estimating sensitivities of water and carbon budgets. *J. Geophys. Res.-Biogeosci.*, 114, -.

Charnock, H., 1955: Wind Stress Over a Water Surface. *Quart. J. Roy. Meteorol. Soc.*, 81, 639-640.

Cristofor, S., A. Vadineanu, G. Ignat, and C. Ciubuc, 1994: Factors Affecting Light Penetration in Shallow Lakes. *Hydrobiologia*, 275, 493-498.

Dai, Y. J., and Coauthors, 2003: The Common Land Model. *Bulletin of the American Meteorological Society*, 84, 1013-+.

Donelan, M. A., F. W. Dobson, S. D. Smith, and R. J. Anderson, 1993: On the Dependence of Sea-Surface Roughness on Wave Development. *J. Phys. Oceanogr.*, 23, 2143-2149.

Downing, J. A., and Coauthors, 2006: The global abundance and size distribution of lakes, ponds, and impoundments. *Limnology and Oceanography*, 51, 2388-2397.

Duarte, C. M., Y. T. Prairie, C. Montes, J. J. Cole, R. Striegl, J. Melack, and J. A. Downing, 2008: CO2 emissions from saline lakes: A global estimate of a surprisingly large flux. *J. Geophys. Res.-Biogeosci.*, 113.

Dutra, E., V. M. Stepanenko, G. Balsamo, P. Viterbo, P. M. A. Miranda, D. Mironov, and C. Schar, 2010: An offline study of the impact of lakes on the performance of the ECMWF surface scheme. *Boreal Environment Research*, 15, 100-112.

Ellis, C. R., H. G. Stefan, and R. Gu, 1991: Water Temperature Dynamics and Heat-Transfer Beneath the Ice Cover of a Lake. *Limnology and Oceanography*, 36, 324-335.

Elo, P. A. R., 2007: The energy balance and vertical thermal structure of two small boreal lakes in summer. *Boreal Environment Research*, 12, 585-600.

Fairall, C. W., E. F. Bradley, D. P. Rogers, J. B. Edson, and G. S. Young, 1996: Bulk parameterization of air-sea fluxes for Tropical Ocean Global Atmosphere Coupled Ocean Atmosphere Response Experiment. *J. Geophys. Res.-Oceans*, 101, 3747-3764.

Fang, X., and H. G. Stefan, 1996: Long-term lake water temperature and ice cover simulations/measurements. *Cold Reg. Sci. Tech.*, 24, 289-304.

——, 1998: Temperature variability in lake sediments. *Water Resources Research*, 34, 717-729.

——, 2009: Simulations of climate effects on water temperature, dissolved oxygen, and ice and snow covers in lakes of the contiguous United States under past and future climate scenarios. *Limnology and Oceanography*, 54, 2359-2370.

Farouki, O. T., 1981: The Thermal-Properties of Soils in Cold Regions. *Cold Reg. Sci. Tech.*, 5, 67-75.

Feddema, J., K. Oleson, G. Bonan, L. Mearns, W. Washington, G. Meehl, and D. Nychka, 2005a: A comparison of a GCM response to historical anthropogenic land cover change and model sensitivity to uncertainty in present-day land cover representations. *Climate Dynamics*, 25, 581-609.

Feddema, J. J., K. W. Oleson, G. B. Bonan, L. O. Mearns, L. E. Buja, G. A. Meehl, and W. M. Washington, 2005b: The importance of land-cover change in simulating future climates. *Science*, 310, 1674-1678.

Flanner, M. G., and C. S. Zender, 2006: Linking snowpack microphysics and albedo evolution. *Journal of Geophysical Research-Atmospheres*, 111.

Flanner, M. G., C. S. Zender, J. T. Randerson, and P. J. Rasch, 2007: Present-day climate forcing and response from black carbon in snow. *Journal of Geophysical Research-Atmospheres*, 112.

Foken, T., 2008: The energy balance closure problem: An overview. *Ecological Applications*, 18, 1351-1367.

Freilich, M. H., and R. T. Guza, 1984: Nonlinear Effects on Shoaling Surface Gravity-Waves. *Philos. Trans. R. Soc. Lond. Ser. A-Math. Phys. Eng. Sci.*, 311, 1-41.

Freilich, M. H., R. T. Guza, and S. L. Elgar, 1990: Observations of Nonlinear Effects in Directional Spectra of Shoaling Gravity-Waves. *J. Geophys. Res.-Oceans*, 95, 9645-9656.

Gao, Z. Q., Q. Wang, and M. Y. Zhou, 2009: Wave-Dependence of Friction Velocity, Roughness Length, and Drag Coefficient over Coastal and Open Water Surfaces by Using Three Databases. *Adv. Atmos. Sci.*, 26, 887-894.

Gebhart, B., and J. C. Mollendorf, 1977: New Density Relation for Pure and Saline Water. *Deep-Sea Research*, 24, 831-848.

Geernaert, G. L., S. E. Larsen, and F. Hansen, 1987: Measurements of the Wind-Stress, Heat-Flux, and Turbulence Intensity During Storm Conditions over the North-Sea. *J. Geophys. Res.-Oceans*, 92, 13127-13139.

Gent, P. R., and Coauthors, 2011: The Community Climate System Model Version 4. *Journal of Climate*, 24, 4973-4991.

Golosov, S., and G. Kirillin, 2010: A parameterized model of heat storage by lake sediments. *Environmental Modelling & Software*, 25, 793-801.

Gomez, J. A. D., E. C. Salinero, and A. S. Merlin, 2009: Monitoring transparency in inland water bodies using multispectral images. *Int. J. Remote Sens.*, 30, 1567-1586.

Goudsmit, G. H., H. Burchard, F. Peeters, and A. Wuest, 2002: Application of k-epsilon turbulence models to enclosed basins: The role of internal seiches. *J. Geophys. Res.-Oceans*, 107, 13.

Goyette, S., N. McFarlane, and G. Flato, 2000: Application of the Canadian Regional Climate Model to the Laurentian Great Lakes region: Implementation of a lake model. *Atmosphere-Ocean*, 38, 481-503.

Gu, R. C., and H. G. Stefan, 1993: Validation of Cold Climate Lake Temperature Simulation. *Cold Reg. Sci. Tech.*, 22, 99-104.

Hagemann, S., K. Arpe, and E. Roeckner, 2006: Evaluation of the hydrological cycle in the ECHAM5 model. *Journal of Climate*, 19, 3810-3827.

Hakanson, L., 1995: Models to Predict Secchi Depth in Small Glacial Lakes. *Aquat. Sci.*, 57, 31-53.

Hazewinkel, M., 1995: *Encyclopaedia of mathematics : an updated and annotated translation of the Soviet "Mathematical Encyclopaedia".* Kluwer.

Hocking, G. C., and M. Straskraba, 1999: The effect of light extinction on thermal stratification in reservoirs and lakes. *International Review of Hydrobiology*, 84, 535-556.

Hondzo, M., and H. G. Stefan, 1993: Lake Water Temperature Simulation-Model. *J. Hydraul. Eng.-ASCE*, 119, 1251-1273.

Hostetler, S., and P. Bartlein, 1990: Simulation of Lake Evaporation with Application to Modeling Lake Level Variations of Harney-Malheur Lake, Oregon. *Water Resources Research*, 26, 2603-2612.

Houser, J. N., 2006: Water color affects the stratification, surface temperature, heat content, and mean epilimnetic irradiance of small lakes. *Canadian Journal of Fisheries and Aquatic Sciences*, 63, 2447-2455.

Hutchinson, G. E., 1957: *A treatise on limnology: Geography, Physics and Chemistry.* Vol. 1, Wiley.

Idso, S. B., and R. G. Gilbert, 1974: On the Universality of the Poole and Atkins Secchi Disk-Light Extinction Equation. *Journal of Applied Ecology*, 11, 399-401.

Jeffries, M., T. Zhang, K. Frey, and N. Kozlenko, 1999: Estimating late-winter heat flow to the atmosphere from the lake-dominated Alaskan North Slope. *J. Glaciol.*, 45, 315-324.

Jin, J., X. Gao, Z. Yang, R. Bales, S. Sorooshian, and R. Dickinson, 1999: Comparative analyses of physically based snowmelt models for climate simulations. *J. Clim.*, 12, 2643-2657.

King, J. R., B. J. Shuter, and A. P. Zimmerman, 1997: The response of the thermal stratification of South Bay (Lake Huron) to climatic variability. *Can. J. Fish. Aquat. Sci.*, 54, 1873-1882.

Kirillin, G., 2010: Modeling the impact of global warming on water temperature and seasonal mixing regimes in small temperate lakes. *Boreal Environment Research*, 15, 279-293.

Koponen, S., J. Pulliainen, K. Kallio, and M. Hallikainen, 2002: Lake water quality classification with airborne hyperspectral spectrometer and simulated MERIS data. *Remote Sens. Environ.*, 79, 51-59.

Kosten, S., V. L. M. Huszar, N. Mazzeo, M. Scheffer, L. D. L. Sternberg, and E. Jeppesen, 2009: Lake and watershed characteristics rather than climate influence nutrient limitation in shallow lakes. *Ecological Applications*, 19, 1791-1804.

Kourzeneva, E., 2010: External data for lake parameterization in Numerical Weather Prediction and climate modeling. *Boreal Environment Research*, 15, 165-177.

Krinner, G., 2003: Impact of lakes and wetlands on boreal climate. *J. Geophys. Res.-Atmos.*, 108, 18.

Krinner, G., and J. Boike, 2010: A study of the large-scale climatic effects of a possible disappearance of high-latitude inland water surfaces during the 21st century. *Boreal Environment Research*, 15, 203-217.

Kristovich, D. A. R., and R. R. Braham, 1998: Mean profiles of moisture fluxes in snow-filled boundary layers. *Boundary-Layer Meteorology*, 87, 195-215.

Laird, N. F., J. Desrochers, and M. Payer, 2009: Climatology of Lake-Effect Precipitation Events over Lake Champlain. *J. Appl. Meteorol. Climatol.*, 48, 232-250.

Larson, G. L., R. L. Hoffman, D. C. McIntire, M. W. Buktenica, and S. F. Girdner, 2007: Thermal, chemical, and optical properties of Crater Lake, Oregon. *Hydrobiologia*, 574, 69-84.

Lawrence, D. M., and A. G. Slater, 2008: Incorporating organic soil into a global climate model. *Climate Dynamics*, 30, 145-160.

Lawrence, D. M., A. G. Slater, V. E. Romanovsky, and D. J. Nicolsky, 2008: Sensitivity of a model projection of near-surface permafrost degradation to soil column depth and representation of soil organic matter. *Journal of Geophysical Research-Earth Surface*, 113, 14.

Lawrence, D. M., and Coauthors, 2011: Parameterization improvements and functional and structural advances in version 4 of the Community Land Model. *J. Adv. Model. Earth Sys.*, **3**, 27 pp.

Lehner, B., and P. Doll, 2004: Development and validation of a global database of lakes, reservoirs and wetlands. *Journal of Hydrology*, 296, 1-22.

Leon, L. F., D. C. L. Lam, W. M. Schertzer, D. A. Swayne, and J. Imberger, 2007: Towards coupling a 3D hydrodynamic lake model with the Canadian Regional Climate Model: Simulation on Great Slave Lake. *Environmental Modelling & Software*, 22, 787-796.

Lofgren, B. M., 1997: Simulated effects of idealized Laurentian Great Lakes on regional and large-scale climate. *J. Clim.*, 10, 2847-2858.

——, 2004: A model for simulation of the climate and hydrology of the Great Lakes basin. *Journal of Geophysical Research-Atmospheres*, 109.

Long, Z., W. Perrie, J. Gyakum, D. Caya, and R. Laprise, 2007: Northern lake impacts on local seasonal climate. *J. Hydrometeorol.*, 8, 881-896.

Maat, N., C. Kraan, and W. A. Oost, 1991: The Roughness of Wind-Waves. *Boundary-Layer Meteorology*, 54, 89-103.

MacKay, M. D., and Coauthors, 2009: Modeling lakes and reservoirs in the climate system. *Limnology and Oceanography*, 54, 2315-2329.

Mahrt, L., 1999: The Coastal Zone. *Air-Sea Exchange: Physics, Chemistry, and Dynamics*, G. L. Geernaert, Ed., Kluwer Academic Publishers, 247-267.

Martynov, A., L. Sushama, and R. Laprise, 2010: Simulation of temperate freezing lakes by one-dimensional lake models: performance assessment for interactive coupling with regional climate models. *Boreal Environment Research*, 15, 143-164.

Mazumder, A., and W. D. Taylor, 1994: Thermal Structure of Lakes Varying in Size and Water Clarity. *Limnology and Oceanography*, 39, 968-976.

Mazumder, A., W. D. Taylor, D. J. McQueen, and D. R. S. Lean, 1990: Effects of Fish and Plankton on Lake Temperature and Mixing Depth. *Science*, 247, 312-315.

McCormick, M., and J. Pazdalski, 1993: Monitoring Midlake Water Temperature in Southern Lake-Michigan for Climate-Change Studies. *Clim. Change*, 25, 119-125.

McCormick, M. J., and G. L. Fahnenstiel, 1999: Recent climatic trends in nearshore water temperatures in the St. Lawrence Great Lakes. *Limnology and Oceanography*, 44, 530-540.

Mironov, D., L. Rontu, E. Kourzeneva, and A. Terzhevik, 2010a: Towards improved representation of lakes in numerical weather prediction and climate models: Introduction to the special issue of Boreal Environment Research. *Boreal Environment Research*, 15, 97-99.

Mironov, D., A. Terzhevik, G. Kirillin, T. Jonas, J. Malm, and D. Farmer, 2002: Radiatively driven convection in ice-covered lakes: Observations, scaling, and a mixed layer model. *J. Geophys. Res.-Oceans*, 107, 16.

Mironov, D., E. Heise, E. Kourzeneva, B. Ritter, N. Schneider, and A. Terzhevik, 2010b: Implementation of the lake parameterisation scheme FLake into the numerical weather prediction model COSMO. *Boreal Environment Research*, 15, 218-230.

Morris, E. M., 1989: Turbulent Transfer over Snow and Ice. *Journal of Hydrology*, 105, 205-223.

Mueller, D. R., P. Van Hove, D. Antoniades, M. O. Jeffries, and W. F. Vincent, 2009: High Arctic lakes as sentinel ecosystems: Cascading regime shifts in climate, ice cover, and mixing. *Limnology and Oceanography*, 54, 2371-2385.

Nordbo, A., S. Launiainen, I. Mammarella, M. Lepparanta, J. Huotari, A. Ojala, and T. Vesala, 2011: Long-term energy flux measurements and energy balance over a small boreal lake using eddy covariance technique. *Journal of Geophysical Research-Atmospheres*, 116.

Oleson, K., and Coauthors, 2010: Technical description of version 4.0 of the Community Land Model (CLM). National Center for Atmospheric Research, NCAR/TN-478+STR.

Panin, G. N., A. E. Nasonov, T. Foken, and H. Lohse, 2006: On the parameterisation of evaporation and sensible heat exchange for shallow lakes. *Theoretical and Applied Climatology*, 85, 123-129.

Peeters, F., D. Straile, A. Lorke, and D. M. Livingstone, 2007: Earlier onset of the spring phytoplankton bloom in lakes of the temperate zone in a warmer climate. *Glob. Change Biol.*, 13, 1898-1909.

Perroud, M., and S. Goyette, 2010: Impact of warmer climate on Lake Geneva water-temperature profiles. *Boreal Environment Research*, 15, 255-278.

Perroud, M., S. Goyette, A. Martynov, M. Beniston, and O. Anneville, 2009: Simulation of multiannual thermal profiles in deep Lake Geneva: A comparison of one-dimensional lake models. *Limnology and Oceanography*, 54, 1574-1594.

Persson, I., and I. D. Jones, 2008: The effect of water colour on lake hydrodynamics: a modelling study. *Freshw. Biol.*, 53, 2345-2355.

Pivovarov, A. A., 1972: *Thermal Conditions in Freezing Lakes and Reservoirs.* John Wiley.

Plummer, D. A., and Coauthors, 2006: Climate and climate change over North America as simulated by the Canadian RCM. *J. Clim.*, 19, 3112-3132.

Qian, T. T., A. G. Dai, K. E. Trenberth, and K. W. Oleson, 2006: Simulation of global land surface conditions from 1948 to 2004. Part I: Forcing data and evaluations. *J. Hydrometeorol.*, 7, 953-975.

Robarts, R. D., and P. R. B. Ward, 1978: Vertical Diffusion and Nutrient Transport in a Tropical Lake (Lake McIlwaine, Rhodesia). *Hydrobiologia*, 59, 213-221.

Rouse, W. R., P. D. Blanken, N. Bussieres, C. J. Oswald, W. M. Schertzer, C. Spence, and A. E. Walker, 2008: Investigation of the Thermal and Energy Balance Regimes of Great Slave and Great Bear Lakes. *J. Hydrometeorol.*, 9, 1318-1333.

Rouse, W. R., and Coauthors, 2005: The role of northern lakes in a regional energy balance. *J. Hydrometeorol.*, 6, 291-305.

Saloranta, T. M., M. Forsius, M. Jarvinen, and L. Arvola, 2009: Impacts of projected climate change on the thermodynamics of a shallow and a deep lake in Finland: model simulations and Bayesian uncertainty analysis. *Hydrol. Res.*, 40, 234-248.

Samuelsson, P., and M. Tjernstrom, 2001: Mesoscale flow modification induced by land-lake surface temperature and roughness differences. *Journal of Geophysical Research-Atmospheres*, 106, 12419-12435.

Samuelsson, P., E. Kourzeneva, and D. Mironov, 2010: The impact of lakes on the European climate as simulated by a regional climate model. *Boreal Environment Research*, 15, 113-129.

Schindler, D. W., 2009: Lakes as sentinels and integrators for the effects of climate change on watersheds, airsheds, and landscapes. *Limnology and Oceanography*, 54, 2349-2358.

Skamarock, W. C., and Coauthors, 2008: A Description of the Advanced Research WRF Version 3. Mesoscale and Microscale Meteorology Division, National Center for Atmospheric Research, NCAR/TN–475+STR.

Sleator, F. E., 1995: GLERL Great Lakes ice thickness data base, 1966-1979. National Snow and Ice Data Center.

Small, E. E., F. Giorgi, L. C. Sloan, and S. Hostetler, 2001: The effects of desiccation and climatic change on the hydrology of the Aral Sea. *J. Clim.*, 14, 300-322.

Smith, L., Y. Sheng, G. MacDonald, and L. Hinzman, 2005: Disappearing Arctic lakes. *SCIENCE*, 308, 1429-1429.

Smith, S. D., 1988: Coefficients for Sea-Surface Wind Stress, Heat-Flux, and Wind Profiles as a Function of Wind-Speed and Temperature. *J. Geophys. Res.-Oceans*, 93, 15467-15472.

Smith, S. D., and Coauthors, 1992: Sea-Surface Wind Stress and Drag Coefficients - The HEXOS Results. *Boundary-Layer Meteorology*, 60, 109-142.

Song, Y., F. H. M. Semazzi, L. Xie, and L. J. Ogallo, 2004: A coupled regional climate model for the Lake Victoria basin of East Africa. *Int. J. Climatol.*, 24, 57-75.

Stepanenko, V. M., and V. N. Lykossov, 2005: Numerical modeling of heat and moisture transfer processes in a system lake – soil. *Russian Journal for Meteorology and Hydrology*, 3, 95-104.

Stepanenko, V. M., E. E. Machulskaya, M. V. Glagolev, and V. N. Lykosov, 2011: Modeling of methane emissions from lakes in the permafrost zone. *Izvestiya, Atmospheric and Ocean Physics*, 47, 1-14.

Stepanenko, V. M., S. Goyette, A. Martynov, M. Perroud, X. Fang, and D. Mironov, 2010: First steps of a Lake Model Intercomparison Project: LakeMIP. *Boreal Environment Research*, 15, 191-202.

Tranvik, L. J., and Coauthors, 2009: Lakes and reservoirs as regulators of carbon cycling and climate. *Limnology and Oceanography*, 54, 2298-2314.

Vassiljev, J., S. P. Harrison, S. Hostetler, and P. J. Bartlein, 1994: Simulation of Long-Term Thermal-Characteristics of 3 Estonian Lakes. *Journal of Hydrology*, 163, 107-123.

Vavrus, S. J., R. H. Wynne, and J. A. Foley, 1996: Measuring the sensitivity of southern Wisconsin lake ice to climate variations and lake depth using a numerical model. *Limnology and Oceanography*, 41, 822-831.

Verburg, P., and R. E. Hecky, 2009: The physics of the warming of Lake Tanganyika by climate change. *Limnology and Oceanography*, 54, 2418-2430.

Vesala, T., and Coauthors, 2006: Eddy covariance measurements of carbon exchange and latent and sensible heat fluxes over a boreal lake for a full open-water period. *Journal of Geophysical Research-Atmospheres*, -.

Vickers, D., and L. Mahrt, 1997: Fetch limited drag coefficients. *Boundary-Layer Meteorology*, 85, 53-79.

Vincent, A. C., D. R. Mueller, and W. F. Vincent, 2008: Simulated heat storage in a perennially ice-covered high Arctic lake: Sensitivity to climate change. *Journal of Geophysical Research-Oceans*, 113.

Walter, K. M., L. C. Smith, and F. S. Chapin, 2007: Methane bubbling from northern lakes: present and future contributions to the global methane budget. *Philosophical Transactions of the Royal Society a-Mathematical Physical and Engineering Sciences*, 365, 1657-1676.

Walter, K. M., S. A. Zimov, J. P. Chanton, D. Verbyla, and F. S. Chapin, 2006: Methane bubbling from Siberian thaw lakes as a positive feedback to climate warming. *Nature*, 443, 71-75.

Wetzel, R., and G. E. Likens, 1991: *Limnological analyses.* Springer-Verlag.

Yeates, P. S., and J. Imberger, 2003: Pseudo two-dimensional simulations of internal and boundary fluxes in stratified lakes and reservoirs. *International Journal of River Basin Management*, 1, 297 - 319.

Zeng, X., M. Shaikh, Y. Dai, R. Dickinson, and R. Myneni, 2002: Coupling of the common land model to the NCAR community climate model. *J. Clim.*, 15, 1832-1854.

Zhang, T., and M. O. Jeffries, 2000: Modeling interdecadal variations of lake-ice thickness and sensitivity to climatic change in northernmost Alaska. *Annals of Glaciology, Vol 31, 2000*, K. Steffen, Ed., 339-347.

Zhang, Y. Z., J. Pulliainen, S. Koponen, and M. Hallikainen, 2003: Empirical algorithms for Secchi disk depth using optical and microwave remote sensing data from the Gulf of Finland and the Archipelago Sea. *Boreal Environment Research*, 8, 251-261.

Zilitinkevich, S. S., 1972: *The dynamics of the atmospheric boundary layer.* National Lending Library for Science and Technology.

Zilitinkevich, S. S., A. A. Grachev, and C. W. Fairall, 2001: Scaling reasoning and field data on the sea surface roughness lengths for scalars. *Journal of the Atmospheric Sciences*, 58, 320-325.

Chapter 3: Boreal Lakes Moderate Seasonal and Diurnal Temperature Variation and Perturb Atmospheric Circulation: Analyses in CESM1

Chapter 3 Table of Contents

3. Boreal Lakes Moderate Seasonal and Diurnal Temperature Variation and Perturb Atmospheric Circulation: Analyses in CESM1

This chapter is based on the article published in 2012 in the Tellus A, with co-authors Lisa N. Murphy (Lawrence Berkeley National Lab), Fuyu Li (Lawrence Berkeley National Lab), Céline Bonfils (Lawrence Livermore National Lab), and William J. Riley (Lawrence Berkeley National Lab). The article was published open-access by Co-Action Publishing.

Citation:

Subin, Z. M., L. N. Murphy, F. Li, C. Bonfils, and W. J. Riley, 2012. Boreal Lakes Moderate Seasonal and Diurnal Temperature Variation and Perturb Atmospheric Circulation: Analyses in CESM1. *Tellus A* 64, 15639. doi:10.3402/tellusa.v64i0.15639

http://www.tellusa.net/index.php/tellusa/article/view/15639

3.1 Summary

We used a lake thermal physics model recently coupled into CESM1 to study the effects of lake distribution in present and future climate.

Under present climate, correcting the large under-estimation of lake area in CESM1 (denoted CCSM4 in the configuration used here) caused 1°C spring decreases and fall increases in surface air temperature throughout large areas of Canada and the U.S. Simulated summer surface diurnal air temperature range decreased by up to 4°C, reducing CCSM4 biases. These changes were much larger than those resulting from prescribed lake disappearance in some present-day permafrost regions under doubled-CO_2 conditions.

Correcting the under-estimation of lake area in present climate caused widespread high-latitude summer cooling at 850 hPa. Significant remote changes included decreases in the strength of fall Southern Ocean westerlies. We found significantly different winter responses when separately analyzing 45-year sub-periods, indicating that relatively long simulations are required to discern the impacts of surface changes on remote conditions. We also investigated the surface forcing of lakes using idealized aqua-planet experiments, which showed that surface changes of 2°C in the Northern Hemisphere extra-tropics could cause substantial changes in precipitation and winds in the tropics and Southern Hemisphere. Shifts in the Inter-Tropical Convergence Zone were opposite in sign to those predicted by some previous studies. Zonal mean circulation changes were consistent in character but much larger than those occurring in the lake distribution experiments, due to the larger magnitude and more uniform surface forcing in the idealized aqua-planet experiments.

3.2 Introduction

Lakes have different surface properties than surrounding land, altering surface fluxes enough to cause significant changes in regional temperature (Dutra et al. 2010; Krinner 2003; Samuelsson et al. 2010). These changes are important for accurate prediction of climate in regions with large lake area, such as the Great Lakes, Northern Canada, and Scandinavia (Dutra et al. 2010; Krinner 2003; Lofgren 1997; Long et al. 2007; Rouse et al. 2005; Samuelsson et al. 2010). Temperate and high-latitude lakes tend to be cooler than surrounding land in the spring

and summer due to increased seasonal thermal inertia and shifts from sensible to latent heat fluxes (Dutra et al. 2010; Krinner 2003; Lofgren 1997; Rouse et al. 2008). The heat absorbed by lakes during the summer tends to be released during the fall, increasing both latent and sensible heat fluxes and causing local warming (Dutra et al. 2010; Lofgren 1997; Long et al. 2007; Rouse et al. 2008; Samuelsson et al. 2010). During the winter, snow insulation moderates the effects of frozen lakes on the atmosphere (Brown and Duguay 2010; Dutra et al. 2010), but melting lakes can cause spring cooling (Samuelsson et al. 2010).

The effects of lakes on atmospheric conditions other than temperature have been less comprehensively studied, especially at large spatial scales. In Samuelsson et al. (2010), the addition of lakes to a regional climate model caused early summer decreases in simulated cloudiness and precipitation in Northern Europe in and increases in late summer and early fall. Krinner (2003) found increases in summer precipitation and cloudiness in Europe due to moisture recycling, but in Quebec the opposite occurred due to reduced evaporation and increased atmospheric stability; the latter effect is consistent with the findings of Lofgren (1997). Lake-effect precipitation occurring when cold air advects over unfrozen lakes has been extensively studied at the regional scale (Bates et al. 1993; Goyette et al. 2000; Kristovich and Braham 1998; Laird et al. 2009; Lofgren 2004; Samuelsson and Tjernstrom 2001).

Lake distributions may interact with climate change and other anthropogenic forcings. Changes in the balance of precipitation and evaporation in lake watersheds may change lake depth or distribution (Schindler 2009; Small et al. 2001), as can anthropogenic manipulation of watersheds (Small et al. 2001). About 10% of current global lake area consists of artificial reservoirs (Lehner and Doll 2004). Climate warming also interacts with lake area in permafrost regions, reviewed in Krinner and Boike (2010). Thaw subsidence is expanding the area of thermokarst lakes in some regions (Jorgenson et al. 2006; Jorgenson et al. 2001; Kaab and Haeberli 2001; Plug et al. 2008). In other regions, decreases in lake area have been observed (Plug et al. 2008; Riordan et al. 2006; Smith et al. 2005; Smith et al. 2007), as the loss of impervious underlying permafrost encourages sub-surface drainage, and increased surface erosion can increase surface runoff. Smith et al. (2007) suggested that the balance between increasing and decreasing lakes in permafrost area correlated with the degree of permafrost degradation: small increases in lake area can result as continuous permafrost begins to thaw, while large decreases in lake area can occur as discontinuous permafrost disappears. Increased lateral drainage after an initial expansion in thermokarst lake area as permafrost degrades is consistent with recent pan-Arctic thermokarst lake modeling (van Huissteden et al. 2011).

While lake distributions may change in the future, even present lake distributions are poorly represented in many climate models, as datasets often underestimate current global lake area. In the Community Earth System Model 1 (CESM1; http://www.cesm.ucar.edu/), the lake area (Cogley 1991) is three times smaller than found in the Global Lake and Wetland Database (GLWD) (Lehner and Doll 2004) with lake area in Northern Canada especially underestimated. Furthermore, Downing et al. (2006) concluded that global lake distribution datasets like the GLWD may themselves be as much as a factor of two too small by missing lakes smaller than $0.1 – 1$ km^2 which are difficult to resolve in satellite data; Grosse at al. (2008) found even larger under-estimation in some Siberian field sites. As 60% of global lake area is found north of 45°N (Lehner and Doll 2004), representation of lakes is especially important for climate studies in this region.

Accurately simulating diurnal surface air temperature range (DTR) requires climate models to correctly represent a number of meteorological processes and geographical features (Karl et al. 1993; Vose et al. 2005): (1) the distance from a large body of water (Geerts 2003); (2) evapotranspiration (ET), cloud cover, precipitation, and soil moisture (Dai et al. 1999); and (3) phenological properties and land-use (Bonfils et al. 2005; Collatz et al. 2000; Kalnay and Cai 2003). The Climate Model Intercomparison Project 3 (CMIP3) climate models have mixed performance in simulating continental DTR. The large-scale spatial patterns (Geerts 2003) are generally replicated by the CMIP3 climate models, but the absolute value is typically underestimated by as much as 50% in many regions, including the Canadian Shield [Randall et al. (2007), Figure S8.3]. The models also generally fail to reproduce the observed decadal variability in DTR (Wild 2009) or the full magnitude of its long-term decline (Braganza et al. 2004; Zhou et al. 2010). In some models, these discrepancies may result from deficiencies in simulating convective clouds (Randall et al. 2007), freezing and thawing soil (Randall et al. 2007), or the responses to changing sulfate aerosols and greenhouse gases (Wild et al. 2007). The degree of land-atmosphere hydrological coupling affects the realism of seasonal variation in surface air temperature (Nigam and Ruiz-Barradas 2006) and could plausibly affect DTR predictions in some models. Since unfrozen lakes tend to suppress diurnal temperature variation in their vicinity (Geerts 2003; Samuelsson et al. 2010), climate model representation of lake properties and distribution may affect DTR biases.

Widespread changes in terrestrial surface properties and the resulting energy fluxes have the potential to cause changes in large-scale circulation (Chase et al. 2000; Feddema et al. 2005a; Feddema et al. 2005b). Several mechanisms can result in linked changes in climate at distant locations [teleconnections (Nigam 2003; Wallace and Gutzler 1981)]. Zonally asymmetric topographic and land-sea temperature contrasts force atmospheric stationary waves (Held et al. 2002; Hoskins and Karoly 1981; Nigam and DeWeaver 2003; Shaman and Tziperman 2005). Wave trains (Kushnir and Wallace 1989), which may be affected by terrestrial surface changes, are associated with changes in upper-tropospheric zonal winds (Branstator 2002; Nigam and Lindzen 1989) and energy transport between the equator and the poles. Another type of teleconnection can result from changes in dominant dynamic modes of variability, several of which could interact with extra-tropical continental climate: the North Atlantic Oscillation (NAO) (Kutzbach 1970; Rogers 1981; Trenberth and Paolino 1981), the Northern Annular Mode (NAM) (Thompson and Wallace 1998), the El Niño-Southern Oscillation (ENSO) (Graham and White 1988; Kawamura 1994; Tourre and White 1995; White and Pazan 1987), the Northern Pacific Oscillation (NPO) (Linkin and Nigam 2008), and the Atlantic Multi-Decadal Oscillation (AMO) (Guan and Nigam 2009). Changes in terrestrial surface properties or climate change may cause changes in the statistical properties of these modes (Bonfils and Santer 2010; Chase et al. 2000; Corti et al. 1999; Timmermann 1999).

A final type of teleconnection could be mediated by changes in the zonal mean atmospheric circulation, which can be described by three interacting cells of vertical and meridional wind flow in each hemisphere: the Hadley, Ferrell, and polar cells (Holton 2004; Oort and Rasmusson 1970). The meridional stream function (MSF) can be used to detect changes to these cells, and is defined as the integral of the meridional mass flow across each latitude line from the surface to each pressure level. Some studies have found that changes in NH extra-tropical surface properties could impact remote regions such as the tropics or Southern Hemisphere (SH). For

instance, North Atlantic cooling episodes during the Quarternary could have displaced the Inter-Tropical Convergence Zone (ITCZ) southward (Kang et al. 2009; Kang et al. 2008), enhanced wind-driven Southern Ocean upwelling (Anderson et al. 2009; Toggweiler and Lea 2010), and caused 20 – 60 ppm increases in atmospheric CO_2 (Lee et al. 2011).

Large magnitudes of North Atlantic cooling were imposed in previous experiments [e.g., 12°C in Lee et al. (2011)]. The effects of terrestrial surface forcing could be comparatively weaker. To our knowledge, changes in simulated lake distribution have not been shown to cause changes in large-scale atmospheric circulation, remote temperatures, or remote precipitation. However, this absence could be the result of using relatively short simulations of 20 years or less [as in Krinner (2003) and Krinner and Boike (2010)]. Longer simulations may be required for several reasons. First, high inter-annual variability occurs in many meteorological variables of interest, such as high latitude temperatures and tropical precipitation. Second, spatial autocorrelation of meteorological fields complicates the detection of coherent signals at small spatial scales (Livezey and Chen 1983). While single-gridcell statistical significance is typically used (and is used cautiously here), a more complete analysis would explicitly consider this autocorrelation (Feddema et al. 2005a), or evaluate significance for each spherical harmonic mode, as a spectral decomposition better represents the spatial degrees of freedom in a GCM than does the number of gridcells (Stott and Tett 1998). Third, dynamic modes of variability can cause temporal autocorrelation of meteorological fields on inter-annual and even inter-decadal timescales. In particular, natural Arctic variability may contain dominant multi-decadal modes (Delworth and Mann 2000; Frankcombe and Dijkstra 2010; Levitus et al. 2009; Minobe 1997; Polyakov and Johnson 2000; Polyakov et al. 2003; Venegas and Mysak 2000) including the NAM (Ogi and Yamazaki 2010) and AMO (Guan and Nigam 2009), and timescales of these modes may be as long as ~70 years (Delworth and Mann 2000; Minobe 1997; Polyakov and Johnson 2000; Polyakov et al. 2003).

In this study, we used an improved lake model coupled into CESM1 (Subin et al. 2012) to assess the effects of lake distribution on climate. We investigated the sensitivity of the simulation of present climate to lake area by comparing (1) the Lehner and Döll (2004) 2.3 million km^2 of lake area to (2) the less realistic 0.7 million km^2 default value. We also investigated the sensitivity of future climate to potential changes in lake area in permafrost regions and compared our results to those of Krinner and Boike (2010), who performed an analogous set of model experiments. Each simulation was integrated for 200 years so that we could detect remote changes in regions with high inter-annual and decadal variability.

Because several studies have investigated the regional effects of changing lake distribution in climate models, but few studies have investigated the remote responses to any type of terrestrial-surface change, we focused equally on local and remote atmospheric responses, even though local responses may be stronger or more robust. In order to better understand the mechanisms causing large-scale changes, we performed simulations in an aqua-planet model with idealized versions of this surface forcing.

3.3 Methods

3.3.1 Model Description

3.3.1.1 Lake Model

The Lake, Ice, Sediment, and Snow Simulator added to the Community Land Model 4 (CLM4-LISSS) (Subin et al. 2012) solves the 1-dimensional thermal diffusion equation by dividing the sub-surface into several discrete layers for each of the following: snow, lake body water and ice, and underlying sediment and bedrock. After calculating energy and momentum fluxes between the surface and the atmosphere, the residual surface energy flux is used as a top boundary condition for the thermal diffusion between snow, lake body, and sediment. Saturated sediments and constant lake body water content are assumed, although snow depth and properties are prognosed. Thermal mixing between simulated lake layers is driven by wind-driven eddies (Hostetler and Bartlein 1990), convection (Hostetler and Bartlein 1990), molecular diffusion, and additional background diffusivity to represent unresolved processes (Fang and Stefan 1996). Shortwave radiation absorption is predicted according to the diagnosed optical properties of snow and lake water. The submodels for friction velocity, aerodynamic resistances, snow, and sediment are similar to those in CLM4 (Oleson et al. 2010), which is the land surface component of CESM1. Surface aerodynamic roughness lengths are calculated as a function of forcing wind and friction velocity. A technical note detailing the lake model is available in the Supplementary Information.

CLM4-LISSS simulated lake temperature and surface fluxes well for shallow lakes, while mixing in deep lakes was under-predicted using the default model configuration; predictions were improved by increasing thermal conductivity by a factor of 10 or more. However, errors using the default configuration for deep lakes were comparable to those resulting from the typical difficulties in representing lake depth and opacity in global simulations (Subin et al. 2012). The default model configuration should suffice for this study, as we focused on the lake area missing from current datasets and the potential changes in lake area in regions of thawing permafrost: most of the lakes in these areas are relatively shallow. For simplicity, we assumed no small-fetch limitation on wave development when calculating the roughness length; the sensitivity to this assumption was shown to be small (Subin et al. 2012).

3.3.1.2 Climate Model

CESM1 consists of five components: CLM4, an atmospheric model (CAM4 or CAM5), an ocean model (POP2), a sea ice model (CICE4), and a land ice sheet model (GLIMMER – CISM) (http://www.cesm.ucar.edu/). The model can be run either in fully coupled mode or with some components inactive or replaced by prescribed data. In this study, we ran simulations in three modes: (1) the "CLM4 offline" mode forced by historical meteorological data (Qian et al. 2006); (2) the "slab ocean" mode with active CLM4, CAM4, and CICE4 active along with a slab ocean model that includes the heat capacity of the ocean mixed layer and prescribes lateral heat transport between ocean gridcells consistent with present climate simulations; and (3) the "aqua-planet" mode, based on an older atmospheric model version, CAM3, described below. For (2), CAM4 (Gent et al. 2010; Neale et al. 2008; Neale et al. 2010; Richter and Rasch 2008; Vavrus and Waliser 2008) was run at 1.9° x 2.5° resolution with prescribed aerosol, greenhouse gas, and ozone concentrations. We note that CESM1 with CAM4 physics rather than the newer CAM5 physics is generally referred to as the Community Climate System Model 4 (CCSM4) (Gent et al. 2011); to avoid confusion with other published analyses, we refer to CCSM4 below.

CLM4 (Lawrence et al. 2011a) divides each gridcell into a hierarchy of independent subgrid tiles with undefined spatial distribution; the gridcell flux to the atmosphere is calculated by averaging the fluxes from each tile. The highest level of the hierarchy below the gridcell (the "landunit") can be soil (vegetated), urban, lake, wetland, or glacier (Oleson et al. 2010). CLM4 currently only models a single 1-dimensional lake column in each gridcell, although relatively simple changes to the existing software could allow multiple lakes to be simulated in each gridcell in future versions. CLM4 can be run with prescribed satellite phenology ("SP") and biogeochemistry turned off, or with prognostic phenology and biogeochemistry turned on ("CN"). Unless otherwise specified, all model simulations used CLM4SP with the 1.9° x 2.5° grid and year 2000 conditions for aerosol deposition, nitrogen deposition, and land use. In order to increase the realism of the high-latitude simulations, we included the provisional changes to frozen soil hydrology, peat physical properties, and rooting depth described in Riley et al. (2011) that were developed by S.C. Swenson and D.M. Lawrence (D.M. Lawrence, personal communication, 2010). These high-latitude biogeophysical changes have the effect of moistening and cooling the near-surface atmosphere during the summer in permafrost regions relative to the standard CLM4.

The CCSM4 terrestrial climatology and hydroclimate are being evaluated by the CESM community; many studies will appear in an upcoming CCSM4 *Journal of Climate* special issue. Offline, CLM4SP predicts higher temporal variability in soil moisture and lower variability in ET than does CLM3.5; this improves the comparison with Gravity Recovery and Climate Experiment (GRACE) observations (Lawrence et al. 2011a). Variability of ET increases in CLM4CN due to prognostic phenology, and ET tends to be biased high in the tropics and mid-latitudes due to excessive gross primary productivity (Lawrence et al. 2011a), which may affect the simulation of temporal temperature variation (Nigam and Ruiz-Barradas 2006). When CLM4CN is coupled into CCSM4, the improved simulation of seasonal soil moisture storage is retained (Gent et al. 2011; Lawrence et al. 2011b). Preliminary analysis by K. W. Oleson (D. M. Lawrence, personal communication, 2011) suggests that CCSM4 land-atmosphere coupling strength as defined in the Global Land-Atmosphere Coupling Experiment (GLACE) is much weaker than CCSM3, which had a relatively strong coupling (Guo et al. 2006). CCSM4 has a positive annual mean surface air temperature bias in the Canadian Shield, Central U.S., Central Eurasia, and Siberia (Gent et al. 2011; Lawrence et al. 2011b; Peacock 2012), with warm summer biases especially prevalent in Central Canada, Alaska, and Siberia (Lawrence et al. 2011b), which may be partially attributable to deficiencies in simulating frozen soil hydrology (Lawrence et al. 2011b). These deficiencies motivated the high-latitude biogeophysical changes mentioned above and will be the subject of a future study. Precipitation is biased high in the Central U.S., especially during the summer (Gent et al. 2011; Lawrence et al. 2011b; Peacock 2012).

3.3.1.3 Aqua-planet model

The aqua-planet model is based on the spectral version of CAM3 (Collins et al. 2004) at T85 resolution (~ 1.4°), with same model configuration as used in Li et al. (2011). The model uses fixed sea-surface temperatures (SSTs) (Neale and Hoskins 2000), and all forcings are symmetric zonally and about the equator (i.e., no continents and constant equinox solar forcing). The

version applied here does not consider oceanic heat transport or finite ocean mixed layer heat capacity.

3.3.2 Datasets

We used the GLWD to estimate the distribution of existing lakes and reservoirs, as it is based on the best available combinations of satellite and geographic data (Lehner and Doll 2004). Downing et al. (2006) globally extrapolated lake distribution functions from some areas where fine-scale data are available and concluded that databases like the GLWD likely underestimate global lake area by a large factor. However, we wished to avoid extrapolation, and a dataset based on Downing et al. (2006) was not readily available. Consequently, our estimates of climate biases resulting from the unrealistically small lake area used in CESM1 are likely to be conservative. We interpolated the lakes and reservoirs in the GLWD level 3 ("classes" 1 and 2 in the dataset) to the CLM4 1.9° x 2.5° grid and excluded the Caspian Sea (which is masked as ocean in CESM1), yielding 2.30 million km^2 (Fig. 3.1a). In comparison, the default 1.9° x 2.5° CLM4 surface dataset, based on Cogley (1991) and excluding gridcells with less than 1% lake area, contains 0.72 million km^2 (Fig. 3.1b). Much of the missing lake area (Fig. 3.1c) is in Canada.

To characterize the effects of changing lake area in permafrost regions under climate change, we generated a potential future lake distribution dataset following the approach of Krinner and Boike (2010), who assumed that the area of inland water surfaces would decrease in disappearing permafrost by 40% but increase in areas of remaining permafrost by 10%. This assumption is qualitatively consistent with the modeling results of van Huissteden et al. (2011). However, whereas Krinner and Boike (2010) used climate model projections to predict these areas, we simply used the existing Brown et al. (2001) permafrost dataset and applied the 10% increase to areas currently classified as continuous permafrost and the 40% decrease to areas currently classified as containing discontinuous, sporadic, and isolated permafrost. A key difference between our experiment and that of Krinner and Boike (2010) is that we considered only changes in lake area, while they combined changes in lake area with changes in wetland area in the same locations. The resulting 2.16 million km^2 of lake area (Fig. 3.1d) includes very small increases in northern Canada and northeast Asia and small decreases to the south, as compared with current conditions.

We used an interpolated version of a global gridded lake depth dataset (Kourzeneva 2009, 2010) (http://www.flake.igb-berlin.de/ep-data.shtml). This dataset includes real data for over 13,000 lakes, assigns a default depth of 10 m when a lake is present but depth data is not available, and assigns a depth of 3 m for rivers. We interpolated this dataset to 1.9° x 2.5° resolution by using the mean depth from each 1 km gridcell, including those containing the default 10 m depth (Fig. 3.1e). As discussed in Subin et al. (2012), this interpolation is crude, as many gridcells are dominated by missing data where the default depths are assigned. We consider this approach an intermediate step between assuming a constant 50 m depth globally, as in the existing CLM4, and simulating several lakes of different size categories in each gridcell, as has been done for a regional climate model (Samuelsson et al. 2010).

3.3.3 Experimental Design

We performed three primary CCSM4 experiments with two additional simulations for sensitivity to model version and forcing climate, and two idealized aqua-planet experiments described below. The primary experiments were intended to understand the sensitivity of present climate to lake distribution and the sensitivity of future climate to changes in lake distribution in permafrost regions, and they included a total of ten CCSM4 simulations. These simulations were conducted using five combinations of climate and lake area (Table 3.1), with each combination using two model configurations (CLM4 offline and slab ocean modes) to separate the direct changes to surface fluxes caused by lakes from the atmospheric responses to these surface flux changes. The first experiment compared simulations using present climate with the GLWD lake area to simulations with the default CLM4 lake area ("Hi" – "Lo"), to see what biases may be introduced to the CCSM4 climate by using an unrealistically small lake area. The second experiment compared simulations using present climate with the GLWD lake area to simulations with no lake area at all ("Hi" – "No"), to compare with previous studies that have similarly investigated the seasonal effects of lakes on surface fluxes and regional climate (Bonan 1995; Dutra et al. 2010; Krinner 2003; Samuelsson et al. 2010). Finally, the third experiment compared simulations using future climate with the potential future lake distribution (Section 3.3.2) to simulations using future climate with the GLWD lake area ("Fu_2CO_2" – "Hi_2CO_2").

For the simulations using present climate (No, Lo, and Hi), we spun up the land model for 100 years using four cycles of 1980-2004 historical atmospheric forcing in order to equilibrate the lake temperatures, soil temperatures, and soil moisture. The resulting land initial conditions were used for 25-year simulations for the offline simulations and 200-year simulations for the coupled simulations, which used the standard year 2000 initial condition files for the atmosphere, slab ocean, and sea ice. We discarded the first 20 years of the coupled simulations to allow all the model components to equilibrate with the altered terrestrial surface and with fixed year 2000 atmospheric concentrations (i.e., ozone, aerosols, CO_2, and other greenhouse gases). Note that the short thermal relaxation time of the slab ocean means that we effectively simulated an equilibrium climate with year 2000 greenhouse gas concentrations, which will be warmer than observed conditions under transient greenhouse gas concentration increases, where net heat flux to the deep ocean cools the ocean surface and the atmosphere.

For the simulations using future climate (Hi_2CO_2 and Fu_2CO_2), we spun up the land model using 2090-2099 atmospheric forcing from a previous fully coupled CCSM4 RCP 4.5 simulation while retaining the standard year 2000 initial condition files for the other components. The offline simulations continued for another 25 years using repeated 2090-2099 data. The fully coupled simulations using future climate were performed with all species kept at year 2000 concentrations except for CO_2, which was doubled over pre-industrial levels to 569.4 ppm. We ran these simulations for a total of 220 years and discarded the first 40 years to allow the land, sea ice, and slab ocean additional time to equilibrate with the resulting climate.

To isolate the effects of model version and forcing climate on model predictions, we also performed two additional simulations (Table 3.1) with the standard version of CCSM4, which does not include CLM4-LISSS or the high-latitude biogeophysical changes. One simulation ("CCSM4-2000") was configured identically to the coupled simulations with slab ocean under present climate described above, except with only 100 years of simulation, while the second ("CCSM4-Historical") consisted of a transient fully coupled CCSM4 simulation with POP2 from

1850-2000 with historical conditions for atmospheric constituents, land use, nitrogen deposition, and aerosol deposition.

Finally, in order to better understand changes in large-scale atmospheric circulation and remote changes caused by the addition of mid- to high-latitude lake area, we also performed two idealized aqua-planet experiments mimicking the terrestrial surface forcing by perturbing prescribed SSTs from 40° – 70°N relative to a control simulation: (a) "SST-2", a 2°C cooling to resemble the effect of lakes in the summer; and (b) "SST+2", a 2°C warming to resemble the effect of lakes in the fall. In the context of the hierarchy of models proposed by Held (2005), the use of aqua-planet allows the mechanisms of large-scale change to be more easily understood. The effects of terrestrial surface properties, topography, zonal asymmetry, and seasonal cycles are removed, leaving a system which comes to equilibrium within 2 months and varies only on a synoptic time-scale.

3.3.4 Analysis

For the simulations using CLM4 offline, we calculated monthly anomalies for each of the three experiments for each of five surface fluxes: latent heat, sensible heat, net longwave emission, absorbed shortwave, and sub-surface energy flux (the rate of increase of snow, lake, and soil enthalpy from both thermal diffusion at the surface and absorption of shortwave radiation). We examined these anomalies averaged over Canada (land north of 48°N and between 175° and 325°E). As the atmospheric forcing was fixed, there was no interaction of the lakes with internal variability, so no statistical analysis was needed.

For the coupled simulations, we calculated seasonal anomalies for each of the three experiments for: daily mean (T_2), maximum (T_{max}), and minimum (T_{min}) 2 m air temperature; diurnal 2 m air temperature range (DTR); convective, large-scale, and total precipitation; downwelling and absorbed shortwave radiation at the surface; low, medium, high, and total cloud fraction; sea-level pressure (SLP); zonal and meridional wind; atmospheric temperature; geopotential height; and MSF. We highlighted statistically significant anomalies by doing a simple independent t-test for each gridcell or latitude (for zonally-averaged fields) with a 5% significance threshold, with each 3-month season as one observation. However, we were cautious in interpreting significant changes remote from the locations of large lake area change. We compared DTR and precipitation for the simulations under present climate to the Climate Research Unit (CRU) 2.1 (Mitchell and Jones 2005) climatology for the period 1980 – 2002. We also compared cloud fraction to the International Satellite Cloud Climatology Project D2 (ISCCP D2) (Rossow and Duenas 2004) for the period 1984 – 2008.

We investigated whether either the mean states or variances of the NAO, NAM, or ENSO were altered in the coupled experiments. For each season (for NAO, which is strongest during the winter and can vary on short timescales) or year (NAM and ENSO, which vary on multi-year timescales), we calculated the differences in SLP between the Azores and Iceland for NAO (Rogers 1981), between 35°N and 65°N for NAM (Li and Wang 2003), and between Tahiti and Darwin for ENSO (Trenberth 1984), using gridcells within 2° of each point or latitude. We calculated the p-values of the independent t-statistic to detect differences in the means and the Bartlett statistic (Bartlett 1937; Snedecor and Cochran 1989) to detect differences in the variances. Since we performed 10 total tests, we adjusted the p-value required to detect

significant changes down from 5% to 0.5% ($1 - 0.95^{1/10}$) to minimize the chance of a spurious significant result. We were also cautious in interpreting results, as some dynamic modes (i.e., ENSO) depend heavily on ocean dynamics that are not fully represented in slab ocean simulations. As a control, we also performed the same tests for differences between the Hi and Hi_2CO_2 simulations, where we may expect changes (Timmermann 1999).

The three aqua-planet simulations were integrated for 3 years, and we used the mean results for the last year in our analysis, calculating zonal mean anomalies with respect to the control simulation for total surface precipitation, 850 mb zonal windspeed, and 500 mb geopotential height.

3.4 Results

3.4.1 Local Effects of Lake Distribution

3.4.1.1 High (GLWD) vs. Low (CLM4 Default) Lake Area under Year 2000 Climate (Hi – Lo)

With fixed atmospheric forcing, the addition of 0.66 million km^2 of lake area in Canada caused up to 4.0 W m^{-2} changes in monthly surface fluxes averaged over the region (Fig. 3.2). Sub-surface energy absorption increased by an average of 2.2 W m^{-2} from April through July; this energy was released back to the atmosphere at an average rate of 2.7 W m^{-2} from September through November. There was an annual average shift of roughly 0.7 W m^{-2} from sensible heat flux to latent heat flux and longwave emission. Lakes increased albedo during the spring melt more than they decreased albedo during the summer, causing a net annual decrease in absorbed shortwave radiation of 0.4 W m^{-2}.

In coupled simulations, the increased sub-surface thermal inertia and shift from sensible heat fluxes to latent heat and longwave fluxes caused widespread significant seasonal changes in T_{min} and T_{max} in Canada and Northern Europe (Fig. 3.3), with a maximum gridcell change of 2.3 °C (fall increase in T_{min}). In the spring and summer, warming and evaporating lakes caused a day-time cooling (Fig. 3.3a-b). During the summer and fall night-time, lakes released heat back to the atmosphere and caused local warming (Fig. 3.3c-d). Near-surface relative humidity increased significantly by up to 6% in Central Canada in the summer.

Significant T_2 changes in areas adjacent to added lakes were negative in the summer and positive in the fall, indicating a net uptake of energy by lakes during the summer and release to their surroundings in the fall. Moreover, the lower atmosphere is more tightly coupled to the terrestrial surface during the day than night and to sensible heat rather than longwave fluxes. Consequently, 850 hPa summer temperatures decreased by up to 1.2°C over North America and the western North Atlantic (Fig. 3.4a). The mean summer planetary boundary layer (PBL) height decreased significantly by up to 70 m near the location of maximum decrease in 850 hPa temperature. This decrease is consistent with observations and modeling studies that show a lower PBL depth over wet locations (Banta and White 2003; Patton et al. 2005) and with decreased sensible heat flux (Shin and Ha 2007).

3.4.1.2 High (GLWD) vs. No Lake Area under Year 2000 Climate (Hi – No)

With fixed atmospheric forcing, the replacement of vegetation and soil by lakes caused seasonal flux changes that depended on location. High-latitude lakes caused flux changes similar in sign to those resulting in the Hi – Lo experiment. Temperate lakes such as the Great Lakes, which were absent in the No simulation (but not the Lo simulation), stayed unfrozen into part of the winter season, increasing both sensible and latent heat fluxes. Tropical lakes were much smaller in extent, but locally caused slight decreases in albedo, large decreases in sensible heat flux, and large increases in latent heat flux for all seasons.

In coupled simulations, changes were similar in character to those for Hi – Lo, except larger in magnitude and broader in seasonal extent, especially in the vicinity of the Great Lakes. Downwelling shortwave radiation significantly decreased in the eastern U.S. and Canada during all seasons due to increased cloudiness. The decrease in summer T_{max} over Great Lakes area gridcells was as large as 4.6°C. Significant decreases in 850 hPa temperatures were widespread throughout North America, Russia, the Arctic, and Europe and reached a magnitude of 2°C above the Great Lakes (Fig. 3.4b). Winter T_{min} increased over the Great Lakes and to the east by ~1°C.

3.4.1.3 Impacts of lake area changes from permafrost thaw under doubled CO_2 climate ($Fu\_2CO_2 - Hi\_2CO_2$)

The assumed potential changes to future lake distribution resulting from permafrost thaw were small (Fig. 3.1d), with very small increases in northern Canada and Siberia contrasting with small decreases to the south. Consequently, resulting impacts on climate were small compared with the Hi – Lo experiment: the only region showing notable changes was the Canadian Shield, which lost about 0.11 million km^2 of lake area. Changes in surface fluxes with fixed future atmospheric forcing were consistent in seasonality with Hi – Lo, except opposite in sign (because lakes were disappearing rather than being added) and smaller in magnitude. In coupled simulations, significant seasonal changes in T_{min} and T_{max} primarily occurred in the Canadian Shield (Fig. 3.5), with a maximum gridcell change of 1.3°C (fall decrease in T_{min}). Northern Canada and Great Lakes spring and summer T_{max} increased (Fig. 3.5a-b), while summer and fall T_{min} decreased (Fig. 3.5c-d), opposite in sign to, and smaller in magnitude than, the changes that occurred in Hi – Lo (Fig. 3.3).

3.4.2 Comparing predicted and observed DTR, precipitation, and cloud cover (Hi – Lo)

Increasing lake area to more realistic values caused significant decreases in predicted DTR throughout the spring, summer, and fall in Canada and Scandinavia. Decreases were largest in the summer (Fig. 3.6a), up to 3.6°C for individual gridcells. These decreases substantially reduced CCSM4 DTR biases compared to CRU in these affected areas (Fig. 3.6b, c), although large biases remained.

CCSM4 biases in precipitation and low clouds were slightly affected by the increase in lake area. Compared to ISCCP-D2, the Lo simulation under-predicted summer low cloud fraction in Canada and the Baltic by as much as 40%. We note that the summer low cloud bias in our simulations contrasted with the positive annual mean low cloud bias observed in the 1° CCSM4 (Gent et al. 2011). Low cloud fraction increased in the Hi simulation by up to 4%, significantly decreasing downward shortwave at the surface by ~3 – 9 W m^{-2} and causing a slight

improvement in the low cloud bias. Compared to CRU, the Lo simulation had a positive bias in total summer precipitation in the Central U.S. of up to 4 mm d^{-1}. Convective precipitation significantly increased in the Hi simulation over the Central U.S. by ~0.2 mm d^{-1}, while large-scale precipitation was unchanged, slightly worsening the total precipitation bias.

3.4.3 Aqua-planet simulations

As the mid- and high-latitude lake area increases decreased energy fluxes to the atmosphere in the summer and increased them in the fall (Fig. 3.2), we analyzed the resulting remote effects via two idealized aqua-planet experiments with ±2°C perturbed SSTs for 40° – 70°N (Fig. 3.7a). These perturbations caused changes in the tropics and the high-latitude SH. Generally, SST-2 and SST+2 had opposite impacts. In the following analysis, we discuss changes in SST-2. The opposite analysis can be applied to changes in SST+2 unless otherwise noted. The SST-2 induced a 2° northward shift of the ITCZ and a ~10% increase in its strength (Fig. 3.7b).

With NH extra-tropical surface cooling, the magnitude of the temperature gradient across the mid-latitudes increased. The NH Ferrell cell strengthened, associated with strengthening of the mid-latitude surface westerlies (Fig. 3.7c), increased subsidence at 30°N, and increased ascent at 60°N (Fig. 3.7d). The NH Hadley Cell strengthened, associated with increased moisture transport from the sub-tropics to the tropics in the low level branch (not shown). Precipitation (Fig. 3.7b) increased just north of the equator. The mechanism linking the mid-latitude circulation changes to the tropical response will be detailed in a future study.

The ITCZ shift was associated with significant SH responses. The SST-2 northward shift in the ITCZ strengthened the subtropical jet and weakened the subsiding branch of the Hadley cell at 30°S (Fig. 3.7d). The mid-latitude surface westerlies were weakened (Fig. 3.7c). Southern Ocean surface winds were not changed in SST-2. In SST+2, where the SH Hadley and Ferrell cells were strengthened, the westerlies strengthened in mid-latitudes and weakened at 60°S. Further work is required to understand why the SH zonal wind responses were not opposite in the SST-2 and SST+2 scenarios.

3.4.4 Hi – Lo: Large-scale and Remote Changes

3.4.4.1 Atmospheric Circulation

While the surface energy forcing caused by increased lake area in the Hi – Lo experiment was smaller in magnitude than the aqua-planet SST perturbations, due to both seasonal and zonal asymmetry, significant changes in atmospheric circulation and remote temperatures still occurred. Our analysis below focuses on changes in the summer and fall.

An increased summer NH meridional temperature gradient strengthened the upper tropospheric mid-latitude jet by ~0.50 m s^{-1} between 40 – 50°N (Fig. 3.8a). While much smaller in magnitude, this change was consistent with changes found in the SST-2 experiment (Fig. 3.7c). Simulated meridional wind anomalies (not shown) may have indicated a NH wave train in response to changes in the jet (Liu and Alexander 2007).

Small SH temperature changes occurred during the boreal summer (Fig. 3.4a). Significant differences in SH circulation also occurred in this season: increases of up to 1% in the SH

tropical MSF indicated a weakened Hadley circulation, while decreases of up to 5% in the polar MSF indicated a strengthened polar cell. These changes in the MSF were consistent with the decreased subtropical and increased polar subsidence occurring in the SST-2 aqua-planet experiment (Fig. 3.7d). Hi – Lo changes in the summer MSF were not significant for the NH.

Significant changes in SH zonal winds occurred during the boreal fall (Fig. 3.8b-d). A decrease at the poleward edge and increase at the equatorward edge of mid-latitude westerlies resulted from an equatorward shift in the SH mid-latitude jet from 50°S to 45°S; at 60°S westerlies decreased by as much as 1 m s^{-1}. The geography of the westerly decreases followed the contours of the Southern Ocean, with 850 hPa winds decreasing by up to 0.7 m s^{-1} (Fig. 3.8c). Significant changes of about 5% in the MSF (positive at 40°S and negative at 60°S) suggested both a strengthening Ferrell cell and a strengthening polar cell, with the boundary between the two shifting north. Increases in zonal mean SLP of up to 0.5 hPa south of 70°S also indicated a strengthened polar cell and were associated with regional temperature changes of up to 0.8°C (not shown). The zonal mean SH changes were consistent with the pattern in SST+2 (Fig. 3.7c-d). Significant increases in the MSF of up to 3% between 5° and 10°N may have indicated a slight southward shift in the ITCZ, consistent with the SST+2 experiment. However, only slight zonal mean precipitation changes occurred of less than 0.1 mm d^{-1}.

3.4.4.2 Modes of Variability

Changes in the mean and variance of the NAO, NAM, or ENSO for Hi – Lo and Hi – No experiments were not significant at the 0.5% level. In contrast, we found highly significant ($p < 10^{-5}$) shifts in the annual mean phase of the NAO, NAM, and ENSO in Hi_$2CO_2$ as compared to Hi, with a significant increase in winter NAO variance.

3.5 Discussion

3.5.1 Effects of Lakes on Seasonal Surface Fluxes and Local Air Temperature

As discussed in Subin et al. (2012), previous studies (Bonan 1995; Dutra et al. 2010; Krinner 2003; Lofgren 1997; Long et al. 2007; Rouse et al. 2005; Samuelsson et al. 2010) have largely agreed on the seasonal effects of lakes on local surface energy fluxes and surface air temperature, with some disagreement as to the net effect on latent heat flux and air temperature at high latitudes in the summer, and whether atmospheric warming persists into the winter after lakes have frozen. The summer disagreements may be related to how dry the neighboring soil is simulated to be (Krinner and Boike 2010) and how the vegetation is represented there. The winter disagreements may depend on the presence and extent of snow insulation in the model (Dutra et al. 2010).

Local changes in seasonal T_2 in the Hi – Lo, Hi – No, and Fu_$2CO_2$ – Hi_$2CO_2$ experiments were within the range of those reported in previous studies. We found that high-latitude lakes caused net local cooling in the spring and summer, and net warming in the fall. Slight net cooling during the summer resulted from the balance of day-time cooling and night-time warming, with slight increases in latent heat flux and longwave emission, and large decreases in sensible heat flux. Some studies (Dutra et al. 2010; Krinner 2003) have found decreases in summer latent heat flux due to lower surface temperatures and decreased roughness lengths. We

also found slight decreases in latent heat flux in the early summer; the largest contribution to summer decreased sensible heat flux at high latitudes was increased energy uptake by lakes, not increased latent heat flux.

In the winter, we found that high latitude lakes did not cause significant warming, which was likely due to the inclusion of snow insulation in CLM4-LISSS (Dutra et al. 2010; Subin et al. 2012). Although CCSM4 moderately over-predicts snow depth at high latitudes due to excessive winter precipitation (Lawrence et al. 2011b), offline CLM4 slightly under-predicts high-latitude snow cover fraction (Lawrence et al. 2011a), and lakes caused little change in winter surface fluxes in the offline Hi – Lo experiment. At lower latitudes, the Great Lakes remained unfrozen for part of the winter in the coupled Hi simulation, causing significant winter warming in this region compared to the coupled No simulation.

3.5.2 Implications for CCSM4 Evaluation

While most CMIP3 climate models underestimated DTR throughout land areas (Randall et al. 2007), we found that CCSM4 overestimated summer DTR in boreal regions (Fig. 3.6c), including regions where lake area is underestimated (Fig. 3.1b, c). This overestimation was due both to excessively high T_{max} and low T_{min} (not shown). This bias was reduced in those regions when more realistic lake area was used (Fig. 3.6a-c), although it was not eliminated. As the T_2 changes in our experiments and those of Krinner and Boike (2010) were linear with lake area change and independent of baseline climate, we hypothesize that increasing lake area to the values suggested to be realistic by Downing et al. (2006) would further reduce the DTR bias. However, the concurrent underestimation in simulated low cloud fraction may also have contributed to the high DTR bias (Dai et al. 1999). Indeed, some of the decrease in DTR with more realistic lake area may have resulted indirectly from the increase in low cloud fraction rather than the direct effect of lakes on surface energy fluxes.

Using the CCSM4-2000 and CCSM4-Historical simulations, we investigated the sensitivity of DTR biases to the model version and the climate forcing. The CCSM4-2000 simulation differed from the coupled Lo simulation only in duration and in lacking CLM4-LISSS and the high-latitude biogeophysical changes under development by S. C. Swenson and D. M. Lawrence. The positive summer DTR bias was larger in boreal regions in CCSM4-2000 than in the Lo simulation (Fig. 3.6d), notably in the Great Lakes region. This finding is consistent with the existing CLM4 lake model deficiencies, including excessive surface diurnal temperature range (Subin et al. 2012). However, much of the improvement in permafrost regions in the Lo simulation may have resulted from the biogeophysical changes.

The simulations using equilibrium 2000 conditions with slab ocean should have had a slightly warmer atmosphere than the 1980-2002 period, both due to changes between 1980 and 2000 and the lack of transient heat flux to the deep ocean. Consequently, interactions between DTR and atmospheric warming could have caused the simulated DTR to differ from the CRU observations. To test the importance of this caveat, we evaluated the summer DTR predicted in the CCSM4-Historical simulation during 1980-1999 (Fig. 3.6e). We found that the positive DTR bias, while slightly lower in some regions than in the CCSM4-2000 simulation, remained large in almost all regions with unrealistic lake area.

While increasing lake area in the Hi – Lo experiment slightly improved the large negative bias in summer low cloud fraction in Canada, even larger improvements occurred over Arctic land when we compared the Lo simulation to the CCSM4-2000 simulation, likely related to the high-latitude biogeophysical changes. The negative summer low cloud fraction bias was improved over the Great Lakes in CCSM4-Historical relative to CCSM4-2000, but not elsewhere at high latitudes. The bias toward excessive summer precipitation in the Central U.S. plains in the Lo simulation (which was slightly worsened in the Hi simulation) was unchanged in the CCSM4-2000 simulation but larger in the CCSM4-Historical simulation.

Assessing improvements to GCM simulations after changing one model component is difficult; compensating errors may cause a reduction in bias for the wrong reasons. We cannot be confident that the reduced DTR bias from adding lake area did not either come at the expense of other hydroclimate variables or compensate for other sources of bias; further work should investigate the DTR bias in CCSM4 and other CMIP5 climate models more systematically. As long as there are no interactions between lake area change and model biases, our predicted changes in climate variables with the addition of lake area will be relatively robust. Biases that would interact with lake area change include unrealistic soil moisture or stomatal limitation of ET in areas replaced by lakes, or an unrealistic land-atmosphere coupling strength. CCSM4 tends to have excessive summer soil moisture limitation in permafrost regions (Lawrence et al. 2011b), which would tend to increase the effects of adding lakes. However, CCSM4 tends to have excessive transpiration (Lawrence et al. 2011b) and a relatively weak land-atmosphere coupling strength (D. M. Lawrence, personal communication, 2011) in tropical and temperate regions, which would tend to reduce the effects of adding lakes.

3.5.3 Climate Effects of Changing Lake Area in Permafrost Regions

We found that decreasing lake area in regions currently characterized by discontinuous permafrost could cause mild seasonal changes in T_2, up to a 1.3°C decrease in T_{min}. However, these changes were modest compared to the biases that may result in the simulation of current climate from using unrealistically small lake area. Krinner and Boike (2010) found significant changes consistent in seasonal sign but somewhat larger and more widespread. These slightly larger changes were likely because they considered the combined disappearance of lake and wetland area, while we considered only changes in lake area. Differences in present and future lake area distributions and lake model structure and parameterization were not likely causes of the discrepancy, except during the winter season, when Krinner and Boike (2010) found significant winter cooling from decreased inland water surface area. We did not find significant winter impacts of lakes at high latitudes, as discussed in Section 3.5.1.

Our simulations could underestimate the climate impacts of changing lakes in permafrost regions. While we followed the assumption of Krinner and Boike (2010) [based loosely on the analysis by Smith et al. (2007) and consistent with the observations in Plug et al. (2008) and simulations by van Huissteden et al. (2011)] that lake area in remaining or currently continuous permafrost would only increase by 10%, it is possible that thermokarst activity could increase lake area by larger percentages in some regions. Our estimates are also sensitive to our assumed existing high-latitude lake area, which is likely an underestimate (Downing et al. 2006). Moreover, we have only considered the physical impacts of changing lake area. The biogeochemical impact of expanding thermokarst lakes and increasing emissions of CO_2 and

CH_4 from these lakes is more difficult to quantify (Riley et al. 2011; Wania et al. 2010), and may be large (Schuur et al. 2008; Walter et al. 2007).

3.5.4 Large-Scale Changes Resulting from Mid- and High-Latitude NH Surface Forcing

Shifts in the ITCZ in response to decreases in NH extra-tropical surface temperatures in our aqua-planet experiments were in the opposite direction of those predicted by previous studies (Kang et al. 2009; Kang et al. 2008), likely due to our use of prescribed SSTs rather than a slab ocean model. We hypothesize that this difference is representative of some differences in the atmospheric responses to terrestrial rather than ocean cooling. We highlight two of these differences: (1) a cooling due to a change in ocean circulation would imply a compensating remote warming [e.g., Kang et al. (2009; 2008) imposed an implied cross-equatorial sub-surface heat flux], while a cooling due to a change in terrestrial surface properties (e.g., albedo) may decrease the top-of-atmosphere energy balance without a direct compensation elsewhere; (2) an ocean cooling would generally persist for a long enough time for remote ocean temperatures to respond, while a terrestrial cooling, such as that resulting from increased sub-surface energy storage due to increased lake area, may be seasonal or otherwise transient. We may tentatively reject (1) as an explanation: while the cross-equatorial heat flux imposed in Kang et al. (2009; 2008) may have reinforced the southward ITCZ shift, several other studies (Chiang and Bitz 2005; Lee et al. 2011) found a southward ITCZ shift from extra-tropical NH cooling without imposing any compensating cross-equatorial heat flux. In particular, the Chiang and Bitz (2005) experiment simulated the responses to an increase of Arctic sea ice, which may act similarly to an increase in terrestrial albedo. However, regarding (2), we are not aware of previous studies investigating the transient response to extra-tropical cooling, so it is possible that the initial atmospheric response would be different in character than the equilibrium response once tropical SSTs have adjusted to the forcing. Further research should investigate these potentially contrasting responses.

Interpreting significant changes in geographic fields at the gridcell level requires caution due to spatial and temporal autocorrelation. To illustrate the limitations of using relatively short simulations to detect signals smaller than typical inter-annual variability, we divided the 180 years analyzed for the Hi – Lo experiment into four 45-year periods, and we compared statistical significance evaluated for each individual period with that evaluated for the entire period. Even in the winter, when the surface forcing caused by the addition of lakes was small (Fig. 3.2), some regions with statistically significant changes occurred when evaluated over the entire 180-year period (Fig. 3.9). However, the changes in individual periods within these regions were not always consistent in sign or significant: the Barents Sea cooled in three of the periods but warmed in the fourth. Moreover, the regions appearing to be significant in each period were not always contained within the regions found to be significant for the entire 180-year period. In particular, most of the Arctic experienced an apparently statistically significant cooling of 1°C or more during one of the periods ("Period 3", Fig. 3.9c), but this cooling did not occur during the other three periods. We note that the previously discussed significant changes occurring in the summer and fall showed much more consistency among the four periods than the winter changes in Fig. 3.9.

Because of these challenges in interpreting statistical significant changes, we have attempted to be cautious in interpreting remote changes such as the Hi – Lo SH changes in boreal summer

temperature and boreal fall zonal winds by examining whether changes were mechanistically consistent among several variables (e.g., temperature, pressure, wind, and MSF), linked to changes in the NH tropics, and similar to analogous changes in the idealized aqua-planet simulations. Many of the remote changes occurring in Hi – Lo failed to satisfy all these criteria, including some localized changes in temperature, precipitation, and surface pressure that we did not analyze in Section 3.4.4.1. The changes in zonal winds in the boreal summer and fall may be the most compelling. Both the summer increases in NH mid-latitude westerlies and the boreal fall decreases in Southern Ocean westerlies were consistent among several variables and with the analogous aqua-planet experiments, although changes in the NH tropics were very small compared to changes in the aqua-planet experiments. We note that many terrestrial surface changes associated with climate change (e.g., vegetation distribution changes, loss of land ice or snow cover, or changes in wetland area) may be of much larger magnitude than the lake area changes simulated here. While previous studies may have used simulations of insufficient duration to detect remote changes, our results suggest that these changes may be significant.

3.6 Conclusions

The presence of large lake area in boreal regions, particularly the Canadian Shield, causes widespread changes in North American surface air temperatures of 1 – 2°C during the spring, summer, and fall, as compared to a comparable system with much less lake area. Increased sub-surface thermal inertia reduces diurnal temperature variation, causes increases in low cloud fraction, and causes net spring and summer cooling and fall warming. Increasing the realism of modeled lake area and properties in climate models may improve simulated biases in diurnal temperature range in some regions, although this evaluation is complicated by the large number of processes affecting diurnal temperature range.

Relatively small changes of 2°C in extra-tropical surface temperatures can cause changes in atmospheric circulation and remote precipitation and winds, although realistic zonally and seasonally asymmetric forcings have less coherent impacts than idealized forcings of similar maximum magnitude. A consistent response to increases in extra-tropical Northern Hemisphere surface energy fluxes in our experiments was decreases in westerly flow over the Southern Ocean; according to previous analyses, these changes could alter ocean upwelling and affect the global carbon cycle. A more detailed investigation of this mechanism is warranted. Further research is also needed to understand potentially contrasting atmospheric responses to extra-tropical surface temperature changes depending on the character of the imposed forcing and remote ocean responses.

The disappearance of lakes from present regions of discontinuous permafrost could cause small (0.5 – 1°C) changes in surface air temperature in certain regions, such as central northern Canada, increasing diurnal temperature variation and amplifying summer warming. However, these changes may be relatively small compared to the effects of global climate change in the same regions or to errors in simulation caused by the under-estimation of lake area in current datasets. To confirm this, research should focus on improving datasets of existing high-latitude lake area and improving understanding of the potential for increases in lake area due to thermokarst activity in remaining permafrost regions. Furthermore, the biogeochemical changes associated with melting permafrost are likely more uncertain than the direct physical responses to changes in lake area.

3.7 Acknowledgements

Michael Wehner (Lawrence Berkeley National Lab), John Chiang (University of California, Berkeley), Benjamin Santer (Lawrence Livermore National Lab), William Collins (Lawrence Berkeley National Lab), and Sarah Kang (Columbia University) provided helpful comments on interpreting large-scale atmospheric responses to regional changes in terrestrial surface forcing. David Lawrence (National Center for Atmospheric Research) facilitated interaction with the CESM Land Model Working Group and support in running and interpreting the model. One anonymous reviewer and one named reviewer (Sumant Nigam) provided helpful comments in clarifying and improving the manuscript. This work was supported by the Director, Office of Science, Office of Biological and Environmental Research, Climate and Environmental Science Division, of the U.S. Department of Energy under Contract No. DE-AC02-05CH11231 to Berkeley Lab.

3.8 Figures

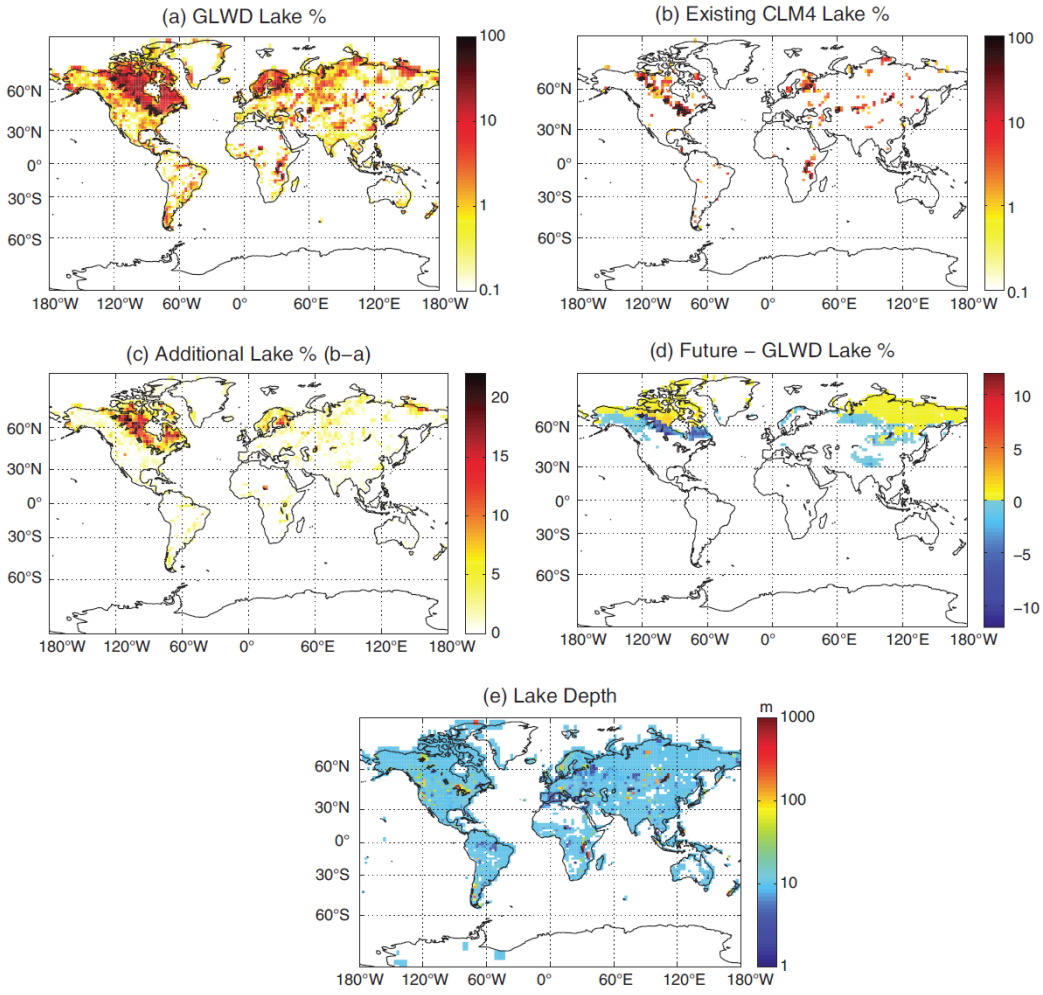

Fig. 3.1: Area and depth datasets at 1.9° x 2.5°: (a) interpolated GLWD lake percent (2.3 million km^2) (Lehner and Doll 2004); (b) default CLM4 lake percent (0.72 million km^2) (Cogley 1991); (c) additional lake percent in GLWD compared to default CLM4; (d) potential future lake percent compared to GLWD (net 0.14 million km^2 decrease); and (e) interpolated lake depth based on Kourzeneva (2009, 2010).

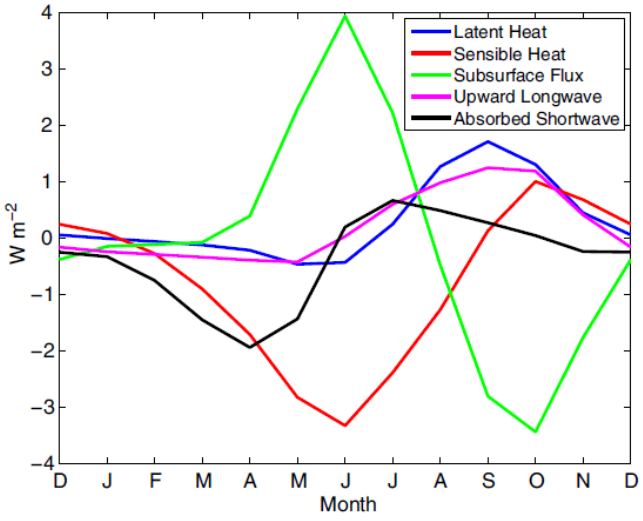

Fig. 3.2: Hi (GLWD lake area) – Lo (default CLM4 lake area) offline monthly average surface flux anomalies for Canada (land north of 48°N and between 175° and 325°E) under present climate: latent heat flux, sensible heat flux, rate of increase of sub-surface enthalpy, upwelling longwave radiation, and absorbed shortwave radiation.

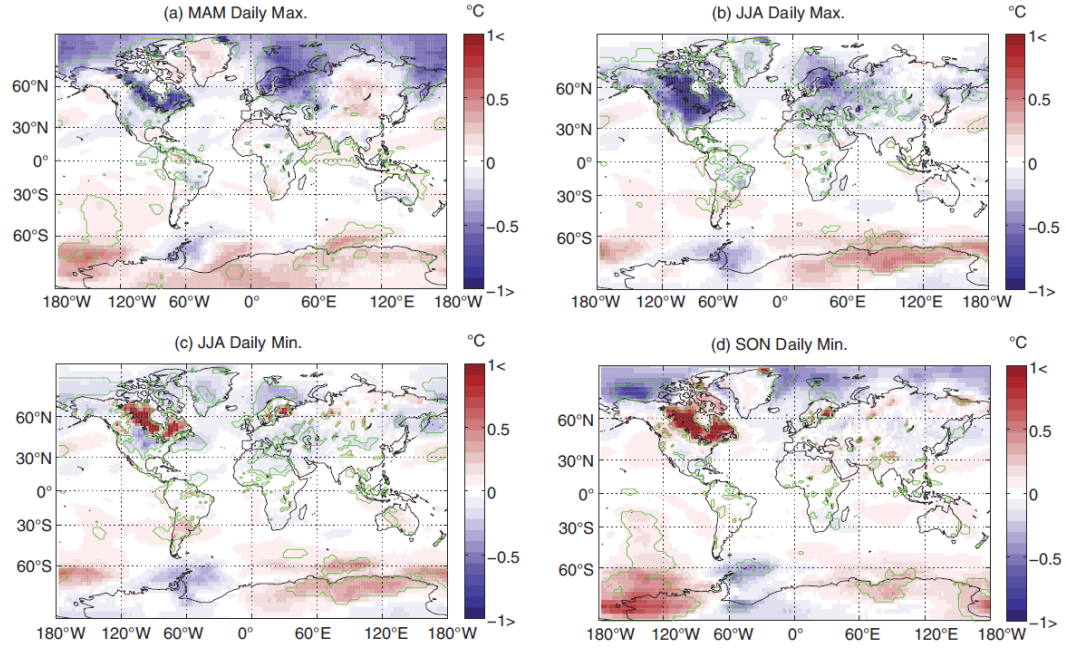

Fig. 3.3: Hi (GLWD lake area) – Lo (default CLM4 lake area) coupled seasonal average 2 m temperature anomalies under year 2000 conditions: (a) MAM daily maximum; (b) JJA

daily maximum; (c) JJA daily minimum; and (d) SON daily minimum. Green contours encircle gridcells experiencing statistically significant changes.

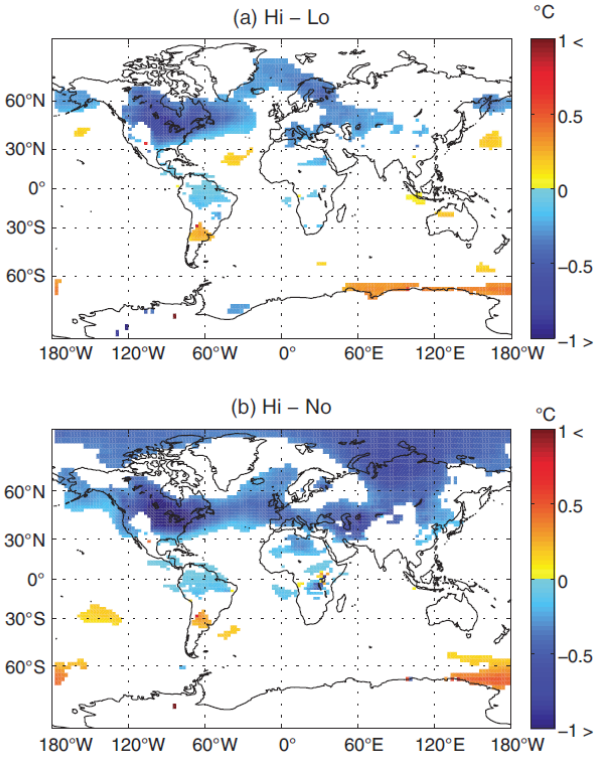

Fig. 3.4: Significant JJA average atmospheric temperature anomalies at 850 hPa in coupled simulations under year 2000 conditions for (a) Hi (GLWD lake area) – Lo (default CLM4 lake area); and (b) Hi (GLWD lake area) – No (no lake area).

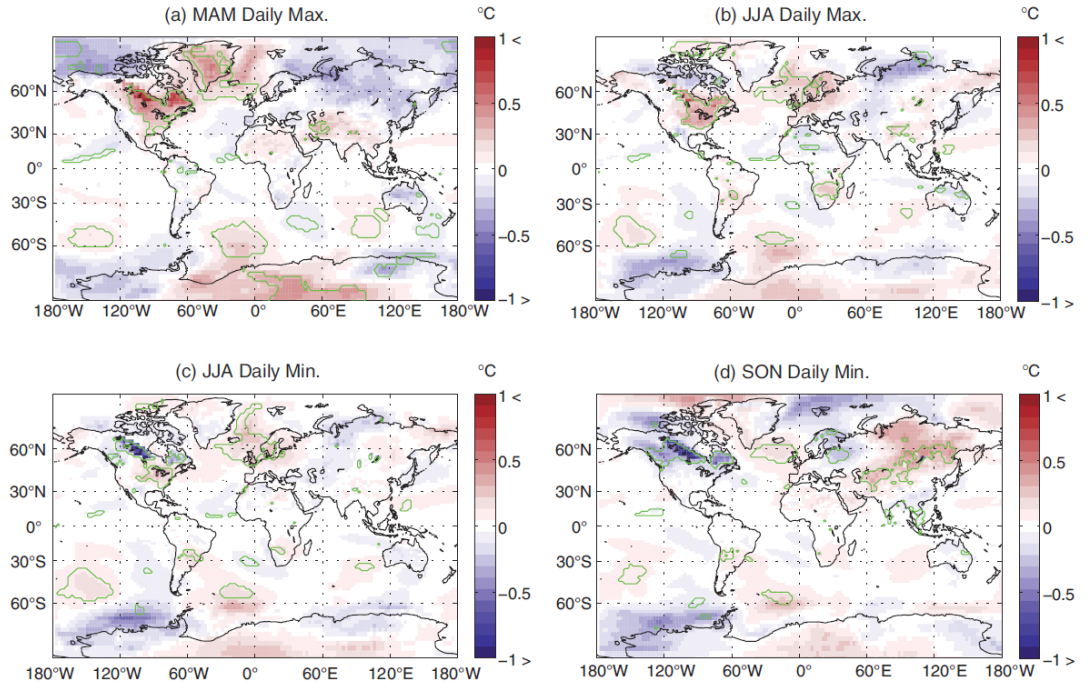

Fig. 3.5: Fu (potential future lake area) – Hi (GLWD lake area) coupled seasonal average 2 m temperature anomalies under doubled CO_2 conditions: (a) MAM daily maximum; (b) JJA daily maximum; (c) JJA daily minimum; and (d) SON daily minimum. Green contours encircle gridcells experiencing statistically significant changes.

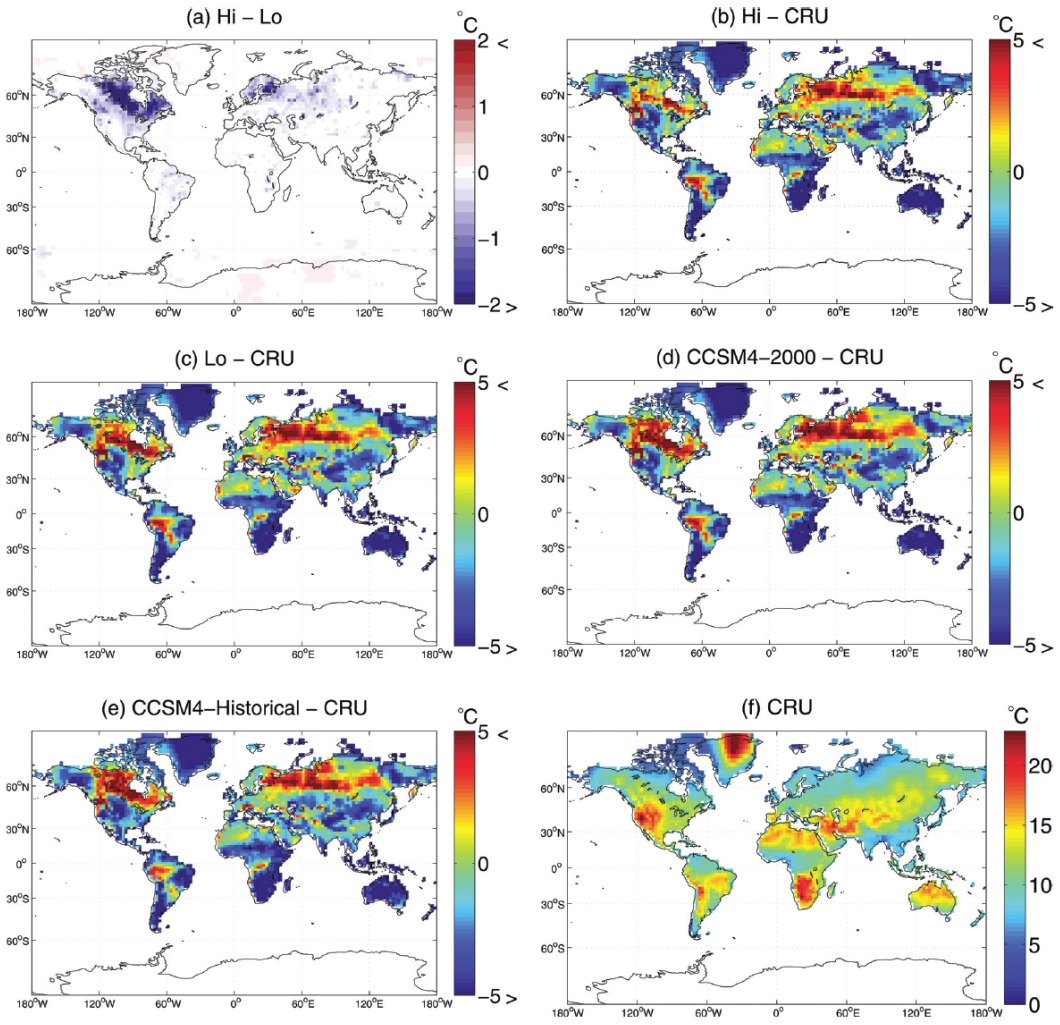

Fig. 3.6: JJA diurnal 2 m temperature range: coupled anomalies for (a) Hi – Lo (significant only); (b) Hi – CRU; (c) Lo – CRU; (d) CCSM4-2000 – CRU; and (e) CCSM4-Historical (1980-1999 mean) – CRU; and absolute JJA 2 m diurnal temperature range for (f) CRU (1980-2002).

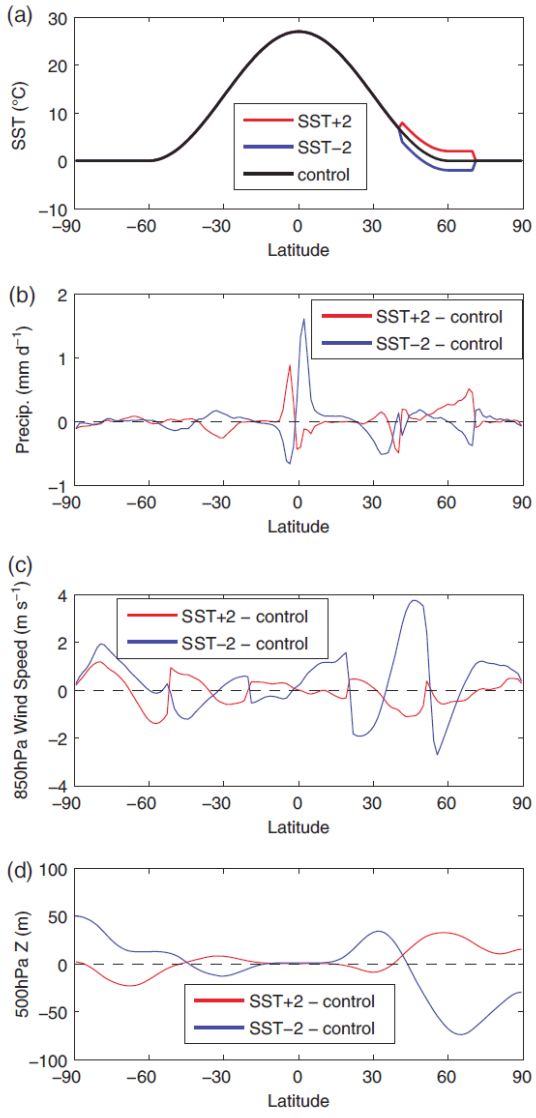

Fig. 3.7: Zonally averaged fields for the three aqua-planet simulations: (a) prescribed SST for control, SST+2, and SST-2; (b) precipitation anomalies with respect to control; (c) 850 mb zonal wind speed anomalies with respect to control; and (d) 500 mb geopotential height anomalies with respect to control.

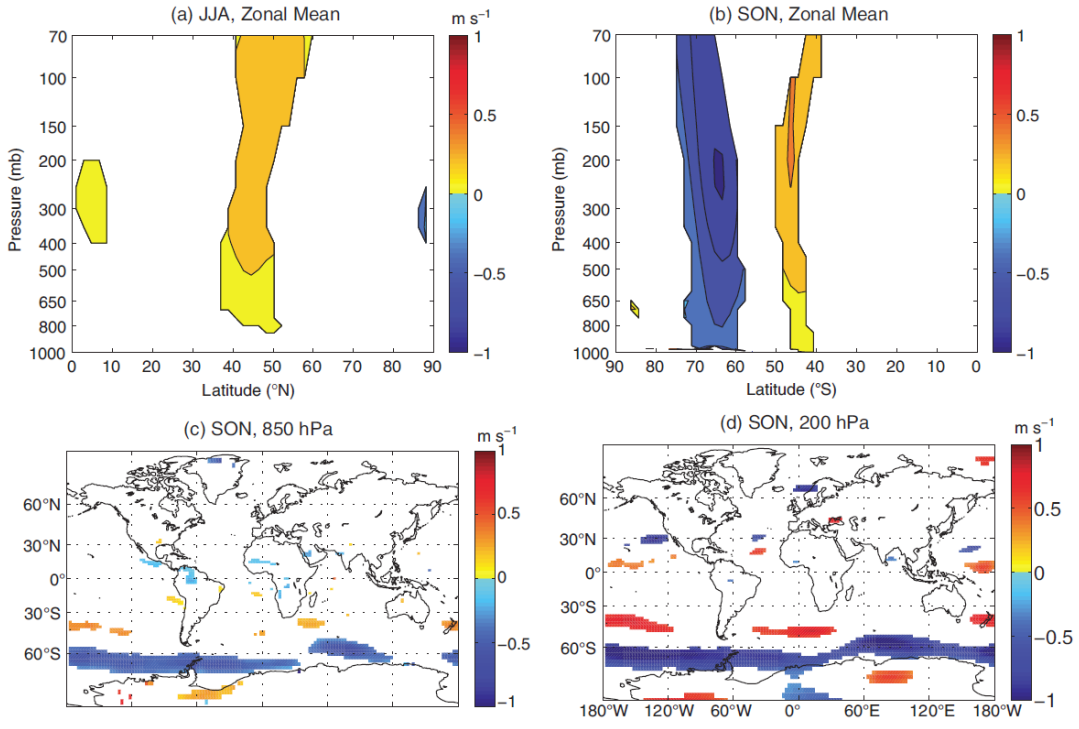

Fig. 3.8: Significant seasonal average atmospheric zonal mean wind anomalies (+ to the east) in coupled simulations under year 2000 conditions for Hi (GLWD lake area) – Lo (default CLM4 lake area): (a) JJA, zonal mean; (b) SON, zonal mean; (c) SON, 850 hPa; and (d) SON, 200 hPa.

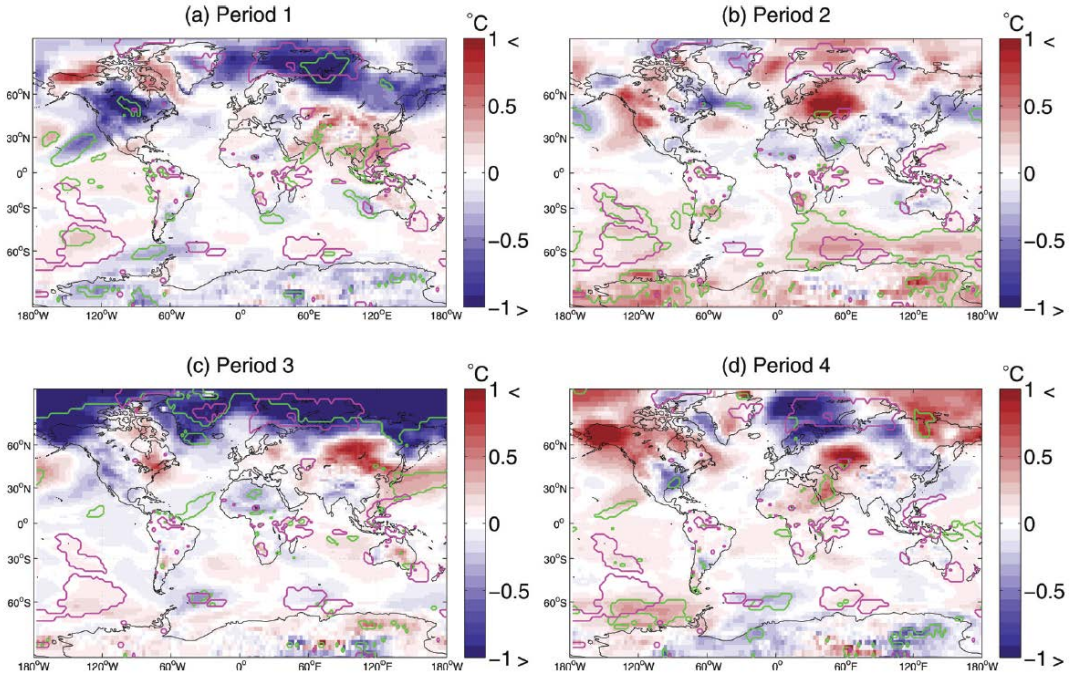

Fig. 3.9: Hi (GLWD lake area) – Lo (default CLM4 lake area) coupled DJF 2 m temperature anomalies under year 2000 conditions for the four 45-year periods composing the full 180 analyzed years of simulation: (a) Period 1; (b) Period 2; (c) Period 3; and (d) Period 4. Green contours encircle significant changes evaluated for each 45-year period, while magenta contours encircle regions where significant changes were found for the full 180 years.

3.9 Tables

Table 3.1: CCSM4 Experimental Design

Climate	**Lake Area**			
	Zero	CLM4	GLWD	Future
1850-2000*		CCSM4-Historical*		
Eq. 2000	**No**	**Lo**; CCSM4-2000	**Hi**	
Eq. 2 x CO_2			**Hi_2CO_2**	**Fu_2CO_2**

Each bold entry represents 2 simulations, one with CLM4 offline for 25 years and one in slab ocean mode with equilibrium (eq.) climate using fixed aerosol, greenhouse gas, and ozone concentrations. The three primary experimental comparisons were Hi – Lo, Hi – No, and Fu_2CO_2 – Hi_2CO_2. Note that the offline CLM4 simulations with "2 x CO_2" actually used 2090-2099 atmospheric forcing from a previous RCP 4.5 simulation, as equilibrium doubled-CO_2 atmospheric forcing was not available. In addition, non-bold entries indicate simulations with the standard CCSM4, lacking CLM4-LISSS and the high-latitude biogeophysical changes. *The CCSM4-Historical simulation was transient and included the full ocean model.

3.10 References

Anderson, R. F., S. Ali, L. I. Bradtmiller, S. H. H. Nielsen, M. Q. Fleisher, B. E. Anderson, and L. H. Burckle, 2009: Wind-Driven Upwelling in the Southern Ocean and the Deglacial Rise in Atmospheric CO2. *Science*, **323,** 1443-1448.

Banta, R. M., and A. B. White, 2003: Mixing-height differences between land use types: Dependence on wind speed. *Journal of Geophysical Research-Atmospheres*, **108**.

Bartlett, M. S., 1937: Properties of sufficiency and statistical tests. *Proceedings of the Royal Society of London Series a-Mathematical and Physical Sciences*, **160,** 0268-0282.

Bates, G. T., F. Giorgi, and S. W. Hostetler, 1993: Towards the Simulation of the Effects of the Great-Lakes on Regional Climate. *Mon. Weather Rev.*, **121,** 1373-1387.

Bonan, G. B., 1995: Sensitivity of a GCM Simulation to Inclusion of Inland Water Surfaces. *J. Clim.*, **8,** 2691-2704.

Bonfils, C., and B. Santer, 2010: Investigating the possibility of a human component in various pacific decadal oscillation indices. *Climate Dynamics***,** 1-12-12.

Bonfils, C., A. Angert, C. C. Henning, S. Biraud, S. C. Doney, and I. Fung, 2005: Extending the record of photosynthetic activity in the eastern United States into the presatellite period using surface diurnal temperature range. *Geophysical Research Letters*, **32**.

Braganza, K., D. J. Karoly, and J. M. Arblaster, 2004: Diurnal temperature range as an index of global climate change during the twentieth century. *Geophysical Research Letters*, **31**.

Branstator, G., 2002: Circumglobal teleconnections, the jet stream waveguide, and the North Atlantic oscillation. *Journal of Climate*, **15,** 1893-1910.

Brown, J., O. J. J. Ferrians, J. A. Heginbottom, and E. S. Melnikov, 2001: *Circum-Arctic map of permafrost and ground-ice conditions*. N.S.I.D.C. http://nsidc.org/data/ggd318.html

Brown, L. C., and C. R. Duguay, 2010: The response and role of ice cover in lake-climate interactions. *Prog. Phys. Geogr.*, **34,** 671-704.

Chase, T. N., R. A. Pielke, T. G. F. Kittel, R. R. Nemani, and S. W. Running, 2000: Simulated impacts of historical land cover changes on global climate in northern winter. *Climate Dynamics*, **16,** 93-105.

Chiang, J. C. H., and C. M. Bitz, 2005: Influence of high latitude ice cover on the marine Intertropical Convergence Zone. *Climate Dynamics*, **25,** 477-496.

Cogley, J. G., 1991: GGHYDRO – Global Hydrographic Data Release 2.0. Dept. Geography, Trent University.

Collatz, G. J., L. Bounoua, S. O. Los, D. A. Randall, I. Y. Fung, and P. J. Sellers, 2000: A mechanism for the influence of vegetation on the response of the diurnal temperature range to changing climate. *Geophysical Research Letters*, **27,** 3381-3384.

Collins, W. D., and Coauthors, 2004: Description of the NCAR Community Atmosphere Model (CAM3). National Center for Atmospheric Research, NCAR/TN-478+STR.

Corti, S., F. Molteni, and T. N. Palmer, 1999: Signature of recent climate change in frequencies of natural atmospheric circulation regimes. *Nature*, **398,** 799-802.

Dai, A., K. E. Trenberth, and T. R. Karl, 1999: Effects of clouds, soil moisture, precipitation, and water vapor on diurnal temperature range. *Journal of Climate*, **12,** 2451-2473.

Delworth, T. L., and M. E. Mann, 2000: Observed and simulated multidecadal variability in the Northern Hemisphere. *Clim. Dyn.*, **16,** 661-676.

Downing, J. A., and Coauthors, 2006: The global abundance and size distribution of lakes, ponds, and impoundments. *Limnology and Oceanography*, **51,** 2388-2397.

Dutra, E., V. M. Stepanenko, G. Balsamo, P. Viterbo, P. M. A. Miranda, D. Mironov, and C. Schar, 2010: An offline study of the impact of lakes on the performance of the ECMWF surface scheme. *Boreal Environment Research*, **15,** 100-112.

Fang, X., and H. G. Stefan, 1996: Long-term lake water temperature and ice cover simulations/measurements. *Cold Reg. Sci. Tech.*, **24,** 289-304.

Feddema, J., K. Oleson, G. Bonan, L. Mearns, W. Washington, G. Meehl, and D. Nychka, 2005a: A comparison of a GCM response to historical anthropogenic land cover change and model sensitivity to uncertainty in present-day land cover representations. *Climate Dynamics*, **25,** 581-609.

Feddema, J. J., K. W. Oleson, G. B. Bonan, L. O. Mearns, L. E. Buja, G. A. Meehl, and W. M. Washington, 2005b: The importance of land-cover change in simulating future climates. *Science*, **310,** 1674-1678.

Frankcombe, L. M., and H. A. Dijkstra, 2010: Internal Modes of Multidecadal Variability in the Arctic Ocean. *Journal of Physical Oceanography*, **40,** 2496-2510.

Geerts, B., 2003: Empirical estimation of the monthly-mean daily temperature range. *Theoretical and Applied Climatology*, **74,** 145-165.

Gent, P. R., S. G. Yeager, R. B. Neale, S. Levis, and D. A. Bailey, 2010: Improvements in a half degree atmosphere/land version of the CCSM. *Climate Dynamics*, **34,** 819-833.

Gent, P. R., and Coauthors, 2011: The Community Climate System Model Version 4. *Journal of Climate*, **24,** 4973-4991.

Goyette, S., N. McFarlane, and G. Flato, 2000: Application of the Canadian Regional Climate Model to the Laurentian Great Lakes region: Implementation of a lake model. *Atmosphere-Ocean*, **38,** 481-503.

Graham, N. E., and W. B. White, 1988: The El-Nino Cycle- A Natural Oscillator of the Pacific-Ocean Atmosphere System. *Science*, **240,** 1293-1302.

Grosse, G., V. E. Romanovsky, K. M. Walter, A. Morgenstern, H. Lantuit, and S. Zimov, 2008: Distribution of Thermokarst Lakes and Ponds at Three Yedoma Sites in Siberia. *Proceedings of the 9th International Conference on Permafrost*, University of Alaska, Fairbanks, USA, 551-556.

Guan, B., and S. Nigam, 2009: Analysis of Atlantic SST Variability Factoring Interbasin Links and the Secular Trend: Clarified Structure of the Atlantic Multidecadal Oscillation. *Journal of Climate*, **22,** 4228-4240.

Guo, Z., and Coauthors, 2006: GLACE: The Global Land-Atmosphere Coupling Experiment. Part II: Analysis. *Journal of Hydrometeorology*, **7,** 611-625.

Held, I. M., 2005: The gap between simulation and understanding in climate modeling. *Bulletin of the American Meteorological Society*, **86,** 1609-+.

Held, I. M., M. F. Ting, and H. L. Wang, 2002: Northern winter stationary waves: Theory and modeling. *Journal of Climate*, **15,** 2125-2144.

Holton, J. R., 2004: *An Introduction to Dynamic Meteorology.* 4th ed. Elselvier Academic Press.

Hoskins, B. J., and D. J. Karoly, 1981: The Steady Linear Response of a Spherical Atmosphere to Thermal and Orographic Forcing. *Journal of the Atmospheric Sciences*, **38,** 1179-1196.

Hostetler, S., and P. Bartlein, 1990: Simulation of Lake Evaporation with Application to Modeling Lake Level Variations of Harney-Malheur Lake, Oregon. *Water Resources Research*, **26,** 2603-2612.

Jorgenson, M. T., Y. L. Shur, and E. R. Pullman, 2006: Abrupt increase in permafrost degradation in Arctic Alaska. *Geophysical Research Letters*, **33**.

Jorgenson, M. T., C. H. Racine, J. C. Walters, and T. E. Osterkamp, 2001: Permafrost degradation and ecological changes associated with a warming climate in central Alaska. *Climatic Change*, **48,** 551-579.

Kaab, A., and W. Haeberli, 2001: Evolution of a high-mountain thermokarst lake in the Swiss Alps. *Arctic Antarctic and Alpine Research*, **33,** 385-390.

Kalnay, E., and M. Cai, 2003: Impact of urbanization and land-use change on climate. *Nature*, **423,** 528-531.

Kang, S. M., D. M. W. Frierson, and I. M. Held, 2009: The Tropical Response to Extratropical Thermal Forcing in an Idealized GCM: The Importance of Radiative Feedbacks and Convective Parameterization. *Journal of the Atmospheric Sciences*, **66,** 2812-2827.

Kang, S. M., I. M. Held, D. M. W. Frierson, and M. Zhao, 2008: The response of the ITCZ to extratropical thermal forcing: Idealized slab-ocean experiments with a GCM. *J. Clim.*, **21,** 3521-3532.

Karl, T. R., and Coauthors, 1993: A New Perspective on Recent Global Warming- Asymmetric Trends of Daily Maximum and Minimum Temperature. *Bulletin of the American Meteorological Society*, **74,** 1007-1023.

Kawamura, R., 1994: A Rotated EOF Analysis of Global Sea-Surface Temperature Variability with Interannual and Interdecadal Scales. *Journal of Physical Oceanography*, **24,** 707-715.

Kourzeneva, E., 2009: Global dataset for the parameterization of lakes in Numerical Weather Prediction and Climate modeling. *ALADIN Newsletter*, F. Bouttier, and C. Fischer, Eds., Meteo-France, 46-53.

——, 2010: External data for lake parameterization in Numerical Weather Prediction and climate modeling. *Boreal Environment Research*, **15,** 165-177.

Krinner, G., 2003: Impact of lakes and wetlands on boreal climate. *J. Geophys. Res.-Atmos.*, **108,** 18.

Krinner, G., and J. Boike, 2010: A study of the large-scale climatic effects of a possible disappearance of high-latitude inland water surfaces during the 21st century. *Boreal Environment Research*, **15,** 203-217.

Kristovich, D. A. R., and R. R. Braham, 1998: Mean profiles of moisture fluxes in snow-filled boundary layers. *Boundary-Layer Meteorology*, **87,** 195-215.

Kushnir, Y., and J. M. Wallace, 1989: Low-Frequency Variability in the Northern Hemisphere Winter- Geographical-Distribution, Structure and Time-Scale Dependence. *Journal of the Atmospheric Sciences*, **46,** 3122-3142.

Kutzbach, J. E., 1970: Large-Scale Features of Monthly Mean Northern Hemisphere Anomaly Maps of Sea-Level Pressure. *Monthly Weather Review*, **98,** 708-&.

Laird, N. F., J. Desrochers, and M. Payer, 2009: Climatology of Lake-Effect Precipitation Events over Lake Champlain. *J. Appl. Meteorol. Climatol.*, **48,** 232-250.

Lawrence, D., and Coauthors, 2011a: Parameterization Improvements and Functional and Structural Advances in Version 4 of the Community Land Model. *Journal of Advances in Modeling Earth Systems*, **3,** 27 pp.

Lawrence, D. M., and Coauthors, 2011b: The CCSM4 Land Simulation, 1850–2005: Assessment of Surface Climate and New Capabilities. *Journal of Climate*, **25,** 2240-2260.

Lee, S.-Y., J. C. H. Chiang, K. Matsumoto, and K. S. Tokos, 2011: Southern Ocean wind response to North Atlantic cooling and the rise in atmospheric CO2: Modeling perspective and paleoceanographic implications. *Paleoceanography*, **26,** PA1214.

Lehner, B., and P. Doll, 2004: Development and validation of a global database of lakes, reservoirs and wetlands. *Journal of Hydrology*, **296,** 1-22.

Levitus, S., G. Matishov, D. Seidov, and I. Smolyar, 2009: Barents Sea multidecadal variability. *Geophysical Research Letters*, **36,** 5.

Li, F., W. D. Collins, M. F. Wehner, D. L. Williamson, J. G. Olson, and C. Algieri, 2011: Impact of horizontal resolution on simulation of precipitation extremes in an aqua-planet version of Community Atmospheric Model (CAM3). *Tellus A***, 63**, 5.

Li, J. P., and J. Wang, 2003: A modified zonal index and its physical sense. *Geophysical Research Letters*, **30**.

Linkin, M. E., and S. Nigam, 2008: The north pacific oscillation-west Pacific teleconnection pattern: Mature-phase structure and winter impacts. *Journal of Climate*, **21,** 1979-1997.

Liu, Z. Y., and M. Alexander, 2007: Atmospheric bridge, oceanic tunnel, and global climatic teleconnections. *Reviews of Geophysics*, **45**.

Livezey, R. E., and W. Y. Chen, 1983: Statistical Field Significance and its Determination by Monte-Carlo Techniques. *Monthly Weather Review*, **111,** 46-59.

Lofgren, B. M., 1997: Simulated effects of idealized Laurentian Great Lakes on regional and large-scale climate. *J. Clim.*, **10,** 2847-2858.

——, 2004: A model for simulation of the climate and hydrology of the Great Lakes basin. *Journal of Geophysical Research-Atmospheres*, **109**.

Long, Z., W. Perrie, J. Gyakum, D. Caya, and R. Laprise, 2007: Northern lake impacts on local seasonal climate. *J. Hydrometeorol.*, **8,** 881-896.

Minobe, S., 1997: A 50-70 year climatic oscillation over the North Pacific and North America. *Geophysical Research Letters*, **24,** 683-686.

Mitchell, T. D., and P. D. Jones, 2005: An improved method of constructing a database of monthly climate observations and associated high-resolution grids. *International Journal of Climatology*, **25,** 693-712.

Neale, R. B., and B. J. Hoskins, 2000: A standard test for AGCMs including their physical parametrizations: I: The proposal. *Atmospheric Science Letters*, **1,** 101-107.

Neale, R. B., J. H. Richter, and M. Jochum, 2008: The Impact of Convection on ENSO: From a Delayed Oscillator to a Series of Events. *Journal of Climate*, **21,** 5904-5924.

Neale, R. B., and Coauthors, 2010: Description of the NCAR Community Atmosphere Model (CAM 4.0). National Center for Atmospheric Research.

Nigam, S., 2003: Teleconnections. *Encyclopedia of Atmospheric Sciences*, R. H. James, Ed., Academic Press, 2243-2269.

Nigam, S., and R. S. Lindzen, 1989: The Sensitivity of Stationary Waves to Variations in the Basic State Zonal Flow. *Journal of the Atmospheric Sciences*, **46,** 1746-1768.

Nigam, S., and E. DeWeaver, 2003: Stationary Waves (Orographic and Thermally Forced). *Encyclopedia of Atmospheric Sciences*, R. H. James, Ed., Academic Press, 2121-2137.

Nigam, S., and A. Ruiz-Barradas, 2006: Seasonal hydroclimate variability over north America in global and regional reanalyses and AMIP simulations: Varied representation. *Journal of Climate*, **19,** 815-837.

Ogi, M., and K. Yamazaki, 2010: Trends in the Summer Northern Annular Mode and Arctic Sea Ice. *Sola*, **6,** 41-44.

Oleson, K., and Coauthors, 2010: Technical description of version 4.0 of the Community Land Model (CLM). National Center for Atmospheric Research, NCAR/TN-478+STR.

Oort, A. H., and E. M. Rasmusson, 1970: On Annual Variation of Monthly Mean Meridional Circulation. *Monthly Weather Review*, **98,** 423-&.

Patton, E. G., P. P. Sullivan, and C. H. Moeng, 2005: The influence of idealized heterogeneity on wet and dry planetary boundary layers coupled to the land surface. *Journal of the Atmospheric Sciences*, **62,** 2078-2097.

Peacock, S., 2012: Projected 21st century changes in temperature, precipitation and snow cover over North America in CCSM4. *Journal of Climate*. 10.1175/JCLI-D-11-00214.1

Plug, L. J., C. Walls, and B. M. Scott, 2008: Tundra lake changes from 1978 to 2001 on the Tuktoyaktuk Peninsula, western Canadian Arctic. *Geophysical Research Letters*, **35,** 5.

Polyakov, I. V., and M. A. Johnson, 2000: Arctic decadal and interdecadal variability. *Geophysical Research Letters*, **27,** 4097-4100.

Polyakov, I. V., and Coauthors, 2003: Variability and trends of air temperature and pressure in the maritime Arctic, 1875-2000. *J. Clim.*, **16,** 2067-2077.

Qian, T. T., A. G. Dai, K. E. Trenberth, and K. W. Oleson, 2006: Simulation of global land surface conditions from 1948 to 2004. Part I: Forcing data and evaluations. *J. Hydrometeorol.*, **7,** 953-975.

Randall, D. A., and Coauthors, 2007: Climate Models and Their Evaluation. *Climate Change 2007: The Physical Science Basis. Contribution of Working Group I to the Fourth Assessment Report of the Intergovernmental Panel on Climate Change*, S. Solomon, D. Qin, M. Manning, Z. Chen, M. Marquis, K.B. Averyt, M.Tignor and H.L. Miller, Ed., Cambridge University Press.

Richter, J. H., and P. J. Rasch, 2008: Effects of convective momentum transport on the atmospheric circulation in the community atmosphere model, version 3. *Journal of Climate*, **21,** 1487-1499.

Riley, W. J., and Coauthors, 2011: Barriers to predicting changes in global terrestrial methane fluxes: analyses using CLM4Me, a methane biogeochemistry model integrated in CESM. *Biogeosciences*, **8,** 1925-1953.

Riordan, B., D. Verbyla, and A. D. McGuire, 2006: Shrinking ponds in subarctic Alaska based on 1950-2002 remotely sensed images. *J. Geophys. Res.-Biogeosci.*, **111,** 11.

Rogers, J. C., 1981: Spatial Variability of Seasonal Sea-Level Pressure and 500 mb Height Anomalies. *Monthly Weather Review*, **109,** 2093-2106.

Rossow, W. B., and E. N. Duenas, 2004: The International Satellite Cloud Climatology Project (ISCCP) Web site - An online resource for research. *Bulletin of the American Meteorological Society*, **85,** 167-172.

Rouse, W. R., P. D. Blanken, N. Bussieres, C. J. Oswald, W. M. Schertzer, C. Spence, and A. E. Walker, 2008: Investigation of the Thermal and Energy Balance Regimes of Great Slave and Great Bear Lakes. *J. Hydrometeorol.*, **9,** 1318-1333.

Rouse, W. R., and Coauthors, 2005: The role of northern lakes in a regional energy balance. *J. Hydrometeorol.*, **6,** 291-305.

Samuelsson, P., and M. Tjernstrom, 2001: Mesoscale flow modification induced by land-lake surface temperature and roughness differences. *Journal of Geophysical Research-Atmospheres*, **106,** 12419-12435.

Samuelsson, P., E. Kourzeneva, and D. Mironov, 2010: The impact of lakes on the European climate as simulated by a regional climate model. *Boreal Environment Research*, **15,** 113-129.

Schindler, D. W., 2009: Lakes as sentinels and integrators for the effects of climate change on watersheds, airsheds, and landscapes. *Limnology and Oceanography*, **54,** 2349-2358.

Schuur, E., and Coauthors, 2008: Vulnerability of permafrost carbon to climate change: Implications for the global carbon cycle. *Bioscience*, **58,** 701-714.

Shaman, J., and E. Tziperman, 2005: The effect of ENSO on Tibetan plateau snow depth: A stationary wave teleconnection mechanism and implications for the south Asian monsoons. *Journal of Climate*, **18,** 2067-2079.

Shin, S. H., and K. J. Ha, 2007: Effects of spatial and temporal variations in PBL depth on a GCM. *Journal of Climate*, **20,** 4717-4732.

Small, E. E., F. Giorgi, L. C. Sloan, and S. Hostetler, 2001: The effects of desiccation and climatic change on the hydrology of the Aral Sea. *J. Clim.*, **14,** 300-322.

Smith, L., Y. Sheng, G. MacDonald, and L. Hinzman, 2005: Disappearing Arctic lakes. *Science*, **308,** 1429-1429.

Smith, L. C., Y. W. Sheng, and G. M. MacDonald, 2007: A first pan-Arctic assessment of the influence of glaciation, permafrost, topography and peatlands on northern hemisphere lake distribution. *Permafrost and Periglacial Processes*, **18,** 201-208.

Snedecor, G. W., and W. G. Cochran, 1989: *Statistical Methods.* 8th ed. Iowa State University Press.

Stott, P. A., and S. F. B. Tett, 1998: Scale-dependent detection of climate change. *Journal of Climate*, **11,** 3282-3294.

Subin, Z. M., W. J. Riley, and D. Mironov, 2012: An improved lake model for climate simulations: Model structure, evaluation, and sensitivity analyses in CESM1. *J. Adv. Model. Earth Syst.*, **4,** M02001.

Thompson, D. W. J., and J. M. Wallace, 1998: The Arctic Oscillation signature in the wintertime geopotential height and temperature fields. *Geophysical Research Letters*, **25,** 1297-1300.

Timmermann, A., 1999: Detecting the nonstationary response of ENSO to greenhouse warming. *Journal of the Atmospheric Sciences*, **56,** 2313-2325.

Toggweiler, J. R., and D. W. Lea, 2010: Temperature differences between the hemispheres and ice age climate variability. *Paleoceanography*, **25**.

Tourre, Y. M., and W. B. White, 1995: ENSO Signals in Global Upper-Ocean Temperature. *Journal of Physical Oceanography*, **25,** 1317-1332.

Trenberth, K. E., 1984: Signal Versus Noise in the Southern Oscillation. *Monthly Weather Review*, **112,** 326-332.

Trenberth, K. E., and D. A. Paolino, 1981: Characteristic Patterns of Variability of Sea-Level Pressure in the Northern Hemisphere. *Monthly Weather Review*, **109,** 1169-1189.

van Huissteden, J., C. Berrittella, F. J. W. Parmentier, Y. Mi, T. C. Maximov, and A. J. Dolman, 2011: Methane emissions from permafrost thaw lakes limited by lake drainage. *Nature Clim. Change*, **1,** 119-123.

Vavrus, S., and D. Waliser, 2008: An Improved Parametrization for Simulating Arctic Cloud Amount in the CCSM3 Climate Model. *Journal of Climate*, **21,** 5673-5687.

Venegas, S. A., and L. A. Mysak, 2000: Is there a dominant timescale of natural climate variability in the Arctic? *Journal of Climate*, **13,** 3412-3434.

Vose, R. S., D. R. Easterling, and B. Gleason, 2005: Maximum and minimum temperature trends for the globe: An update through 2004. *Geophysical Research Letters*, **32**.

Wallace, J. M., and D. S. Gutzler, 1981: Teleconnections in the Geopotential Height Field During the Northern Hemisphere Winter. *Monthly Weather Review*, **109,** 784-812.

Walter, K. M., L. C. Smith, and F. S. Chapin, 2007: Methane bubbling from northern lakes: present and future contributions to the global methane budget. *Philosophical Transactions of the Royal Society a-Mathematical Physical and Engineering Sciences*, **365,** 1657-1676.

Wania, R., I. Ross, and I. C. Prentice, 2010: Implementation and evaluation of a new methane model within a dynamic global vegetation model: LPJ-WHyMe v1.3.1. *Geosci. Model Dev.*, **3,** 565-584.

White, W. B., and S. E. Pazan, 1987: Hindcast Forecast of ENSO Events Based upon the Redistribution of Observed and Model Heat-Content in the Western Tropical Pacific, 1964-86. *Journal of Physical Oceanography*, **17,** 264-280.

Wild, M., 2009: Global dimming and brightening: A review. *Journal of Geophysical Research-Atmospheres*, **114**.

Wild, M., A. Ohmura, and K. Makowski, 2007: Impact of global dimming and brightening on global warming. *Geophysical Research Letters*, **34**.

Zhou, L. M., R. E. Dickinson, A. G. Dai, and P. Dirmeyer, 2010: Detection and attribution of anthropogenic forcing to diurnal temperature range changes from 1950 to 1999: comparing multi-model simulations with observations. *Climate Dynamics*, **35,** 1289-1307.

Chapter 4: Effects of Soil Moisture on Soil Temperature in Freezing Soils Could Alter Responses to Anthropogenic Forcing

Chapter 4 Table of Contents

4. Effects of Soil Moisture on Soil Temperature in Freezing Soils Could Alter Responses to Anthropogenic Forcing

This chapter is being developed into a version to be submitted to *Geophysical Research Letters*, with co-authors Charlie D. Koven (Lawrence Berkeley National Lab), William J. Riley (Lawrence Berkeley National Lab), Margaret S. Torn (Lawrence Berkeley National Lab), David M. Lawrence (National Center for Atmospheric Research), and Sean C. Swenson (National Center for Atmospheric Research).

4.1 Summary

At high latitudes, changes in soil moisture could alter soil temperatures independently of air temperature changes by interacting with the snow thermal rectifier. We investigated this mechanism with experiments in the Community Land Model 4 (CLM4) with prescribed atmospheric forcing and leaf area. Under equilibrium historical conditions, increasing CO_2 concentrations experienced by plants from 285 ppm to 857 ppm caused widespread increases in water-filled pore space of 0.1-0.2. In permafrost gridcells that experienced this moistening, vertical- and annual- mean soil temperatures increased by 1-2°C. A similar pattern of moistening and warming occurred when increasing JJAS rainfall over historical values by 25%, comparable to expected future rainfall increases. When increasing JJAS rainfall from 75% to 100% of historical values, much more pronounced moistening and warming occurred, showing a large sensitivity to baseline hydrological state. Experiments with perturbed physics confirmed that the simulated warming in permafrost soils was caused by increases in the soil latent heat of fusion per unit volume and in the soil thermal conductivity due to the increased moisture. In transient experiments forced by an RCP8.5 scenario, warming due to increased CO_2 or JJAS rainfall was smaller in magnitude and spatial extent than in the equilibrium experiments. Permafrost areas experiencing active-layer deepening were less than 8%, as increased heat of fusion and soil thermal conductivity have compensating effects on active-layer depth.

4.2 Introduction

Permafrost-zone soils contain about 1700 Pg C (Tarnocai et al. 2009), and recent research has focused on investigating the potential vulnerability of this carbon to mineralization under climate warming (Schuur et al. 2008; Schuur et al. 2011). A number of modeling studies have investigated the magnitude of expected near-surface permafrost thaw (Schaefer et al. 2011), which may be a precursor to large losses of soil carbon, but these studies typically simulated or analyzed only surface air temperature (SAT; precise definitions of common terms in Section 4.8.1) changes as the primary driver of soil temperature increases. However, other factors can be at least as important in determining soil temperature and active layer thickness (ALT; Section 4.8.1): the seasonally asymmetric presence of snow insulation (the "snow thermal rectifier") is a major control on soil temperature (Goodrich 1982; Zhang 2005). Many studies have shown the potential for changes in snowfall, snow properties, and snow season length to alter soil temperatures (Iijima et al. 2010; Lawrence and Slater 2010; Pavlov and Moskalenko 2002; Stieglitz et al. 2003; Westermann et al. 2011; Zhang et al. 2005).

Modeling has shown that increased soil moisture could cause mean annual warming of permafrost soils by interacting with the snow thermal rectifier, due to increased latent heat of

fusion per unit soil volume (LHF; Section 4.8.1) (Goodrich 1982) and increased soil thermal conductivity (Zhang and Stamnes 1998). Several mechanisms could alter soil moisture independently of air temperature under 21st century climate change. An experimental synthesis found significant increases in soil moisture across a range of ecosystems due to reduced transpiration in open-air elevated CO_2 experiments (van Groenigen et al. 2011). Modeling studies typically find decreased transpiration resulting from elevated CO_2 (Boucher et al. 2009; Cao et al. 2010; de Boer et al. 2011; Gopalakrishnan et al. 2011; Sellers et al. 1996b), consistent with recent observed increases in continental runoff (Gedney et al. 2006). Such reduced transpiration could result in increases in SAT due to an increased Bowen ratio (Boucher et al. 2009; Cao et al. 2010; Sellers et al. 1996b). Additional warming could result from decreased albedo due to increased leaf area associated with CO_2-fertilization (Bala et al. 2006; Notaro et al. 2007; Notaro et al. 2005). Nevertheless, we are unaware of any studies investigating the effects of elevated CO_2-physiological forcing on soil temperatures.

A robust prediction in future climate simulations is increased precipitation at high latitudes throughout the year (Christensen et al. 2007), although the net effects on soil moisture are uncertain due to likely increases in potential evapotranspiration (ET) (Hinzman et al. 2005) and possible increases in drainage due to the retreat of underlying impervious permafrost (Avis et al. 2011; Smith et al. 2005). Some studies have discussed permafrost soil temperature increases co-occurring with increases in rainfall, but these studies did not isolate changes in soil thermal properties associated with increased moisture from other influences on soil temperature, including changes in summer Bowen ratio and in snow properties (Iijima et al. 2010; Saito 2008; Westermann et al. 2011; Zhang et al. 2001). Observational evidence for increased ALT or warmer soils in areas with higher soil moisture is mixed (Hinkel and Nelson 2003; Hinkel et al. 2001; Jorgenson et al. 2010; Shiklomanov et al. 2007), which could be due to the confounding warming effects of surface water and cooling effects of increased near-surface moss and soil organic content in wet ecosystems (Jorgenson et al. 2010). One recent Arctic experimental manipulation partially attributed observed summer soil warming to increased sub-surface thermal conductivity associated with flooding treatment (Zona et al. 2012).

In this study, we investigated whether increased soil moisture from elevated CO_2 or increased summer rainfall could cause soil warming in addition to that caused by increases in air temperature, quantifying the mechanisms by which soil moisture affects soil temperature. We include conceptual and simplified analyses of the seasonal cycle in Section 4.4.3.3 to illustrate the thermal dynamics occurring in the model experiments.

4.3 Methods

We performed experiments with the Community Land Model 4 (CLM4) (Lawrence et al. 2011a), the land-surface component of the Community Climate System Model 4 (CCSM4) (Gent et al. 2011) and the Community Earth System Model 1 (CESM1) (http://www.cesm.ucar.edu/models/cesm1.0/). Transpiration is calculated iteratively during the evaluation of surface and canopy energy fluxes, using formulations for stomatal conductance (Collatz et al. 1991; Oleson et al. 2010; Sellers et al. 1996a) and photosynthesis (Collatz et al. 1991; Farquhar et al. 1980) that include soil-moisture stress (Oleson et al. 2008). CLM4 soil physics includes vertically-resolved thermal and hydrological diffusion in 10 soil layers down to 3.8 m, with 5 hydrologically inactive bedrock layers continuing down to 42 m (Lawrence et al.

2011a; Oleson et al. 2010). The effects of observed vertically-resolved gridcell-mean soil organic content on soil physical properties are prescribed (Lawrence and Slater 2008). At each timestep, thermal diffusion is solved in the absence of phase change, and then temperatures are corrected for LHF (Oleson et al. 2010), with allowance for the persistence of unfrozen soil moisture below the nominal freezing point (Niu and Yang 2006) (sensitivity to this parameterization in Section 4.8.2). While CLM4 contains a number of sub-grid land types, we only analyzed changes occurring in the vegetated landunit (Section 4.8.1). The snow model includes up to 5 resolved layers with state variables of temperature, ice density, water density, snow grain radius, and deposited aerosol concentration (Flanner and Zender 2006; Flanner et al. 2007; Lawrence et al. 2011a). Predictions of snow cover, snow accumulation, and permafrost extent in the offline CLM4 compare satisfactorily with observations, while positive snowfall biases in the coupled CCSM4 increase soil temperatures and ALT and decrease permafrost extent, somewhat degrading their realism (Lawrence et al. 2011a; Lawrence et al. 2011b; Lawrence et al. 2011c). In the simulations performed here, we included preliminary changes to CLM4 soil hydrology that correct for unrealistic conduction of liquid water through frozen soils (Section 4.8.3).

We performed simulations using prescribed leaf area and atmospheric forcing in order to isolate the direct interactions of soil moisture and soil temperature (Table 4.1; detailed model-configuration information in Section 4.8.4). Using prescribed leaf area allows transpiration and diagnostic photosynthesis to vary but with inactive model biogeochemistry. For equilibrium historical simulations, we used repeated cycles of 1948-1972 atmospheric forcing from a bias-corrected reanalysis dataset of historical conditions (Qian et al. 2006). For equilibrium 1850-1874 and for transient climate change simulations, we used atmospheric forcing generated from an 1850-2099 historical and Representative Concentration Pathway 8.5 (RCP8.5) (Riahi et al. 2011) scenario from a coupled CCSM4 simulation (Section 4.8.5). June, July, August, and September (JJAS) rainfall for the permafrost region (Section 4.8.1) increased by 27% in this scenario from the 1850s to the 2090s (Supp. Fig. 4.1).

4.4 Interactions of Soil Moisture and Soil Temperature Under Equilibrium Historical Conditions

4.4.1 Results

To set the context for the results presented here, we found that eliminating snow insulation (experiment *NoSnowIns – CTL*; Table 4.1), while maintaining other snow properties unchanged (Section 4.8.6), caused a mean of 7°C and a maximum of 18°C decreases in annual-mean soil temperatures under historical conditions north of 45° latitude (Supp. Fig. 4.2a); for comparison to previous published estimates (Zhang 2005), differences between soil surface temperature and SAT in *CTL* (the "snow offset") were about 1°C smaller in magnitude than this decrease (Supp. Fig. 4.2b). This result indicates a very large effect of the snow thermal rectifier in CLM4 compared to projected future SAT increases, implying a large potential sensitivity to processes which modify or interact with this effect.

Increasing atmospheric CO_2 concentrations experienced by plants from 285 ppm (pre-industrial levels) to 857 ppm ($CO_2 - CTL$), as projected for 2100 in the A2 scenario (Nakicenovic and Swart 2000), caused increases in water-filled pore space (WFPS; Section

4.8.1) of 0.1-0.2 in many regions throughout the globe, due to reduced transpiration (Supp. Fig. 4.3a). Increasing JJAS rainfall by 25% (*HiRain − CTL*) caused similarly widespread WFPS increases (Supp. Fig. 4.3b), although the increases extended farther north into the Canadian archipelago where there was insufficient vegetation to cause reduced transpiration in $CO_2 - CTL$. Increasing JJAS rainfall from 75% of the climatological value to 100% (*CTL – LoRain*) caused even larger increases in WFPS, especially in Northeastern Siberia (Supp. Fig. 4.3c), indicating substantial sensitivity to the baseline hydrological state.

In these three experiments, increases in WFPS of 0.1-0.2 were associated with increases in vertical- and annual-mean soil temperatures of 1-2°C in permafrost regions (Fig. 4.1a-c), particularly northeast Siberia, northern Canada, and northern Alaska; these regions exhibited a confluence of unsaturated soils in *CTL*, cold winter air, substantial winter snow accumulation, and non-negligible leaf area or summer rainfall. Warming was strongest in the *CTL – LoRain* experiment, where the largest soil moisture increases also occurred. Soil temperature changes outside of present-day permafrost regions were less than 0.5°C in magnitude, and we did not analyze changes in these regions.

4.4.2 Perturbed Physics Simulations

In order to test the hypothesis that these soil temperature increases were caused by increased LHF and soil thermal conductivity due to increased soil moisture, we repeated the elevated CO_2 experiment with perturbed physics (Section 4.8.6) that selectively eliminated these mechanisms. In $tkSat\_CO_2 - tkSat$, soil conductivity was prescribed to saturated values (either for frozen or unfrozen soils, respectively); in $NoHfus\_CO_2 - NoHfus$, LHF was turned off beneath the top soil layer; and in $tkSat\_NoHfus\_CO_2 - tkSat\_NoHfus$, both these modifications were applied. While the patterns of WFPS increases in these three experiments were similar to those in $CO_2 - CTL$ (Supp. Fig. 4.3a, d-f), the magnitude of warming was reduced by about half in both $tkSat\_CO_2 - tkSat$ and $NoHfus\_CO_2 - NoHfus$ (Fig. 4.1d,e). In $tkSat\_NoHfus\_CO_2 - tkSat\_NoHfus$, the warming was negligible (Fig. 4.1f). These results demonstrate that these two mechanisms coupling soil moisture and soil temperature were necessary to cause the warming we observed in Section 4.4.1.

4.4.3 Analysis

4.4.3.1 Vertical and seasonal patterns of soil temperature change

We computed a mean annual cycle over the 25-year climatology in the elevated CO_2 experiments, averaging over all gridcells showing greater than 1°C soil temperature increases in $CO_2 - CTL$ (Fig. 4.1a), weighting each gridcell equally. In $CO_2 - CTL$, these gridcells tended to accumulate moisture in the middle to lower active layer, increasing WFPS from about 0.7 to 0.9 (Supp. Fig. 4.4). The mean ALT in *CTL* was 1.5 m (Fig. 4.2a). Near-surface soil temperature changes in $CO_2 - CTL$ (Fig. 4.2b) showed a winter warming peaking at 3.3°C alternating with a summer cooling of less than 0.4°C; this seasonal cycle was rectified to a nearly constant 1.3°C warming below 4.5 m. The mean ALT increased by 0.1 m in $CO_2 - CTL$, and the fall freeze-up was delayed by about 3 days.

The soil temperature changes in the elevated-CO_2 experiments with perturbed physics (Fig. 4.2c,d) showed a complementary vertical-seasonal pattern from the two mechanisms coupling

soil moisture and soil temperature, roughly adding linearly to produce the pattern in Fig. 4.2b. With increased LHF only (*tkSat_CO₂ – tkSat*), winter warming and summer cooling were relatively vertically symmetric (Fig. 4.2c), as increased energy diverged from the freeze front in the fall and winter and converged to the thaw front in the summer (Supp. Fig. 4.5c); the increase in the energy transport requirement caused delays in freeze and thaw and reduced ALT by 0.4 m. With increased soil conductivity only (*NoHfus_CO₂ – NoHfus*), near-surface winter warming and summer cooling contrasted with winter cooling and summer warming at the top of the permafrost table (Fig. 4.2d), causing an ALT increase of 0.5 m; winter energy fluxes increased upwards in the winter and downwards in the summer (Supp. Fig. 4.5d). In both cases, we can infer that the longer seasonal extent and larger magnitude of winter warming as compared with summer cooling required the seasonally asymmetric presence of snow insulation; when the *CO₂ – CTL* experiment was repeated with snow insulation eliminated, no net warming occurred (not shown).

4.4.3.2 Changes in surface energy fluxes

We examined the annual cycle of surface energy flux changes in the gridcells experiencing greater than 1°C soil temperature increases in *CO₂ – CTL* (Fig. 4.3). Due to elevated CO_2 (*CO₂ – CTL*), the downwards sub-surface energy flux (Section 4.8.1) increased by as much as 4 W m^{-2} in the summer and decreased by about 2 W m^{-2} throughout the winter (Fig. 4.3a), enhancing the baseline seasonal cycle of energy exchange between the soil and the atmosphere. In the summer, decreased transpiration caused an increase in the Bowen ratio. Some increased shortwave absorption occurred in the spring and summer due to earlier snowmelt (a positive feedback to the soil warming) and to the moister and therefore darker soil. (Snow thickness decreases occurred entirely in the spring, leaving winter snow insulation unchanged.) In the perturbed physics cases isolating mechanisms coupling soil moisture and soil temperature (Fig. 4.3b,c), the enhanced seasonal energy exchange simulated in *CO₂ – CTL* was decreased by about half; when both these mechanisms were removed (Fig. 4.3d), it was negligible, leaving only the summer Bowen ratio change due to decreased transpiration. Increasing JJAS rainfall (*HiRain − CTL*; Fig. 4.3e) caused nearly identical changes in downwards sub-surface energy flux as *CO₂ – CTL*, although the summer Bowen ratio change was reversed. Summer SAT changes (Supp. Fig. 4.6) were smaller in magnitude than 0.2°C in these uncoupled experiments and inconsistent in sign with surface temperature changes, highlighting that Bowen ratio changes had only minor contributions to the soil temperature changes.

4.4.3.3 Conceptual and simple analytical representations

Conceptually, the LHF mechanism warms the soils after moistening because the extra LHF released during freeze tends to be trapped under the snow in the winter, while the extra LHF needed to melt the extra soil ice in the summer can be conducted in relatively easily from the atmosphere when snow is not present. Likewise, increased soil thermal conductivity acts to conduct more heat through the active layer during the summer but cannot contribute equally to heat loss during the winter because the snow is the dominant thermal resistance. [Without the winter snow, the greater thermal conductivity of ice compared with liquid water would reverse the sign of this mechanism, i.e., due to the "thermal offset" (Goodrich 1982).]

Analytically, we first examine the LHF mechanism by considering the regime where $L >> c\Delta T$: L is LHF, c is the soil heat capacity per unit volume, and ΔT is the amplitude of

seasonal temperature variation. In this regime, the Stefan equation approximates the instantaneous thaw depth X during the unfrozen season (Riseborough et al. 2008):

$$X = \sqrt{\frac{2kT}{L}}, \qquad \textbf{Eq. 4.1}$$

where k is the soil thermal conductivity and T is proportional to the thawing degree days (the time-integral of the temperature above freezing). In the Stefan equation, increasing L decreases the seasonal-maximum X by a factor proportional to $1/\sqrt{L}$ but increases the integrated summer ground heat flux (XL) by a factor of $\sqrt{L}$. In *tkSat_CO₂ – tkSat*, reduced transpiration added 110 kg m^{-2} of water to the active layer of the gridcells experiencing warming (Supp. Fig. 4.4c), corresponding to an increased XL, to first order, of 55 kg m^{-2} * 3.3 x 10^5 J kg^{-1} = 1.8 x 10^7 J m^{-2} that must be exchanged seasonally with the atmosphere: about 1.2 W m^{-2} averaged over 6 months of "winter" (November through April). This change in energy flux across a mean 0.33 m of snow with conductivity ~0.25 W m^{-1} K^{-1} is consistent with increasing the difference between the soil and snow surface temperatures by 1.5°C, similar to the 1.2°C increase occurring in *tkSat_CO₂ – tkSat*.

Secondly, the thermal conductivity mechanism applies in both the $L >> c\Delta T$ regime and in the opposite, purely diffusive, regime (Riseborough et al. (2008), Eq. 4.2): in both cases, the integrated summer ground heat flux is proportional to $\sqrt{k}$. As the summer k increased by ~25% in *NoHfus_CO₂ – NoHfus* (not shown), the total summer heat absorption of 9.5 x 10^7 J m^{-2} would have been expected to increase, to first order, by about 1.2 x 10^7 J m^{-2}. This increased energy exchange requirement is consistent with an increased winter energy flux of 0.76 W m^{-2} across 0.35 m of snow in *NoHfus_CO₂ – NoHfus* causing a soil surface temperature increase of 1.1°C compared to the snow surface, similar to the simulated increase of 1.3°C in the model experiment.

4.5 Effects on Future Permafrost Thaw Vulnerability

To investigate whether the mechanisms illustrated in Section 4.4 may be important factors affecting permafrost thaw during future climate change, we performed additional land-model experiments forced with atmospheric conditions generated by a CCSM4 historical and RCP8.5 1850-2099 simulation (Section 4.8.5). We first repeated equilibrium experiments forced by the 1850-1874 period in order to identify the sensitivity of the responses to the forcing. For elevated CO_2 (*1850_CO₂ − 1850*) and increased JJAS rainfall (*1850_HiRain − 1850*), regions of moistening (Supp. Fig. 4.7a,b) and warming (Fig. 4.4a,b) permafrost soils occurred, but these regions were smaller in spatial extent and magnitude of warming than, and generally did not overlap with, the regions warming in *CO₂ – CTL* and *HiRain − CTL*. This result reinforces the high sensitivity of these moistening mechanisms to the modeled hydrological state.

We investigated these mechanisms under transient climate change by comparing a baseline RCP8.5 land model simulation to one with fixed 1850 CO_2 concentrations of 285 ppm (*RCP8.5 − RCP8.5_FixCO₂*) and to one with decadal JJAS rainfall forcing detrended (Section 4.8.7) to maintain the 1850-1874 climatology (*RCP8.5 − RCP8.5_FixRain*). Regions of moistening (Supp. Fig. 4.7c-f) and warming (Fig. 4.4c-f) permafrost soils occurred during the 2025-2049 and 2050-2074 periods, but these were smaller in spatial extent and warming magnitude than

those occurring in the equilibrium 1850-1874 experiments. Warming of ~0.5°C from increased CO_2 also occurred in some areas that had already lost near-surface permafrost by the end of the 21st century (Fig. 4.4e), associated with up to 0.2 m increases in annual-mean thickness of unfrozen soil. This warming was largest during the 2075-2099 period and during the fall season (not shown).

Temporal and regional mis-matches between the hydrological forcing and the areas susceptible to warming drove the smaller impacts of soil moistening in the future simulations as compared to those predicted under historical conditions. By the latter half of the 21st century, when the JJAS rainfall and the CO_2 trends became large (Supp. Fig. 4.1 and Supp. Fig. 4.8), permafrost extent was already substantially reduced (Fig. 4.4) and air temperatures had dramatically increased (Supp. Fig. 4.9), especially during winter, reducing susceptibility to the mechanisms coupling soil moisture and soil temperature. The rapid loss of permafrost may have been accentuated by the CCSM4 excessive snowfall bias (Lawrence et al. 2011b), although increased snow insulation would have also tended to strengthen the effects of soil moisture on soil temperature. The late-21st-century regional mis-match was also exacerbated in *RCP8.5 − RCP8.5_FixCO₂* because the permafrost had retreated to high Arctic regions lacking much leaf area at present. Our prescribed-leaf-area simulations were inherently unable to show much sensitivity to CO_2 concentrations in these regions, but future increases in leaf area could increase this sensitivity.

In addition to mean annual soil temperatures, increased ALT and vulnerability to complete thaw are crucial metrics for assessing the potential for loss of permafrost carbon. In the equilibrium historical simulations with both reanalysis and CCSM4 forcing, effects of the soil warming on ALT area distributions were small (Supp. Fig. 4.10a): area with ALT less than 2 m or 4 m decreased by up to 3×10^5 km^2 (2%). Small changes also were predicted in the future simulations (Supp. Fig. 4.10b): area with ALT less than 4 m decreased by up to 2×10^5 km^2 in *RCP8.5 − RCP8.5_FixRain*. This change represented an 8% decrease in area in 2075-2099, but relative to an already very low remaining area of 2.2×10^6 km^2. These results indicate that soil moistening, despite causing substantial increases in mean annual soil temperatures, likely has only modest effects on ALT or permafrost vulnerability to thaw. This contrast is likely due to the compensating effects on ALT of the two mechanisms coupling soil moisture and soil temperatures (Section 4.4.3.1 and Section 4.4.3.3): while increased soil thermal conductivity tends to increase ALT, increased LHF tends to decrease it, resulting in a small net increase in our experiments.

4.6 Discussion

4.6.1 Applicability of Results

We showed that mechanisms that could increase WFPS in permafrost regions by 0.1-0.2 could increase mean soil temperatures by 1-2°C. A number of additional factors not simulated here could modify these results, discussed below. Experimental manipulations should be conducted to investigate these mechanisms and the additional factors not simulated here.

Compared to our predictions, coupling with the atmosphere could alter soil temperatures via feedback from changes in SAT, if changes in surface energy fluxes occurred over large regions. Such feedbacks would likely increase the soil warming associated with the spring and summer

albedo decreases (Fig. 4.3), cause additional soil warming associated with decreased transpiration from elevated CO_2 (Fig. 4.3a), and reduce the soil warming associated with increased rainfall because of increased ET (Fig. 4.3e).

Allowing leaf area to increase with elevated CO_2 or increased rainfall would likely reduce the net soil moisture increases, as some additional transpiration would be associated with increased plant growth. However, the increased leaf area would also likely reduce albedo at high latitudes and facilitate snowmelt (Bala et al. 2006; Notaro et al. 2007; Notaro et al. 2005), which could cause spring and summer soil warming. Preliminary experiments suggest that these two factors may compensate under historical conditions to yield similar mean annual soil warming (not shown).

Persistent increases in soil moisture could increase anoxia (Section 4.6.2), which could cause more moss and near-surface soil organic matter to accumulate, decreasing summer soil thermal conductivity and mitigating soil warming. More generally, the effects of increasing CO_2 and rainfall on vegetation abundance will have uncertain effects on soil temperatures.

Our results show that the potential for soil moistening and subsequent warming is very sensitive to the simulated hydrology; if soils are already relatively moist, then additional precipitation or reduced transpiration will be unable to cause warming. Conversely, moist soils may be more susceptible to drying mechanisms, with subsequent cooling that could mitigate future warming. Unfortunately, we are unaware of sufficiently comprehensive observations of present-day soil moisture in permafrost regions that would allow us to evaluate our hydrological predictions or the vulnerability to future moistening or drying.

4.6.2 Interactions with Soil Biogeochemistry

Increased soil moisture will likely cause little summer warming or ALT increases and thus be unlikely to increase accessibility of deep permafrost carbon, but it may affect greenhouse gas budgets resulting from decomposition in actively cycling soils. For instance, the persistent soil warming following near-surface permafrost thaw in some areas (Fig. 4.4e) could enhance the mineralization of newly thawed permafrost carbon. Moistening could increase anoxia, which may be enhanced because the delayed fall freeze-up increases the time when unfrozen soil remains under impervious frozen soil. Decreased freeze depth in seasonally frozen soils, as occurred late in the 21st century from increased CO_2, could also increase the potential for winter anaerobic decomposition under frozen soil.

4.6.3 Implications for Carbon Cycle Feedbacks

If elevated CO_2 increases soil carbon mineralization or enhances anoxic conditions, increased emissions of CO_2, CH_4, and N_2O could occur independently of climate warming. Previous analyses, such as Ringeval et al. (2011), considered the effects of increased soil moisture due to elevated CO_2 on CH_4 emissions, but they did not examine the direct temperature response due to this moistening. While our results do not suggest the likelihood of large increases in greenhouse gas emissions due to the effects of soil moisture on soil temperature, there were large sensitivities to modeled hydrology in equilibrium simulations, and model biases and limitations may have reduced the magnitude of future soil warming (Section 4.5). Consequently, the effects of soil moisture on soil temperature should be considered in future analyses.

4.7 Acknowledgements

I would like to recognize Joe Melton (University of Victoria) and the other members of the Wetland WETland and Wetland CH_4 Inter-comparison of Models Project (WETCHIMP); experiments conducted by the authors for this project inspired the research detailed here. William Collins (Lawrence Berkeley Lab) contributed comments on a draft manuscript. This work was supported by the Director, Office of Science, Office of Biological and Environmental Research, Climate and Environmental Science Division, of the U.S. Department of Energy under Contract No. DE-AC02-05CH11231 to Berkeley Lab.

4.8 Appendix

4.8.1 Definitions

SAT: Surface air temperature, calculated at 2 m above the surface.

ALT: Active layer thickness, here calculated as the annual-maximum depth of the interpolated 0°C isotherm.

LHF: Latent heat of fusion per unit volume of soil, i.e., 3.3×10^5 J kg^{-1} multiplied by the kg H_2O per m^3 of soil volume.

Permafrost region: non-glaciated land area north of 45°N and with mean-annual SAT colder than 0°C.

Vegetated landunit: CLM4 contains 5 different sub-grid landunits, including *vegetated*, *lake*, *wetland*, *urban*, and *glacier* (Lawrence et al. 2011a; Oleson et al. 2010). We only analyze the vegetated landunit here, which consists of vegetation over snow (if present) over soil and bedrock. We also generally exclude from analysis gridcells containing vegetated landunits which do not experience at least one month in the mean annual cycle with surface temperature above freezing.

WFPS: Water-filled pore space, the fraction of available pore volume in the soil occupied by liquid or solid H_2O, i.e., volumetric saturated fraction.

Downwards sub-surface energy flux: the sum of downwards heat flux and shortwave radiation penetrating the top resolved CLM4 soil or snow (if present) layer.

4.8.2 Sensitivity to Treatment of Unfrozen Soil Moisture

In CLM4, soil layers cooling below the freezing point are not forced to convert liquid water to ice (with release of LHF) until the soil moisture potential predicted to be associated with the temperature below freezing (Niu and Yang 2006) becomes more negative than the soil moisture potential based on the WFPS (Oleson et al. 2010). This parameterization was used for all of our simulations defined in Table 4.1. In addition, we repeated the *CO_2 – CTL* simulation with no allowance for the persistence of liquid water below 0°C: all liquid water was forced to freeze before soil layers could cool below 0°C. This modification caused only slight changes in the spatial pattern and magnitude of soil warming as compared with the original *CO_2 – CTL* simulation; mean differences in vertical- and annual-mean soil temperatures due to elevated CO_2 for gridcells experiencing >1°C increases in the original *CO_2 – CTL* decreased by 0.2°C in the

modified experiment, but some permafrost gridcells showed greater soil warming in the modified experiment as compared with the original.

4.8.3 Modifications to CLM4 Hydrology

Permafrost soils in CLM4 may be biased dry (Lawrence et al. 2011a; Lawrence et al. 2011b); a likely contribution (Swenson et al., submitted to *J. Adv. Mod. Earth Sys.*) is excessive conduction of liquid water through frozen soils to the groundwater. The CLM4 formulation calculates an unfrozen fraction of soil pore volume (Niu and Yang 2006; Oleson et al. 2008) and allows liquid water to be conducted through that fraction (Oleson et al. 2010) without sufficiently accounting for the large effective tortuosity in soils with substantial ice-filled pore space (Lundin 1990). We tentatively correct this error here by eliminating the Niu and Yang (2006) unfrozen fraction calculation and replacing it with a power-law ice impedance I (-) that reduces the hydraulic conductivity according to (Hansson et al. 2004; Lundin 1990):

$$I = 10^{-\Omega F_{ice}} \qquad \textbf{Eq. 4.3}$$

where F_{ice} (-) is the ice-filled pore space (fraction of total pore volume), and here $\Omega = 8$. As the CLM4 1-dimensional soil water budget is closed by calculating horizontal drainage as a function of the diagnosed water table depth, we compute a "perched" water table depth z_p (m) in gridcells with saturated layers occurring above a frost table z_f (m), and calculate horizontal drainage Q_p (mm H_2O s^{-1}) according to:

$$Q_p = \alpha\left(z_f - z_p\right)k_p \qquad \textbf{Eq. 4.4}$$

where $\alpha = 10^{-3}$ m^{-1} and k_p (mm H_2O s^{-1}) is the vertical-mean hydraulic conductivity in the perched water table, including the ice impedance (Equation 4.3). These modifications yield wetter active layers in permafrost gridcells.

4.8.4 Details of CLM4 Simulation Configurations

All simulations (Table 4.1) used CLM4 offline (i.e., with prescribed atmospheric conditions) with prescribed leaf area (satellite phenology; "SP") (Lawrence et al. 2011a). Historical equilibrium simulations with Qian et al. (2006) atmospheric forcing ("NCEP" in Table 4.1) were global with 1.9° x 2.5° resolution. The CESM1 (http://www.cesm.ucar.edu/models/cesm1.0/) standard "I_1850" case was used, with 1850 conditions for aerosol deposition and land use (i.e., plant functional type spatial distributions). An initial simulation (with identical configuration to the *CTL* simulation) was spun up for 200 years with repeated 1948-1972 atmospheric forcing. The ending state from this simulation was used as initial conditions for an additional 200 years of spinup for each of the "NCEP" simulations with the respective conditions for CO_2 concentration, JJAS rainfall, and perturbed physics for each experiment. Note that for the rainfall perturbation simulations *HiRain* and *LoRain*, JJAS rainfall was only altered for timesteps when the lower atmospheric temperature was greater than or equal to 0°C to prevent alteration of snow properties. Finally, an additional 25-year period was integrated and analyzed for each simulation.

Simulations using CCSM4 atmospheric forcing (Section 4.8.5; "CCSM4" and "RCP8.5" in Table 4.1) were for a northern domain (> 45°N) extracted from the global 0.9° x 1.25° resolution dataset. For the equilibrium historical simulations ("CCSM4" in Table 4.1), an "I_1850" case

was modified to accept atmospheric forcing data from the archived CCSM4 simulation (Section 4.8.5), with 1850 conditions for aerosol deposition and land use. These three equilibrium historical simulations were separately spun up for 200 years with repeated 1850-1874 forcing from the CCSM4 data, with the respective conditions for CO_2 concentration and JJAS rainfall for each simulation. Finally, an additional 25-year period was integrated and analyzed for each simulation.

For the transient simulations ("RCP8.5" in Table 4.1), an "I_RCP8.5_CN" case was modified to use satellite phenology and to accept atmospheric forcing data from the archived CCSM4 simulation (Section 4.8.5), with transient 1850-2099 conditions for aerosol deposition and land use. Atmospheric forcing data followed the transient 1850-2099 data. The same initial conditions as for the *1850* simulation were used for the three transient simulations, which then proceeded for 250 years from 1850-2099.

4.8.5 2° CCSM4 Climate Forcing

For the "CCSM4" and "RCP8.5" simulations in Table 4.1, we used atmospheric forcing generated from a previously archived CCSM4 historical and RCP8.5 simulation. This simulation was fully coupled (with active land, atmosphere, ocean, and sea ice models) and used the 1.9° x 2.5° resolution datasets for the land and atmosphere and the "gx1v6" resolution dataset for the ocean. The land model included prognostic biogeochemistry ("CN"), and the atmosphere used "CAM4" physics. Atmospheric concentrations of greenhouse gases were prescribed. We used the standard "B_RCP8.5_CN" case (http://www.cesm.ucar.edu/models/cesm1.0/). Other than the resolution, this simulation was configured similarly to those used in the CCSM4 RCP8.5 ensemble (Vavrus et al. 2011) archived for the Climate Model Intercomparison Project 5 (CMIP5); the projected >70°N 21st century warming (2090-2099 – 2000-2009) in our 2° resolution CCSM4 simulation was 9.8°C, within the range projected in the 1° ensemble (Vavrus et al. 2011). The global-mean temperature increase from the 1850-1874 period to the 2075-2099 period was 4.3°C (Supp. Fig. 4.9a,b). High-latitude rainfall increased at most locations from the 1850-1874 period to the 2075-2099 period (Supp. Fig. 4.9c,d), while snowfall increased in the coldest areas and decreased in warmer areas (Supp. Fig. 4.9e,f). The archived data used as forcing for CLM4 included half-hourly lower-atmosphere incident solar radiation data and 3-hourly data for lower-atmosphere downward longwave radiation, temperature, specific humidity, wind, pressure, and precipitation rates.

4.8.6 Perturbed Physics

No snow insulation: for the *NoSnowIns* simulation (Table 4.1), the thermal conductivity of each snow layer calculated by CLM4 (Oleson et al. 2010), as based on SNTHERM (Jin et al. 1999), was multiplied by a factor of 10^6. As the energy fluxes in CLM4 from the snow surface are calculated based on a fixed top layer temperature from the last timestep and then updated after the soil thermal diffusion solution based on the change in top layer temperature and the first derivative of sensible and latent heat fluxes with surface temperature (Oleson et al. 2010), and because heat fluxes into the soil were limited by the conductivity of the top soil layer, no numerical stability problems occurred.

Soil conductivity prescribed to saturated values: soil thermal conductivity in CLM4 (Oleson et al. 2010), based on Farouki (1981), depends on soil texture, soil organic matter content,

temperature, WFPS, and ice-filled pore space. For the *tkSat*, *tkSat_CO$_2$*, *tkSat_NoHfus*, and *tkSat_NoHfus_CO$_2$* simulations (Table 4.1), the soil thermal conductivity was set for all hydrologically active soil layers (1-10) regardless of the WFPS and ice-filled pore space at each timestep. Instead, the value corresponding to WFPS = 1 for unfrozen soils was used if the soil layer temperature exceeded 0°C, while the value corresponding to ice-filled pore space of 1 for frozen soils was used otherwise.

No heat of fusion: for the *NoHfus*, *NoHfus_CO$_2$*, *tkSat_NoHfus*, and *tkSat_NoHfus_CO$_2$* simulations (Table 4.1), the latent heat of fusion for soil pore H_2O was eliminated for soil layers 2-10. It was maintained in the top 0.01 m soil layer and in the snow layers; the CLM4 bedrock layers are assumed dry with fixed thermal properties. While normally the requirement of absorbing or releasing 3.3×10^5 J kg^{-1} H_2O for thaw or freeze, respectively, limits soil temperature changes near freezing in CLM4 (Oleson et al. 2010), in these simulations the heat of fusion was set to 1 J kg^{-1} for soil layers 2-10. Consequently, no energy transport requirements for thaw and freeze restricted soil temperature change. We made sure that after our modifications, the soil energy balance check in CLM4 remained valid to 10^{-6} W m^{-2}.

4.8.7 Precipitation Detrending

The *RCP8.5_FixRain* simulation (Table 4.1) used "detrended" precipitation forcing from the archived CCSM4 historical and RCP8.5 coupled simulation data (Section 4.8.5), as compared to the fully transient precipitation forcing used directly from the coupled simulation for the other "RCP8.5" and "CCSM4" simulations (Table 4.1). We calculated the 1850-1874 JJAS rainfall climatology for each gridcell by averaging the rainfall for each 3-hour timestep during this period, separately for convective and large-scale liquid precipitation. To generate the detrended forcing for the *RCP8.5_FixRain* simulation, we calculated the anomalous ratio of decadal JJAS rainfall for each decade from 1850 to 2099 (i.e., 1850-1859; 1860-1869; … 2090-2099) as compared with the 1850-1874 climatology. Then, at each JJAS timestep from 1850-2099, for each gridcell, and separately for convective and large-scale liquid precipitation, we multiplied the precipitation in the forcing data by the inverse of this ratio (when finite) to obtain the detrended forcing data. This method preserved daily, seasonal, and inter-annual rainfall variation while maintaining a fixed decadal-mean climatology.

4.9 Figures

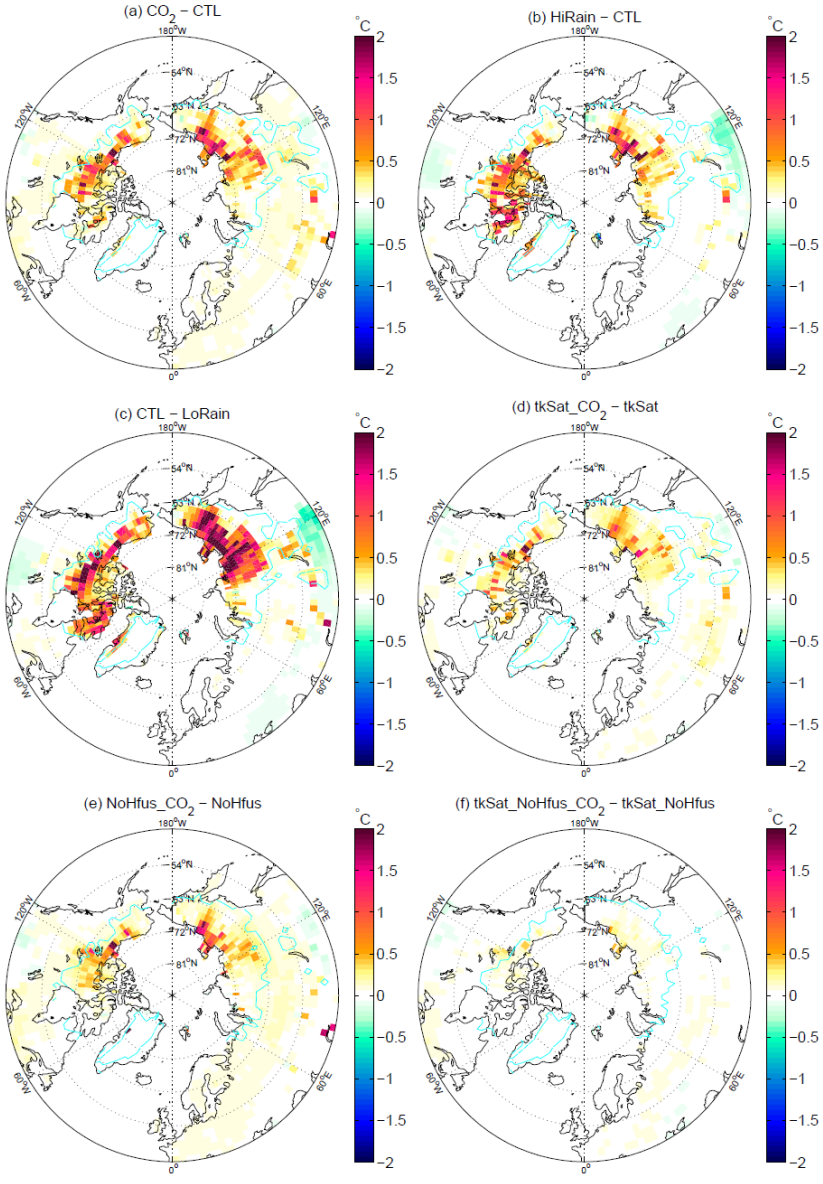

Fig. 4.1: Vertical- (to 3.8 m depth) and annual-mean soil temperature differences (°C) for experiments under equilibrium historical conditions: (a) elevated CO_2; (b) increased JJAS rainfall; (c) increased JJAS rainfall relative to reduced baseline; (d) elevated CO_2 with saturated soil thermal conductivity; (e) elevated CO_2 with no LHF; and (f) elevated CO_2 with both modifications to soil physics. Cyan lines encircle regions with ALT less than 5 m in the control (i.e., cooler) simulations for each panel.

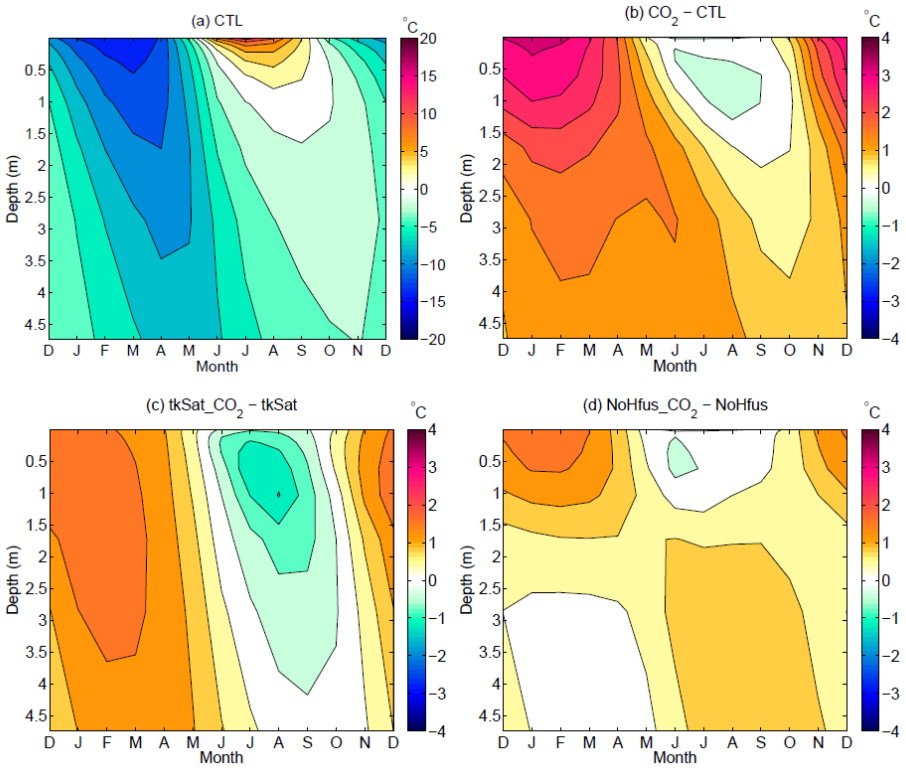

Fig. 4.2: Monthly-mean soil temperatures or soil temperature differences (°C) for experiments under equilibrium historical conditions, averaged over gridcells experiencing greater than 1°C soil temperature increases in the *CO_2 – CTL* experiment: (a) absolute temperatures occurring in the baseline simulation; (b) changes due to elevated CO_2; (c) changes due to elevated CO_2 with saturated soil thermal conductivity; and (d) changes due to elevated CO_2 with no LHF.

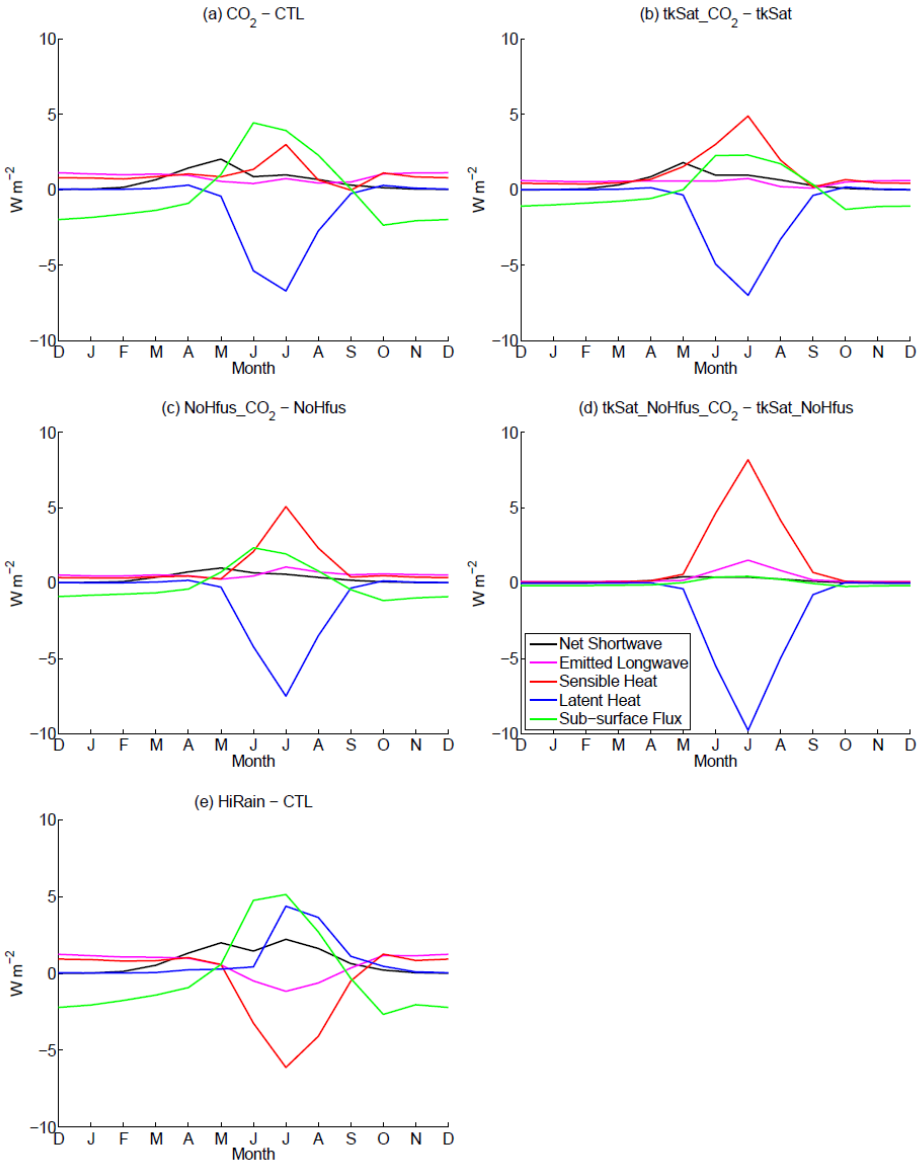

Fig. 4.3: Monthly-mean surface energy flux differences (W m^{-2}) for experiments under equilibrium historical conditions, averaged over gridcells experiencing greater than 1°C soil temperature increases in *CO_2 – CTL* (except for panel e): (a) elevated CO_2; (b) elevated CO_2 with saturated soil thermal conductivity; (c) elevated CO_2 with no LHF; (d) elevated CO_2 with both modifications to soil physics; and (e) increased JJAS rainfall (averaged over gridcells experiencing greater than 1°C soil temperature increases in this experiment). Longwave, sensible, and latent energy fluxes are positive upwards; net shortwave and sub-surface energy fluxes are positive downwards.

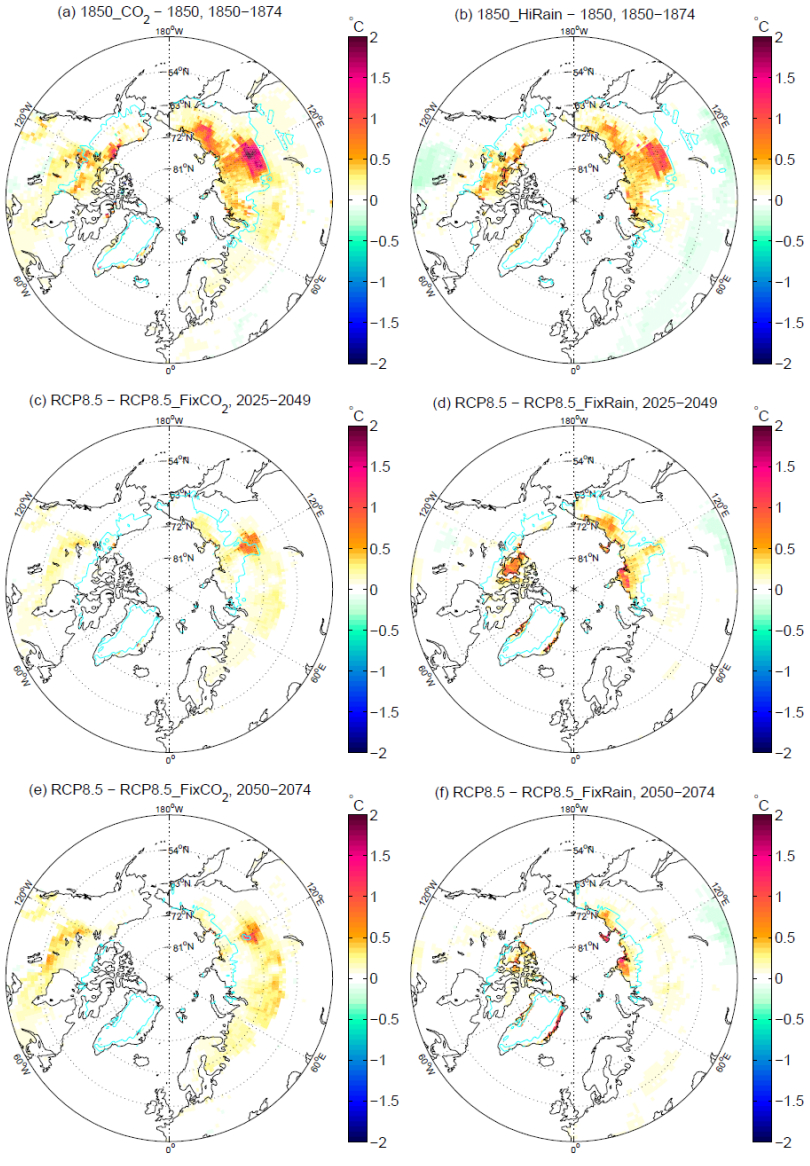

Fig. 4.4: Vertical- (to 3.8 m depth) and annual-mean soil temperature differences (°C) for experiments forced by an 1850-2099 CCSM4 historical and RCP8.5 scenario: (a) elevated CO_2 in 1850-1874 equilibrium; (b) increased JJAS rainfall in 1850-1874 equilibrium; (c) transient effects of increasing CO_2 during 2025-2049; (d) transient effects of increasing JJAS rainfall during 2025-2049; (e) transient effects of increasing CO_2 during 2050-2074; and (f) transient effects of increasing JJAS rainfall during 2050-2074. Cyan lines encircle regions with ALT less than 5 m in the control (i.e., cooler) simulations for each panel.

4.10 Tables

Table 4.1: Experimental Design[a]

Simulation Name	Forcing	CO_2 (ppm)	JJAS Rainfall	Soil Physics
CTL	NCEP	285	---	---
NoSnowIns	NCEP	285	---	NoSnowIns
CO_2	NCEP	857	---	---
HiRain	NCEP	285	+25%	---
LoRain	NCEP	285	-25%	---
tkSat	NCEP	285	---	tkSat
tkSat_CO_2	NCEP	857	---	tkSat
NoHfus	NCEP	285	---	NoHfus
NoHfus_CO_2	NCEP	857	---	NoHfus
tkSat_NoHfus	NCEP	285	---	tkSat; NoHfus
tkSat_NoHfus_CO_2	NCEP	857	---	tkSat; NoHfus
1850	CCSM4	285	---	---
1850_CO_2	CCSM4	857	---	---
1850_HiRain	CCSM4	285	+25%	---
RCP8.5	RCP8.5	Transient	---	---
RCP8.5_FixCO_2	RCP8.5	285	---	---
RCP8.5_FixRain	RCP8.5	Transient	Detrended	---

[a]CO_2 concentrations refer only to those experienced by plants, while radiative concentrations were implicit in the prescribed atmospheric forcing; JJAS = June, July, August, September; NCEP = repeated 1948-1972 cycles from Qian et al. (2006); CCSM4 = repeated 1850-1874 cycles from a 2° historical fully coupled 2° CCSM4 simulation; equilibrium fully coupled CCSM4 simulation (Section 4.8.5); RCP8.5 = 1850-2099 from a historical and RCP8.5 fully coupled 2° CCSM4 simulation (Section 4.8.5); NoSnowIns = no snow insulation (Section 4.8.6); tkSat = soil conductivity prescribed to saturated values (Section 4.8.6); NoHfus = no LHF in soil (Section 4.8.6); Detrended = transient rainfall adjusted to maintain decadal climatology at 1850-1874 values (Section 4.8.7). All simulations used prescribed leaf area and atmospheric conditions.

4.11 References

Avis, C. A., A. J. Weaver, and K. J. Meissner, 2011: Reduction in areal extent of high-latitude wetlands in response to permafrost thaw. *Nature Geoscience*, **4,** 444-448.

Bala, G., K. Caldeira, A. Mirin, M. Wickett, C. Delire, and T. J. Phillips, 2006: Biogeophysical effects of CO(2) fertilization on global climate. *Tellus Series B-Chemical and Physical Meteorology*, **58,** 620-627.

Boucher, O., A. Jones, and R. A. Betts, 2009: Climate response to the physiological impact of carbon dioxide on plants in the Met Office Unified Model HadCM3. *Climate Dynamics*, **32,** 237-249.

Cao, L., G. Bala, K. Caldeira, R. Nemani, and G. Ban-Weiss, 2010: Importance of carbon dioxide physiological forcing to future climate change. *Proceedings of the National Academy of Sciences of the United States of America*, **107,** 9513-9518.

Christensen, J. H., and Coauthors, 2007: Regional Climate Projections. *Climate Change 2007: The Physical Science Basis. Contribution of Working Group I to the Fourth Assessment Report of the Intergovernmental Panel on Climate Change*, S. Solomon, and Coauthors, Eds., Cambridge University Press.

Collatz, G. J., J. T. Ball, C. Grivet, and J. A. Berry, 1991: Physiological and Environmental-Regulation of Stomatal Conductance, Photosynthesis, and Transpiration- A Model that Includes a Laminar Boundary-Layer. *Agricultural and Forest Meteorology*, **54,** 107-136.

de Boer, H. J., E. I. Lammertsma, F. Wagner-Cremer, D. L. Dilcher, M. J. Wassen, and S. C. Dekker, 2011: Climate forcing due to optimization of maximal leaf conductance in subtropical vegetation under rising CO(2). *Proceedings of the National Academy of Sciences of the United States of America*, **108,** 4041-4046.

Farouki, O. T., 1981: The Thermal-Properties of Soils in Cold Regions. *Cold Regions Science and Technology*, **5,** 67-75.

Farquhar, G. D., S. V. Caemmerer, and J. A. Berry, 1980: A Biogeochemical-Model of Photosynthetic CO2 Assimilation in Leaves of C-3 Species. *Planta*, **149,** 78-90.

Flanner, M. G., and C. S. Zender, 2006: Linking snowpack microphysics and albedo evolution. *Journal of Geophysical Research-Atmospheres*, **111**.

Flanner, M. G., C. S. Zender, J. T. Randerson, and P. J. Rasch, 2007: Present-day climate forcing and response from black carbon in snow. *Journal of Geophysical Research-Atmospheres*, **112**.

Gedney, N., P. M. Cox, R. A. Betts, O. Boucher, C. Huntingford, and P. A. Stott, 2006: Detection of a direct carbon dioxide effect in continental river runoff records. *Nature*, **439,** 835-838.

Gent, P. R., and Coauthors, 2011: The Community Climate System Model Version 4. *Journal of Climate*, **24,** 4973-4991.

Goodrich, L. E., 1982: The Influence of Snow Cover on the Ground Thermal Regime. *Canadian Geotechnical Journal*, **19,** 421-432.

Gopalakrishnan, R., G. Bala, M. Jayaraman, L. Cao, R. Nemani, and N. H. Ravindranath, 2011: Sensitivity of terrestrial water and energy budgets to CO 2 -physiological forcing: an investigation using an offline land model. *Environmental Research Letters*, **6,** 044013.

Hansson, K., J. Simunek, M. Mizoguchi, L. C. Lundin, and M. T. van Genuchten, 2004: Water flow and heat transport in frozen soil: Numerical solution and freeze-thaw applications. *Vadose Zone Journal*, **3,** 693-704.

Hinkel, K. M., and F. E. Nelson, 2003: Spatial and temporal patterns of active layer thickness at Circumpolar Active Layer Monitoring (CALM) sites in northern Alaska, 1995-2000. *Journal of Geophysical Research-Atmospheres*, **108,** 13.

Hinkel, K. M., F. Paetzold, F. E. Nelson, and J. G. Bockheim, 2001: Patterns of soil temperature and moisture in the active layer and upper permafrost at Barrow, Alaska: 1993-1999. *Global and Planetary Change*, **29,** 293-309.

Hinzman, L. D., and Coauthors, 2005: Evidence and implications of recent climate change in northern Alaska and other arctic regions. *Climatic Change*, **72,** 251-298.

Iijima, Y., A. N. Fedorov, H. Park, K. Suzuki, H. Yabuki, T. C. Maximov, and T. Ohata, 2010: Abrupt Increases in Soil Temperatures following Increased Precipitation in a Permafrost Region, Central Lena River Basin, Russia. *Permafrost and Periglacial Processes*, **21,** 30-41.

Jin, J., X. Gao, Z. Yang, R. Bales, S. Sorooshian, and R. Dickinson, 1999: Comparative analyses of physically based snowmelt models for climate simulations. *Journal of Climate*, **12,** 2643-2657.

Jorgenson, M. T., and Coauthors, 2010: Resilience and vulnerability of permafrost to climate change. *Canadian Journal of Forest Research-Revue Canadienne De Recherche Forestiere*, **40,** 1219-1236.

Lawrence, D., and Coauthors, 2011a: Parameterization Improvements and Functional and Structural Advances in Version 4 of the Community Land Model. *Journal of Advances in Modeling Earth Systems*, **3,** 27 pp.

Lawrence, D. M., and A. G. Slater, 2008: Incorporating organic soil into a global climate model. *Climate Dynamics*, **30,** 145-160.

——, 2010: The contribution of snow condition trends to future ground climate. *Climate Dynamics*, **34,** 969-981.

Lawrence, D. M., A. G. Slater, and S. C. Swenson, 2011b: Simulation of Present-Day and Future Permafrost and Seasonally Frozen Ground Conditions in CCSM4. *Journal of Climate*, **25,** 2207-2225.

Lawrence, D. M., and Coauthors, 2011c: The CCSM4 Land Simulation, 1850–2005: Assessment of Surface Climate and New Capabilities. *Journal of Climate*, **25,** 2240-2260.

Lundin, L. C., 1990: Hydraulic-Properties in an Operational Model of Frozen Soil. *Journal of Hydrology*, **118,** 289-310.

Nakicenovic, N., and R. Swart, Eds., 2000: *Special Report on Emissions Scenarios*. Cambridge University Press.

Niu, G.-Y., and Z.-L. Yang, 2006: Effects of frozen soil on snowmelt runoff and soil water storage at a continental scale. *Journal of Hydrometeorology*, **7,** 937-952.

Notaro, M., S. Vavrus, and Z. Y. Liu, 2007: Global vegetation and climate change due to future increases in CO2 as projected by a fully coupled model with dynamic vegetation. *Journal of Climate*, **20,** 70-90.

Notaro, M., Z. Y. Liu, R. Gallimore, S. J. Vavrus, J. E. Kutzbach, I. C. Prentice, and R. L. Jacob, 2005: Simulated and observed preindustrial to modern vegetation and climate changes. *Journal of Climate*, **18,** 3650-3671.

Oleson, K., and Coauthors, 2010: Technical description of version 4.0 of the Community Land Model (CLM). National Center for Atmospheric Research, NCAR/TN-478+STR.

Oleson, K. W., and Coauthors, 2008: Improvements to the Community Land Model and their impact on the hydrological cycle. *Journal of Geophysical Research-Biogeosciences*, **113**.

Pavlov, A. V., and N. G. Moskalenko, 2002: The thermal regime of soils in the north of Western Siberia. *Permafrost and Periglacial Processes*, **13,** 43-51.

Qian, T. T., A. G. Dai, K. E. Trenberth, and K. W. Oleson, 2006: Simulation of global land surface conditions from 1948 to 2004. Part I: Forcing data and evaluations. *Journal of Hydrometeorology*, **7,** 953-975.

Riahi, K., and Coauthors, 2011: RCP 8.5-A scenario of comparatively high greenhouse gas emissions. *Climatic Change*, **109,** 33-57.

Ringeval, B., P. Friedlingstein, C. Koven, P. Ciais, N. de Noblet-Ducoudre, B. Decharme, and P. Cadule, 2011: Climate-CH(4) feedback from wetlands and its interaction with the climate-CO(2) feedback. *Biogeosciences*, **8,** 2137-2157.

Riseborough, D., N. Shiklomanov, B. Etzelmuller, S. Gruber, and S. Marchenko, 2008: Recent advances in permafrost modelling. *Permafrost and Periglacial Processes*, **19,** 137-156.

Saito, K., 2008: Arctic land hydrothermal sensitivity under warming: Idealized off-line evaluation of a physical terrestrial scheme in a global climate model. *Journal of Geophysical Research-Atmospheres*, **113**.

Schaefer, K., T. J. Zhang, L. Bruhwiler, and A. P. Barrett, 2011: Amount and timing of permafrost carbon release in response to climate warming. *Tellus Series B-Chemical and Physical Meteorology*, **63,** 165-180.

Schuur, E., and Coauthors, 2008: Vulnerability of permafrost carbon to climate change: Implications for the global carbon cycle. *Bioscience*, **58,** 701-714.

Schuur, E. A. G., B. Abbott, and N. Permafrost Carbon, 2011: High risk of permafrost thaw. *Nature*, **480,** 32-33.

Sellers, P. J., and Coauthors, 1996a: A revised land surface parameterization (SiB2) for atmospheric GCMs .1. Model formulation. *Journal of Climate*, **9,** 676-705.

Sellers, P. J., and Coauthors, 1996b: Comparison of radiative and physiological effects of doubled atmospheric CO2 on climate. *Science*, **271,** 1402-1406.

Shiklomanov, N. I., O. A. Anisimov, T. Zhang, S. Marchenko, F. E. Nelson, and C. Oelke, 2007: Comparison of model-produced active layer fields: Results for northern Alaska. *Journal of Geophysical Research-Earth Surface*, **112,** 12.

Smith, L., Y. Sheng, G. MacDonald, and L. Hinzman, 2005: Disappearing Arctic lakes. *Science*, **308,** 1429-1429.

Stieglitz, M., S. J. Dery, V. E. Romanovsky, and T. E. Osterkamp, 2003: The role of snow cover in the warming of arctic permafrost. *Geophysical Research Letters*, **30,** 4.

Tarnocai, C., J. G. Canadell, E. A. G. Schuur, P. Kuhry, G. Mazhitova, and S. Zimov, 2009: Soil organic carbon pools in the northern circumpolar permafrost region. *Global Biogeochemical Cycles*, **23**.

van Groenigen, K. J., C. W. Osenberg, and B. A. Hungate, 2011: Increased soil emissions of potent greenhouse gases under increased atmospheric CO(2). *Nature*, **475,** 214-U121.

Vavrus, S. J., M. M. Holland, A. Jahn, D. A. Bailey, and B. A. Blazey, 2011: 21st-century Arctic climate change in CCSM4. *Journal of Climate*.

Westermann, S., J. Boike, M. Langer, T. V. Schuler, and B. Etzelmuller, 2011: Modeling the impact of wintertime rain events on the thermal regime of permafrost. *Cryosphere*, **5,** 945-959.

Zhang, T., and K. Stamnes, 1998: Impact of climatic factors on the active layer and permafrost at Barrow, Alaska. *Permafrost and Periglacial Processes*, **9,** 229-246.

Zhang, T., R. G. Barry, D. Gilichinsky, S. S. Bykhovets, V. A. Sorokovikov, and J. P. Ye, 2001: An amplified signal of climatic change in soil temperatures during the last century at Irkutsk, Russia. *Climatic Change*, **49,** 41-76.

Zhang, T. J., 2005: Influence of the seasonal snow cover on the ground thermal regime: An overview. *Reviews of Geophysics*, **43,** 26.

Zhang, Y., W. J. Chen, S. L. Smith, D. W. Riseborough, and J. Cihlar, 2005: Soil temperature in Canada during the twentieth century: Complex responses to atmospheric climate change. *Journal of Geophysical Research-Atmospheres*, **110,** 15.

Zona, D., D. A. Lipson, K. T. Paw U, S. F. Oberbauer, P. Olivas, B. Gioli, and W. C. Oechel, 2012: Increased CO2 loss from vegetated drained lake tundra ecosystems due to flooding. *Global Biogeochem. Cycles*, **26,** GB2004.

Chapter 5: Conclusions and Discussion

Chapter 5 Table of Contents

5. Conclusions and Discussion

5.1 Summary and Primary Conclusions

In Chapter 2, I identified deficiencies in the existing Community Land Model 4 (CLM4) lake model, developed a new lake model (the "Lake, Ice, Snow, and Sediment Simulator"; CLM4-LISSS), evaluated the new model, and identified important processes and parameters for regional climate. The performance of the current CLM4 lake model was poor, with large differences from observations of water temperatures and surface fluxes for all four lakes simulated, attributable to deficiencies in model structure and to errors in surface flux and lake temperature calculations. CLM4-LISSS matched observations of water temperatures and surface fluxes very well for three small temperate and boreal lakes, while biases in larger lakes were modest and comparable to those associated with uncertainty in empirical lake characterizations (e.g., depth, opacity). However, the results reinforce previous conclusions (Martynov et al. 2010; Perroud et al. 2009; Stepanenko et al. 2010) that wind-driven eddy mixing predicted by the Hostetler Lake Model is insufficient for large, deep lakes, which are likely mixed largely by advective processes induced by horizontal temperature gradients.

Missing processes in lake models and insufficient parameter data for global simulations (as compared to measured parameters at some sites) can cause very large seasonal biases in local surface flux predictions of up to 30 W m^{-2}, which amounts to about 1 W m^{-2} averaged over the lake-rich area of Canada. Either neglecting snow insulation or the energy exchanges associated with phase change will lead to large declines in predicted winter lake ice temperatures, but with opposite effects on predicted surface fluxes and summer lake water temperatures. Global datasets of lake opacity could be developed based on existing remote sensing capabilities, and these datasets would improve predictions of surface fluxes as much as would improved global datasets of lake depth, and research should be undertaken to predict how lake optical properties might change under anthropogenic climate change and watershed manipulation. Decreases in lake albedo associated with disintegration and changes in ice properties during initial spring thaw can accelerate melt by a week or more at high latitudes, but current 1D model parameterizations [e.g., Mironov et al. (2010), included in CLM4-LISSS] of the albedo of thawing lakes are relatively crude and have not been systematically evaluated.

In Chapter 3, I investigated the local and large-scale effects of changes in lake distribution on regional climate, finding that the inclusion of realistic lake area can have large impacts on model predictions. The large area of lakes in Boreal regions, particularly the Canadian Shield, causes widespread differences in North American surface air temperatures of 1 – 2°C during the spring, summer, and fall, as compared to a comparable system lacking this lake area. The large sub-surface thermal inertia of lakes reduces diurnal temperature variation in their vicinity, causes increases in low cloud fraction, and causes net spring and summer cooling and fall warming. Given these effects of lakes, if warming were to result in the disappearance of lakes from present regions of discontinuous permafrost, 0.5 – 1°C changes in surface air temperature could occur in certain regions, such as central northern Canada. While this is not a large magnitude of temperature change compared to expected large-scale high-latitude air temperature changes, it may be of concern for impacts of climate change on ecosystems and human systems, as it would exacerbate daily maximum temperatures during the summer. Furthermore, existing datasets may

underestimate lake area (Downing et al. 2006; Grosse et al. 2008), meaning that future losses of lake area in regions of thawing permafrost could be larger than those that I prescribed in my experiments in Chapter 3.

Changes of 2°C in extra-tropical surface temperatures, relatively small in comparison to previous studies (Kang et al. 2008; Lee et al. 2011), could cause changes in atmospheric circulation and remote precipitation and winds. Although realistic zonally and seasonally asymmetric forcings from modifying lake area had less coherent impacts than idealized forcings of similar maximum magnitude, I found consistent directions of large-scale circulation responses resulting from both forcings. One such response to increases in extra-tropical Northern Hemisphere surface energy fluxes was decreases in westerly flow over the Southern Ocean; while the decreases simulated in this dissertation were tentative and small in magnitude, requiring confirmation in future studies, such changes would have implications for the global carbon cycle (Lee et al. 2011).

In Chapter 4, I showed that mechanisms that increase soil moisture could increase mean annual soil temperatures by interacting with the snow thermal rectifier, independent of air temperature increases. Increases in moisture of 10 – 20% of volumetric saturation increased mean annual soil temperatures by 1 – 2°C via increases in soil thermal conductivity and in the latent heat of fusion. In equilibrium historical experiments, elevated CO_2 and increased summer rainfall increased soil moisture and soil temperatures over substantial areas of Northern Canada and Northwest Siberia. However, isolating increases in CO_2 and summer rainfall from other forcings associated with a severe transient 21st century warming scenario (RCP 8.5) caused moistening and warming of reduced magnitude and spatial extent compared to the equilibrium experiments. This relatively smaller effect may have been due to spatial and temporal mis-matches in the forcing and the areas susceptible to warming, as winter air temperatures and permafrost area decreased dramatically by the late 21st century in this scenario. Nevertheless, future empirical and modeling studies should investigate this novel mechanism of response to anthropogenic forcing, as it is possible that it could alter rates of soil carbon mineralization or fractions mineralized anaerobically in permafrost soils experiencing climate change. Some Climate Model Intercomparison Project 5 (CMIP5) models may implicitly show this, without identifying or quantifying the mechanism; simulations of future climate conditions should be careful to isolate changes in soil temperature resulting from increased soil moisture from those resulting directly from increased air temperatures.

Taken together, these results show that vertically resolved modeling of thermal diffusion and phase change in both lakes and soils, in addition to explicit representation of snow insulation and vertical soil hydrology, can change the character of predictions of high-latitude terrestrial responses to climate change. Energy and water stocks and exchanges in this system are tightly coupled, and they are in turn coupled to biogeochemistry. ESMs would benefit from comprehensive inclusion of well-validated implementations of these processes at the level of complexity required to quantify the most important interactions, with continuing empirical research and investigations in fine-scale models to identify these interactions.

5.2 Thematic Discussion and Opportunities for Future Research

5.2.1 Modulation of Sub-Surface Energy Fluxes by Lakes, Snow, and Ice

Winter snow, overlying lakes, and active-layer soil moisture can all act to warm permafrost soils by increasing downwards summer sub-surface energy fluxes more readily than upwards winter fluxes out of the soil. The results shown in this dissertation illustrate the importance of hydrology, including phase change and seasonal snow insulation, in regulating sub-surface temperatures. Parallels in surface-flux regulation by lakes and snow, or by snow and ice for both lakes and soils, highlight the importance of interactions of water and energy at high latitudes.

The presence of winter snow insulation warms lakes in both the winter and summer and decreases seasonal energy exchange with the atmosphere by as much as 30 W m^{-2}, by isolating the lakes from cold winter air. Snow insulation has similar effects on permafrost soils, increasing mean-annual soil temperatures and reducing seasonal energy exchange throughout the high-latitude region.

The latent heat of fusion taken up by freezing lake water and released by melting lake ice causes near-surface lake warming in the winter, without summer warming, and also causes increases in seasonal energy exchange between lakes and the atmosphere. Similarly, increases in latent heat of fusion from increased soil moisture cause winter warming and summer cooling in the active layer of permafrost soils, in addition to increases in seasonal energy exchange between soils and the atmosphere.

Snow insulation and the latent heat of fusion interact in both lakes and soils. In lakes and in seasonally frozen soils, the presence of snow insulation substantially limits the depth of winter freeze and release of latent heat, reducing the effects of sub-surface freeze on winter energy fluxes to the atmosphere and near-surface air temperatures. In permafrost soils, where the depth of winter freeze is predominately set by summer conditions, the presence of snow insulation acts to enhance the winter warming as compared to the summer cooling from increased heat of fusion due to increased soil moisture, causing mean annual warming of soils.

Like winter snow, lakes tend to warm their underlying soils by decreasing the effective heat conductance between soils and the atmosphere in the winter as compared to the summer. Lakes deeper than the depth of winter ice tend to have taliks beneath them, and some soils under lakes can be free of permafrost even while surrounding areas have nearly continuous permafrost (Jorgenson et al. 2010). This effect results because in the unfrozen season, vigorous wind-driven and buoyant convective mixing of lake water tends to homogenize water temperatures in shallow lakes; in contrast, frozen lakes have little turbulent mixing, and the large specific heat of fusion per unit volume acts as thermal insulation for water beneath 1 – 2 m. Moreover, because the maximum density of fresh water occurs near 4°C, and lakes tend to remain stably stratified in the winter, lake bottom water and adjacent sediment can remain well above freezing. All of these effects were apparent in the lakes simulated in Chapter 2.

However, the effects of lakes on underlying soil temperatures in permafrost regions have not been studied at a pan-Arctic scale. While we generally expect lakes to cause talik formation, the rates of permafrost thaw and dependence on soil and lake properties and forcing climate have only been modeled for a few lake sites (Kessler et al. 2012; Plug and West 2009; West and Plug 2008). A model like CLM4-LISSS or the one evaluated in Stepanenko et al. (2011) should be used in a spatially distributed mode, forced by present climate for evaluation and future climate for understanding the effects of lake properties on the thaw of underlying permafrost. This modeling could address the question of how much the addition of new shallow thermokarst lakes

could accelerate permafrost thaw, and the sensitivity of this thaw to soil and lake properties and forcing climate. In order to have confidence in the predictions, observations of present-day soil temperatures underneath and near lakes are needed. Fortunately, such observations are now becoming more available (Arp et al. 2011; Jones et al. 2011).

Excess ground ice can moderate permafrost thaw in several ways. The loss of ground ice creates thermokarst, which generally accelerates permafrost thaw by increasing surface water and mechanically mixing the soil. The West and Plug model (2008) predicted lake deepening via thaw subsidence with loss of excess ice, and such a formulation could be used in spatially distributed 1D lake models in the context of the experiments in the previous paragraph. However, ground ice is also believed to stabilize permafrost by providing a large transient heat sink (Burn and Nelson 2006). At the same time, ice has a greater thermal conductivity than soil, so the net effect is unclear and may depend on the ice spatial configuration. None of the GCM-scale permafrost models yet include excess ground ice, but some of these effects may be able to be relatively easily parameterized by altering the thermal conductivity, heat of fusion, and heat capacity in the presence of prescribed excess ice; once thawed, ice could be assumed to be lost on centennial timescales. It is noteworthy that in West and Plug (2008), increased ground ice concentration had little net effect on the rate of lake deepening. This result should be confirmed with a variety of assumed ice geometries, including vertically oriented ice wedges in addition to horizontally oriented ice lenses, to see if the geometry affects the relative strength of the thaw-retarding heat sink as compared with the thaw-enhancing increases in conductivity and thaw subsidence volume.

Experiments in Chapter 4 highlight the importance of snow insulation to high-latitude soil thermal regimes: eliminating snow insulation caused a mean of 7°C and a maximum of 18°C decreases in annual-mean soil temperatures under historical conditions north of 45°. Few similar experiments have been performed at a global scale, but these numbers are within the range of those reported in previous modeling and observational studies comparing annual-mean differences between soil surface and surface air temperatures (Zhang 2005). Because snow insulation is a large control on high-latitude soil temperatures compared to expected 21st century air temperature changes, future changes in snow properties could substantially alter the response of soil temperatures to climate change. These issues were reviewed and investigated in model simulations in Lawrence and Slater (2010). They found that winter snowfall is likely to increase in the present-day permafrost zone, increasing snow accumulation and contributing to soil temperature increases, though decreases in albedo and increases in snow density may offset some of the increases in insulation. As General Circulation Models (GCMs) consistently predict increased precipitation in all seasons for high-latitude ecosystems (Christensen et al. 2007), and air temperatures throughout most of the permafrost zone will very likely remain below freezing during the winter, these model predictions of Lawrence and Slater (2010) are likely to be accurate. The timing of spring snowmelt is a related control on soil temperatures (Zhang 2005). Lawrence and Slater (2010) found that snow will melt more rapidly in the spring with climate warming, exposing soils to sunlight and to warm late-spring air temperatures more quickly. In general, the results of Lawrence and Slater (2010) suggest that changes in snow properties may act as a positive feedback to high-latitude climate change by increasing soil temperatures, increasing the susceptibility of permafrost carbon to mineralization (Section 5.2.6).

5.2.2 Modulation of Hydrology by Thawing Permafrost

Permafrost thaw can increase soil wetness and can increase microtopographic roughness and surface water via thermokarst activity, increasing surface water. However, increasing active layer thicknesses (ALT) and loss of impervious permafrost can increase drainage. These effects are summarized in Smith et al. (2007), who suggested that lake area may tend to increase in areas of continuous permafrost that begins to thaw but decrease in areas of discontinuous permafrost experiencing complete thaw. We prescribed lake area changes consistent with this generalization in Chapter 3 and examined effects on regional air temperatures. One recent study (van Huissteden et al. 2011) found that drainage of thermokarst lakes limited regional methane emissions, but the drainage mechanism investigated there was primarily lateral drainage through overflow or erosion of drainage channels rather than thaw of underlying impervious permafrost.

Research is needed to investigate whether increased drainage after loss of permafrost could be an important mechanism for drying soils in addition to reducing lake area. Simple parameterizations of inundated area as a function of soil moisture predicted loss of inundated area and thus reduced methane emissions in some areas losing permafrost in recent analyses (Avis et al. 2011; Koven et al. 2011; Riley et al. 2011; Ringeval et al. 2011), but I do not know of observations confirming these predictions. A mechanism that results in increasing drainage with increased active layer depth will be included in an upcoming version of CLM (Swenson et al., submitted to *J. Adv. Mod. Earth Sys.*).

5.2.3 Vulnerability of Northern Peatlands to Changes in Hydrological Regime

Northern peat soils contain about 400-600 Pg of carbon (Tarnocai et al. 2009; Yu et al. 2010). The vegetation and organic matter near the surface of peatlands, specifically live moss and fibric peat with high porosity and low thermal conductivity, contrasts with the heavily decomposed sapric peat, which has high water retention and very low hydraulic conductivity, that is typically beneath the water table (Letts et al. 2000; Limpens et al. 2008). The high porosity of near-surface peat and low hydraulic conductivity of the sapric peat helps to maintain the wetness of the peatland by increasing water storage capacity, inducing groundwater convergence, and inhibiting drainage. Beneath the water table, persistent anoxia induces changes in biogeochemistry that strongly inhibit decomposition (Beer and Blodau 2007; Freeman et al. 2001), allowing the potentially indefinite accumulation of carbon in an aggrading peat profile in the absence of disturbance. In some permafrost areas, the permafrost table tends to rise over time, further sequestering the aggrading peat (Kuhry et al. 2010).

As peat carbon is currently stabilized primarily by anoxia and permafrost, it could potentially be destabilized if climate change alters peatland hydrological or thermal regimes (Frolking et al. 2011; Grosse et al. 2011; Limpens et al. 2008). Large-scale drying could occur via local changes in precipitation and potential evapotranspiration, a reduction in water inflow, or by the degradation of underlying impervious permafrost that currently prevents drainage (Section 5.2.2).

Because peat physical properties arise from the depth and quality of organic matter, peatland biogeophysics are strongly coupled to biogeochemistry, creating the opportunity for strong positive feedbacks. Warming, fire, or altered hydrological regime could accelerate peat mineralization. If this loss eliminated thermally insulating, gas-diffusion resistant, and hydraulically buffering peat layers, further mineralization of the remaining peat could be enhanced in a positive feedback loop. One site-scale modeling study (Ise et al. 2008) illustrated

this potential, but this needs to be further explored using a spatially distributed model fully validated under historical and present conditions (Frolking et al. 2010; 2011). Observations of fire chronosequences and the results of intentional peatland drainage provide some information about expected responses, but additional modeling can help to understand the vulnerability of peatlands to unprecedented 21st century climate change and the potential for positive internal feedbacks to increase this vulnerability (Frolking et al. 2011).

Investigating the coupling between biogeophysics and biogeochemistry in near-surface, organic soils of high-latitude areas could also provide an extension of the biogeophysical analysis of the coupling of soil moisture and soil temperature in Chapter 4. Increased soil moisture could increase summer soil thermal insulation by increasing the accumulation of moss and near-surface organic matter (Jorgenson et al. 2010; Yi et al. 2007), reducing the impact of the warming mechanisms identified in Chapter 4. Conversely, drying caused by increased drainage could cause warming by degrading thermally insulating peat. Wisser et al. (2011) investigated the potential for permafrost thaw in existing peatlands, but without considering dynamic soil properties in response to changing organic content.

While large-scale drying of peatlands could cause a positive climate feedback by increasing CO_2 emissions, warming peatlands that remain wet could experience increases in methane fluxes. A more mechanistic treatment of wetland hydrology in an ESM would allow for improved confidence in predictions of such dynamics (Riley et al. 2011).

5.2.4 Role of Lakes in Regulating Regional Climate

I confirmed the importance of lakes in regulating regional climate by showing that large lake area in Boreal regions causes widespread modulation of surface fluxes and near-surface air temperatures. Over Canada, the realistic inclusion of about 700,000 km^2 of additional small lakes in the Canadian Shield caused up to 4 W m^{-2} differences in monthly surface fluxes with prescribed atmospheric conditions. In coupled experiments, lakes caused net spring and summer cooling and fall warming, with up to 4°C decreases in summer diurnal air temperature range, enhanced by increases in low cloud fraction.

These results in Chapter 3 are within the range of findings in previous studies (Bonan 1995; Dutra et al. 2010; Krinner 2003; Lofgren 1997; Long et al. 2007; Rouse et al. 2005; Samuelsson et al. 2010), but these studies have sometimes disagreed about the net effects of lakes on summer latent heat fluxes and about the importance of lakes in warming the winter atmosphere. Based on results in Chapters 2 and 3, we can identify some potential reasons for these discrepancies.

Neglecting the presence of snow insulation over lakes, as do many existing lake models in climate models (Bonan 1995; Samuelsson et al. 2010), could lead to over-predicting the effects of high latitude lakes on climate by over-estimating energy fluxes from freezing lake water in winter. With snow insulation included, the addition of lakes had little effect on winter climate at high latitude in my simulations (Chapter 3). However, large, temperate lakes like the Great Lakes, that may remain unfrozen for longer into the winter and accumulate less snow, may still have a noticeable warming effect on nearby regions.

I also showed that the small effective surface roughness of lakes and their high seasonal thermal inertia may reduce both sensible and latent heat fluxes in the early summer as compared to nearby land. This effect implies that summer cooling associated with lakes is primarily due to

increased sub-surface heat storage rather than a decrease in Bowen ratio, and is more prominent during the day than at night. With the high air temperatures and small seasonal lake water temperature variation characteristic of tropical lakes, however, tropical lakes consistently increase latent heat fluxes.

While increases in high-latitude lakes may be expected warm nearby soils (Section 5.2.1), this warming may not be associated with mean increases in air temperatures. While unfrozen lakes do have lower albedo than surrounding land, the impact of this difference in albedo is reduced at high zenith angles and can be compensated by increased low clouds resulting from lakes, so Boreal lakes did not increase summer net shortwave radiation in coupled experiments in Chapter 3. In my experiments, lakes stratified rapidly at the beginning of the fall freezing season and formed lake ice shortly after the beginning of snow accumulation, with little net effects on absorbed shortwave. In the spring, lake ice persisted with higher albedo than nearby land during snowmelt, reducing net shortwave absorption more than it increased in the summer. However, mean annual changes in surface fluxes were much smaller than changes in gross seasonal surface fluxes. The Chapter 3 model predictions of these effects, and specifically net seasonal changes in surface albedo due to lakes and changes in cloudiness due to lakes should be verified by observations.

Air temperature changes caused by changing lake area in regions of thawing permafrost may be relatively small compared to the effects of global climate change in the same regions or to errors in simulation caused by the under-estimation of lake area in current datasets. To confirm this expectation, research should focus on improving datasets of existing high-latitude lake area and improving understanding of the potential for increases in lake area due to thermokarst activity in cold permafrost regions beginning to thaw. Furthermore, the biogeochemical changes associated with thawing permafrost are likely more uncertain than the direct physical responses to changes in lake area (Riley et al. 2011).

5.2.5 Large-Scale Atmospheric Effects of Changes in Extra-Tropical Surface Properties

In Chapter 3, large-scale differences in seasonal mean zonal winds and meridional stream function (MSF) occurred both in coupled experiments representing increased lake area and in idealized aqua-planet experiments using prescribed surface forcing consistent with the local effects of increased lake area in the coupled experiments. Many of the large-scale differences from increased lake area in the Boreal summer in the coupled experiments were consistent with those resulting from prescribed extra-tropical Northern Hemisphere (NH) surface cooling in the aqua-planet experiments, including a strengthened mid-latitude NH westerly jet and MSF changes consistent with a northward-shifting intertropical convergence zone (ITCZ). Similarly, many of the large-scale differences from increased lake area in the Boreal fall were consistent with those resulting from prescribed extra-tropical NH surface warming in the aqua-planet experiments, including MSF changes consistent with a southward-shifting ITCZ, increases in mid-latitude Southern Hemisphere westerlies, and decreases in Southern Ocean westerlies. However, the atmospheric circulation differences in the coupled experiments, with relatively small surface forcing due to zonal and seasonal asymmetry, were small and sometimes barely significant. Likewise, the aqua-planet simulations were relatively short (i.e., 3 years), and while aqua-planet with prescribed sea-surface temperatures (SSTs) and fixed diurnal equinox solar forcing should only vary on a synoptic timescale and come to equilibrium very quickly, the

results should be confirmed in longer experiments. In addition, analogous experiments should be conducted with other atmospheric GCMs to make sure that the results are not model-dependent.

If the northward shifts in ITCZ in response to extra-tropical surface cooling found in Chapter 3 are confirmed with additional modeling experiments, research should investigate the dynamics causing this shift to be in the opposite direction of those predicted by previous studies (Broccoli et al. 2006; Chiang and Bitz 2005; Kang et al. 2009; Kang et al. 2008; Lee et al. 2011). The most obvious difference between the experimental setup used in the Chapter 3 aqua-planet experiments and aqua-planet experiments used in previous studies (Broccoli et al. 2006; Kang et al. 2008) is the use of fixed SSTs in Chapter 3. As similar responses also occurred seasonally in my coupled experiments with increased lake area that included a responsive (slab) ocean model, I hypothesize that the contrasting direction of ITCZ shift is representative of real-world differences in the atmospheric responses to terrestrial rather than ocean cooling. One such difference is that extra-tropical ocean surface temperature changes would generally persist for a long enough time for tropical ocean temperatures to respond, while a terrestrial forcing, such as changes in sub-surface energy storage due to changes in lake area, or changes in albedo from changes in snowcover, may be seasonal, interannually variable, or otherwise transient. Continued work by Shih-Yu Lee and John Chiang highlight the importance of tropical SST responses in mediating southward ITCZ shifts resulting from North Atlantic cooling (S.-Y. Lee, personal communication, 2011). Research should investigate the transient response to extra-tropical cooling, in case it is possible that the initial atmospheric response would be different in character than the equilibrium response once tropical sea-surface temperatures have adjusted to the forcing.

While the surface forcing due to increasing lake area was relatively small compared with the surface forcing investigated by previous experiments that was intended to represent a slowdown in the oceanic thermohaline circulation, a number of other high-latitude terrestrial surface changes could have much larger forcings. For instance, large albedo changes could result from shifts in vegetation distribution (Chapin et al. 2005; Eugster et al. 2000), loss of seasonal snowcover (Dery and Brown 2007), and increased deposition of dark aerosols on snow (Flanner et al. 2007; Flanner et al. 2009). I have shown in Chapter 3 that relatively long simulations (i.e., 200 years) may be necessary for robust detection of remote effects of these terrestrial surface changes due to temporal autocorrelation resulting from internal dynamical modes of climate variability, particularly in the Arctic. As in Chapter 3, idealized aqua-planet simulations may help to interpret significant remote effects. Additional research should also place ITCZ shifts induced by high-latitude terrestrial responses to climate change in the context of other ITCZ shifts expected to result from hemispheric asymmetries in anthropogenic forcing (Zhang et al. 2007): terrestrial amplification of well-mixed greenhouse gas forcing could induce a northward ITCZ shift (Johns et al. 2003), while increased albedo associated with the aerosol indirect effect could induce a southward shift (Rotstayn and Lohmann 2002).

5.2.6 What Mechanisms Could Cause Large, Positive High-Latitude Terrestrial Climate Feedbacks in the 21st Century?

As detailed in Chapter 1, high-latitude terrestrial ecosystems could act to enhance regional or global climate change (i.e., provide positive feedbacks) via four principle mechanisms: (1) decreased albedo, due to decreased extent of seasonal snow cover or land ice, or due to

expansion of dark vegetation cover (Chapin et al. 2005; Eugster et al. 2000); (2) increased CO_2 fluxes due to increased mineralization of soil carbon (especially in present-day permafrost) (Schuur et al. 2008; Zimov et al. 2006); (3) increased methane fluxes due to increased mineralization of soil carbon or to increases in anaerobic soil conditions (Ringeval et al. 2011; Schuur et al. 2008; Walter et al. 2007); and (4) increased atmospheric water vapor due to increases in evapotranspiration (Bonfils et al. 2012; Swann et al. 2010). In this dissertation, I investigated whether changes in lake area or soil moisture could trigger these mechanisms. In particular (Chapter 1), lakes could decrease albedo or increase evapotranspiration, or alter seasonal energy fluxes so as to increase mean surface air temperatures and soil temperatures in surrounding regions; increased soil moisture could warm soils.

The results shown in Chapters 2-4, while subject to a number of model limitations and needing to be verified in other models and in empirical studies, do not indicate a likelihood of large, positive terrestrial climate feedbacks occurring in the 21st century resulting from the effects of lakes and soil moisture on surface energy fluxes. In Chapter 3, in regions prescribed with increases in lake area (as may occur in regions of present-day continuous permafrost), annual-mean increases in surface air temperatures due to decreased albedo, increased evapotranspiration, or warming of stable winter atmospheric boundary layers did not occur; increases in spring surface albedo and increases in summer low cloud cover caused compensating cooling, and winter snow insulation isolated lakes from the winter atmosphere. In regions of present-day discontinuous permafrost prescribed with decreases in lake area, summer warming was slight and localized. In Chapter 4, I showed how an increase in soil moisture can lead to annual-mean warming in permafrost soils, but this warming had little effect on ALT and permafrost thaw due to compensating effects on ALT of the two mechanisms coupling soil moisture and soil temperature; also, 21st century annual-mean soil warming associated with expected future hydrological forcings was small in the model and forcing scenario used. I also participated in research suggesting that future loss of inundated area in regions of thawing permafrost (Section 5.2.2) could limit increases in high-latitude methane emissions (Riley et al. 2011).

These results suggest priorities for future research. In contrast to the weak evidence for positive feedbacks via the mechanisms investigated here, I have participated in research examining other biogeophysical and biogeochemical feedback mechanisms that could be large. Inclusion of vertically resolved soil carbon with cryoturbative diffusion converted high-latitude terrestrial ecosystems from a net sink to a net source by the end of the 21st century in a recent analysis (Koven et al. 2011), and I am helping to extend these results to a CLM4 experiment that includes nitrogen cycling and more comprehensive treatment of anaerobic decomposition processes (Koven et al., In Prep.). Currently, none of the spatially explicit (i.e., spatially distributed regional dynamic vegetation models, or terrestrial land-surface models within GCMs) estimates of future methane emissions include contributions from methanogenesis of newly thawed permafrost carbon, but the model being developed by Koven et al. would include this. I also contributed to a recent analysis showing the large potential for northern shrub encroachment to warm the Arctic via both decreases in albedo and increases in atmospheric water vapor (Bonfils et al. 2012); this analysis could be extended to investigate remote changes or changes in atmospheric circulation following the approach of Chapter 3, with long (~200 yr) experiments and with analogous surface forcing investigated in idealized aqua-planet simulations.

The large potential for changes in snow properties to affect soil temperatures (Section 5.2.1) should be further investigated; the results of Lawrence and Slater (2010) suggesting that increased snowfall and faster spring snowmelt would enhance soil temperature increases (which could increase the vulnerability of permafrost carbon) should be confirmed. Increases in fire frequency or severity could represent another source of large terrestrial feedbacks that I have not investigated in this dissertation: fire could increase vulnerability of soil carbon to mineralization (Grosse et al. 2011), although it could also be associated with increases in albedo (Randerson et al. 2006).

Many researchers are continuing to investigate the potential vulnerability of permafrost carbon to thaw and mineralization, the potential for increases in anaerobic decomposition in Arctic soils, the likelihood and impacts of vegetation shifts in the Arctic tundra, and the likelihood and impacts of changing fire regimes in the Boreal forest. Based on the work in this dissertation, future research priorities should also emphasize: (1) better understanding of the 3-dimensional geomorphological changes caused by thermokarst (Kessler et al. 2012) and extension to regional scales; (2) more comprehensive observations and modeling of the interaction of thermokarst processes with biogeochemistry (Grosse et al. 2011; Kessler et al. 2012); and (3) improved assessment of the vulnerability of northern wetlands to warming and changes in hydrological and fire regimes (Frolking et al. 2011; Limpens et al. 2008).

5.3 References

Arp, C. D., B. M. Jones, F. E. Urban, and G. Grosse, 2011: Hydrogeomorphic processes of thermokarst lakes with grounded-ice and floating-ice regimes on the Arctic coastal plain, Alaska. *Hydrological Processes*, **25,** 2422-2438.

Avis, C. A., A. J. Weaver, and K. J. Meissner, 2011: Reduction in areal extent of high-latitude wetlands in response to permafrost thaw. *Nature Geoscience*, **4,** 444-448.

Beer, J., and C. Blodau, 2007: Transport and thermodynamics constrain belowground carbon turnover in a northern peatland. *Geochimica Et Cosmochimica Acta*, **71,** 2989-3002.

Bonan, G. B., 1995: Sensitivity of a GCM Simulation to Inclusion of Inland Water Surfaces. *J. Clim.*, **8,** 2691-2704.

Bonfils, C. J. W., T. J. Phillips, D. M. Lawrence, P. Cameron-Smith, W. J. Riley, and Z. M. Subin, 2012: On the influence of shrub height and expansion on northern high latitude climate. *Environ. Res. Lett.*, **7**.

Broccoli, A. J., K. A. Dahl, and R. J. Stouffer, 2006: Response of the ITCZ to Northern Hemisphere cooling. *Geophysical Research Letters*, **33,** 4.

Burn, C. R., and F. E. Nelson, 2006: Comment on "A projection of severe near-surface permafrost degradation during the 21st century" by David M. Lawrence and Andrew G. Slater. *Geophysical Research Letters*, **33**.

Chapin, F. S., and Coauthors, 2005: Role of land-surface changes in Arctic summer warming. *Science*, **310,** 657-660.

Chiang, J. C. H., and C. M. Bitz, 2005: Influence of high latitude ice cover on the marine Intertropical Convergence Zone. *Climate Dynamics*, **25,** 477-496.

Christensen, J. H., and Coauthors, 2007: Regional Climate Projections. *Climate Change 2007: The Physical Science Basis. Contribution of Working Group I to the Fourth Assessment Report of the Intergovernmental Panel on Climate Change*, S. Solomon, and Coauthors, Eds., Cambridge University Press.

Dery, S. J., and R. D. Brown, 2007: Recent Northern Hemisphere snow cover extent trends and implications for the snow-albedo feedback. *Geophysical Research Letters*, **34**.

Downing, J. A., and Coauthors, 2006: The global abundance and size distribution of lakes, ponds, and impoundments. *Limnology and Oceanography*, **51,** 2388-2397.

Dutra, E., V. M. Stepanenko, G. Balsamo, P. Viterbo, P. M. A. Miranda, D. Mironov, and C. Schar, 2010: An offline study of the impact of lakes on the performance of the ECMWF surface scheme. *Boreal Environment Research*, **15,** 100-112.

Eugster, W., and Coauthors, 2000: Land-atmosphere energy exchange in Arctic tundra and boreal forest: available data and feedbacks to climate. *Glob. Change Biol.*, **6,** 84-115.

Flanner, M. G., C. S. Zender, J. T. Randerson, and P. J. Rasch, 2007: Present-day climate forcing and response from black carbon in snow. *Journal of Geophysical Research-Atmospheres*, **112**.

Flanner, M. G., C. S. Zender, P. G. Hess, N. M. Mahowald, T. H. Painter, V. Ramanathan, and P. J. Rasch, 2009: Springtime warming and reduced snow cover from carbonaceous particles. *Atmospheric Chemistry and Physics*, **9,** 2481-2497.

Freeman, C., N. Ostle, and H. Kang, 2001: An enzymic 'latch' on a global carbon store - A shortage of oxygen locks up carbon in peatlands by restraining a single enzyme. *Nature*, **409,** 149.

Frolking, S., N. T. Roulet, E. Tuittila, J. L. Bubier, A. Quillet, J. Talbot, and P. J. H. Richard, 2010: A new model of Holocene peatland net primary production, decomposition, water balance, and peat accumulation. *Earth Syst. Dynam.*, **1,** 1-21.

Frolking, S., J. Talbot, M. C. Jones, C. C. Treat, J. B. Kauffman, E. S. Tuittila, and N. Roulet, 2011: Peatlands in the Earth's 21st century climate system. *Environmental Reviews*, **19,** 371-396.

Grosse, G., V. E. Romanovsky, K. M. Walter, A. Morgenstern, H. Lantuit, and S. Zimov, 2008: Distribution of Thermokarst Lakes and Ponds at Three Yedoma Sites in Siberia. *Proceedings of the 9th International Conference on Permafrost*, University of Alaska, Fairbanks, USA, 551-556.

Grosse, G., and Coauthors, 2011: Vulnerability of high-latitude soil organic carbon in North America to disturbance. *Journal of Geophysical Research-Biogeosciences*, **116**.

Ise, T., A. L. Dunn, S. C. Wofsy, and P. R. Moorcroft, 2008: High sensitivity of peat decomposition to climate change through water-table feedback. *Nature Geoscience*, **1,** 763-766.

Johns, T., and Coauthors, 2003: Anthropogenic climate change for 1860 to 2100 simulated with the HadCM3 model under updated emissions scenarios. *Climate Dynamics*, **20,** 583-612.

Jones, B. M., G. Grosse, C. D. Arp, M. C. Jones, K. M. W. Anthony, and V. E. Romanovsky, 2011: Modern thermokarst lake dynamics in the continuous permafrost zone, northern Seward Peninsula, Alaska. *Journal of Geophysical Research-Biogeosciences*, **116**.

Jorgenson, M. T., and Coauthors, 2010: Resilience and vulnerability of permafrost to climate change. *Canadian Journal of Forest Research-Revue Canadienne De Recherche Forestiere*, **40,** 1219-1236.

Kang, S. M., D. M. W. Frierson, and I. M. Held, 2009: The Tropical Response to Extratropical Thermal Forcing in an Idealized GCM: The Importance of Radiative Feedbacks and Convective Parameterization. *Journal of the Atmospheric Sciences*, **66,** 2812-2827.

Kang, S. M., I. M. Held, D. M. W. Frierson, and M. Zhao, 2008: The response of the ITCZ to extratropical thermal forcing: Idealized slab-ocean experiments with a GCM. *J. Clim.*, **21,** 3521-3532.

Kessler, M. A., L. J. Plug, and K. M. Walter Anthony, 2012: Simulating the decadal- to millennial-scale dynamics of morphology and sequestered carbon mobilization of two thermokarst lakes in NW Alaska. *J. Geophys. Res.*, **117,** G00M06.

Koven, C. D., and Coauthors, 2011: Permafrost carbon-climate feedbacks accelerate global warming. *Proc. Natl. Acad. Sci. U. S. A.*, **108,** 14769-14774.

Krinner, G., 2003: Impact of lakes and wetlands on boreal climate. *Journal of Geophysical Research-Atmospheres*, **108,** 18.

Kuhry, P., E. Dorrepaal, G. Hugelius, E. A. G. Schuur, and C. Tarnocai, 2010: Potential Remobilization of Belowground Permafrost Carbon under Future Global Warming. *Permafrost and Periglacial Processes*, **21,** 208-214.

Lawrence, D. M., and A. G. Slater, 2010: The contribution of snow condition trends to future ground climate. *Climate Dynamics*, **34,** 969-981.

Lee, S.-Y., J. C. H. Chiang, K. Matsumoto, and K. S. Tokos, 2011: Southern Ocean wind response to North Atlantic cooling and the rise in atmospheric CO2: Modeling perspective and paleoceanographic implications. *Paleoceanography*, **26,** PA1214.

Letts, M. G., N. T. Roulet, N. T. Comer, M. R. Skarupa, and D. L. Verseghy, 2000: Parametrization of peatland hydraulic properties for the Canadian Land Surface Scheme. *Atmosphere-Ocean*, **38,** 141-160.

Limpens, J., and Coauthors, 2008: Peatlands and the carbon cycle: from local processes to global implications - a synthesis. *Biogeosciences*, **5,** 1475-1491.

Lofgren, B. M., 1997: Simulated effects of idealized Laurentian Great Lakes on regional and large-scale climate. *J. Clim.*, **10,** 2847-2858.

Long, Z., W. Perrie, J. Gyakum, D. Caya, and R. Laprise, 2007: Northern lake impacts on local seasonal climate. *J. Hydrometeorol.*, **8,** 881-896.

Martynov, A., L. Sushama, and R. Laprise, 2010: Simulation of temperate freezing lakes by one-dimensional lake models: performance assessment for interactive coupling with regional climate models. *Boreal Environment Research*, **15,** 143-164.

Mironov, D., E. Heise, E. Kourzeneva, B. Ritter, N. Schneider, and A. Terzhevik, 2010: Implementation of the lake parameterisation scheme FLake into the numerical weather prediction model COSMO. *Boreal Environment Research*, **15,** 218-230.

Perroud, M., S. Goyette, A. Martynov, M. Beniston, and O. Anneville, 2009: Simulation of multiannual thermal profiles in deep Lake Geneva: A comparison of one-dimensional lake models. *Limnology and Oceanography*, **54,** 1574-1594.

Plug, L., and J. West, 2009: Thaw lake expansion in a two-dimensional coupled model of heat transfer, thaw subsidence, and mass movement. *Journal of Geophysical Research-Earth Surface*, **114,** -.

Randerson, J. T., and Coauthors, 2006: The impact of boreal forest fire on climate warming. *Science*, **314,** 1130-1132.

Riley, W. J., and Coauthors, 2011: Barriers to predicting changes in global terrestrial methane fluxes: analyses using CLM4Me, a methane biogeochemistry model integrated in CESM. *Biogeosciences*, **8,** 1925-1953.

Ringeval, B., P. Friedlingstein, C. Koven, P. Ciais, N. de Noblet-Ducoudre, B. Decharme, and P. Cadule, 2011: Climate-CH(4) feedback from wetlands and its interaction with the climate-CO(2) feedback. *Biogeosciences*, **8,** 2137-2157.

Rotstayn, L. D., and U. Lohmann, 2002: Tropical Rainfall Trends and the Indirect Aerosol Effect. *J. Clim.*, **15,** 2103-2116.

Rouse, W. R., and Coauthors, 2005: The role of northern lakes in a regional energy balance. *J. Hydrometeorol.*, **6,** 291-305.

Samuelsson, P., E. Kourzeneva, and D. Mironov, 2010: The impact of lakes on the European climate as simulated by a regional climate model. *Boreal Environment Research*, **15,** 113-129.

Schuur, E., and Coauthors, 2008: Vulnerability of permafrost carbon to climate change: Implications for the global carbon cycle. *Bioscience*, **58,** 701-714.

Smith, L. C., Y. W. Sheng, and G. M. MacDonald, 2007: A first pan-Arctic assessment of the influence of glaciation, permafrost, topography and peatlands on northern hemisphere lake distribution. *Permafrost and Periglacial Processes*, **18,** 201-208.

Stepanenko, V. M., E. E. Machulskaya, M. V. Glagolev, and V. N. Lykosov, 2011: Modeling of methane emissions from lakes in the permafrost zone. *Izvestiya, Atmospheric and Ocean Physics*, **47,** 1-14.

Stepanenko, V. M., S. Goyette, A. Martynov, M. Perroud, X. Fang, and D. Mironov, 2010: First steps of a Lake Model Intercomparison Project: LakeMIP. *Boreal Environment Research*, **15,** 191-202.

Swann, A. L., I. Y. Fung, S. Levis, G. B. Bonan, and S. C. Doney, 2010: Changes in Arctic vegetation amplify high-latitude warming through the greenhouse effect. *Proc. Natl. Acad. Sci. U. S. A.*, **107,** 1295-1300.

Tarnocai, C., J. G. Canadell, E. A. G. Schuur, P. Kuhry, G. Mazhitova, and S. Zimov, 2009: Soil organic carbon pools in the northern circumpolar permafrost region. *Global Biogeochemical Cycles*, **23**.

van Huissteden, J., C. Berrittella, F. J. W. Parmentier, Y. Mi, T. C. Maximov, and A. J. Dolman, 2011: Methane emissions from permafrost thaw lakes limited by lake drainage. *Nature Climate Change*, **1,** 119-123.

Walter, K. M., L. C. Smith, and F. S. Chapin, 2007: Methane bubbling from northern lakes: present and future contributions to the global methane budget. *Philosophical Transactions of the Royal Society a-Mathematical Physical and Engineering Sciences*, **365,** 1657-1676.

West, J. J., and L. J. Plug, 2008: Time-dependent morphology of thaw lakes and taliks in deep and shallow ground ice. *Journal of Geophysical Research-Earth Surface*, **113**.

Wisser, D., S. Marchenko, J. Talbot, C. Treat, and S. Frolking, 2011: Soil temperature response to 21st century global warming: the role of and some implications for peat carbon in thawing permafrost soils in North America. *Earth Syst. Dynam.*, **2,** 121-138.

Yi, S. H., M. K. Woo, and M. A. Arain, 2007: Impacts of peat and vegetation on permafrost degradation under climate warming. *Geophysical Research Letters*, **34**.

Yu, Z. C., J. Loisel, D. P. Brosseau, D. W. Beilman, and S. J. Hunt, 2010: Global peatland dynamics since the Last Glacial Maximum. *Geophysical Research Letters*, **37**.

Zhang, T. J., 2005: Influence of the seasonal snow cover on the ground thermal regime: An overview. *Rev. Geophys.*, **43,** 26.

Zhang, X., and Coauthors, 2007: Detection of human influence on twentieth-century precipitation trends. *Nature*, **448,** 461-465.

Zimov, S., S. Davydov, G. Zimova, A. Davydova, E. Schuur, K. Dutta, and F. Chapin, 2006: Permafrost carbon: Stock and decomposability of a globally significant carbon pool. *Geophysical Research Letters*, **33,** -.

Appendix 1: Supplemental Figures for Chapter 2

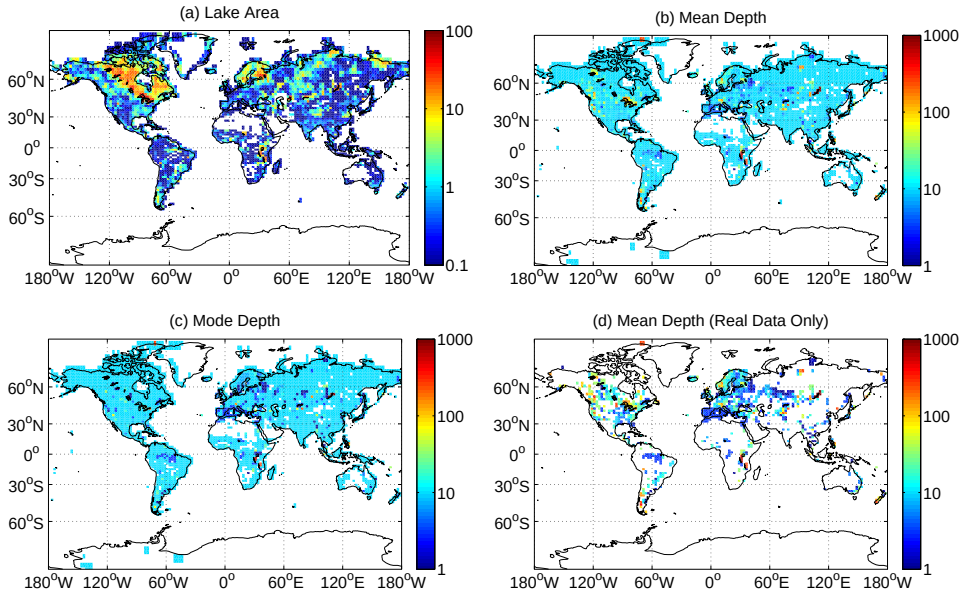

Figure 1: (a) % lake area used in this study (Lehner and Doll 2004), and (b-d) comparison of gridded lake depth (m) interpolated from 1 km resolution in Kourzeneva et al. (2010) to 1.9 x 2.5° resolution used in CLM with alternative interpolation approaches: (b) mean depth of all lakes (weighted by fraction of 1 km gridcells); (c) mode depth of lakes in 1 km gridcells; and (d) mean depth of all lakes for which real data was available, rather than the default 10 m.

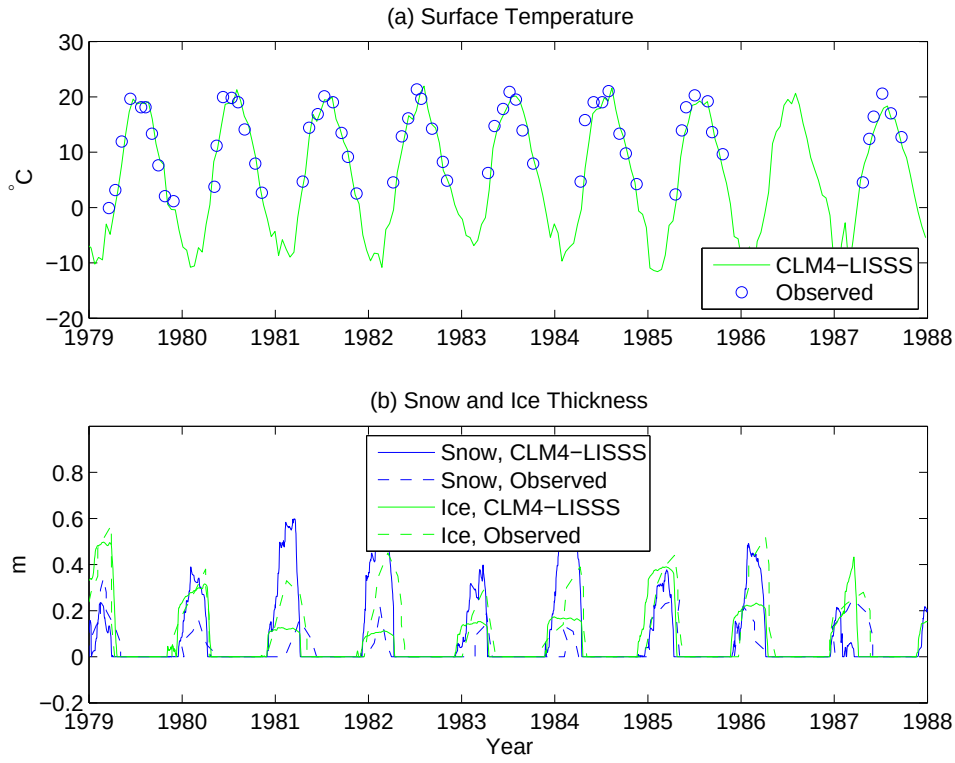

Figure 2: Lake Karujarv, 1979-1988, observed and simulated by CLM4-LISSS: (a) surface temperature; and (b) snow and ice thickness.

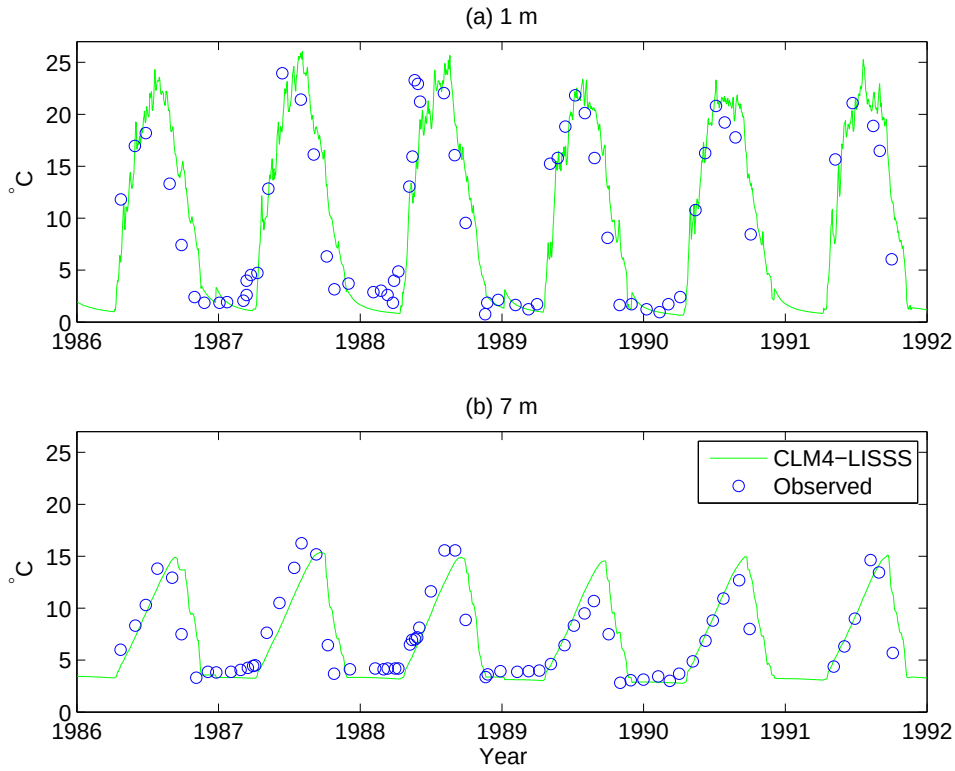

Figure 3: Thrush Lake water temperatures, observed and simulated by CLM4-LISSS, 1986-1991: (a) 1 m; (b) 7 m.

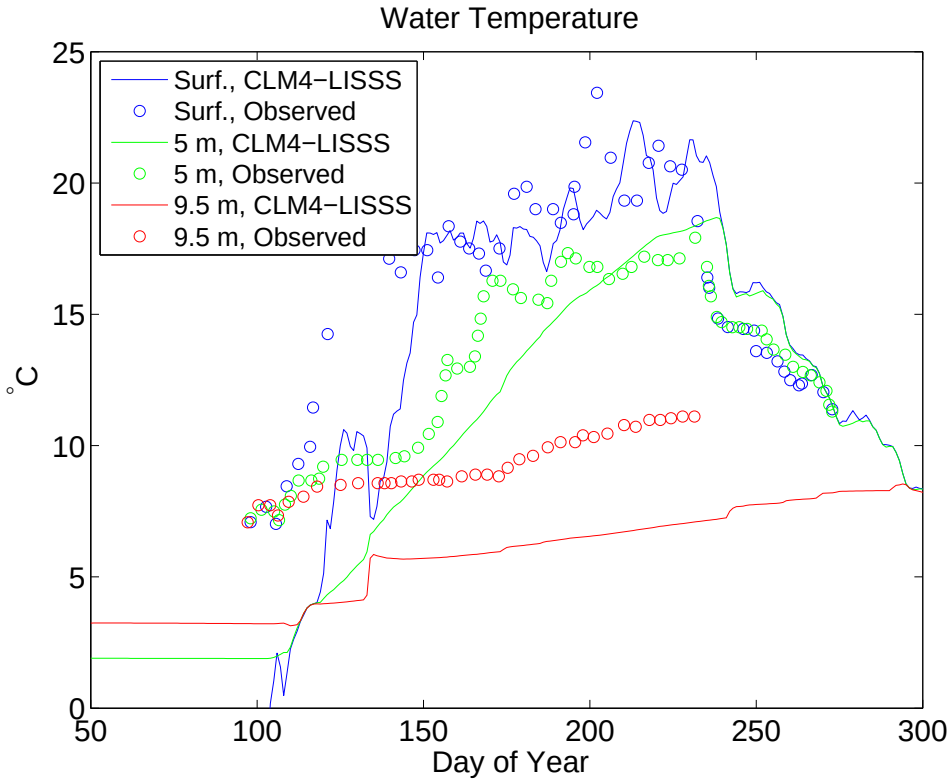

Figure 4: Lake Raksjo water temperatures, observed and simulated by CLM4-LISSS, 1995: surface, 5 m, and 9.5 m.

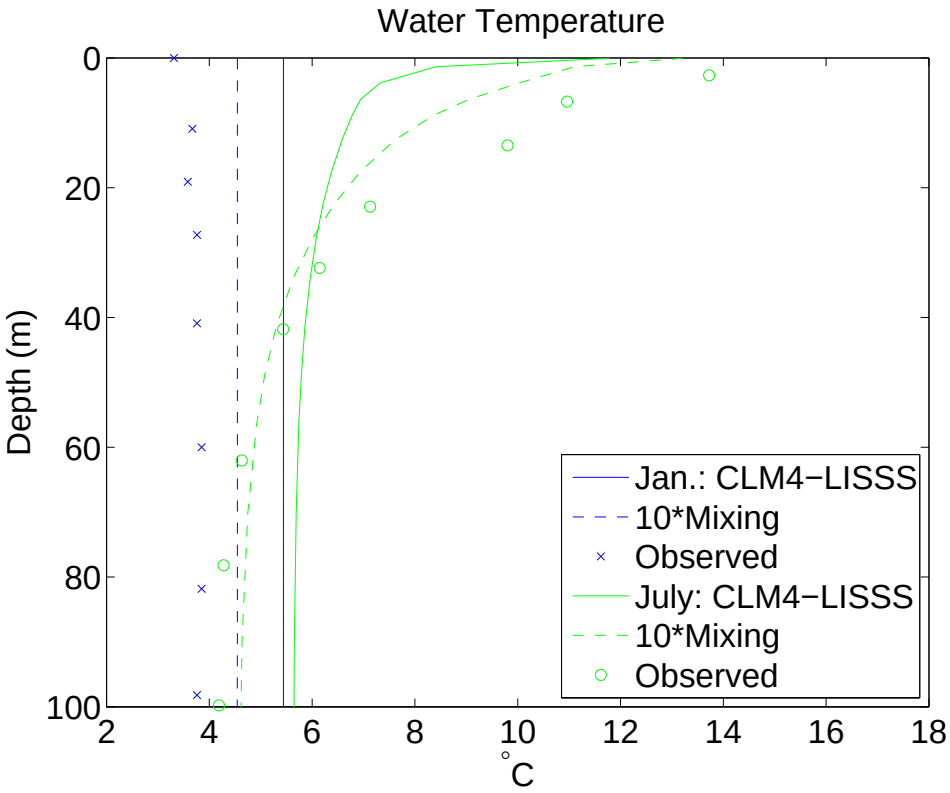

Figure 5: Crater Lake 1988-2000 monthly-averaged water temperatures, simulated by CLM4-LISSS, CLM4-LISSS with eddy diffusivity increased by 10, and observed (Larson et al. 2007), for mean January and mean July.

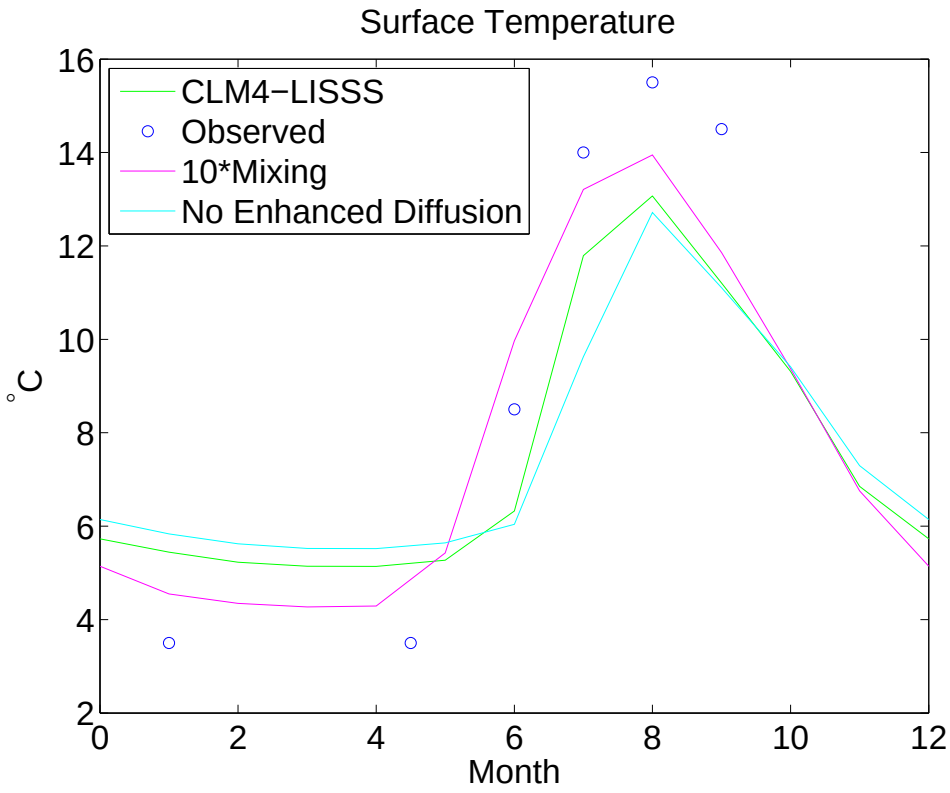

Figure 6: Crater Lake 1988-2000 monthly-averaged surface temperature, simulated by CLM4-LISSS, observed (Larson et al. 2007), CLM4-LISSS with eddy diffusivity increased by 10, and CLM4-LISSS without enhanced diffusion.

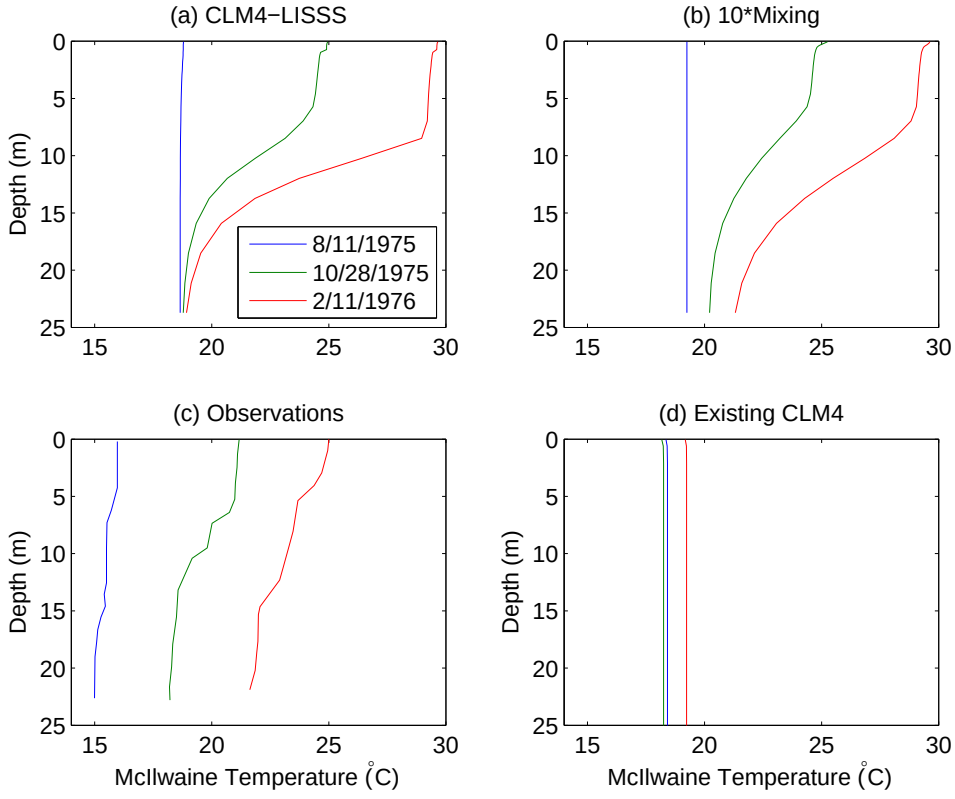

Figure 7: Lake McIlwaine water temperatures for 11 Aug. 1975, 28 Oct. 1975, and 11 Feb. 1976: (a) simulated by CLM4-LISSS; (b) simulated by CLM4-LISSS with eddy diffusivity increased by 10; (c) observed (Robarts and Ward 1978); and (d) simulated by the existing CLM4.

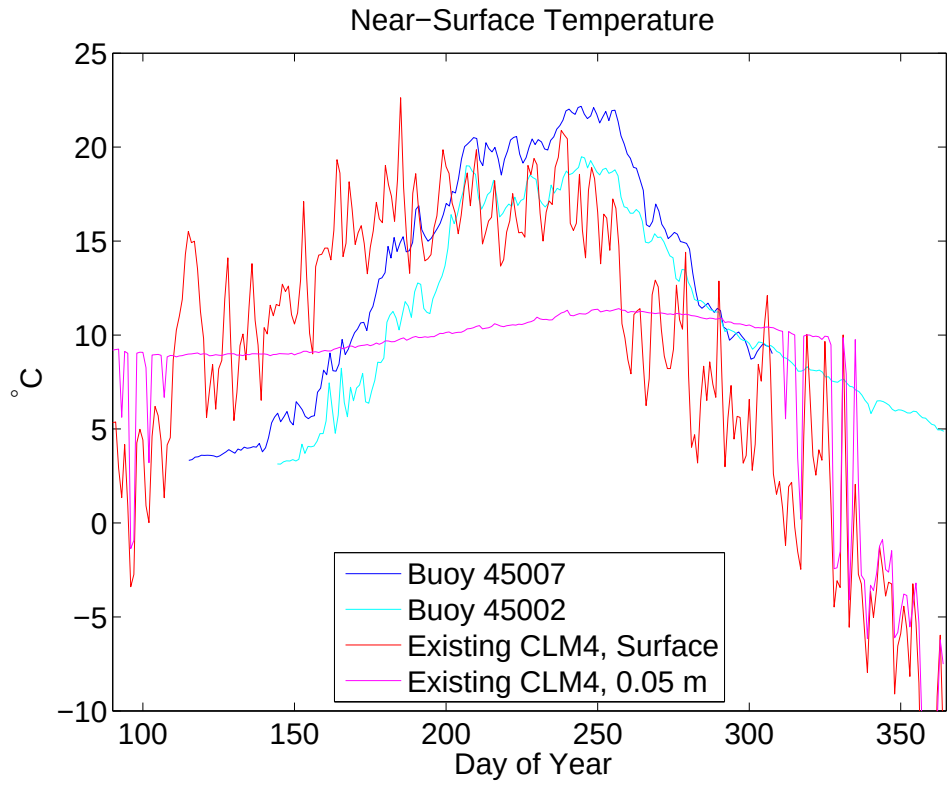

Figure 8: Daily mean Lake Michigan near-surface temperatures for 1990: National Data Buoy Center Station 45007 observations, National Data Buoy Center Station 45002 observations, simulated by the existing CLM4 (surface temperature), and simulated by the existing CLM4 (0.05 m temperature).

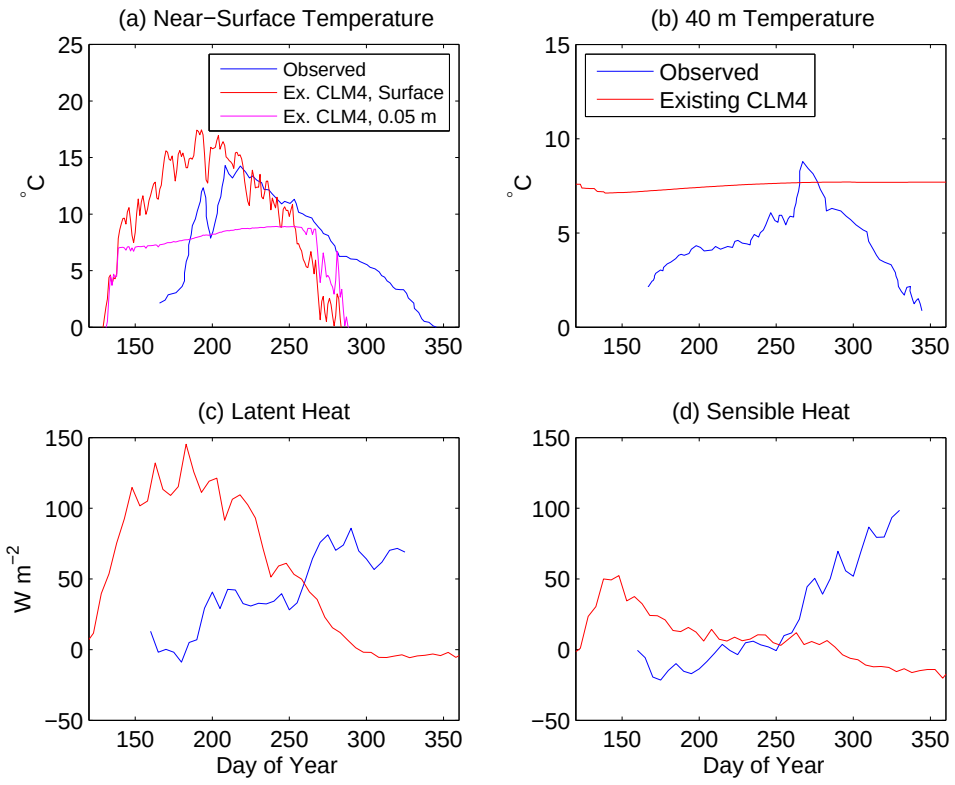

Figure 9: Daily-averaged Great Slave Lake water temperatures and surface fluxes from 1997-2003 excluding 2001, observed (Rouse et al. 2008) and simulated by the existing CLM4: (a) near-surface temperature; (b) temperature at 40 m depth; (c) latent heat; and (d) sensible heat.

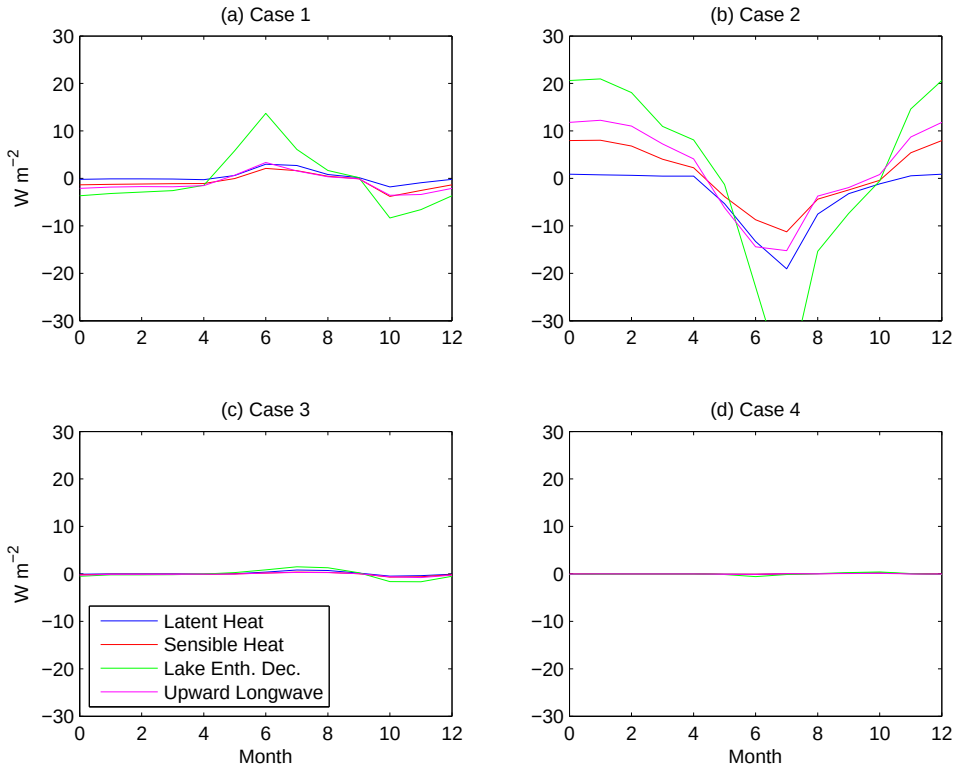

Figure 10: Monthly average surface flux anomalies for North Eurasian (60 - 90 °N, 0 - 175 °E) lakes: Cases 1-4.

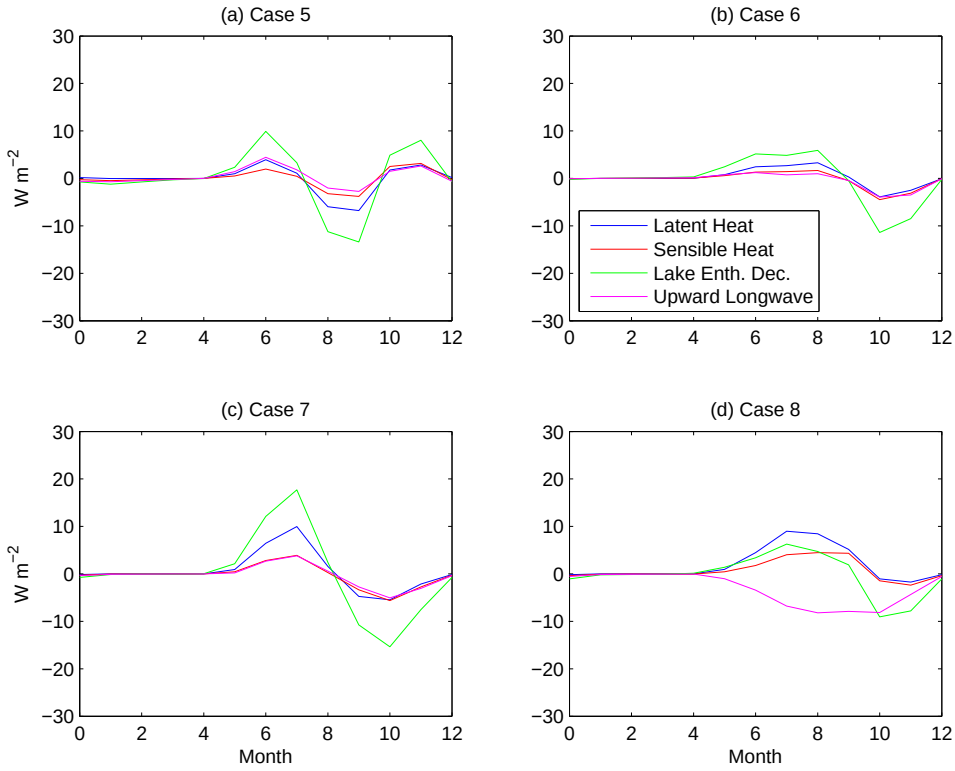

Figure 11: Monthly average surface flux anomalies for North Eurasian (60 - 90 °N, 0 - 175 °E) lakes: Cases 5-8.

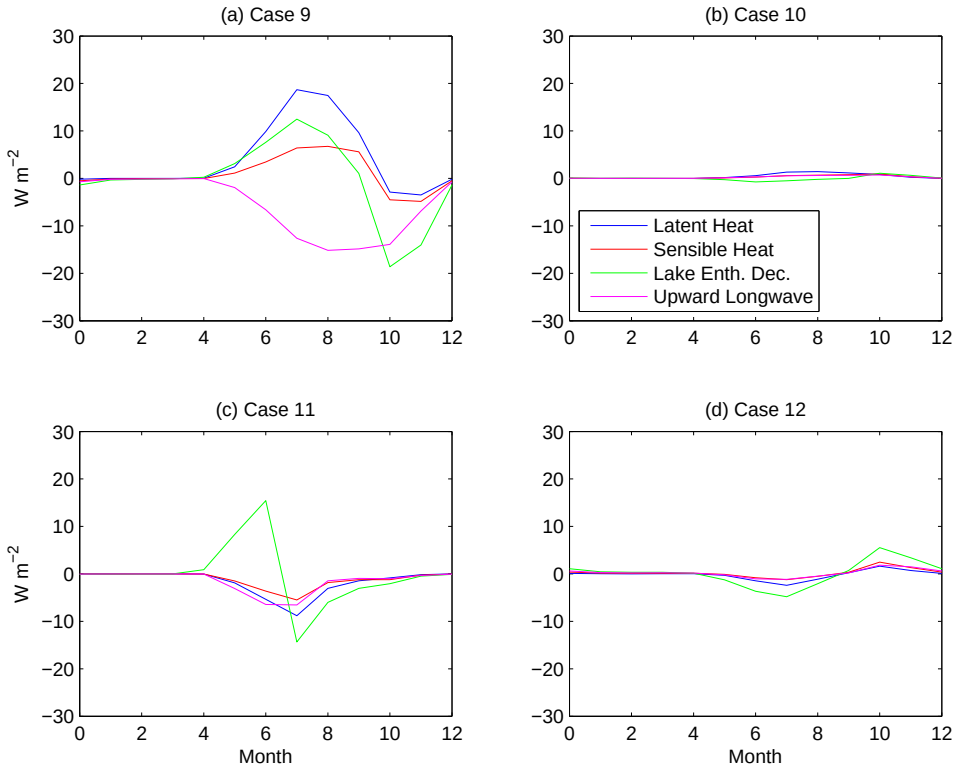

Figure 12: Monthly average surface flux anomalies for North Eurasian (60 - 90 °N, 0 - 175 °E) lakes: Cases 9-12.

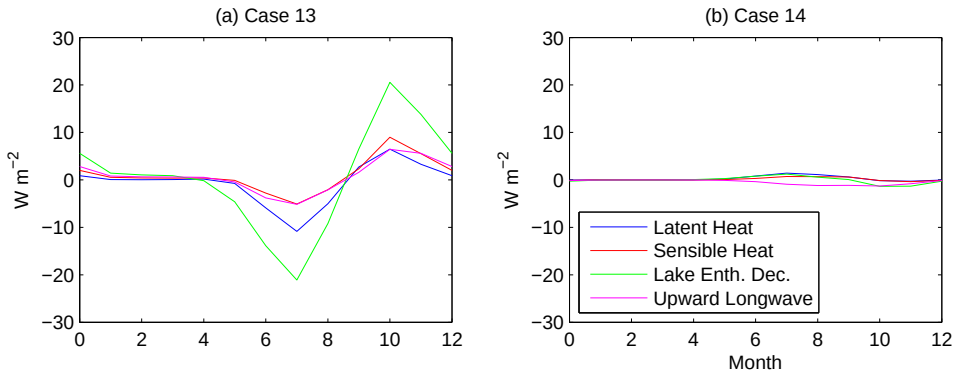

Figure 13: Monthly average surface flux anomalies for North Eurasian (60 - 90 °N, 0 - 175 °E) lakes: Cases 13-14.

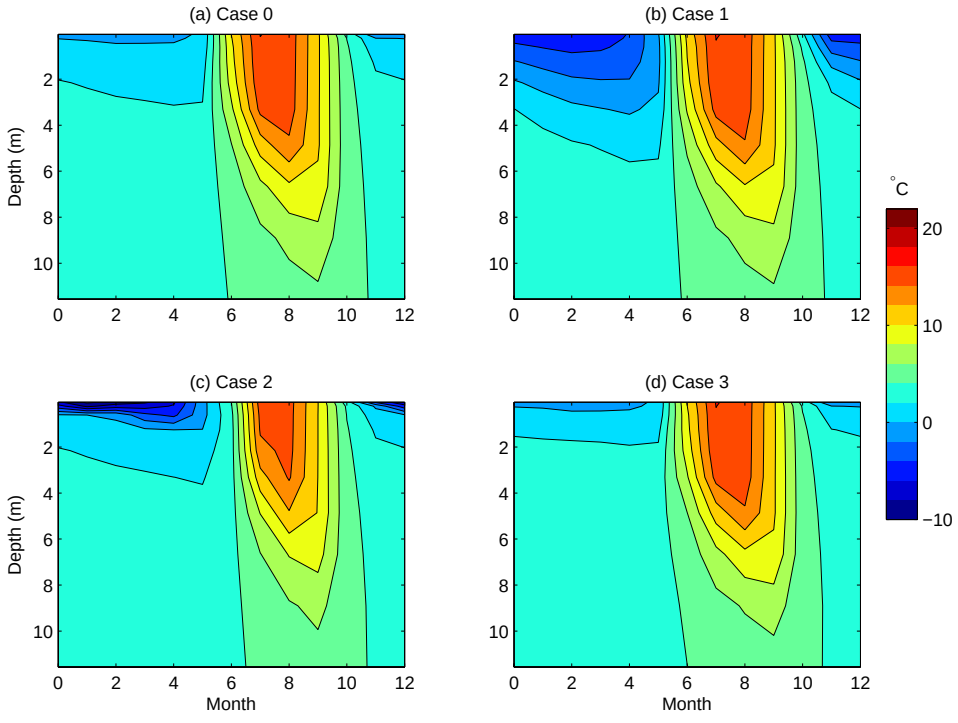

Figure 14: Monthly average water temperatures for the gridcell co-located with Finnish lake Inari: Cases 0-3 (Case 0 is the baseline).

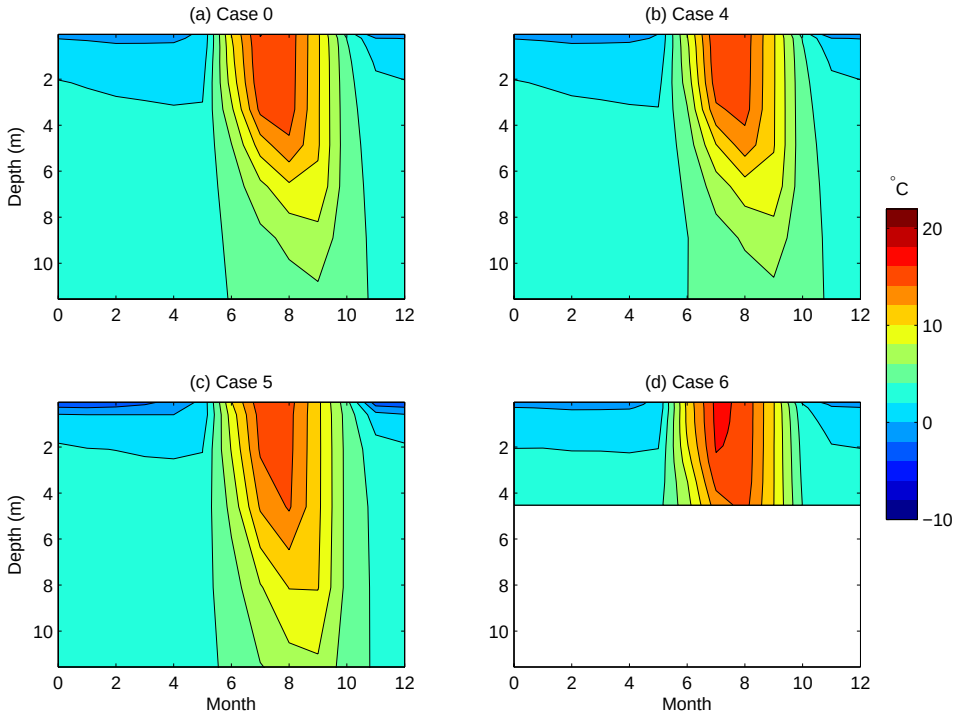

Figure 15: Monthly average water temperatures for the gridcell co-located with Finnish lake Inari: Cases 4-6 (Case 0 is the baseline).

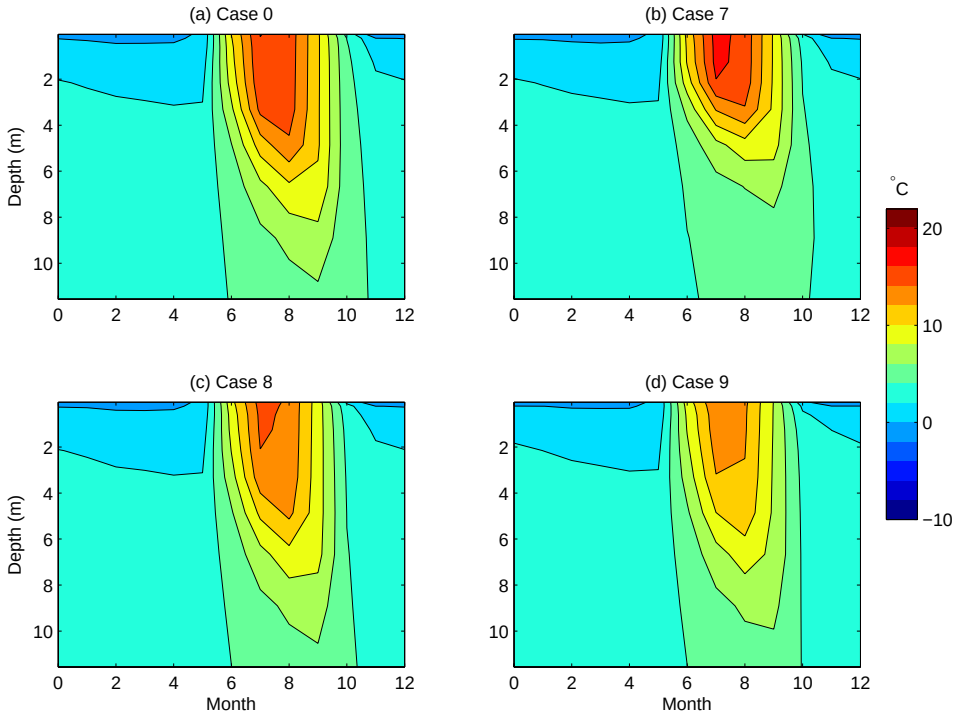

Figure 16: Monthly average water temperatures for the gridcell co-located with Finnish lake Inari: Cases 7-9 (Case 0 is the baseline).

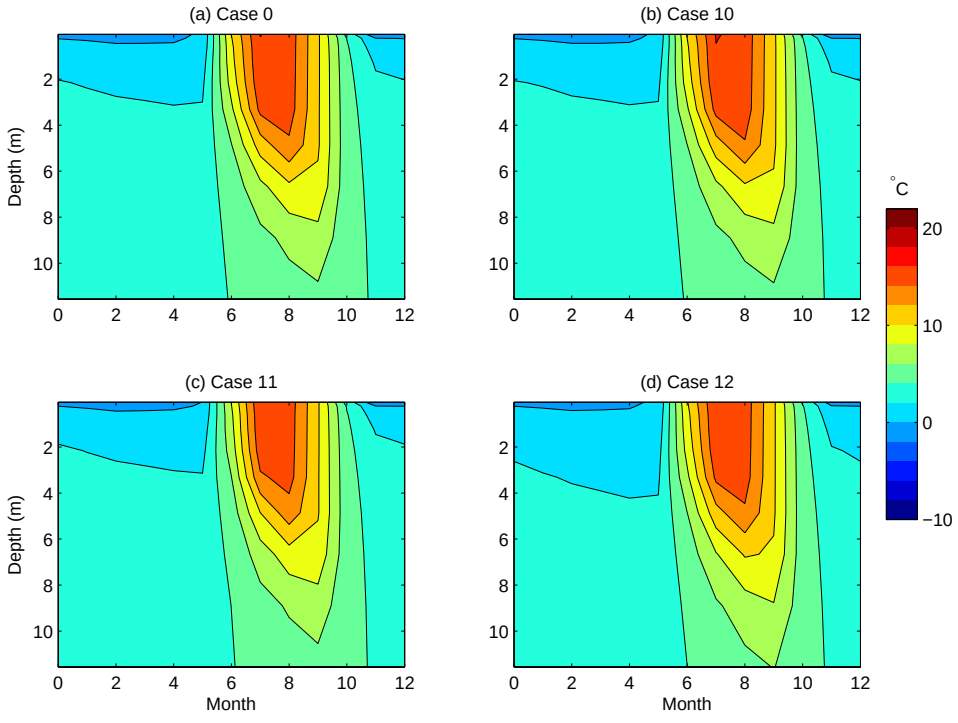

Figure 17: Monthly average water temperatures for the gridcell co-located with Finnish lake Inari: Cases 10-12 (Case 0 is the baseline).

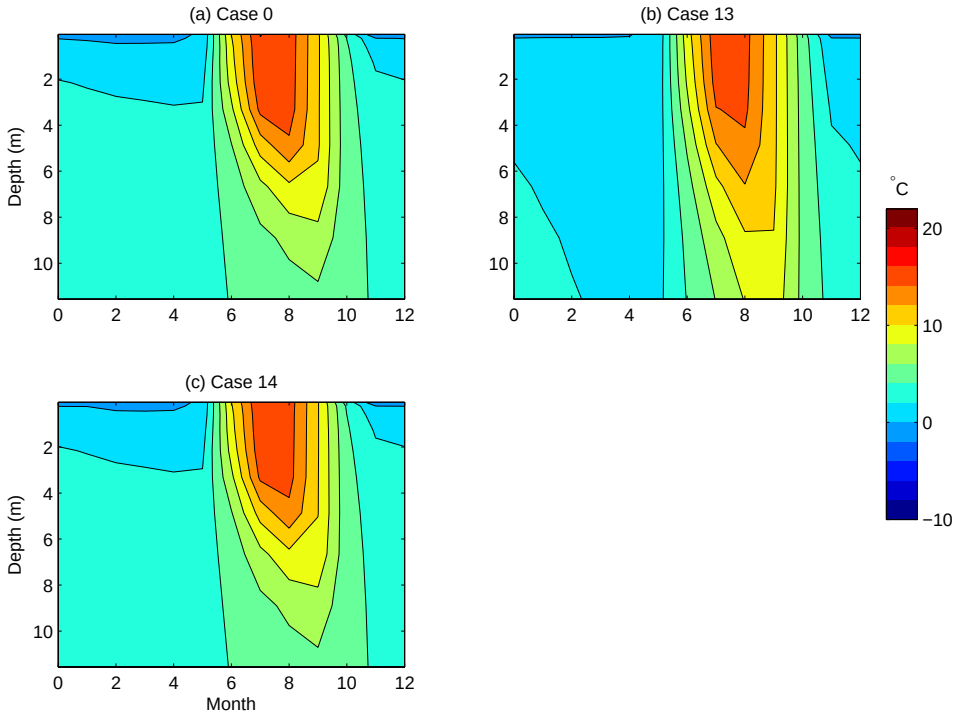

Figure 18: Monthly average water temperatures for the gridcell co-located with Finnish lake Inari: Cases 13-4 (Case 0 is the baseline).

Appendix 2: Supplemental Figures for Chapter 4

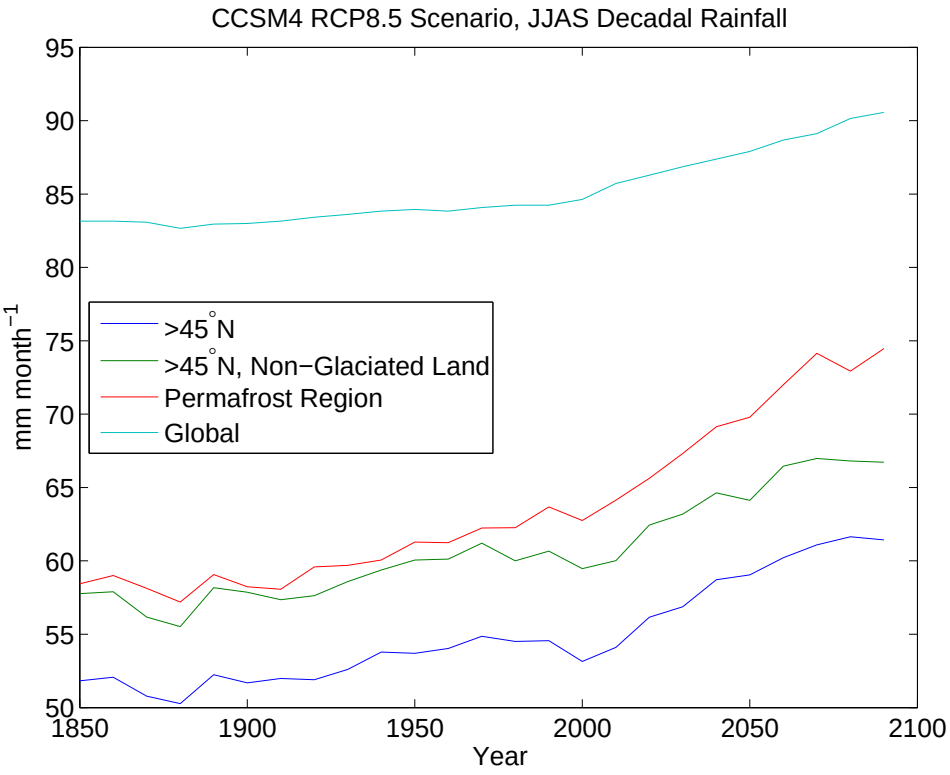

Figure 1: Trends of decadal-mean JJAS rainfall (mm month^{-1}) in the 1850-2099 CCSM4 RCP8.5 forcing.

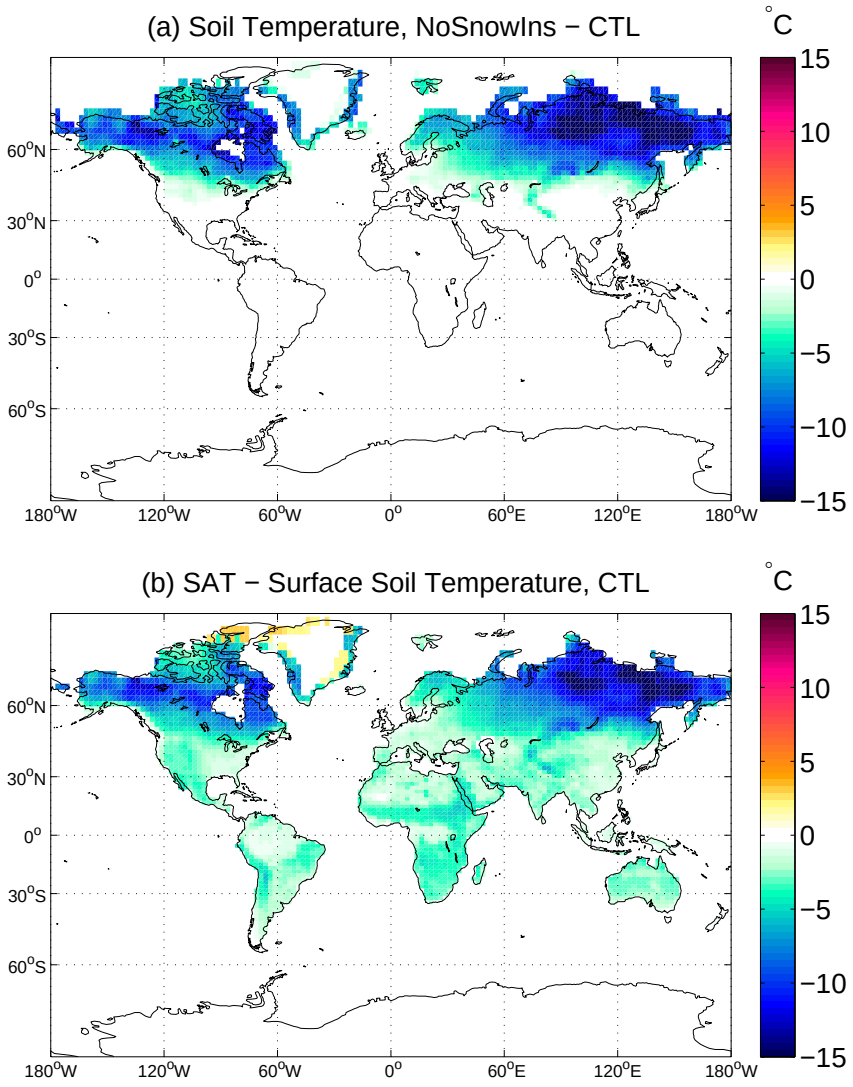

Figure 2: Effects of snow insulation under equilibrium historical conditions: (a) vertical- (to 3.8 m) and annual-mean soil temperature changes (°C) when eliminating snow insulation; and (b) mean differences between surface air temperature and soil surface temperature in the control simulation.

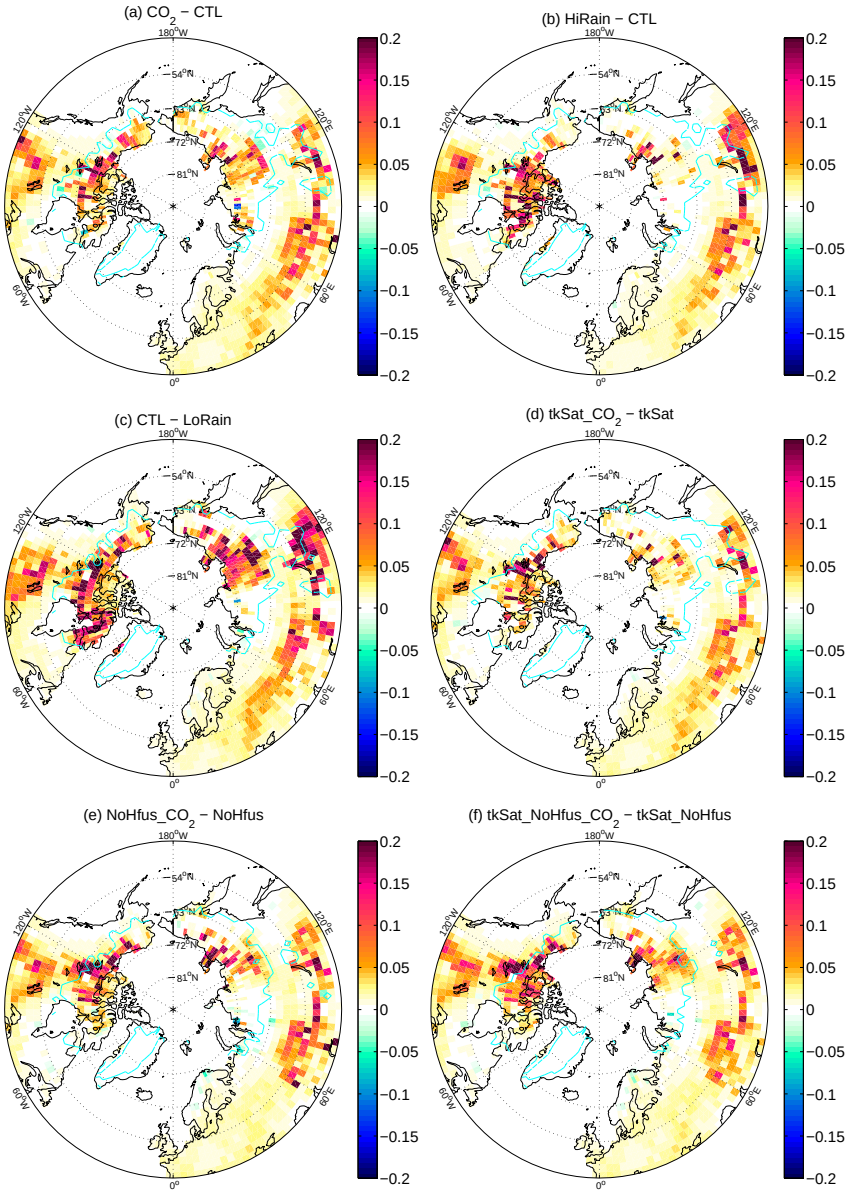

Figure 3: Vertical- (to 3.8 m depth) and annual-mean soil water-filled pore space differences for experiments under equilibrium historical conditions: (a) elevated CO_2; (b) increased JJAS rainfall; (c) increased JJAS rainfall relative to reduced baseline; (d) elevated CO_2 with saturated soil thermal conductivity; (e) elevated CO_2 with no LHF; and (f) elevated CO_2 with both modifications to soil physics. Cyan lines encircle regions with ALT less than 5 m in the control (i.e., drier) simulations for each panel.

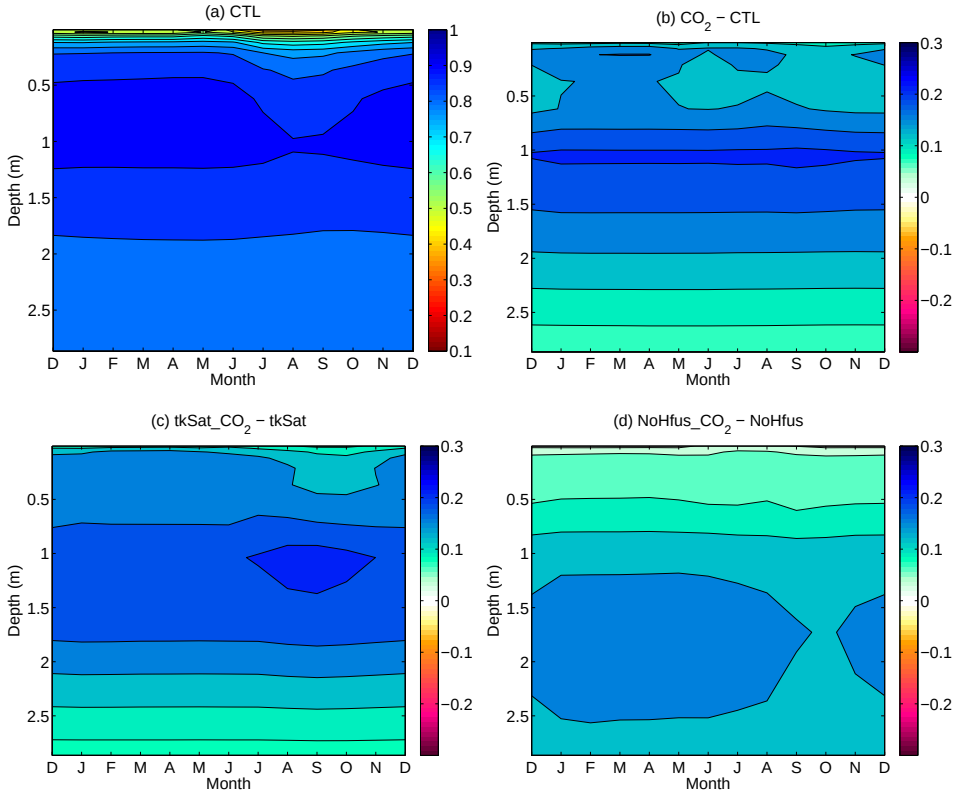

Figure 4: Monthly-mean soil water-filled pore space differences for experiments under equilibrium historical conditions, averaged over gridcells experiencing greater than 1°C soil temperature increases in the *CO*$_2$ - *CTL* experiment: (a) absolute water-filled pore space occurring in the baseline simulation; (b) changes due to elevated CO_2; (c) changes due to elevated CO_2 with saturated soil thermal conductivity; and (d) changes due to elevated CO_2 with no soil LHF.

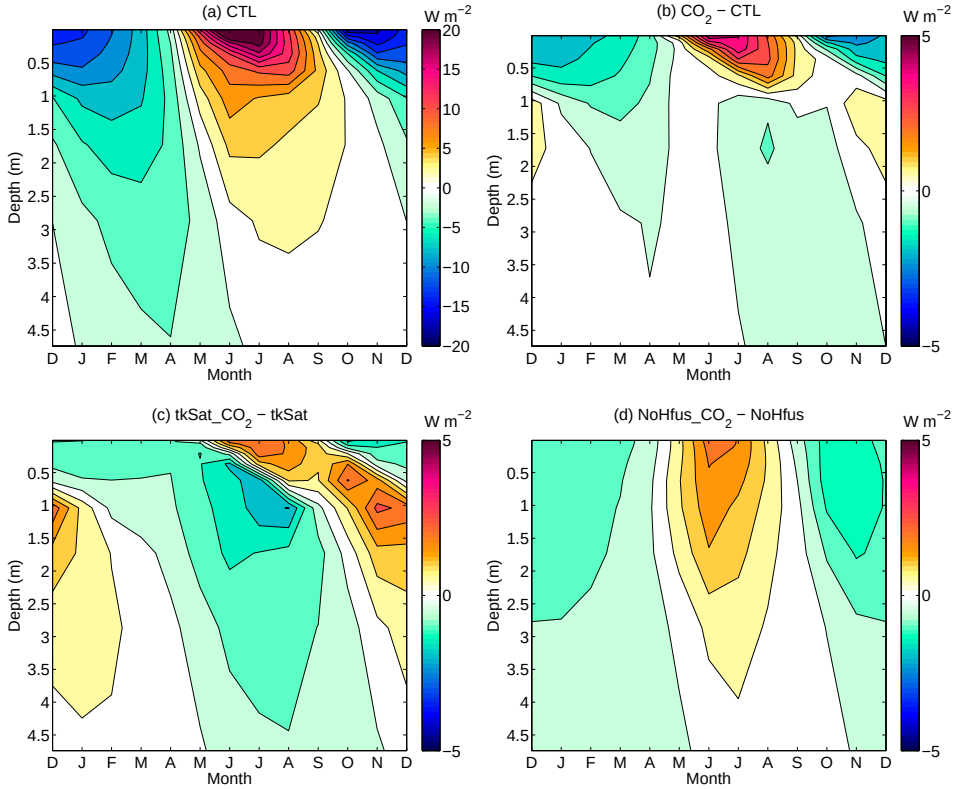

Figure 5: Monthly-mean downwards soil heat flux differences (W m^{-2}) for experiments under equilibrium historical conditions, averaged over gridcells experiencing greater than 1°C soil temperature increases in the CO_2 - CTL experiment: (a) absolute downwards heat flux occurring in the baseline simulation; (b) changes due to elevated CO_2; (c) changes due to elevated CO_2 with saturated soil thermal conductivity; and (d) changes due to elevated CO_2 with no LHF.

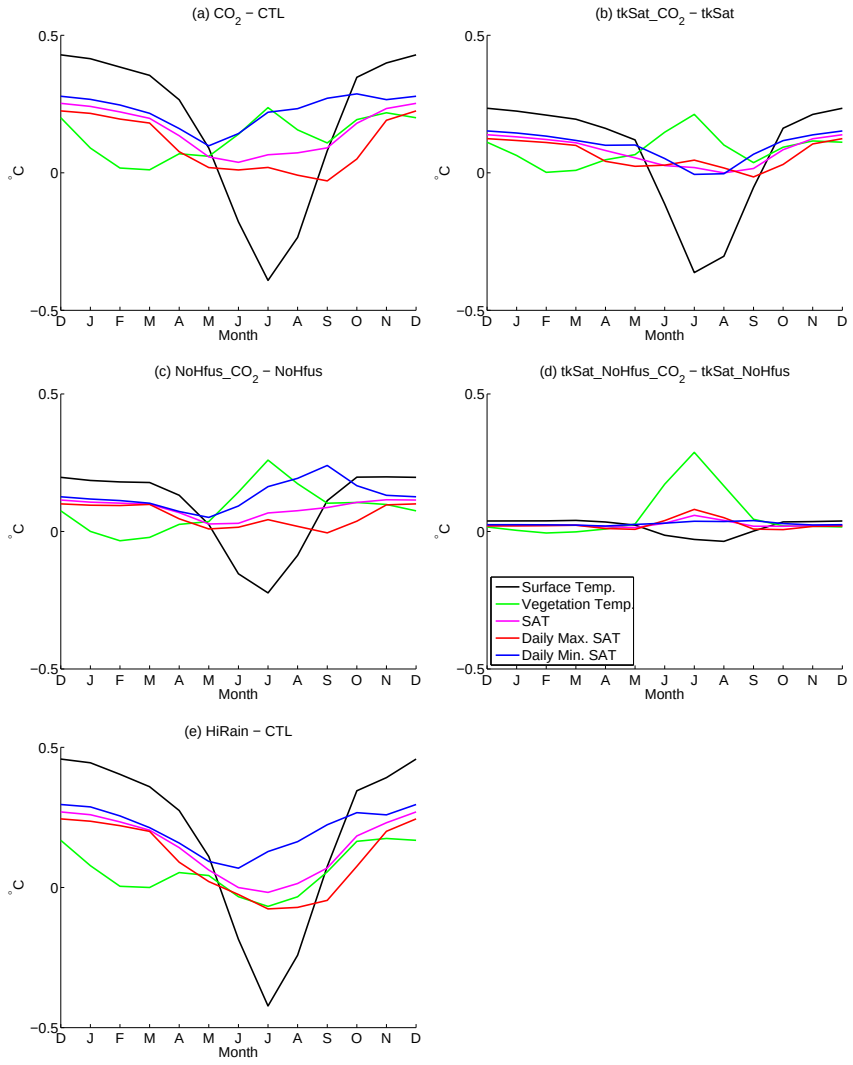

Figure 6: Monthly-mean near-surface temperature differences (°C) for experiments under equilibrium historical conditions, averaged over gridcells experiencing greater than 1°C soil temperature increases in the CO_2 - CTL experiment (except for panel e): (a) elevated CO_2; (b) elevated CO_2 with saturated soil thermal conductivity; (c) elevated CO_2 with no LHF; (d) elevated CO_2 with both modifications to soil physics; and (e) increased JJAS rainfall (averaged over gridcells experiencing greater than 1°C soil temperature increases in this experiment). Surface temperature is defined as the temperature of the top resolved soil or snow (if present) layer; vegetation temperature is defined at the leaf surface when present; SAT = surface air temperature.

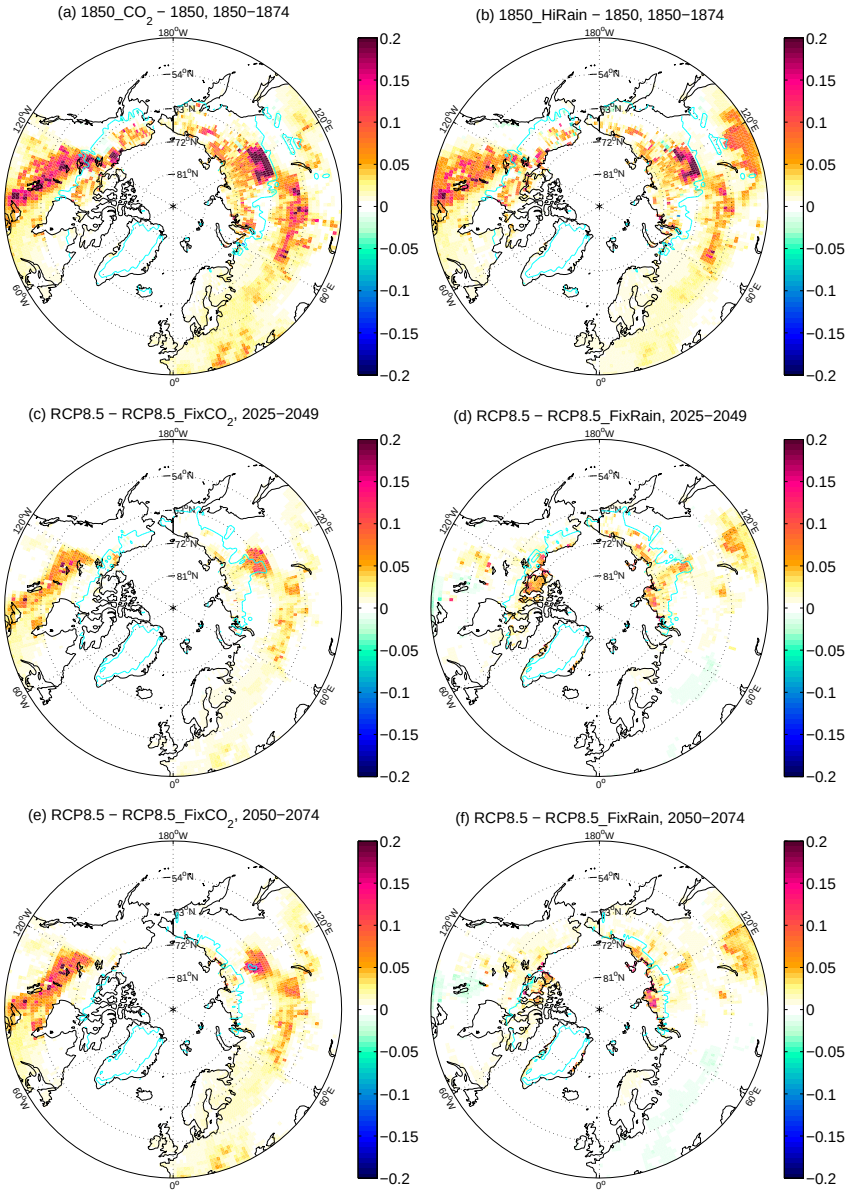

Figure 7: Vertical- (to 3.8 m depth) and annual-mean soil water-filled pore space differences for experiments forced by an 1850-2099 CCSM4 RCP8.5 scenario: (a) elevated CO_2 in 1850-1874 equilibrium; (b) increased JJAS rainfall in 1850-1874 equilibrium; (c) transient effects of increasing CO_2 during 2025-2049; (d) transient effects of increasing JJAS rainfall during 2025-2049; (e) transient effects of increasing CO_2 during 2050-2074; and (f) transient effects of increasing JJAS rainfall during 2050-2074. Cyan lines encircle regions with ALT less than 5 m in the control (i.e., drier) simulations for each panel.

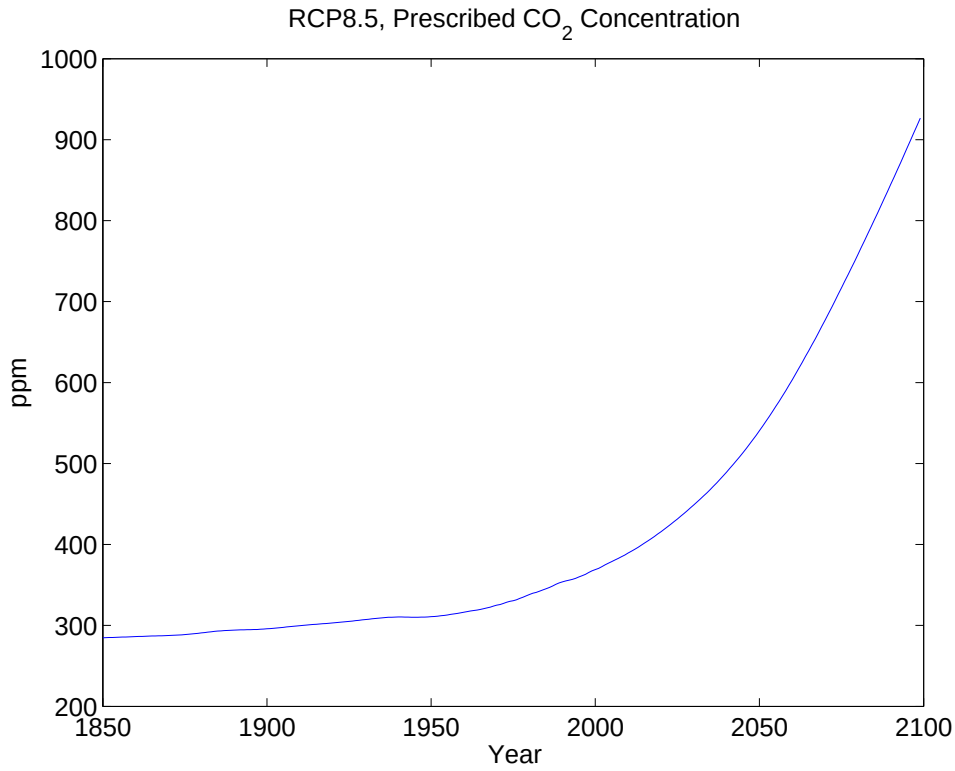

Figure 8: Prescribed atmospheric CO_2 concentrations (ppm) for the RCP8.5 scenario.

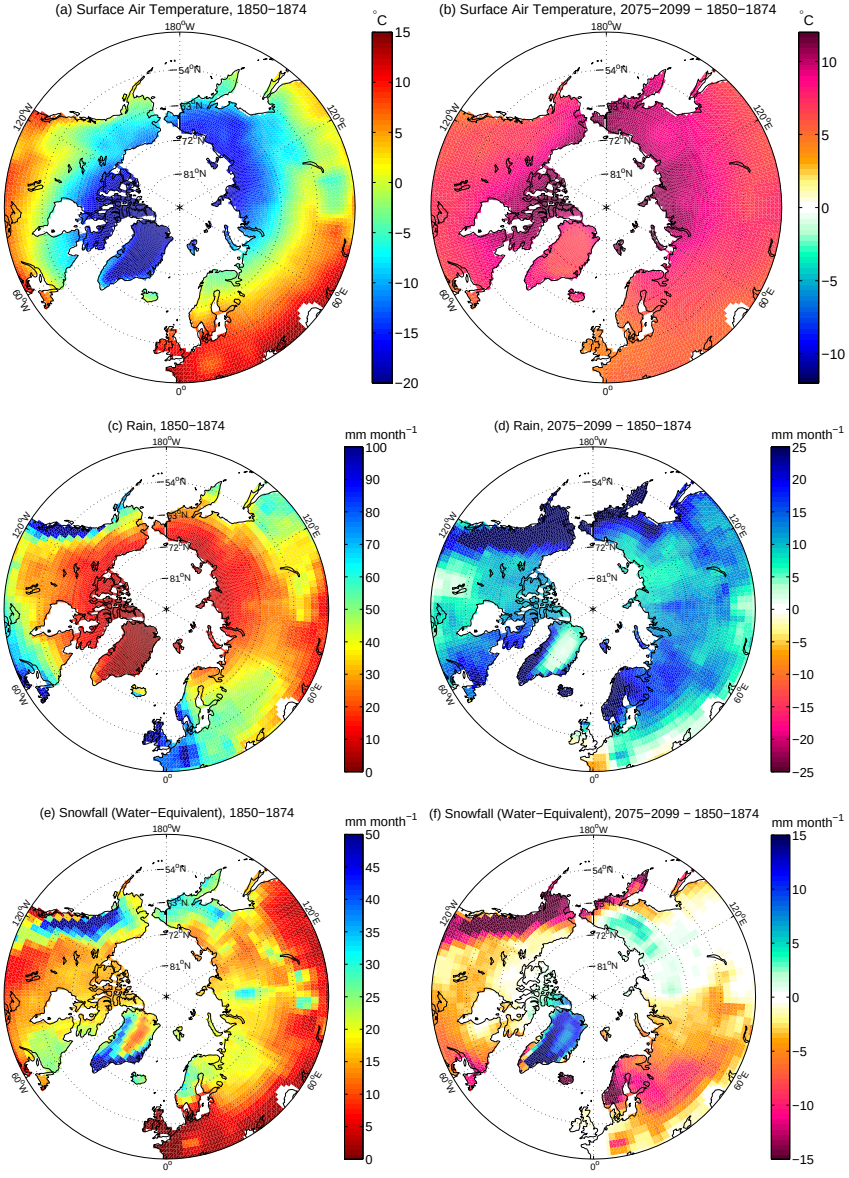

Figure 9: Climatology for the 1850-2099 CCSM4 RCP8.5 forcing: (a) 1850-1874 mean surface air temperatures (°C); (b) mean surface air temperature changes (°C) from 1850-1874 to 2075-2099; (c) 1850-1874 mean rainfall (mm month^{-1}); (d) mean rainfall changes (mm month^{-1}) from 1850-1874 to 2075-2099; (e) 1850-1874 mean snowfall (mm H2O month^{-1}); and (f) mean snowfall changes (mm H2O month^{-1}) from 1850-1874 to 2075-2099.

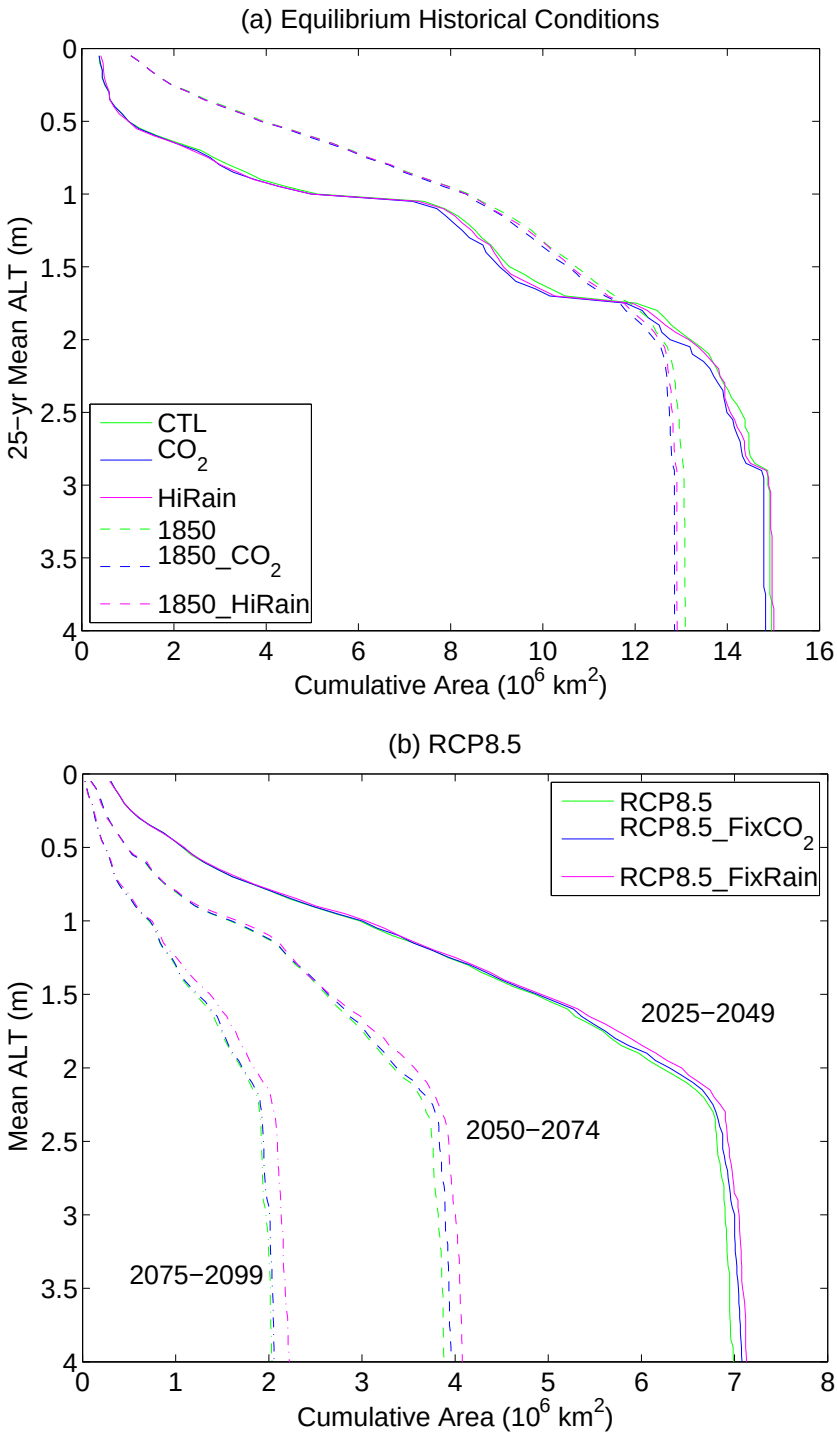

Figure 10: Cumulative distribution functions of increasing 25-year mean active-layer thickness (m) vs. area (10^6 km^2) (a) simulations under equilibrium historical conditions (Table 1); and (b) forced by a transient RCP8.5 scenario.